Performance of Immersed Tunnels subjected to Settlements

Noordtunnel Case Study

Mark van der Heijden

Engineering Doctorate

Rijkswaterstaat
Ministry of Infrastructure and Water Management

TU Delft

COB
Nederlands kenniscentrum voor ondergronds bouwen en ondergronds ruimtegebruik

Performance of Immersed Tunnels subjected to Settlements

Noordtunnel Case Study

by

Mark van der Heijden, MSc

to obtain the degree of

Engineering Doctorate
in Civil and Environmental Engineering

at the Delft University of Technology,
to be defended publicly on Thursday December 21st, 2023 at 11:00 AM.

EngD Committee:	Prof. dr. ir. M.A.N. Hendriks,	Delft University of Technology,	Chairman
	Prof. dr. K.G. Gavin,	Delft University of Technology,	Independent
	Dr. ir. W. Broere,	Delft University of Technology,	Supervisor
	Ir. H.R.E. Dekker,	Rijkswaterstaat	

Rijkswaterstaat
Ministry of Infrastructure and Water Management

Cover photo (1990): Immersion of the first element of the Noordtunnel at the approach (lower one), while the second element is being positioned, retrieved from https://www.wegenwiki.nl/Noordtunnel.

Preface

This thesis entails the completion of the Engineering Doctorate research project, which I have been working on for the past two years. Combining applied scientific research with my regular work at Rijkswaterstaat has been very challenging, absolutely enlightening, and above all extremely valuable. The developed skills, acquired knowledge, and gained experiences, as well as the people I encountered along the way, will serve me in my future endeavours. I am grateful to many people and parties who contributed to the realisation of this research project, there are far too many to all acknowledge individually.

First and foremost, I would like to thank Rijkswaterstaat for the unique opportunity to make this EngD programme possible. This programme has been mutually beneficial, where a relevant research has been conducted for Rijkswaterstaat, while also improving professionally. In particular, I am tremendously grateful to my mentor, Harry Dekker, for being consistently critical on my research from an optimistic and pragmatic perspective, and sharing lots of his valuable knowledge and experiences.

Moreover, I am sincerely grateful to Delft University of Technology for facilitating the EngD programme, including all the experts that were involved in the programme. I would especially like to thank Max Hendriks, Wout Broere and Ken Gavin for their extremely valuable contribution as my committee. I am deeply grateful to Max Hendriks for being my supervisor during this challenging research, where he always shared his critical thoughts, came up with creative ideas, and provided me with truly valuable feedback. In addition, I am extremely grateful to my daily supervisor, Wout Broere, for his invaluable knowledge in the field of tunnels, his critical thinking from multiple perspectives, and above all his constant support when needed. Also, I am very grateful to Ken Gavin for his independent view on my research project, and sharing his extensive knowledge during our meetings. On top of that, I would like to thank Martine van den Boomen and Jaap Vleugel for their expertise and contribution to the research.

Furthermore, I would like to thank all the experts within the tunnelling sector for their outstanding support at various moments. I am especially grateful to Hans de Wit, Jan Kloosterman, Hans Mortier, Adri Vervuurt, Coen van der Vliet, and Gerrit Wolsink for sharing their knowledge and experiences. Additionally, the Centre for Underground Construction (COB) has played a central role in facilitating the connection of people and sharing of knowledge, for which I am very thankful. Also, I have been greatly inspired by the collaboration across different parties, after all we should remember that there are often far more corresponding interests than opposing ones.

Finally, I would like to thank my family, friends and my girlfriend for their unwavering support and belief in me, especially during the most challenging days. I am incredibly grateful for their ever honest opinions, willingness to help, and love!

Mark van der Heijden
Pijnacker, December 2023

Abstract

In the next decades, Rijkswaterstaat will renovate many existing immersed tunnels so they can meet their intended lifespan in a good condition. Ongoing settlements could be a threat to the tunnel structural performance, as deformation may cause structural damage. Currently, immersed tunnels are subjected to greater and more uneven settlements than considered in the design. The issue of these ongoing settlements is mainly concentrated in the segment joints, which have typically been executed by a spigot and socket structure to prevent differential settlements. Significant deformation of the tunnel structure could result in concrete cracking, which entails the risks of structural connection loss, tunnel misalignment, and leakages (leading to durability reduction and damage to installations). This could impact the reliability of the structure over time, and consequently affect the availability of the road network. Therefore, the key objective of this research is how to assess the structural reliability and tunnel availability, and to investigate in which way the performance of existing immersed tunnel structures could be optimised given the ongoing settlements. Assessing the residual lifespan is beyond the scope, but optimising the tunnel performance during the remaining operational life is the main motivation for this research project.

The research methodology consists of a parametric structural model, which determines the tunnel reliability and availability by using a Monte Carlo approach. This approach involves the realisation of an N number of simulations, where each simulation solves the structural model for a random set of input parameters, based on their stochastic distribution. The failure probability follows from the number of simulations with failure, and from this the structural reliability is derived. Subsequently, the availability is estimated based on the reliability, by the mean time between failure and the mean down time, considering the tunnel as a fully repairable system. Also, the (future) critical segment joints are identified, given the determined failure probability for each segment joint. The structural model consists of beam elements, which are supported by distributed springs, connected by discrete springs, and subjected to a vertical distributed load. The model considers the vertical deformation (v), axial deformation (u), and rotation (φ) as degrees of freedom. An output of the displacement, rotation, bending moment, and shear force diagrams is produced by the model, after solving the system of differential equations for a given input. Three different sets of boundary conditions are considered for the differential equations, resulting in three structural models:

- *Model 1* prescribes the displacement at all the immersion and segment joints.
- *Model 2* prescribes displacements at immersion joints and rotations at segment joints.
- *Model 3* prescribes the rotation at all the immersion and segment joints.

The prescribed displacements follow from the settlement data, where the prescribed rotations are based on the bending moments with the rotational joint stiffness. Additionally, the axial deformation of the tunnel is included, by considering various deformation modes with a probability of occurrence, which are based on the tunnel seasonal behaviour. Failure is then defined as the exceedance of the segment joint capacity, examining two failure mechanisms of shear force and rotation. Shear force failure is the most likely mechanism in case of significant deformation, where rotational failure considers the structure more from a geotechnical perspective.

The Noordtunnel case is used to demonstrate the research methodology, as this tunnel showed excessive settlements and a major renovation will be performed in the coming years. The input contains a projection of the settlement developments until 2050, distinguishing between the extreme cases of a logarithmic and linear increase, allowing to quantify the consequence of ongoing settlements. It follows that the reliability of the tunnel decreases over the years, as the settlements increase. Moreover, the unavailability is estimated to be approximately one day annually, assuming a

direct relationship between the loss of structural connection and the appearance of leakages at a segment joint. On top of that, segment joints S12, S13, and S43 are qualitatively identified as the most critical joints of the Noordtunnel, while joints S21, S22, S32, and S42 are semi critical. It follows that three out of the four joints with known leakages are identified as critical according to the research methodology. In the methodology considerable uncertainty is involved in the input parameters, structural models, and failure mechanisms, as follows from the results and sensitivity analysis. Especially the input parameters of the foundation stiffness, segment joint capacity, and settlements involve a large spread in the outcomes, as these parameters have a major impact and contain uncertainty themselves. Furthermore, between the structural models there is a significant spread in the outcomes, where *Model 2* corresponds closest to reality. Moreover, the failure mechanisms contain an even larger spread. The involved uncertainty causes the results to be interpretable as an order of magnitude only. Therefore, it is recommended to continue with the research methodology by gathering more data of the tunnel structure, further developing the soil-structure interaction, and extending the model at the segment joint level.

Next, the maintenance and renovation strategy for the segment joints in immersed tunnels are examined, to optimise the performance throughout the residual lifespan. Five solution alternatives are taken into account, including advanced monitoring and inspection, corrective injection of leakages, repairing the structural connection, installing additional waterproofing, and compensation grouting. These solutions are assessed techno-economically with a societal cost-benefit analysis. First of all, advanced monitoring and inspection induce data gathering, encouraging scientific knowledge development, which supports more efficient maintenance in the long-term. Furthermore, the present corrective way of injecting leakages could be improved, in terms of process and organisation. Moreover, drastic renovation solutions of repairing the structural connection (recovering structural performance), additional waterproofing (ensuring watertightness), and compensation grouting (controlling settlements) may be applicable for critical segment joints. The main practical recommendation is to explicitly include the segment joints of immersed tunnels into the maintenance and renovation scope of Rijkswaterstaat. This involves the installation of advanced monitoring systems in immersed tunnels, the optimisation of correctively injecting leakages in the maintenance strategy, and the further development of the drastic solutions as a part of the renovation strategy.

Contents

List of Figures

List of Tables

1. Introduction

This section presents the introduction of the research. Firstly, the motivation of the research is described in subsection 1.1. Next, subsection 1.2 demonstrates the problem statement. Additionally, the research aim and method are substantiated in subsection 1.3. Finally, subsection 1.4 gives an overview of the thesis outline.

1.1. Motivation

The infrastructure network of the Netherlands contains many immersed tunnels that were built in the previous century. Rijkswaterstaat[1] will renovate multiple existing immersed tunnels[2] in the next decades to meet the intended lifespan of 100 years in a good condition. In South Holland, 9 tunnels will be renovated to maintain safety and availability for the future[3]. The focus of these renovations is predominantly on replacing the tunnel technical installations, while the tunnel structure itself should also be in the scope of the renovation more obviously. This is because the tunnels are facing several challenges nowadays, which could affect their structural condition, e.g. leakages as shown in Figure 1.

One of the potential threats to the immersed tunnel structures concerns ongoing settlements, as deformation of a tunnel may cause damage to the structure. Currently, the impact of ongoing settlements on the residual lifespan of immersed tunnel structures is unknown to Rijkswaterstaat. Therefore, given the intended lifespan that must be met in good condition, it is important to gain insight into the reliability of a tunnel structure over time with respect to these settlements. Furthermore, it is also essential to understand the impact on the availability of the tunnel, as the availability of the road network should always be maintained at a high level of performance.

Figure 1: A leakage in the Drechttunnel in 2002 resulted in ice on the road and icicles on the roof, when the temperature was below zero degrees Celsius (Leeuw, 2008).

[1] Rijkswaterstaat is the executive agency of the Dutch Ministry of Infrastructure and Water Management.
[2] The immersed tunnel technology is usually applied to waterway crossings. An immersed tunnel is made up of several elements, which are connected by immersion joints. Each element is manufactured in a construction dock and contains several segments (with segment joints in between). After completion, the elements are transported over water, immersed in the trench, and attached to each other. In the Netherlands, it is common that immersed tunnels receive a sand jet foundation after positioning (shallow foundation).
[3] Project Tunnel Renovations South Holland (PTZ, Project Tunnelrenovaties Zuid-Holland) will include the renovation of 8 tunnel structures and currently the 1st Heinenoordtunnel is being renovated.

1.2. Problem Statement

Immersed tunnels in the Netherlands are often founded on shallow foundations, for which the occurrence of minor settlements is not extraordinary. However, excessive settlements could lead to significant deformation of a tunnel structure, which could threaten the performance level of the structure. For instance, settlement-related leakages could occur to the tunnel structure, as displayed in Figure 1 for the Drechttunnel, when the temperature was below zero degrees Celsius in 2002.

During the design phase of existing immersed tunnels, only minor uniform deformations were taken into consideration. However, displacement measurements of the tunnel show that several immersed tunnels undergo greater and more uneven settlements than expected in the design, as illustrated in Figure 2 for the Kiltunnel. Similar issues emerge in many immersed tunnels in the Netherlands, including the multiple existing immersed tunnels managed by Rijkswaterstaat.

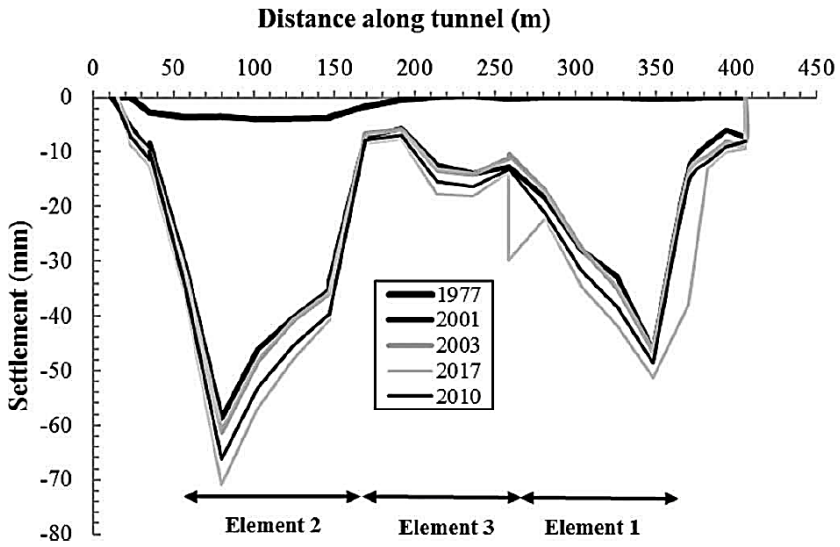

Figure 2: Vertical settlements of the Kiltunnel measured between 1977 to 2017 (Gavin et al., 2019).

The issue of these ongoing settlements is mainly concentrated in the segment joints[4], which have typically been executed by a spigot and socket structure to prevent differential settlements, as shown in Figure 3. Due to the greater and more uneven settlements, larger loads may occur on the segment joints than were initially considered. This could lead to cracking or spalling of the concrete, as the joints are often only equipped with a small amount of practical shrinkage reinforcement. This entails the risks of water leakage, loss of structural connection, reduction of durability, and damage to technical installations, which in the worst case could possibly lead to the end of the useful tunnel life.

An example of the major consequence of settlements is the Kiltunnel, where a sand-carrying leakage of the foundation appeared in 2001, which is displayed in Figure 4 (Leeuw, 2008). This leakage was likely caused by fracture of the spigot and socket structure, due to substantial deformation of the tunnel structure (Leeuw, 2008). In the past, many leakages have appeared in the floors, walls and roofs of immersed tunnels in the Netherlands (Leeuw, 2008; Leeuw, 2018). Almost all leakages appeared in the segment joints, as there is only one known case of an immersion joint leakage in the Dutch and Belgian tunnels, which is the 1st Coentunnel (COB, 2020).

[4] The function of the segment joint is to allow some deformation in the longitudinal direction of the tunnel element (due to temperature effects for instance) and minor rotations around the transverse axis between segments (as a result of the considered settlements in the design).

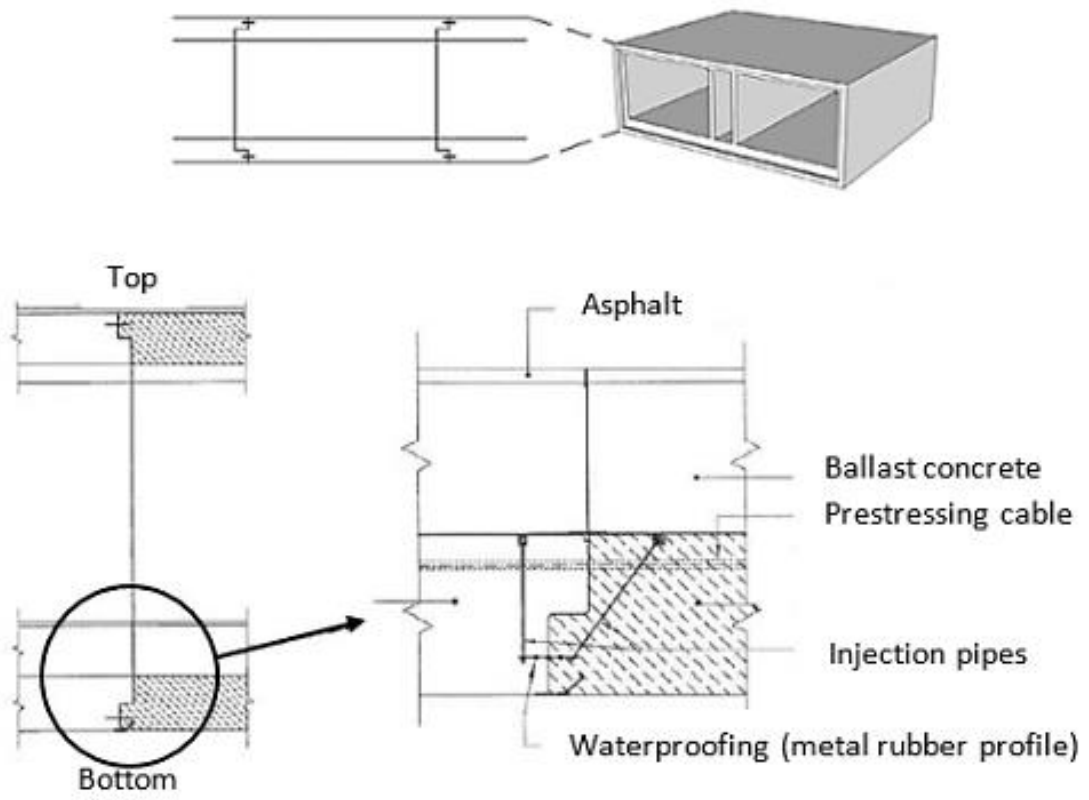

Figure 3: Tunnel segment with a segment joint that is executed as spigot and socket structure, including a rubber waterproofing around the entire joint (Schols, 2012a).

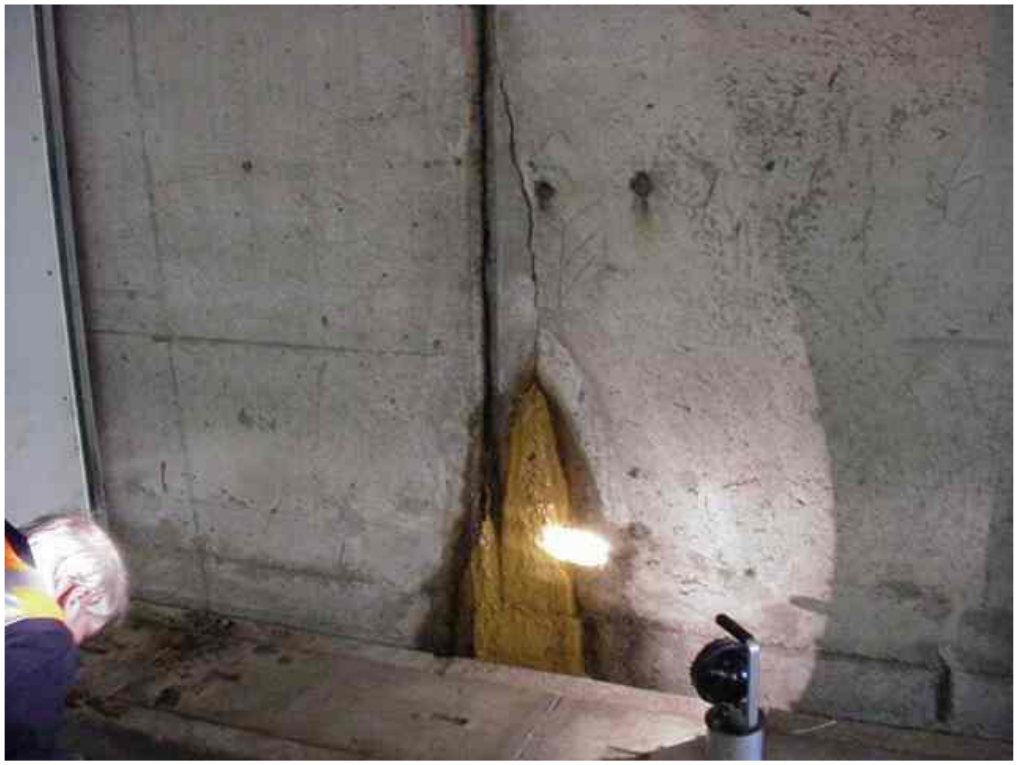

Figure 4: Leakage in the outer wall of a segment joint in the Kiltunnel, where foundation sand was transported into the tunnel (Leeuw, 2008).

1.3. Research Aim & Method

The deformation behaviour of immersed tunnels subjected to ongoing settlements has been studied to a limited extent, especially when relating to the segment joints. In the Netherlands, the segment joints are typically executed with the spigot and socket structure (Figure 3), but there are only a few known examples of tunnels with such a type of joint in other countries[5]. As a result, the international literature on immersed tunnels with this type of segment joint is somewhat shallow. In addition, the behaviour of existing immersed tunnels cannot adequately be explained yet, in relation to the assumed situation during the design, due to the lack of data and poor data quality. Moreover, the remaining structural reliability of the segment joints in existing immersed tunnels is not known given the ongoing settlements. On top of that, the impact on the unavailability of the tunnel has not been considered before, due to a potential decreasing structural reliability of the segment joints. Finally, the effect of predictive maintenance on the residual lifespan of an existing immersed tunnel has not yet been thoroughly investigated.

The key motivation behind the research is therefore to investigate in which way the residual lifespan of existing immersed tunnel structures could be optimised, given the ongoing settlements. To achieve this, the structural reliability and availability of the tunnel should be determined first, using a methodology yet to be developed. In this methodology, a structural model is used to represent an immersed tunnel, with a parametric type of input. In this way, the methodology should be applicable to multiple immersed tunnels in the Netherlands. Moreover, future changes of parameters could easily be implemented, when developments due to new insights appear. Parameters include for instance: the tunnel structure geometry, geotechnical conditions and measured settlements. With the structural model, the methodology should be able to predict the structural reliability and availability over time, based on settlement projection scenarios. In addition, the methodology should be capable of identifying the critical segment joints of the tunnel structure, which could become problematic in the future, due to increasing settlements. This should serve a tunnel manager to clearly have an overview of the possible risks that settlements could induce to the tunnel structure. Furthermore, the developed methodology enables the tunnel manager to optimise the maintenance of the tunnel structure, for example through the utilisation of predictive maintenance. On top of that, the already planned renovations could be used more optimally, when the scope of the settlement threat to the tunnel structure is more evident. Hence, the main research question is the following:

How to assess and optimise the performance of existing immersed tunnels subjected to ongoing settlements, regarding the segment joint functioning?

The research question involves only existing immersed tunnels that are performed with a spigot and socket structure in the segment joints (Figure 3). The main research question is divided into four sub questions, which are as follows:

1. *In which way could a parametric model simulate an immersed tunnel structure subjected to ongoing settlements?*
2. *How to assess the structural reliability and availability over time of an immersed tunnel subjected to ongoing settlements?*

[5] Several examples of immersed tunnels with a spigot and socket type of segment joint are the Medway tunnel (Chatham, UK), the Liefkenshoektunnel (Antwerp, Belgium) and the Warnow tunnel (Rostock, Germany). However, no relevant literature with respect to these tunnels has been found.

3. *To which extent could the (future) critical segment joints of an immersed tunnel be identified?*
4. *Which maintenance and renovation strategy could potentially improve the performance of the segment joints?*

The research is executed by developing a structural model that represents an immersed tunnel, using the Python programming language. The structural reliability of the tunnel could be determined based on a Monte Carlo approach. The tunnel availability and critical segment joints are derived from this. Furthermore, maintenance and renovation solutions are inventoried and their applicability is assessed, considering the techno-economic feasibility. The Noordtunnel is used as a case study, since this tunnel has shown greater settlements than foreseen during the design, and the renovation is planned to be performed before 2030. This provides the opportunity of including (future) critical segment joints in the renovation scope. Note that the methodology of this thesis could also be applied to other immersed tunnels, which face similar challenges regarding ongoing settlements.

The failure definition in the calculation is equal to the exceedance of the structural capacity of a segment joint, and accompanying (temporary) unavailability due to leakages occurring. Noteworthy, this concerns local failure of the joint in practice, as the tunnel segment is still supported by the sand foundation. As a result, this research does not consider the occurrence of global tunnel failure[6]. This is why the remaining tunnel lifespan is not assessed with structural requirements from the standards, but based on the operational limits in terms of unavailability. In addition, this research assumed a direct relationship between the appearance of leakages and the loss of structural connection at a segment joint. Hence, (temporary) unavailability of the tunnel is coupled to the appearance of water leakages in one of the segment joints. It should be noted that the relationship between ongoing settlements and leakages is not unambiguous, as e.g. existing leakage paths could be present in a segment joint, as a result of poor performance quality during the construction phase (Leeuw, 2008).

Noteworthy, this research is part of the COB[7] research programme *Future Proof Tunnels*, in which a scientific basis is laid to solve knowledge gaps with respect to tunnel structures. Within this programme the research touches the domains of joint behaviour and soil-structure interaction.

1.4. Thesis Outline

The outline of the thesis is as follows. First of all, in this section the introduction of the research has been described, including the motivation, problem statement, research aim and method (section 1). Next, section 2 will demonstrate the literature review, which dives deeper into the behaviour of immersed tunnels, and the specific issues with the segment joints. In section 3, the research methodology will be presented to determine the structural reliability and availability of immersed tunnels subjected to ongoing settlements. This includes the substantiation of the structural tunnel model and the Monte Carlo approach used. Thereupon, section 4 describes the Noordtunnel case, with the parameter quantification and the obtained results from the methodology. In section 5, the sensitivity analysis and the discussion of the research methodology are performed. Then, section 6 suggests the maintenance and renovation strategy, which could be implemented to deal with the critical segment joints. Thereafter, the conclusions and recommendations of the research are provided in section 7. Subsequently, the references used in the research are displayed. Finally, the appendices are presented that support the previous sections and add additional depth.

[6] However, in practice it could be imaginable that after local failure of a segment joint, by the influence of differential settlements, a situation arises with (uncontrollable) massive leakages and (unsafe) bumps in the road. As a result, the tunnel could have reached the end of its functional lifespan at some point.
[7] The Centre for Underground Construction (COB) is a network and knowledge organisation.

2. Literature Review

In this section the literature is reviewed. In subsection 2.1, relevant background information of the immersed tunnel technology is presented first. Next, the behaviour of immersed tunnels on a shallow foundation is described in subsection 2.2. Finally, subsection 2.3 focuses on the specific issues related to the segment joints of immersed tunnels.

2.1. Background Immersed Tunnels

The immersed tunnel technology is the ideal way of constructing a tunnel across a waterway, as the technique relies on water for transportation and placement of the tunnel[8] (Lunniss & Baber, 2013). Immersed tunnels typically have a limited length when crossing a waterway, compared to bored tunnels and bridges, which could be beneficial in terms of costs (Olsen et al., 2022). Generally, an immersed tunnel layout consists of three parts (as illustrated in Figure 5): immersed tunnel elements, cut and cover tunnels, and open approaches (Lunniss & Baber, 2013). This research involves the immersed part of the tunnel structure only, thus the immersed tunnel elements.

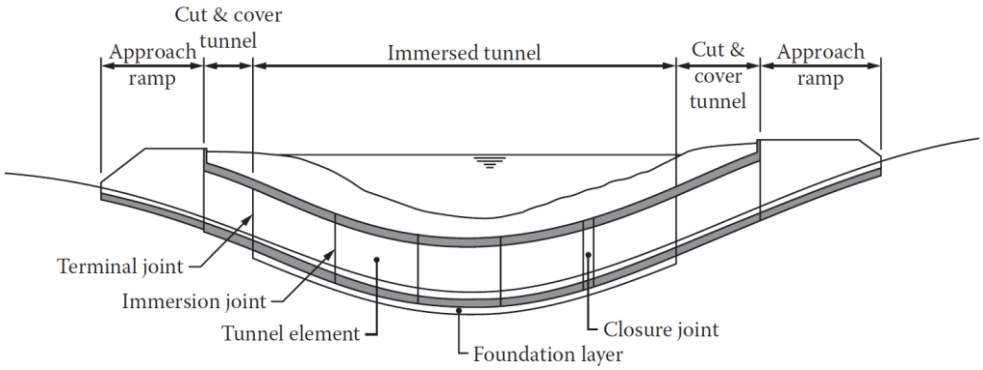

Figure 5: General layout of an immersed tunnel (Lunniss & Baber, 2013).

The construction of an immersed tunnel contains some basic fundamentals (Lunniss & Baber, 2013):

- Manufacturing the tunnel elements in a construction dock, where each element consists of several segments (with segment joints in between).
- Transporting the prefabricated elements over water to the tunnel location[9], while floating.
- Immersing[10] the elements into a dredged trench at the bottom of the waterway, and connecting them by means of immersion joints (and the closure joint)[11].
- Backfilling of the trench and completion of the tunnel from the inside.

This research focusses on the impact of settlements on the structural condition of the segment joints, thus regarding the joints within a tunnel element. The segment joints of the older existing immersed tunnels in the Netherlands have typically been executed by a spigot and socket structure, as shown in Figure 3. The watertightness of these joints is ensured by the application of a rubber gasket with steel plates (W9U) around the entire cross section. The function of a segment joint is to allow for some axial deformations and minor rotations, while differential settlements are prevented.

[8] Although most of the immersed tunnels accommodate roads or railways, they can also serve as utility tunnels by containing water and power supplies, for instance (Lunniss & Baber, 2013).
[9] During transport, the tunnel elements are fitted with watertight bulkheads, and the segments of an element are kept together by applying temporary prestressing.
[10] During immersion, the water pressure at the head of the immersed element prestresses the tunnel.
[11] In the Netherlands, it is common that the elements receive a foundation by sand jetting after positioning.

2.2. Behaviour Immersed Tunnels

Several case studies of immersed tunnels in soft soil conditions are known for undesirable settlement patterns, despite anticipation during the design phase to prevent this (Grantz 2001b). Multiple factors related to the settlements of immersed tunnels are distinguished according to Grantz (2001a): sub-soil conditions[12], tunnel foundation construction method[13], tunnel foundation quality[14], surcharge[15], tunnel geometry[16], and tidal variation[17]. The first three factors relate to the stiffness of the tunnel foundation, while the other factors influence the loading on the tunnel foundation. Gavin et al. (2019) showed a relation between a higher magnitude of ongoing settlements and the presence of a lower soil stiffness beneath the tunnel. Zhang & Broere (2019) performed a case study on settlements of the Yongjiang Tunnel, in which the impact of foundation stiffness and surcharge loading on the settlements was determined with a numerical model. Results showed that surcharge by back-silting significantly increases the settlements developing, but a reduction of stiffness could even lead to larger settlements (Zhang & Broere, 2019). Cyclic loading (by tidal effects, traffic or temperature) and creep were considered as potential causes for the mechanism of ongoing settlements at the Kiltunnel over time (Gavin et al., 2019). These mechanisms lead to a logarithmic settlement increase of the tunnel over time.

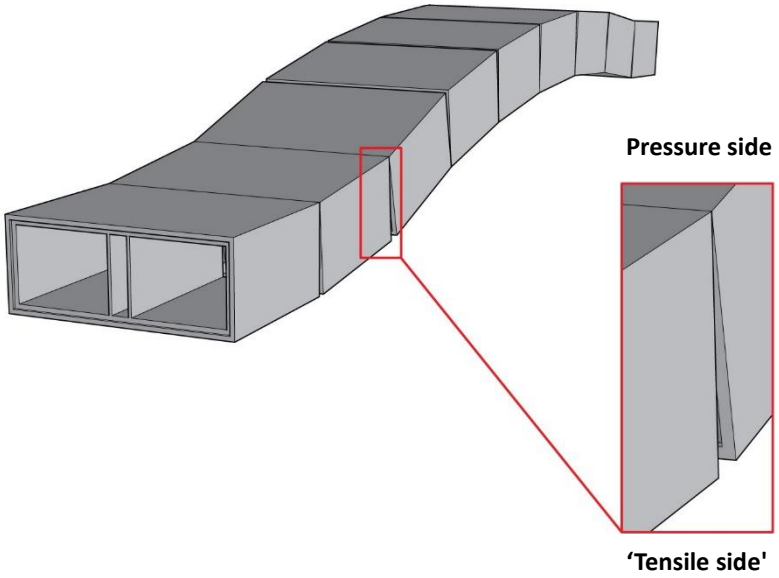

Figure 6: Differential settlements cause the tunnel structure to deform, including opening and rotation of the segment joints (COB, 2023).

[12] In general, a consolidated sandy layer shows lower settlements compared to a compressible clayey soil (Zhang & Broere, 2019).
[13] Besides a shallow sand foundation, immersed tunnels could be founded on (stiffer) gravel beds. However, this type of foundation is not further considered in this research.
[14] The quality of the shallow sand foundation could be influenced by siltation of the trench (before immersion) and the type of trench dredging method (involving more or less irregularities in the foundation) (Grantz, 2001a).
[15] This implies an increasing load on top of the tunnel foundation, as a consequence of backfill on top of the tunnel and the increasing heavy traffic loading (Zhang & Broere, 2019).
[16] A greater tunnel base width means a lower foundation pressure (as the contact area is larger), hence lower settlements will develop (Zhang & Broere, 2019).
[17] Under certain circumstances, large amplitude tidal variation may also cause settlement of sands by their gradual compaction due to daily oscillations in pore pressure (Grantz, 2001a).

Immersed tunnel structures perform time and temperature related behaviour, where differential settlements cause the most structural deformation. Uniform settlements induce the tunnel structure to deform as a whole, like a rigid body, and are therefore less of a concern (Grantz, 2001a; Zhang & Broere, 2019). Meanwhile, differential settlements lead to deformation of tunnel segments, opening and rotation of the joints (visualised in Figure 6), and the cyclic compression and expansion of the rubber Gina gasket (Zhang & Broere, 2019). There is a negative correlation between the increase of temperature and the opening of the tunnel joints[18] (Zhang & Broere, 2023c). This is caused by shortening of the concrete segment due to temperature deformation, while shrinkage[19] and creep can practically be ignored (Saveur & Grantz, 1997). The uneven settlements of a tunnel show a seasonal variation as well, albeit significantly smaller[20] than the joint opening deformation, and for which the correlation with temperature could be positive or negative (Zhang, 2023). Furthermore, tidal variations of the river above an immersed tunnel generate a vertical response. Figure 7 displays the observed behaviour of the 1st Heinenoordtunnel[21], where the tunnel moves upwards and downwards periodically with tidal variations[22], more or less like a rigid body (Broere & Zhang, 2023).

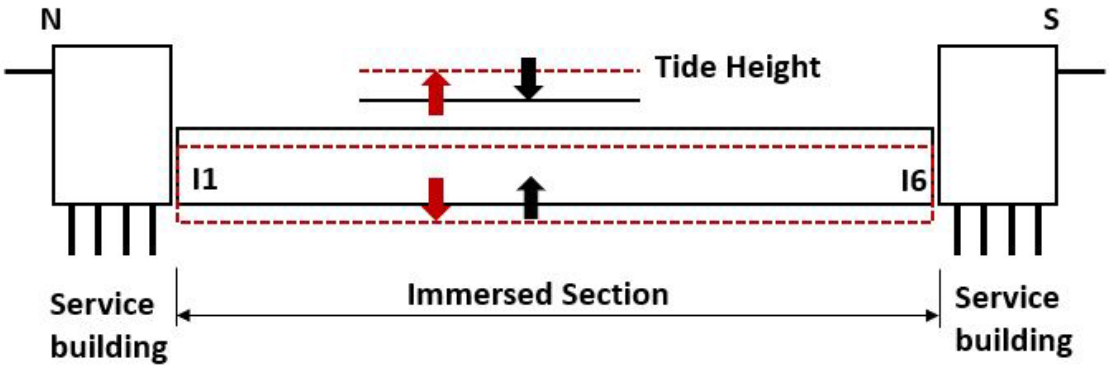

Figure 7: Cyclic behaviour of the 1st Heinenoordtunnel under tidal impact, schematically visualised (Broere & Zhang, 2023).

Structurally seen, each tunnel element initially behaves as a bending beam made up of segments that are pressed against each other, until the bending moment in a joint becomes so great that the joint opens (Arcadis, 2015). Herewith, the stiffness of the immersion and segment joints[23] depends on the joint opening. In addition, the normal pressure force[24] in the tunnel will increase with rising temperature, by the expansion of concrete tunnel segment. Due to this increase in normal force, the tunnel is pre-tensioned, which could slightly lift[25] the segment with the largest settlement in the summer period, as displayed in Figure 8 (Arcadis, 2015). The summer-winter cycle leads to variable joint openings in the center of a tunnel element and to sliding back and forth of segment adjacent to

[18] Measurements in the 1st Heinenoordtunnel showed a time lag between joint opening deformation and temperature, causing a delay of around 1 or 2 days between the temperature change and the subsequent joint opening variation (Zhang, 2023; Zhang & Broere, 2023c).
[19] For the tunnels in the Netherlands, the shrinkage strain is ignored as the concrete is directly exposed to the outside (Saveur & Grantz, 1997).
[20] The uneven settlement amplitude is less than 1 mm at most joints of the 1st Heinenoordtunnel (Zhang, 2023).
[21] The measurement data showed a sub-millimeter movement amplitude of about 0.3 mm (Zhang, 2023).
[22] This cyclic tunnel movement can be explained by a coupled flow and consolidation model of underlying soil layers subjected to tidal variations, at which the soil domain response shows a time lag (of roughly one hour in the order of magnitude) compared to the imposed tidal variation (Zhang, 2023; Zhang & Broere, 2023b).
[23] In the segment joint the stiffness may vary between zero and the cross-sectional stiffness for the joint being fully opened and closed, respectively (COB, 2022).
[24] Aging of the Gina rubber gasket involves stress relaxation, for which the prestressing force in the immersion joint decreases logarithmically over time to approximately 50% after 100 years (COB, 2022).
[25] As rotation of the segment joint causes the pressure line to shift from the neutral line towards the zone of contact, in either the floor or the roof, a pressure arc is created which lifts the tunnel (COB, 2022).

the immersion joint (COB, 2022). This is because the normal forces in the segment joints could easily decrease as a segment shortens, while the elastic Gina gaskets remain more or less under pressure (COB, 2022). Note that, a segment will only move when the shear stresses along the tunnel perimeter are exceeded by the normal force (COB, 2022). In short, the tunnel deformation behaviour is subjected to several (daily and seasonal) mechanisms, which makes it difficult to predict the exact tunnel deformation over time.

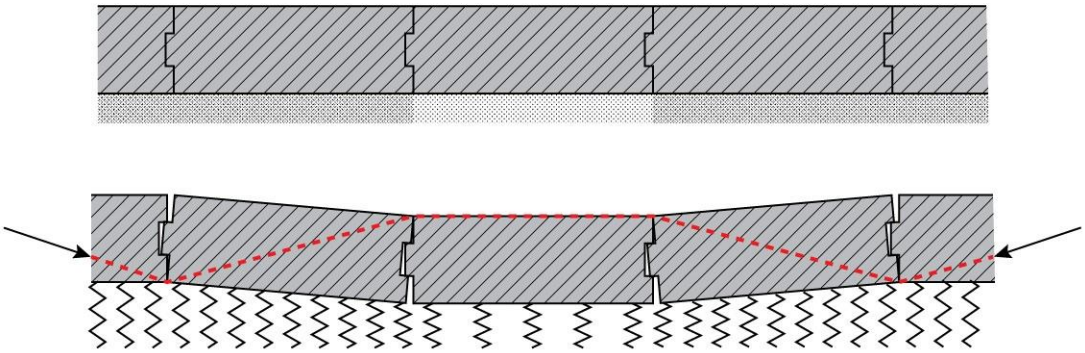

Figure 8: Lifting of a segment with a lower foundation stiffness by the formation of a pressure arc, due to temperature increase (COB, 2023).

2.3. Segment Joint Issues

Settlements, especially differential settlements, could result in cracking of the tunnel structure, leakages and misalignment of the tunnel (Grantz, 2001a). Loads resulting from differential settlements[26] are concentrated at the top or base collar[27] of a segment joint, because the tunnel cross section will deform slightly (Schols et al., 2013a). Figure 9 shows the deformation mode of the collar in a segment joint by the effect of uneven settlements between adjacent segments and the accompanying shear forces (Zhang & Broere, 2023a). As a result of acting shear forces, the collar could potentially crack, which could cause a leakage. This has an impact on the structural tunnel condition, and thereby affecting the operation and durability of the tunnel (Olsen et al., 2022). It is noteworthy that the direction of the shear forces determines whether the load is transferred to the top or base collar. In Figure 9 for instance, the shear forces are concentrated in the top collar, while an opposite shear force direction (_I¯ instead of ¯I_) would lead to a load transfer in the base collar.

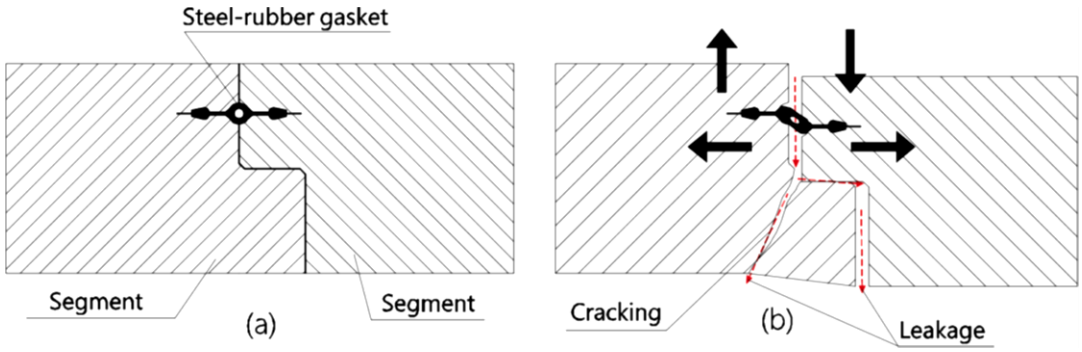

Figure 9: Schematic presentation of the collar structure in a segment joint (a), and the deformation of this collar structure (b), in which the shear forces, horizontal joint opening and resulting leakages are indicated with the vertical arrows, horizontal arrows and red arrows, respectively (Zhang & Broere, 2023a). Note that the left leakage path is preceded by cracking of the concrete due to the acting shear forces.

[26] This is without considering torsion around the longitudinal axis, whereby forces would act in the vertices (Schols et al., 2013b). Torsion is beyond the scope of this research and will therefore not be elaborated upon.
[27] With the collar, the protruding part of the spigot and socket structure is meant.

Figure 10 illustrates the fracture of the collar in a segment joint, where the action of the forces on the collar is being presented more clearly. Besides the shear force, as discussed above, also a tensile force can be exerted on the collar for a rotating segment joint. This horizontal tensile force is a result of the friction between the collars, while the shear force is present (Schols et al., 2013a).

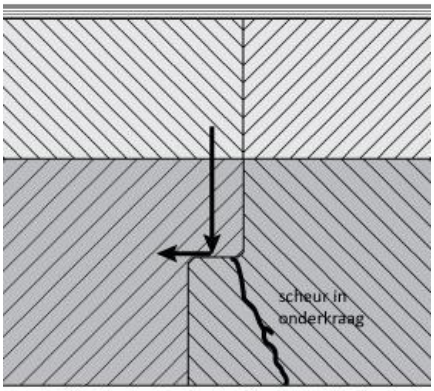

Figure 10: Fracture of the lower collar in the spigot and socket structure of the segment joint, due to a shear force and tensile force acting on the collar (COB, 2023).

Assessing the structural condition of a segment joint for a deformed tunnel is very complex, as the influence of the soil-structure interaction is exerted on both the loading and resistance of the joint. For the Kiltunnel, 2D Finite Element Method (FEM) calculations showed the resistance of the collars[28] to be around $1\ MN/m$ over the effective collar width (Schols et al., 2013b). Note that the effective collar width is smaller than the full width, because the collar near the walls has a greater local stiffness, and therefore attracts more force. Moreover, 3D FEM calculations have proven to be impracticable for the Kiltunnel, due to computational limitations and complexity to include the soil-structure interaction (Parwani, 2014).

By means of a structural model, the forces acting in a segment joint can be determined, with which the reliability of the joints could be established. An analytical model could be used for this, where the tunnel segments are simplified as Timoshenko beams (Wang et al., 2023). In addition, the beams are connected by discrete springs that represent the mechanical behaviour of the joints, and the soil-structure interaction is included by distributed springs (Wang et al., 2023; Tang et al., 2023). For the Drechttunnel case, a reliability assessment was performed regarding the leakages of the immersion joint, using a data-enhanced approach (TNO, 2021). Depending on the possible type of damage that may occur to the tunnel, the segment joint should be assessed in the SLS or ULS[29].

[28] The calculated resistances were respectively $1.3\ MN/m$ for the top outer collar, $0.8\ MN/m$ for the top inner collar, $1.1\ MN/m$ for the base inner collar and $1.2\ MN/m$ for the base outer collar (Schols et al., 2013b).
[29] Water on the road surface or icicles at the roof, unevenness in the road surface and impact on the 'area of free space' (PVR in Dutch) should all be assessed within the Serviceability Limit State (SLS), while unstoppable excessive leakages (especially sand-carrying leakages) and fracture to the structure, leading to loss of the soil and water retaining capacity, should be assessed as Ultimate Limit State (ULS) (Bakker et al., 2012).

3. Research Methodology

This section explains the research methodology to determine the structural reliability and availability of immersed tunnels subjected to ongoing settlements. Subsection 3.1 describes the definitions and limitations underlying the methodology. In subsection 3.2 the structural immersed tunnel model is presented, including the explanation of the three different models. The axial deformation modes of the structural model are discussed more in detail in subsection 3.3. In subsection 3.4 the considered failure mechanisms of the segment joint are expounded. Subsection 3.5 explains the Monte Carlo approach, by which the structural tunnel model is solved for a number of simulations, and the reliability and availability of the tunnel can subsequently be determined.

3.1. Definitions and Limitations

Immersed tunnels can show deformations in three dimensions, of which the degrees of freedom are schematically visualised in Figure 11. The degrees of freedom consist of three displacements and three rotations. A distinction is made between vertical displacements (z-axis), displacements in longitudinal direction (y-axis), and displacements perpendicular to the longitudinal direction (x-axis). In addition, three rotations are possible around the three axes (φ_x, φ_y, φ_z).

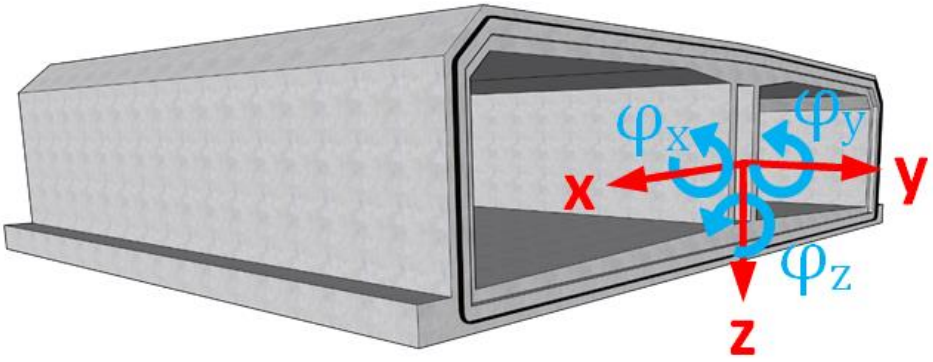

Figure 11: Degrees of freedom for an immersed tunnel in three dimensions.

In this research, only two-dimensional deformations are taken into account, to keep the complexity manageable and to ensure feasibility of the calculations. This implies that the displacements perpendicular to the longitudinal direction (x-axis), and the rotations around the y-axis (φ_y) and z-axis (φ_z), are not considered.

Noticeably, the research methodology takes the global deformations of immersed tunnel structures into consideration, including the accompanying forces within the structure. The focus is on determining the structural reliability of the segment joints and the impact on the tunnel availability, without examining the immersion joints. In addition, local deformation of the immersed tunnel will only be taken into account to a limited extend. This means that deflection of the tunnel walls and slabs has not been looked at specifically, but the principle has been included in a simplified way. Moreover, the distribution of forces over the cross section are not considered at detailed level. It has been assumed that the joints remain flat over the cross section. Furthermore, the resulting normal forces at the segment joints are assumed to act at the neutral axis of the tunnel cross section. Moreover, torsional deformation of the structure around the longitudinal y-axis has not been investigated. Therefore, the research methodology cannot be used for determining the exact deformation, and the force action across the segment joints.

3.2. Structural Tunnel Model

The immersed tunnel structure is modelled as shown in Figure 12, for four tunnel elements consisting of n segments. The model is made up of beam elements with several degrees of freedom that are supported by distributed springs, connected by translation and rotational springs, and subjected to a (vertical) distributed load. Note that, the two approach structures that enclose the immersed tunnel section on two sides, are founded on piles. Thus, the approach structures are assumed to be fixed points in the model, as indicated in the figure. Hereby, the vertical deformation is assumed to be prevented in the outer immersion joints, while horizontal deformation and rotation are allowed.

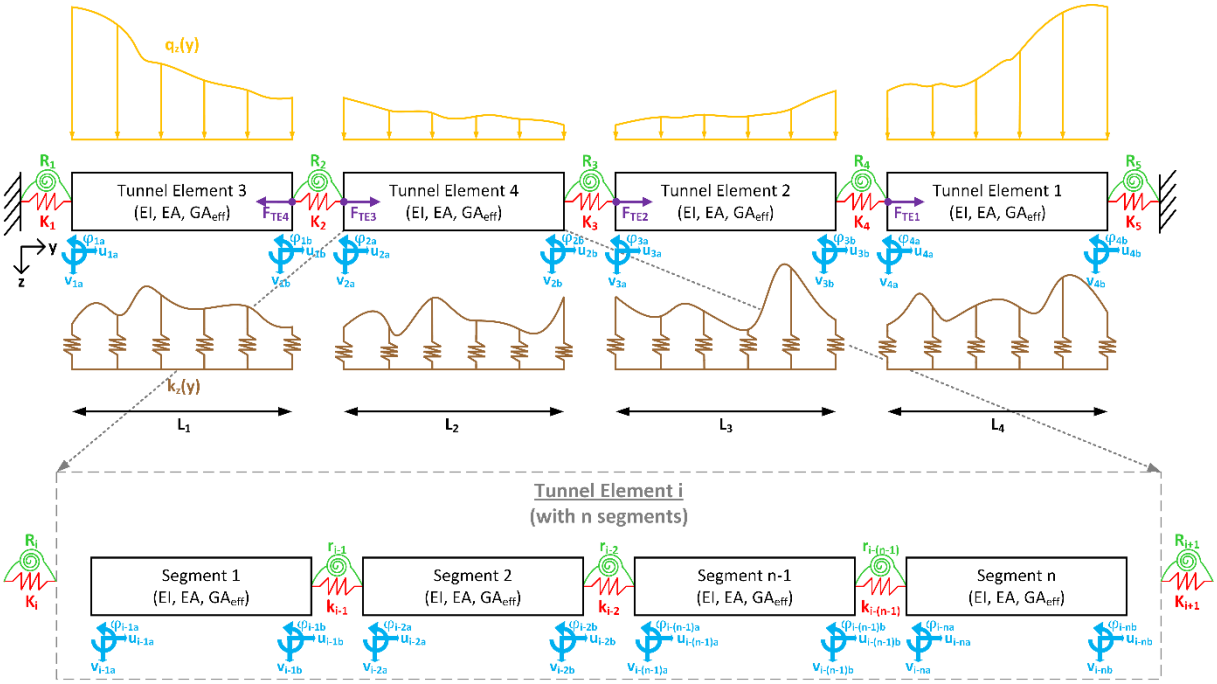

Figure 12: Structural model of an immersed tunnel with an analytical displacement field (in two dimensions), illustrated for the Noordtunnel case, and including each tunnel element consisting of n segments.

The model has three degrees of freedom: vertical deformation (v), axial deformation (u), and rotation around the x-axis (φ_x). Each tunnel element is modelled as a beam structure, where the deformation is given by two differential equations, which is further discussed in Appendix A. The axial behaviour of a tunnel segment is described by Equation 6 (Appendix A.1), and relates to the axial deformation (u). Equation 8 (Appendix A.2) describes the bending deformation[30], and links to the vertical deformation (v) and the rotation (φ)[31]. The immersion and segment joints are modelled as (horizontal) translation springs (K_i, k_i) and rotational springs (R_i, r_i), which connects the segments. No vertical displacement springs are considered between the segments. Note that the closure joint is modelled as a segment joint, because it is contemplated to be structurally less similar to an immersion joint[32]. The model examines the resulting load on the tunnel foundation, which consists of the soil cover weight and the resulting tunnel self-weight, as the vertical load $q_z(y)$. The soil-structure interaction of the tunnel foundation is modelled by the distributed springs $k_z(y)$ at the bottom of the beam elements[33].

[30] The Timoshenko beam is approximated to be equivalent to the Euler-Bernoulli beam if: $3EI/GA_{eff}L^2 \ll 1$. This is considered to apply in this research, as it holds for the Noordtunnel case that: $3EI/GA_{eff}L^2 = 0.10$.
[31] The subscript 'x' of φ_x is omitted for the rest of the thesis, as it is the only rotation direction considered.
[32] As the closure joint does not contain a Gina rubber gasket, it behaves much stiffer than an immersion joint.
[33] When solving the differential equation of bending deformation (Equation 8), the foundation stiffness $k_z(y)$ is averaged over the field of each tunnel segment, to keep the system of equations mathematically solvable.

The structural model delivers an output by solving all the differential equations for a given input. The output includes the displacement, rotation, bending moment, and shear force diagrams of the tunnel[34]. Two differential equations should be solved per tunnel segment, for both the axial and bending deformation, with boundary conditions at the edges. The boundary conditions for the axial differential equation are further described in subsection 3.3. For the differential equation of the bending deformation (Equation 8), different options will be discussed here. Because the differential equation is of fourth order, there are four boundary conditions per tunnel segment (two per edge). First of all, for the outer two immersion joints, the two required boundary conditions follow from a prescribed displacement and rotation[35]. Secondly, for the other three immersion joints (including the closure joint), three required boundary conditions follow from equilibrium at the interface for the displacements, bending moments and shear forces. In addition, the fourth boundary condition can either consist of a prescribed displacement or rotation[36]. Note that in this research, the prescribed rotations are based on the occurring bending moments with the rotational joint stiffness. Finally, all segment joints have the same two boundary conditions options as the three inner immersion joints[37]. In this research, three different sets of boundary conditions for the structural model are considered:

- *Model 1* prescribes the displacement at all the immersion and segment joints.
- *Model 2* prescribes displacements at immersion joints and rotations at segment joints.
- *Model 3* prescribes the rotation at all the immersion and segment joints.

All three models produce particular outcomes, regarding the displacement, rotation, bending moment, and shear force diagrams over the length of the tunnel. Appendix B demonstrates the outcomes of the three structural models, illustrated for the mean values of the Noordtunnel case. The outcomes of *Model 1* are displayed in Figure 60 of Appendix B.1. In this model, the displacements at all the joints are prescribed based on the settlement data, as indicated by the red dots in the figure. The rotations at the joints are not prescribed for this model, allowing them to develop freely, which results in varying joint rotations. *Model 1* shows the greatest bending moment to develop in the fourth immersion joint, and the largest shear forces to occur at the outer immersion joints. In Figure 61 of Appendix B.2, the outcomes of *Model 2* are presented. This model prescribes the displacements at the immersion joints, resulting in the largest rotations there. At the segment joints, the rotations are prescribed, by which the free displacements deviate from the settlement data. As for *Model 1*, also for *Model 2* the greatest bending moment and shear forces appear in the fourth immersion joint and outer immersion joints, respectively. Figure 62 of Appendix B.3 visualises the outcomes of *Model 3*. In this model, the rotations are prescribed at all the joints, causing the free displacements to differ from the settlement data. Unlike *Model 1* and *Model 2*, for *Model 3* the greatest bending moments appear in the middle of the first and last tunnel elements. The largest shear forces occur at the outer immersion joints for *Model 3*, which is in line with the other two models. Because each model has advantages and disadvantages while using, the methodology considers all three models to establish which model best corresponds to reality in the end. As a result, the possibility is also provided to quantitatively gain insight into the model uncertainty.

[34] It should be noted that the rotation, moment and shear force diagram are all related to the displacement. When the displacement depends on x, it holds that: $v = v(x)$, $\varphi = -\frac{dv}{dx}$, $M = -EI \cdot \frac{d^2v}{dx^2}$, $V = -EI \cdot \frac{d^3v}{dx^3}$.

[35] The displacement is considered to be zero (due to the connection with approach structures) and the rotation is related to the occurring bending moment with the rotational spring (R_i): $v_i = 0$ and $\varphi_i = M_i/R_i$.

[36] Thus, two options are considered at these joints, for both it holds that the displacement, moment and shear force of the two intersecting tunnel segments are equal: $v_{i,left} = v_{i,right}$, $M_{i,left} = M_{i,right}$, $V_{i,left} = V_{i,right}$. Moreover, the displacement or rotation could respectively be prescribed by settlement data or related to the bending moment with the rotational spring (R_i): $v_{i,left} = v_{i,right} = v_{data}$ or $\varphi_{i,left} = \varphi_{i,right} + M_i/R_i$.

[37] It should be noted that for the segment joints the rotational stiffness r_i is used instead of R_i in footnote 36.

3.3. Axial Deformation Modes

This subsection discusses the axial deformation of the structural tunnel model in depth. For each tunnel segment, the differential equation of the axial deformation should be solved (Equation 6), as was explained in the previous subsection. Because the differential equation is of second order, each segment has two boundary conditions, one on each side. This means that for all the joints, excluding the outer two immersion joints, two boundary conditions are required at the interface. This implies that both the displacements and normal forces at the boundaries should be prescribed. However, for the immersed tunnels of Rijkswaterstaat there are no long-term axial deformation measurements available. Therefore, a deeper consideration is required, where some necessary assumptions need to be set.

An immersed tunnel experiences a summer-winter cycle regarding the axial behaviour, as a consequence of temperature change[38], described in the literature review (subsection 2.2). This causes the concrete tunnel segments to shrink and expand, inducing the segment joints to open and close. Generally, the summer-winter cycle induces variable joint openings at the center of a tunnel element, while segments adjacent to the immersion joint are sliding back and forth (COB, 2022). A segment could slide when the acting normal force is greater than the friction resistance of the soil around the tunnel, which is schematically shown in Figure 13. In addition, the segment joints are considered to carry no tensile force, as the strength of the W9U rubber gasket is small and the rubber is not very stiff (Van Oorsouw, 2010). Note that the structural reliability of the tunnel is determined for the maximum joint opening over the year, thus indirectly by assuming the winter period.

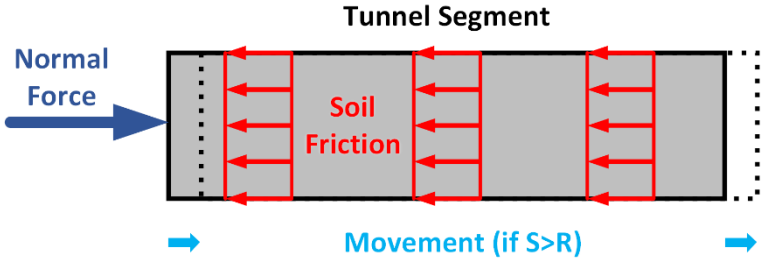

Figure 13: Schematic representation of the considered mechanism working on a tunnel segment (normal force vs soil friction resistance), which forms the basis for the axial deformation of Figure 14, Figure 15 and Figure 16.

In the structural model, the temperature is assumed constant over the entire tunnel[39], the center of the immersion joints is supposed to be fixed in position, and symmetrical axial behaviour is assumed for the segments in between the immersion joints[40]. It can be reasoned that within two immersion joints, the tunnel segments may exhibit different deformation modes. For a tunnel element of five segments and four joints, this leads to three deformation options based on the abovementioned considerations. This implies that all the segment joints could be closed, the inner two joints could be opened, or all the joints could be opened. A fourth deformation mode is added, which is the opening of the two outer segment joints, based on the observations at the 1st Heinenoordtunnel[41].

[38] For the structural model, it is considered that temperature is the only driving force, thus e.g. potential sand behaviour inside an immersed tunnel joint gap is not taken into consideration.
[39] Thus, temperature gradients over the walls or slabs are neglected, as well as possible longitudinal differences.
[40] This is due to the elastic Gina gaskets that remain more or less under pressure, while the normal forces in the segment joints could easily decrease, as a segment shortens (COB, 2022). The closure joint is considered to behave like a segment joint in the structural model, as it lacks the elastic Gina gasket.
[41] Monitoring results of the 1st Heinenoordtunnel showed substantial opening of the two segment joints near the approach structures (Zhang, 2023). This leads to the fourth deformation mode when symmetry is assumed.

Figure 14 shows the possible axial deformation modes considered, illustrated for the Noordtunnel case. It should be noted that the immersed section of the Noordtunnel is divided into three parts: tunnel element 1, tunnel element 2, and the combination of tunnel elements 3 and 4. In this research, each deformation mode is given a probability of occurrence, as a result that the necessary boundary conditions are created per tunnel segment, including all of the possible modes.

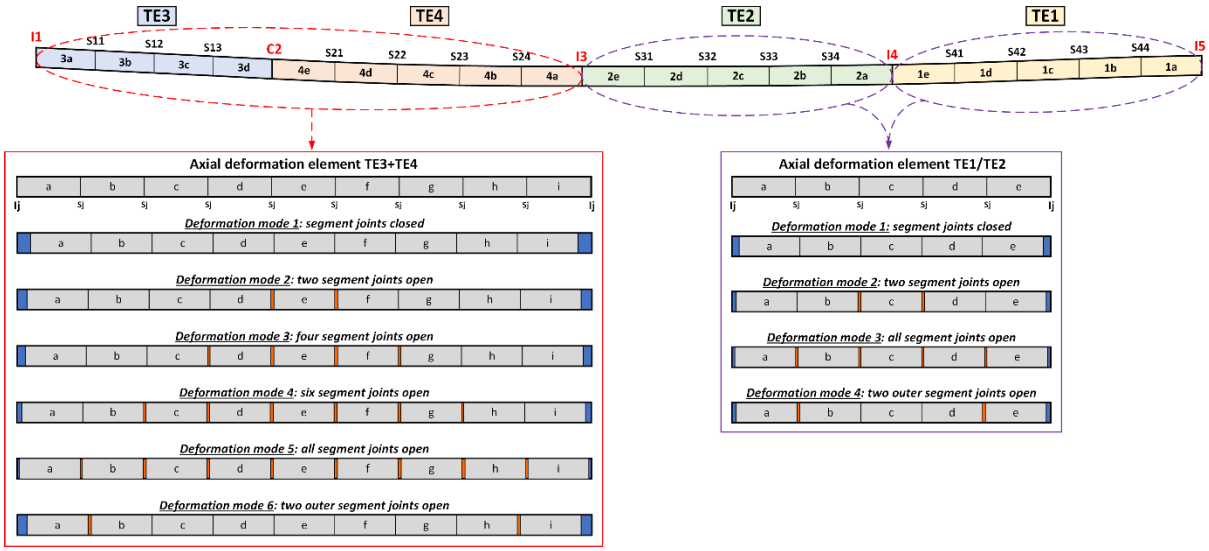

Figure 14: Axial deformation modes of the different tunnel elements, illustrated for the Noordtunnel case.

Figure 15 and Figure 16 provide the axial deformation modes with the normal forces at the joints, for the combination of tunnel elements 3 and 4, and tunnel element 1 or 2, respectively. The opening of each joint for the different axial deformation modes is determined as follows. First of all, the shortening per segment is determined by temperature shrinkage[42], considering the tunnel structure goes from the summer to the winter period. Secondly, the opening of the segment joints is based on the shortening of the adjacent segments, with regard to the distance between the centers of these two segments[43]. Finally, the relaxation of the immersion joints is based on the difference between the total shortening of the segments, and the total opening of the segment joints[44]. Now the normal forces at all the joints can be determined. For the segment joints which are opened, the normal force is equal to zero. The normal forces in the immersion joints can be determined with the respective Force-displacement graph of the Gina rubber gasket, based on the resulting compression (initial compression minus relaxation)[45]. For the closed segment joints, the normal forces are determined by solving the differential equation (Equation 6), for a tunnel part with known boundary conditions[46].

[42] The temperature shrinkage of a tunnel segment is determined by $\Delta L = \alpha \cdot L_0 \cdot \Delta T\ [m]$, where the expansion coefficient of concrete is assumed to be $\alpha = 12 \cdot 10^{-6}\ K^{-1}$, L_0 is the undeformed segment length $[m]$, and ΔT is the temperature difference $[K]$ (Van Montfort, 2018).

[43] The opening of the outer opened segment joints is considered to be an independent stochastic parameter, with a uniform distribution between $\Delta u_i = 0.1 \cdot \Delta L_{seg}$ and $\Delta u_i = 1.0 \cdot \Delta L_{seg}$, in which ΔL_{seg} is the shortening of the tunnel over the distance in between the centers of the two adjacent segments. For the inner opened segment joints, the joint opening is considered as deterministic value of $\Delta u_i = \Delta L_{seg}$.

[44] The relaxation of the Gina gasket in the immersion joints can be determined from the difference between the total shortening of the segments, and the total opening of the segment joints, within the relevant area of the immersion joint (half of all the adjacent 'parts of the tunnel', with the three parts indicated in Figure 14).

[45] Including stress relaxation of the Gina rubber gasket at which the stress decreases logarithmically over time.

[46] So, the differential equation is solved for a field of multiple segments with known normal forces at both ends (zero for opened segment joints, and a calculated force for the immersion joints with the Force-displacement graph of the Gina rubber gasket). When solving Equation 6, k_x is averaged over the field and $q_x = 0$.

For deformation mode 6 (tunnel elements 3 and 4) and mode 4 (tunnel element 1 or 2), it is less obvious to determine the normal forces at the closed segment joints. Therefore, the normal force is assumed to be equal to the maximum soil friction force, which can be exerted over the perimeter of a single segment.

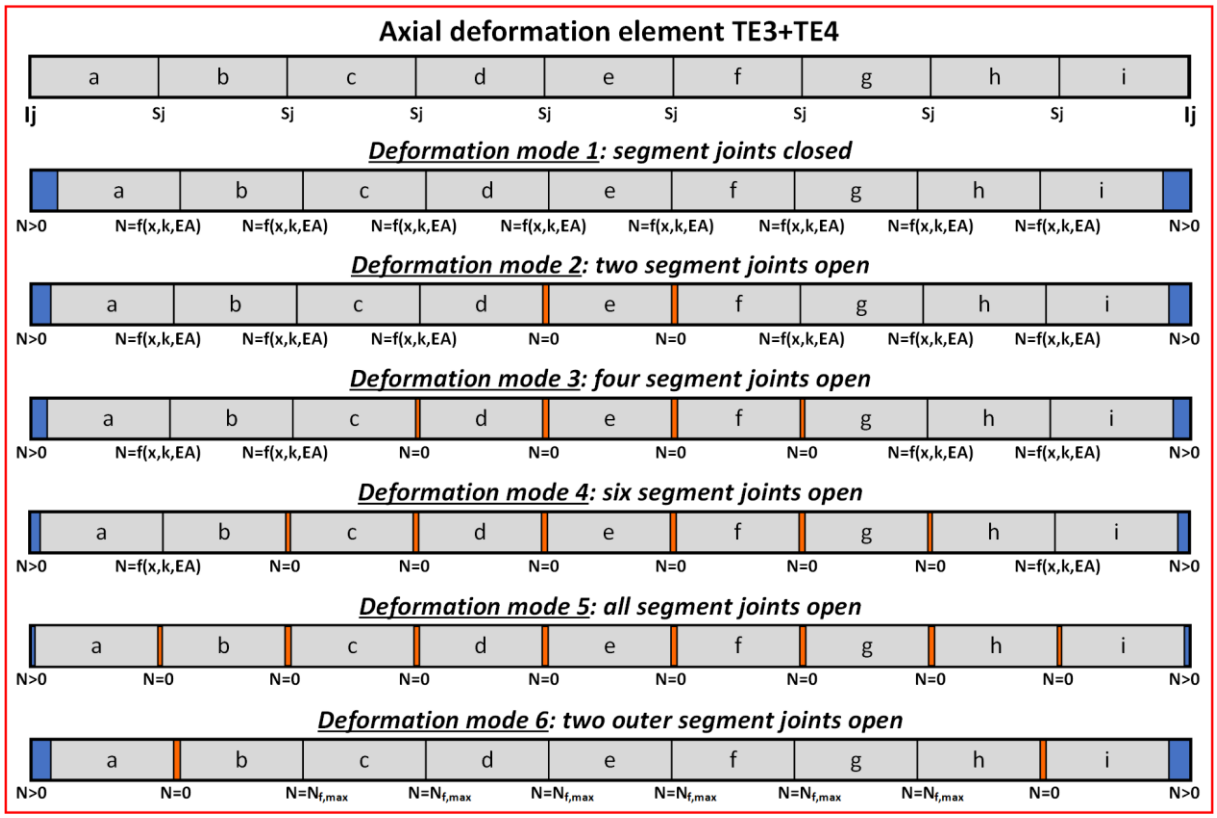

Figure 15: Axial deformation modes of elements 3 and 4 of the Noordtunnel combined (considering the closure joint to behave as a segment joint).

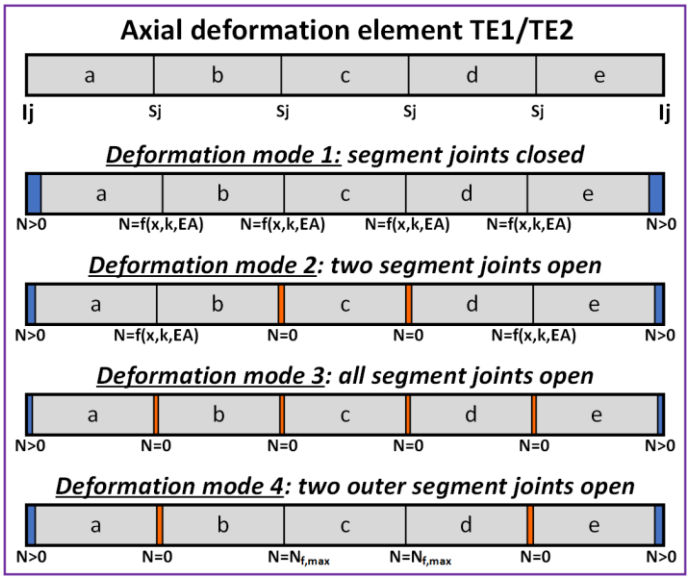

Figure 16: Axial deformation modes of element 1 or 2 of the Noordtunnel.

Noteworthy, with the approach used in this subsection, the axial displacements and normal forces at all the joints of the tunnel structure can be determined. These two parameters are of importance to solve the structural model of the tunnel (displayed in subsection 3.2). The axial deformation over the segments is thus not calculated separately by solving the differential equation.

3.4. Failure Mechanisms

In this research, two failure mechanisms for the segment joint are considered: exceedance of the shear force and rotation capacity. Shear force failure of the segment joint is most likely the structural failure mechanism in case of ongoing settlements, as was described in subsection 2.3. Furthermore, when the tunnel structure is examined from a geotechnical standpoint, the structure has a limit in terms of maximum deformation that it is able to withstand. Therefore, failure due to exceeding the rotational capacity of the joint is acknowledged as the second failure mechanism. The contemplation of the two failure mechanisms induces the opportunity to analyse the influence of the respective mechanisms more clearly. The reason why more mechanisms have not been taken into account, is to ensure the workability and manageability of the entire research method.

The shear force failure Is considered for the collar structure of the segment joint, as illustrated in Figure 9 and Figure 10. It should be noted that the loads will only concentrate in the top or base collar, as the tunnel cross section will slightly deform (Schols et al., 2013a). In addition, the stiffness of the collar varies across the tunnel width, causing the collar to attract more load near the walls (Schols et al., 2013b). Thus, for the shear force capacity, a single collar should be taken into account over an effective width of the tunnel, which is schematically shown in Figure 17. The research method considers a maximum shear force capacity (in kN) for the failure mechanism of the shear force.

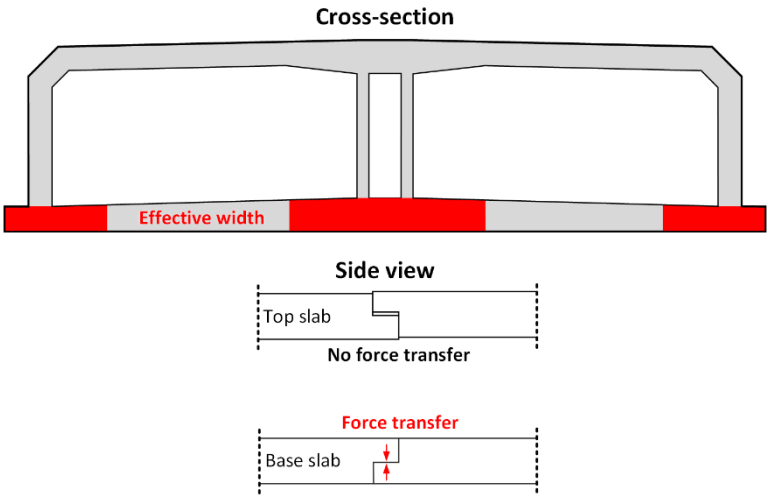

Figure 17: Effective width of the tunnel cross section (above), and load concentration in a single collar from the side (below).

For the rotational failure, a limit is taken into account for the maximum rotation that a structure can withstand. Figure 18 schematically demonstrates this with α_{max} for three rigid structural elements subjected to uneven settlements, according to Eurocode 7[47]. In the research method, a maximum rotation capacity (in radians) will be considered for the failure mechanisms of rotation.

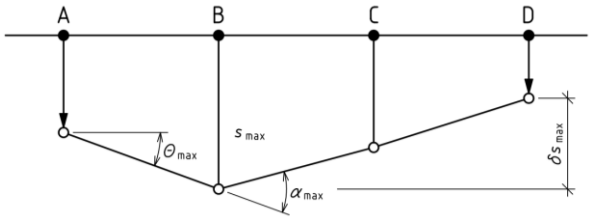

Figure 18: Schematic presentation of the rotational limit with α_{max}, for a geotechnical structure subjected to ongoing settlements (NEN-EN 1997-1+C1+A1:2016, p.177-178).

[47] *NEN-EN 1997-1+C1+A1:2016, Eurocode 7: Geotechnical design - Part 1: General rules* (p.177-178).

3.5. Monte Carlo Approach

A Monte Carlo approach is used, to determine the reliability and availability of the immersed tunnel structure for ongoing settlements. With this approach, an N number of simulations is performed, in which the parameters have a random value each simulation, based on their stochastic distribution. The failure probability can consequently be determined by dividing the number of simulations that lead to failure over the total amount of simulations ($P_f = n_f/N$). The input, method and output of the Monte Carlo approach are successively discussed below. At the end of this subsection, the complete overview of the approach is visually presented in Figure 19. The Monte Carlo approach is executed by using the Python programming language.

3.5.1. Input

Table 1 presents the input parameters for the Monte Carlo approach, that have a deterministic or stochastic distribution, which are expected to contain uncertainty to a lesser or greater extent, respectively. The deterministic parameters are similar in all the simulations[48]. However, for the stochastic parameters, the respective value of a parameter is randomly chosen per simulation, based on its probabilistic distribution. During the simulations, the quantitative values are chosen independently per joint for the stochastic parameters of the segment joint opening, settlements at the joints, vertical load, foundation stiffness, and soil friction stiffness. However, for the stochastic parameters of the shear force and rotational capacity, all the joints have equivalent values in a single simulation. Hence, there is dependency between the joints for the parameters of shear force and rotational capacity, in contrast to the independency of the other stochastic parameters.

Table 1: Overview input parameters of the Monte Carlo approach.

Parameter	Notation	Unit	Distribution
Tunnel geometry	$-$	m	Deterministic
Axial stiffness	EA	kN	Deterministic
Bending stiffness	EI	kNm^2	Deterministic
Stiffness immersion joint (axial)	K_i	kN/m	Deterministic
Stiffness immersion joint (rotational)	R_i	kNm/rad	Deterministic
Stiffness segment joint (rotational)	r_i	kNm/rad	Deterministic
Initial compression Gina gasket	c_{init}	m	Deterministic
Normal force at immersion	F_{TEi}	kN	Deterministic
Moment at immersion	M_{TEi}	kNm	Deterministic
Time	t	$years$	Deterministic
Temperature difference	ΔT	K	Deterministic
Probability axial deformation modes	P_{def}	$-$	Deterministic
Opening segment joints[49]	Δu_i	m	Uniform; Deterministic
Settlements at joints	v_i	m	Lognormal
Vertical load	q_z	kN/m	Normal
Stiffness tunnel foundation	k_z	kN/m^2	Normal
Stiffness soil friction	k_y	kN/m^2	Normal
Shear force capacity	V_R	kN	Normal
Rotational capacity	φ_R	rad	Normal

[48] It should be noted that the joint stiffness depends on either Gina gasket compression (including stress relaxation over time) or opening of the joint, for the immersion and segment joints, respectively.
[49] Note that the outer opened segment joints are considered to be independent stochastic parameters with a uniform distribution, while the inner opened segment joints are considered as deterministic parameters.

3.5.2. Method

The method consists of running an N number of simulations, in which the stochastic parameters have a random value per simulation based on their distribution. The number of simulations that lead to failure is counted as n_f. Based on the number of simulations (N) and the number of failures (n_f), the failure probability can be determined with: $P_f = n_f/N$. The method includes three sub-components, which are further described hereafter.

The first sub-component relates to solving the axial deformation equations (explained in subsection 3.3). For each simulation, the soil friction stiffness (k_y) and the joint opening of the segment joints (Δu_i) are generated, based on the stochastic distribution. Together with the probabilities of the axial deformation modes (P_{def}), the axial deformation can be computed for every simulation. Now that the joint openings (segment joints and closure joint) and Gina gaskets' compression (immersion joints) are known, the stiffnesses of the joints can be derived. The rotational stiffnesses of the segment joints (r_i) and immersion joints (R_i) are used for the rotational springs in the bending deformation model.

The second sub-component involves solving the bending deformation equations (explained in subsection 3.2). The settlements at the joints (v_i), vertical load (q_z), tunnel foundation stiffness (k_z), shear force capacity (V_R), and rotational capacity (φ_R), are generated based on the stochastic distribution for each simulation. For each simulation, the system of differential equations is set up for the immersed tunnel structure model, which is shown in Figure 12, using all the parameters. Solving the system of differential equations gives as outcome the displacement, rotation, bending moment, and shear force functions over the tunnel structure ($v(y)$, $\varphi(y)$, $M(y)$, and $V(y)$). It should be noted that three different structural models could be used for the Monte Carlo analysis[50], as described in subsection 3.2. Appendix B presents the outcomes for *Model 1*, *Model 2* and *Model 3*, illustrated for the Noordtunnel case with the mean values of the parameters.

The third sub-component regards performing the failure criterium, distinguishing between shear force failure and rotational failure. At every simulation, for each joint it is checked whether failure occurs, for both failure mechanisms separately and combined[51]. This is the case when the resistance (V_R or φ_R) is exceeded by the respective shear force or rotation that develops at a segment joint. In addition, it is checked when at least one segment joint of the tunnel fails, which is defined as 'failure of the tunnel'.

3.5.3. Output

The output of the method consists of the calculated failure probabilities, which are estimated for both each segment joint separately and for the entire tunnel, using the failure mechanisms of shear force, rotation, and both combined. Noticeably, as was already stated in the introduction (subsection 1.3), 'failure' involves local failure of the segment joint and not global failure of the tunnel structure as a whole[52]. In addition, it is noteworthy mentioning that the 'failure probability of the tunnel', which is assumed to occur when at least one segment joint fails, is predominantly determined in order to calculate the tunnel its (temporary) unavailability in the end.

[50] *Model 1*, *Model 2* and *Model 3* are considered for the structural model (see subsection 3.2).
[51] Failure for the failure mechanisms combined is defined as failure by one or both mechanisms.
[52] As the segments are still supported by the sand foundation, it is considered that global failure will not occur, as a consequence of settlements. However, it cannot be ruled out either that a situation could arise for which the tunnel reaches its functional lifespan at some point (e.g. massive leakages and unsafe bumps in the road).

The structural reliability is calculated based on the estimated failure probability, by taking the difference between 1.0 and the failure probability: $R = 1 - P_f$. For all the segment joints and the entire tunnel, the reliability has been computed for the failure mechanisms of shear force, rotation, and the combination.

Now, the tunnel availability can be estimated for a certain time period, considering the tunnel as a fully repairable system after the occurrence of failure of a segment joint[53]. The steady state availability (A_{ST}) can be determined for certain time periods, based on the mean time between failure ($MTBF$) and the mean down time (MDT), according to Equation 1. Here, the mean time between failure can be determined by Equation 2, where T is the time of renewal[54]. With this, it is considered that the tunnel is brought to a perfect condition again, by applying preventive maintenance. Thus, the mean time between failure is based upon the calculated structural reliability.

$$A_{ST} = \frac{MTBF}{MTBF + MDT}$$

Equation 1: Average or steady-state availability (Birolini, 2014).

$$MTBF(0,T) = \frac{\int_0^T R(t)dt}{1 - R(T)}$$

Equation 2: Mean time between failure ($MTBF$), for which T is the time of renewal (Birolini, 2014).

Figure 19 presents the complete overview of the approach that was explained in this subsection. The three components of input, method and output are clearly distinguished within the figure on the next page.

[53] In practice this could for instance be a massive (uncontrollable) leakage that arises, as a consequence of excessive settlements. In such a case, solving the leakage causes temporary unavailability.

[54] Note that if T approximates infinity, the mean time between failure equals the mean time to failure with the following expression (Birolini, 2014): $MTBF(0,\infty) = MTTF = \int_0^\infty R(t)dt$

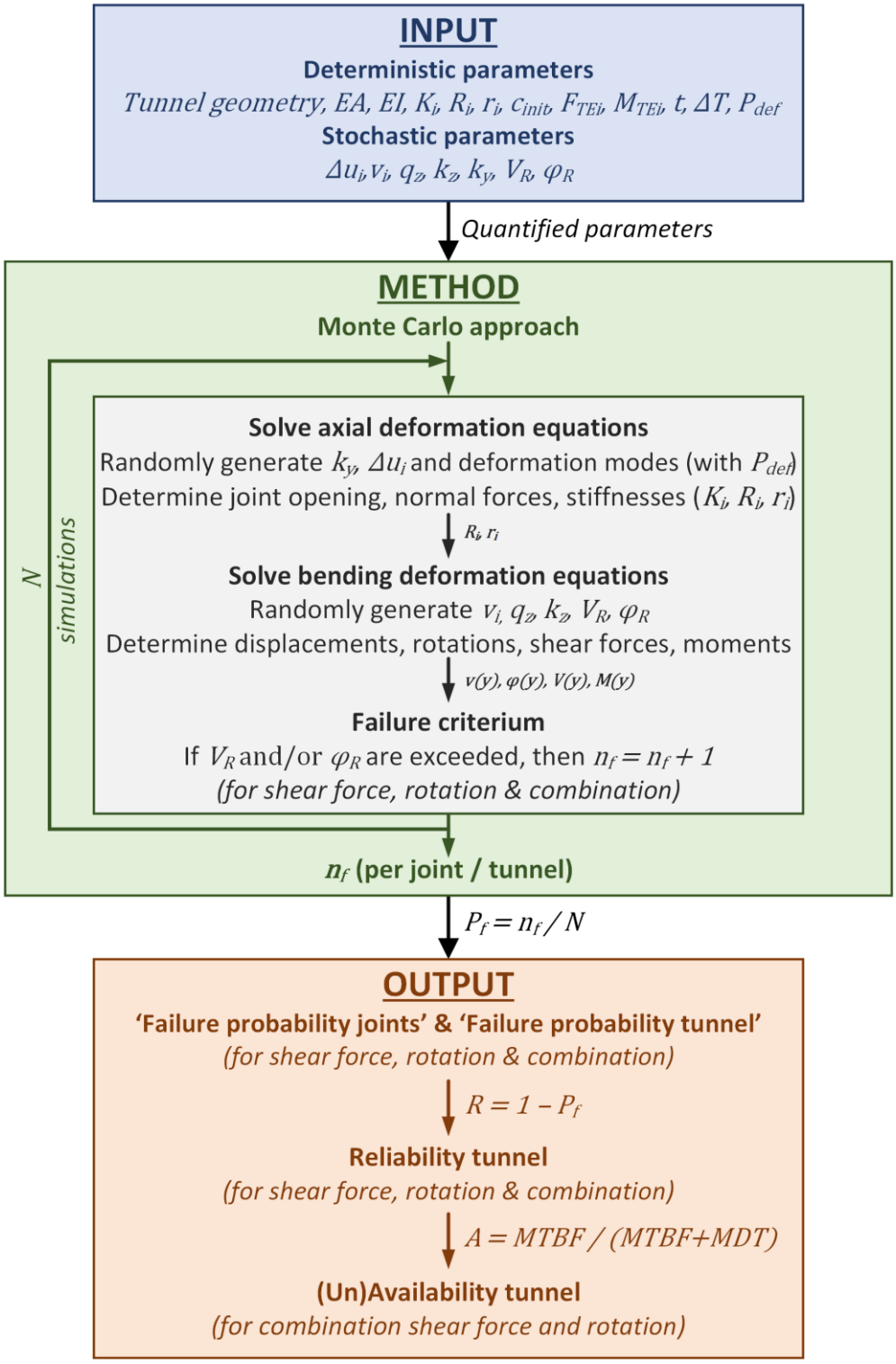

Figure 19: Overview Monte Carlo approach by which the structural reliability and (un)availability are determined for the immersed tunnel subjected to ongoing settlements.

4. The Noordtunnel Case

In this section the research methodology is applied to the Noordtunnel case. Subsection 4.1 describes the introduction of the Noordtunnel case, including the settlements and leakages the tunnel has dealt with. Subsection 4.2 explains the quantification of the input parameters for the Noordtunnel. The results of the Noordtunnel are discussed in subsection 4.3, in which the tunnel reliability (4.3.1), tunnel availability (4.3.2), and the critical segment joints (4.3.3) are presented.

4.1. Case Introduction

The Noordtunnel is part of the A15 motorway and crosses tidal river named the 'Noord'. The tunnel consists of two traffic tubes and a central tunnel channel, as displayed in Figure 20. The immersed part of the tunnel was constructed from November 1990 to January 1991, and is made up four elements (TE1 to TE4). These tunnel elements contain four or five segments, as illustrated in Figure 21. The numbering of the elements follows the order of immersion during construction of the tunnel. The immersion joints are numbered from left to right (I1 to I5), and the same holds for the segment joints (S11 to S13, S21 to S24, S31 to S34 and S41 to S44). Noticeably, the second immersion joint is actually the closure joint (C2), which is structurally different from the immersion joints.

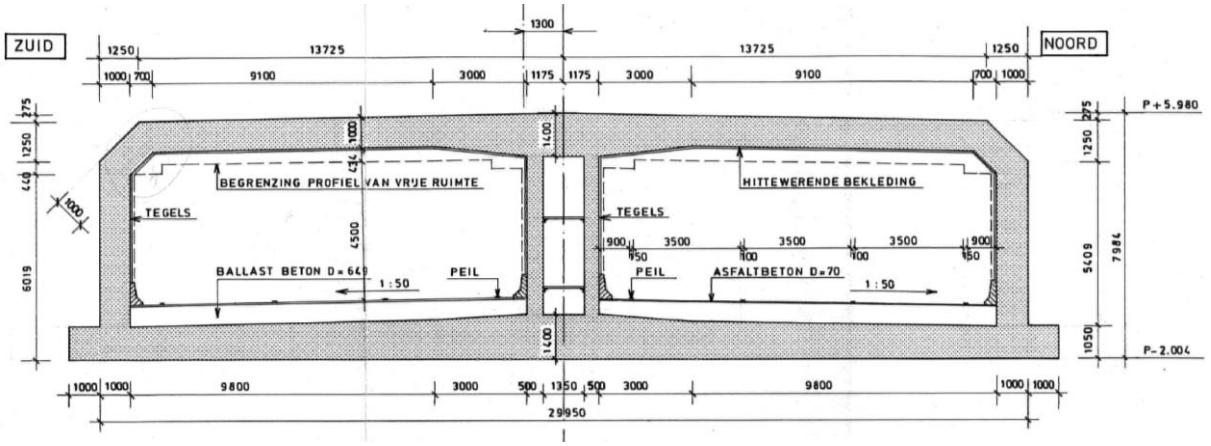

Figure 20: Cross section Noordtunnel (Sweco, 2020).

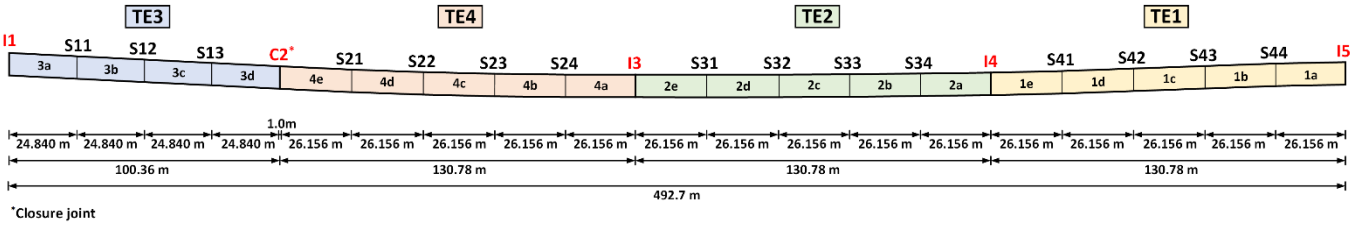

Figure 21: Longitudinal overview of the Noordtunnel, including the numbered immersion and segment joints.

Appendix C provides background information about the case of the Noordtunnel. In Figure 63 and Figure 64 of Appendix C.1, the longitudinal section and detailed cross section of the Noordtunnel are displayed, respectively. Appendix C.2 presents the initial settlement measurements, for tunnel elements 1 to 4, with Figure 65 to Figure 68.

Measurement data of the Noordtunnel shows greater ongoing settlements than were considered in the design[55]. Sweco (2020) predicted a linear increase in settlements, which could lead up to $120\ mm$, when the tunnel reaches a lifespan of 100 years. However, the combination of 2D FEM calculations in PLAXIS with the reconstruction of the settlement history, demonstrated the prediction of a logarithmic settlement increase for the Noordtunnel case (Atmakusuma, 2023). From a geotechnical point of view, a logarithmic settlement increase would be expected, as described in subsection 2.2. When the settlement development would be linear in time, the settlements should be driven by a non-geotechnical mechanism though. Thus, both the logarithmic and linear settlement increase are included in this research, as the exact future settlement development is yet unknown.

Figure 22 displays the measurements of total settlements in the Noordtunnel, retrieved from measurement data of Rijkswaterstaat (2019) and corrected by Sweco (2020). Noteworthy, there is a lot of uncertainty in the settlements, amongst others due to the low measurement frequency, limited accuracy during measuring, and unstable reference points.

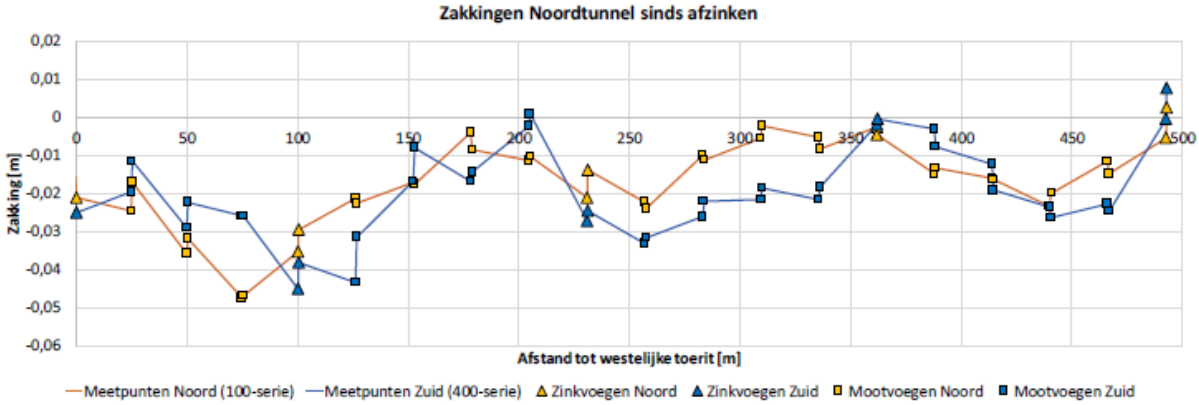

Figure 22: Retrieved and corrected settlements of the Noordtunnel (Sweco, 2020).

In addition, several leakages[56] have occurred in the segment joints of the Noordtunnel over the years. Figure 23 illustrates that several segment joints have been injected over the years, according to the 'Leeuw method' (Kloosterman, 2014).

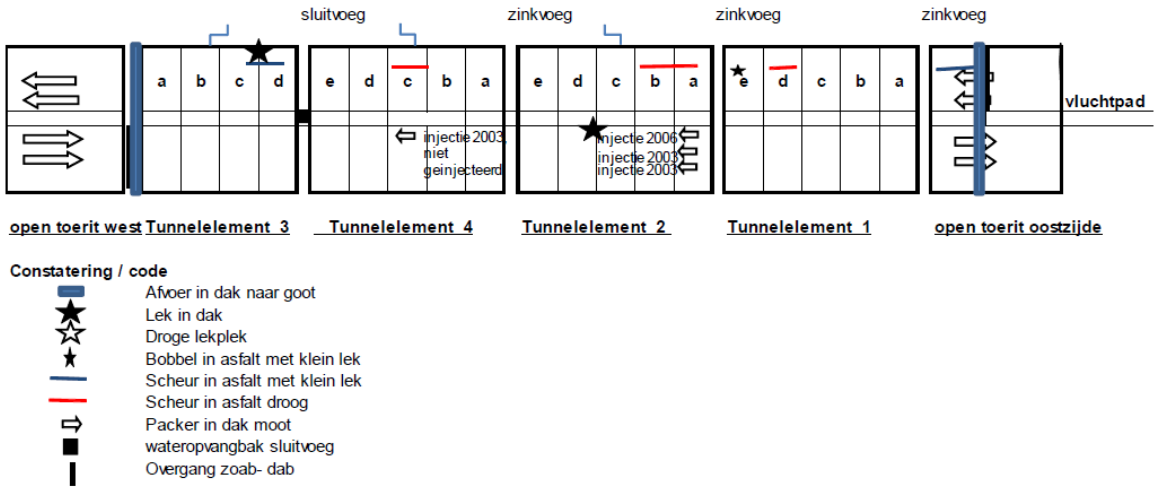

Figure 23: Overview of the past leakages and injections in the Noordtunnel (Kloosterman, 2014).

[55] It should be noted that there is a gap in the settlement data, as the deformation of the segment joints is only being measured from 2013 onwards (before only the immersion joints were measured).
[56] Note that the exact relationship between the settlement data and observed leakages is currently unclear (partly due to the poor data quality).

4.2. Quantification Input Parameters

In this subsection the input parameters are quantified for the Noordtunnel case. Consecutively, the settlements (4.2.1), immersion and segment joint stiffness (4.2.2), vertical load and foundation stiffness (4.2.3), segment joint capacity (4.2.4), and additional parameters with a total overview (4.2.5) will be discussed.

4.2.1. Settlements

The stochastic parameter of the settlements is based on the measurements that have been carried out over the years. In Figure 24 the adapted settlement trend is presented, based on the data of Sweco (2020). The crosses (x) in the figure point out the settlements at the immersion joints, and the dots (·) the settlements at the segment joints. Furthermore, the distinction between settlements of the northern tunnel side (red) and southern tunnel side (blue) has been considered, as obtained from Figure 22. However, the data displays some differences, where the measurements on both sides of the same joint deviate from each other. This is assumed to be caused by measurement errors, as these deviations could only appear after structural failure of the joint. Therefore, the data has been corrected by averaging the settlements for both sides of the same joint. This gives the dashed settlement trends, for both the settlements on the northern (red) and southern side (blue). By averaging these two trends, the mean settlement trend on the tunnel-axis is computed as well (black dashed line). Finally, the settlements at the first and last immersion joint are corrected to be zero (black solid line). The settlements at these two joints are expected to be small in reality, due to the connection with the abutments founded on piles, which should hardly undergo any settlements.

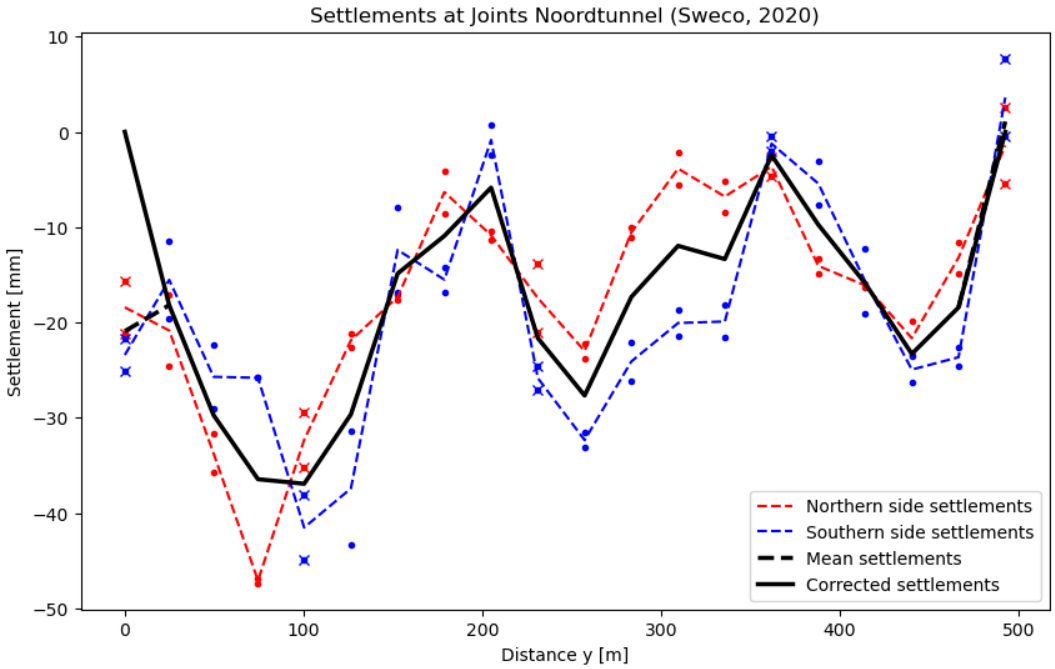

Figure 24: Determined mean settlement trend at the tunnel-axis from the data of Sweco (2020).

The settlements are projected for the years 2030, 2040 and 2050, based on the increase of past settlements over time, distinguishing two extreme projection cases (as described in subsection 4.1):

- *Case A* involves a logarithmic settlement increase, as would be expected from the geotechnical mechanisms, and was demonstrated by Atmakusuma (2023).
- *Case B* entails a linearly increasing settlement development, with a maximum annual increase of 1.2 mm at the most normative location (Sweco, 2020).

In *Case A*, the settlements are assumed to increase logarithmically from the immersion onwards[57]. While in *Case B*, the settlements increase proportionally[58], according to the settlement curve of 2020 (with maximum $12\ mm$ per 10 years). Figure 25 and Figure 26 display the projection of the settlements over the years for both cases.

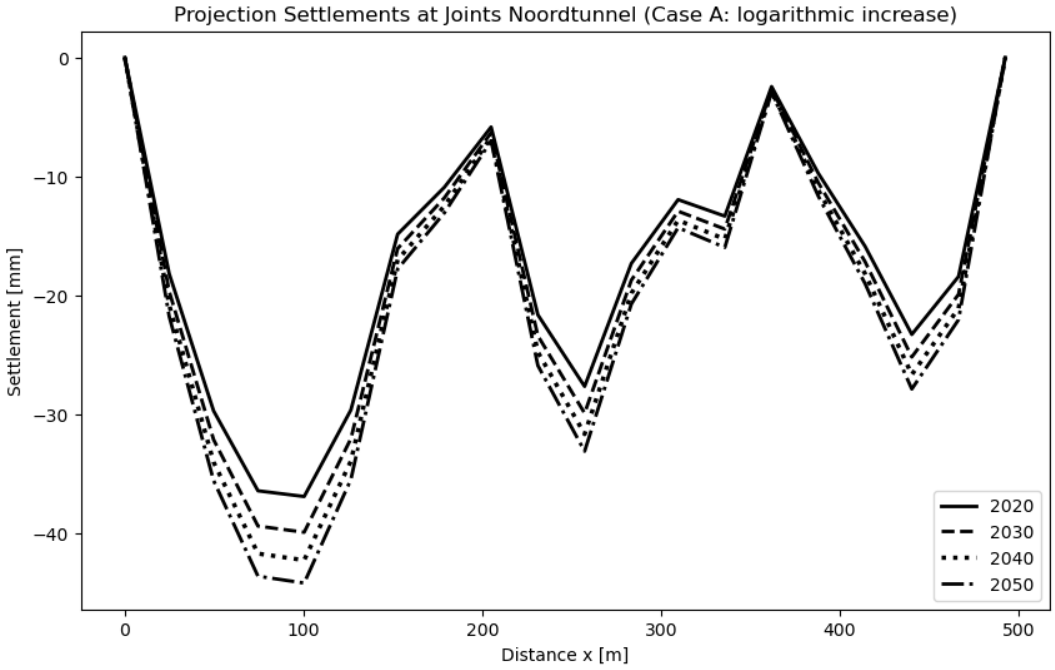

Figure 25: Projection of the settlements over the years, considering the logarithmic settlement increase of Case A.

Figure 26: Projection of the settlements over the years, considering the linear settlement increase of Case B.

[57] Practically this means that the settlement curve of 2020 is multiplied with the factors $\frac{\ln(40)}{\ln(30)}$, $\frac{\ln(50)}{\ln(30)}$ and $\frac{\ln(60)}{\ln(30)}$ for the years 2030, 2040 and 2050, respectively. Here, 2020 is roughly assumed to be 30 years after immersion. The settlement increase until 2090 is $12.7\ mm$ (at C2), compared to $15.1\ mm$ calculated by Atmakusuma (2023).

[58] In the analysis it is assumed that the settlement increases $1.2\ mm$ annually at the joint where the settlement is maximum in 2020. The other settlements are determined proportionally with respect to this value.

The settlements are considered as independent parameters at each joint, with a lognormal distribution. This distribution was chosen because the uncertainty of the maximum settlements is greater than the minimum settlements. A lognormal distribution is assumed[59] for the settlement factor f_v, with $\mu = 0$ and $\sigma = 0.25$, as shown in Figure 27. Multiplying this factor with the settlement curves, gives the lognormal distributed settlement trend for each year. Figure 28 demonstrates the lognormal distribution of the settlements for the year 2020, in which the corrected settlement curve of Figure 24 is used as the median value. The settlement distributions for the years 2030, 2040 and 2050 are derived from the two settlement projection cases, which are presented in Figure 25 and Figure 26. In Appendix D.1, the settlement distributions of these years are displayed in Figure 69 to Figure 71, for the logarithmic settlement increase of *Case A*. Figure 72 to Figure 74 illustrate the settlement distributions with the linear settlement increase of *Case B*. For both cases, the projection curves of Figure 25 and Figure 26 are used as the median values of the settlement distributions. Note that, the settlements are an input for all the joints in structural *Model 1*, while being an input for the immersion joints only in *Model 2*, and no input at all for *Model 3*, as described in paragraph 3.2.

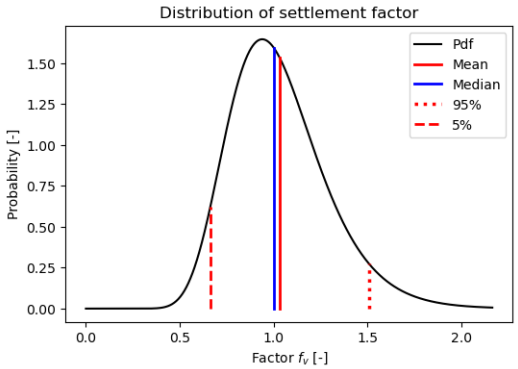

Figure 27: Lognormal distribution of the factor that is multiplied with the settlements at the joints.

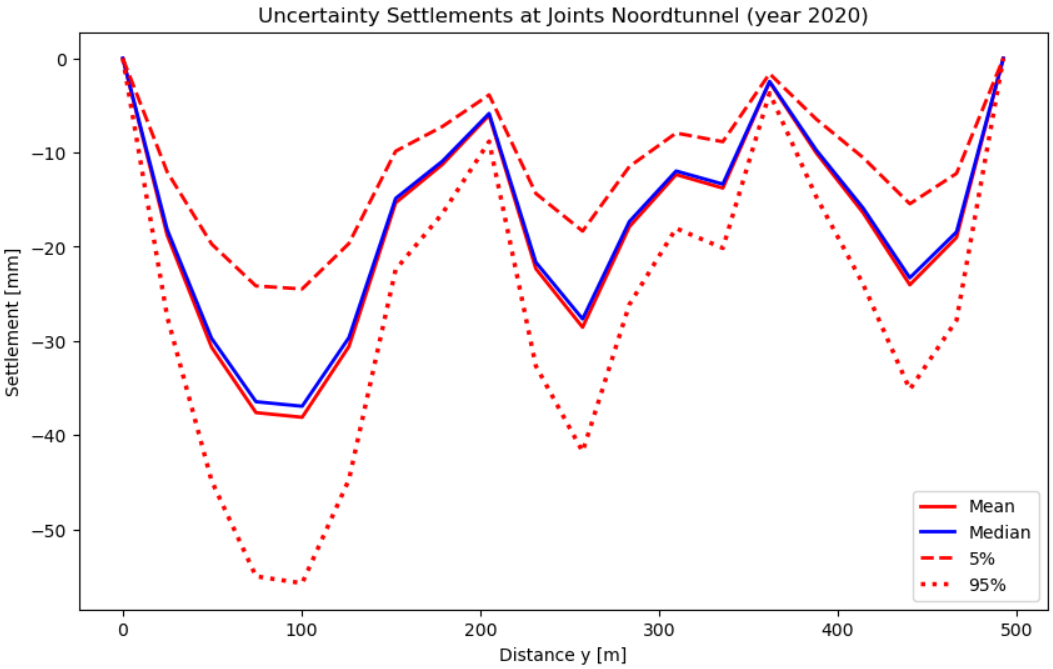

Figure 28: Lognormal distributed settlements at the joints in the year 2020, where the median follows from Figure 24.

[59] These values were chosen so that the 95% upper percentile generates a settlement factor $f_v = 1.5$. This value is based on the fact that roughly one third of the settlements has not been registered in the measurement data (Sweco, 2020). Note that this was corrected in the settlement graphs of Figure 24, Figure 25 and Figure 26.

4.2.2. Immersion and Segment Joint Stiffness

The immersion and segment joint stiffness are derived for the Noordtunnel case. For the immersion joints, the axial and rotational stiffness are based on the rubber Gina gasket characteristics. In Appendix D.2, the derivation of the Gina gasket force-displacement graph is explained, for the applied ETS-130-160 type, while assuming 50% logarithmic stress relaxation of the rubber over 100 years (COB, 2022; Saveur & Grantz, 1997). The resulting force-displacement graph is displayed in Figure 77, and the initial stiffness of the rubber gasket (k_0) is shown in Figure 78. In Equation 3 and Equation 4, the relations of the axial and rotational stiffness are demonstrated, based on the initial stiffness and Gina gasket dimensions[60]. Figure 29 and Figure 30 present the resulting axial and rotational stiffness.

$$k_u = 2 \cdot k_0 \cdot (W_{gasket} + H_{gasket})$$

Equation 3: Axial stiffness of the immersion joints (Van Oorsouw, 2010).

$$k_\phi = k_0 \cdot H_{gasket}^2 \cdot \left(\frac{1}{2} \cdot W_{gasket} + \frac{1}{6} \cdot H_{gasket}\right)$$

Equation 4: Rotational stiffness of the immersion joints (adjusted formula[61] of Van Oorsouw (2010)).

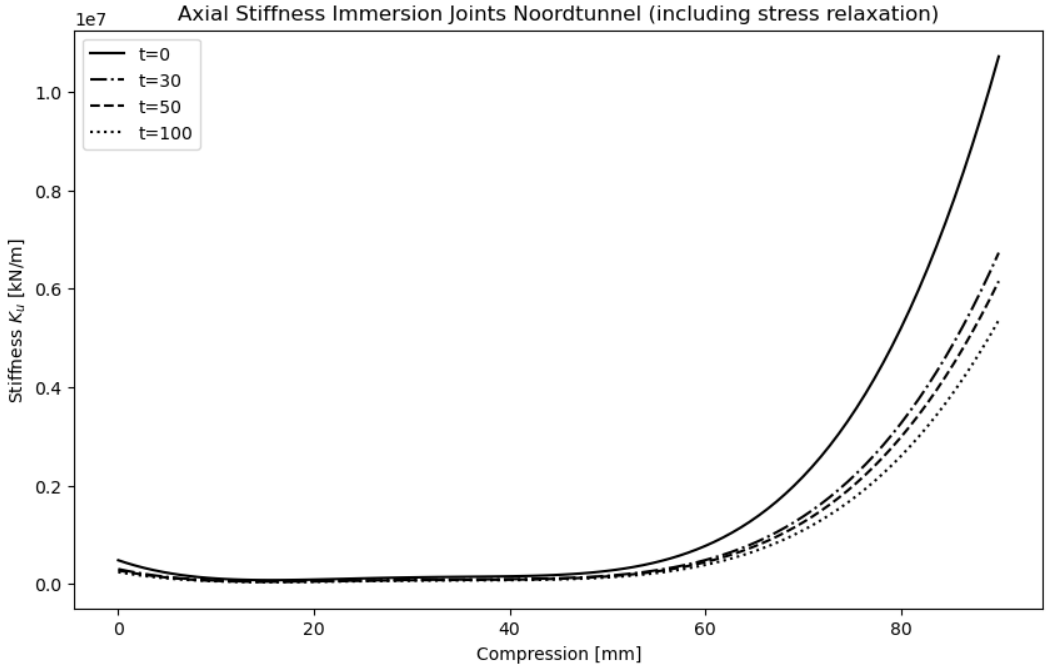

Figure 29: Axial stiffness of the immersion joints of the Noordtunnel, including stress relaxation of the rubber.

[60] For the dimensions of the Gina gasket, the tunnel is assumed to be a rectangular box. The gasket width and height are assumed to be $W_{gasket} = 28.95\ m$ and $H_{gasket} = 6.72\ m$.

[61] The derivation follows from a linear elastic cross section of the rubber gasket, with bending moments due to the resulting forces F_1 and F_2 in the horizontal and vertical rubber gasket parts, respectively:

$$k_\phi = \frac{M}{\phi} = \frac{F_1 \cdot H_{gas} + F_2 \cdot \frac{2}{3} H_{gas}}{\phi} = \frac{\left(\frac{1}{2} k_0 \cdot \phi \cdot W_{gas} \cdot H_{gas}\right) \cdot H_{gas} + \left(\frac{1}{4} k_0 \cdot \phi \cdot H_{gas}^2\right) \cdot \frac{2}{3} H_{gas}}{\phi} = k_0 \cdot H_{gasket}^2 \cdot \left(\frac{1}{2} \cdot W_{gasket} + \frac{1}{6} \cdot H_{gasket}\right)$$

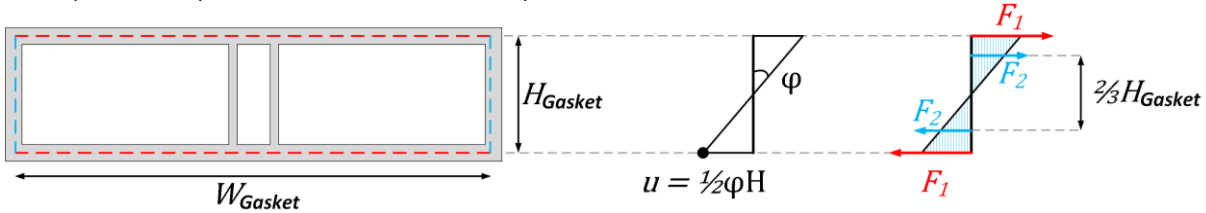

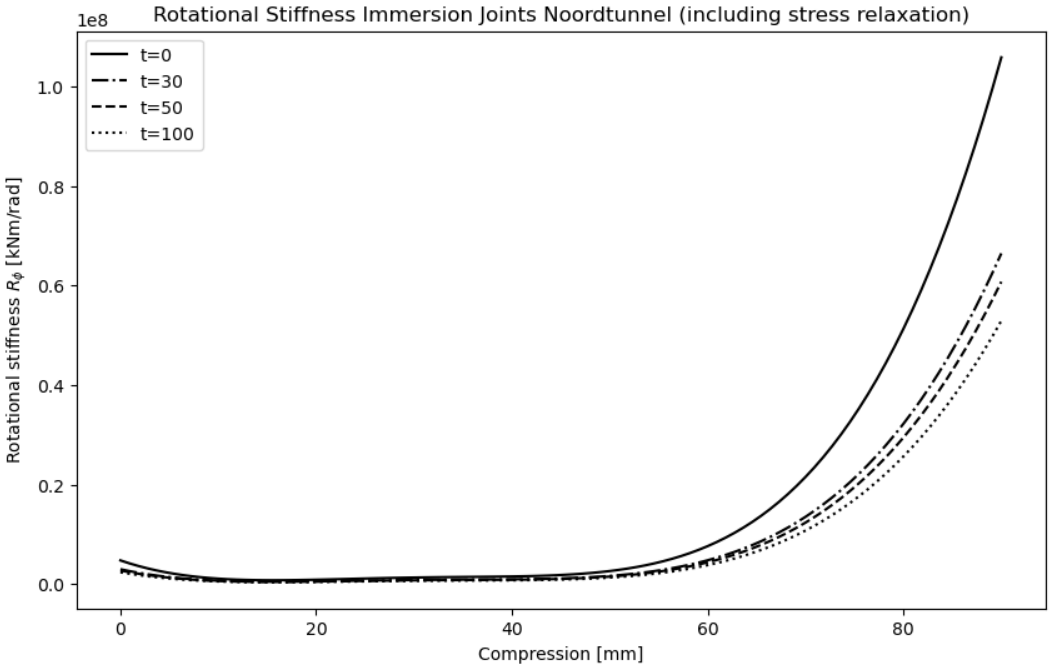

Figure 30: Rotational stiffness of the immersion joints of the Noordtunnel, including stress relaxation of the rubber.

The rotational stiffness of the segment joint is dependent on the joint opening. This stiffness varies between zero and the value of the tunnel cross-sectional stiffness, for the joint being fully opened and closed, respectively (COB, 2022). The maximum rotational stiffness is derived from the bending stiffness with a rule-of-thumb[62], assuming the segment joint to be as stiff as the tunnel cross section. This results in a maximum rotational stiffness of $r_{\phi,u0} = 2.4 \cdot 10^9\ kNm/rad$, when the segment joint is fully closed. The rotational stiffness is assumed to be zero if the joint is fully opened, for which the maximum joint opening value[63] is considered to be $u_{max} = 50\ mm$. Between these two extreme values, a logarithmic relation is assumed, in which the stiffness decreases more rapidly at the initial joint opening. Figure 31 presents the stiffness of the segment joints of the Noordtunnel, as a function of the joint opening. In the figure, a linear relation and square root relation are used as a reference.

The maximum rotational stiffness is close to the calculated rotational stiffness by Van Oorsouw (2010), with $r_\phi = 1.6 \cdot 10^9\ kNm/rad$ for a flat segment joint. Furthermore, the maximum stiffness is close to the calculated stiffness range of the Kiltunnel, with $r_\phi = 2.81 \cdot 10^9$ to $4.71 \cdot 10^9\ kNm/rad$ (Schols, 2012b). The rotational stiffness of the segment joint appears to be around 100 times stiffer than for the immersion joint ($R_\phi = 2.2 \cdot 10^7\ kNm/rad$ for $70\ mm$ gasket compression), as was stated by Schols et al. (2013b). It should be noted that, the influence of the tensile force in the W9U gasket is neglected in the rotational capacity, as the tensile strength of the rubber is small and the rubber is not very stiff (Van Oorsouw, 2010). Because of this, the segment joint will not be able to carry any tensile force in the model of the Noordtunnel. Therefore, the translational springs of the segment joints have not been considered in the structural model for the Noordtunnel case.

[62] The rotational stiffness is based on the rule-of-thumb (*'Vergeet-me-nietje'*) of a two-sided clamped beam under a distributed load (whereby $M = \frac{qL^2}{24}$ and $w = \frac{qL^4}{384EI}$). As two half segments are modelled with a rotational spring in between (clamped supports located halfway both segments), it follows that:

$$k_\phi = \frac{M}{\phi} = \frac{M}{\frac{2 \cdot w}{0.5 \cdot L}} = \frac{\frac{qL^2}{24}}{\frac{qL^3}{96EI}} = \frac{4EI}{L} \text{ with } L = L_{segment}$$

[63] The total width of the collar is about 250 mm, but the rotational stiffness is estimated to be close to zero when the joint opening reaches 50 mm, which is 20% of the collar width.

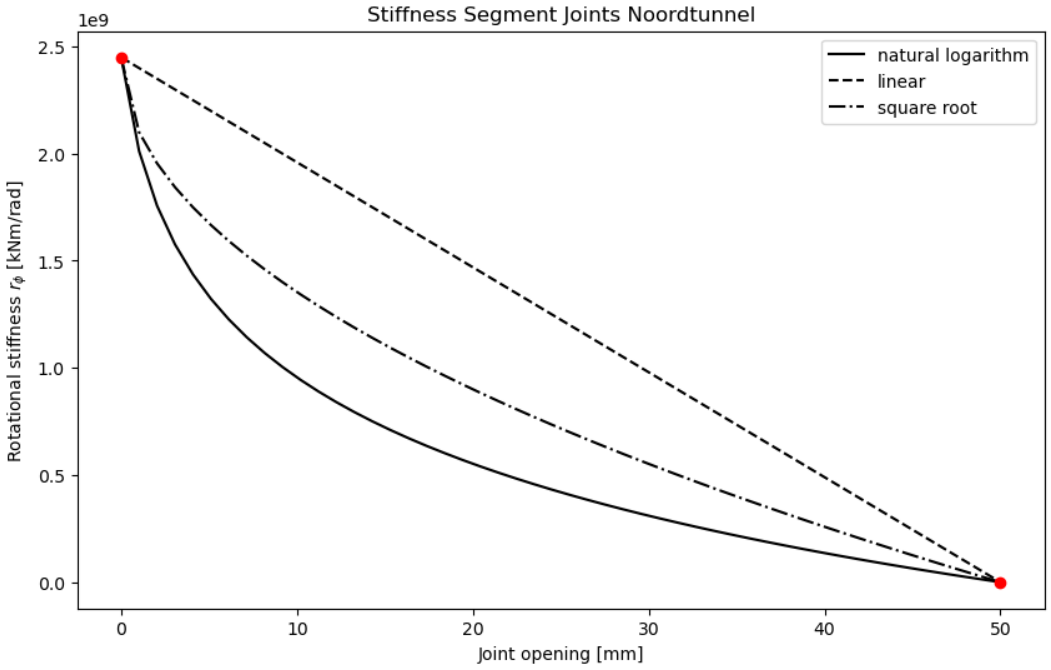

Figure 31: Rotational stiffness of the segment joints of the Noordtunnel (for various mathematical relations).

4.2.3. Vertical Load and Foundation Stiffness

The vertical load and foundation stiffness are substantiated for the Noordtunnel case. Both the resulting tunnel weight and soil cover weight are accounted for the total vertical load on the tunnel. Traffic loads are not considered in this research, since they are not permanent. It should be noted that the loads are determined at the level of the tunnel foundation. Thereby, only the current present loads are included, which means that erosion or sedimentation of the soil cover over the years is not taken into account.

According to TEC (1989), the loads of the tunnel weight[64], soil weight[65], and upward water pressure[66] are 2650.5, 453.6, and 2370 kN/m over the tunnel length, respectively. This includes the assumption of 1 m soil cover on top of the tunnel roof, which is reasonable for the current situation above the middle two tunnel elements (TE2 & TE4), since the cover layer has been restored to this level during maintenance work in March 2022. On the edges of the waterway, the present soil cover on top of the tunnel roof on the outer two tunnel elements (TE1 & TE3) exceeds 2 m (Deltares, 2023). It is assumed that TE1e, TE2 and TE4 have 1 m of soil cover, while TE1abcd and TE3 have 2 m of soil cover, where the joints between these two levels contain an average of 1.5 m. A normal distribution for the soil load is assumed, with a coefficient of variation $CV = 0.1$, as there is some uncertainty[67] in the exact soil cover thickness. Note that the resulting load from the tunnel weight is considered to be a deterministic parameter. By adding up the loads from tunnel weight and soil weight, the total load is obtained. Figure 32 shows the normal distributed vertical load over the length of the Noordtunnel.

[64] The load of the tunnel weight involves the weight of the reinforced concrete, ballast concrete, asphalt and miscellaneous (such as the barriers, fire protection, tiles). The volumetric weight of concrete is 24 kN/m^3 (for both reinforced and ballast concrete), while for asphalt the volumetric weight is 22 kN/m^3 (TEC, 1989).
[65] The load by the soil weight contains both the soil cover on top of the tunnel, and the soil cover on the 'ears' of the tunnel. The resulting soil weight (under water) is considered to be 10 kN/m^3 (TEC, 1989).
[66] The total upward water pressure of the tunnel cross section is determined by multiplying the area of the enclosed tunnel cross section (237 m^2) with volumetric weight of water (10 kN/m^3), according to TEC (1989).
[67] As a consequence of both limited monitoring data quality and developments of erosion/sedimentation.

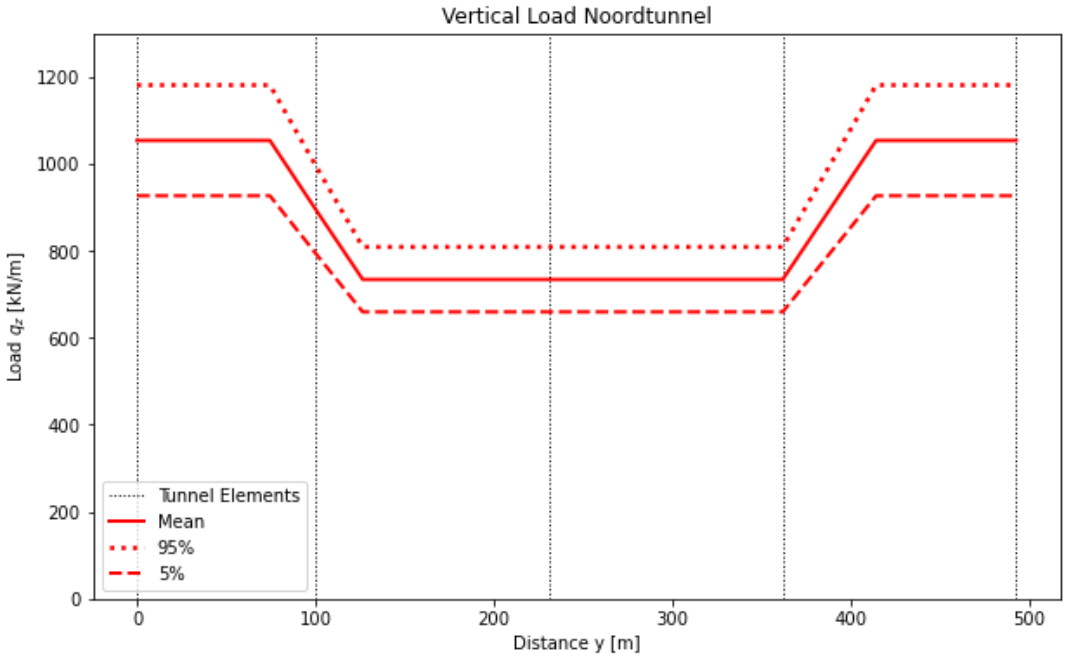

Figure 32: Normally distributed vertical load on the Noordtunnel (at foundation level).

The foundation stiffness is determined based on the initial settlement measurement data for the tunnel elements just after immersion. Appendix C.2 presents the initial settlement diagrams for each of the four tunnel elements[68], over the period of nine to ten months after immersion (TEC, 1992). For each tunnel element, the difference in settlement (Δz) is considered for a period of approximately 91 to 93 days, where the soil cover was already fully completed, and assumed to be constant. The load[69] of the soil cover weight is established for $0.5m$ of soil cover, which was the installed level after immersion (TEC, 1989). The permanent load[70] of the tunnel is assumed to be equal to the reinforced concrete and ballast concrete weight, although the ballast concrete still was partially under construction during the considered time period. Hence, the total resulting load on the tunnel foundation over the initial settlement period amounts to approximately $435\ kN/m$. The foundation stiffness is estimated by dividing this total resulting load on the tunnel foundation, with the settlements increase at the immersion joints[71]. Noteworthy, the settlement increase is determined about four months after immersion, which still causes the geotechnical mechanism of consolidation to occur. Thus, the foundation stiffness is derived at a slightly increasing load and consolidation occurring, while in practice the tunnel will experience a constant load and is subjected to the geotechnical mechanism of creep.

Figure 33 shows the foundation stiffness of the Noordtunnel, with the dashed lines for the four tunnel elements. Here, it is assumed that the foundation stiffness is linear over each tunnel element, between the two data points of the immersion joints. The fitted stiffness curve of the Noordtunnel is obtained (displayed with a solid line), by averaging the differences in stiffness at the interface of the elements, hence assuming a continuous foundation stiffness over the tunnel length. As a reference, for the Limfjord tunnel the foundation stiffness was considered to be about $2\ MN/m^2$, which is a factor of 10 to 20 times smaller (Atkins et al., 2019). In contrast, during the design phase of the

[68] Note that this only contains the settlement data at the immersion joints (primary and secondary end).
[69] The resulting load amounts $293.9\ kN/m$ for $0.5m$ of soil cover (TEC, 1989). It should be noted that this load is assumed to be equal over the entire tunnel by considering no sedimentation or erosion.
[70] This leads to a net permanent load of $141.1\ kN/m$, including the upward water pressure (TEC, 1989).
[71] This results in the following formula: $k_z = q_{total}/v_{initial}$

Noordtunnel a foundation stiffness of 900 MN/m^2 was taken into account, which is roughly a factor of 20 to 30 times greater (TEC, 1989). The foundation stiffness turns out to be a very uncertain parameter, which is difficult to determine precisely. Therefore, the stiffness of the tunnel foundation is assumed to be normally distributed[72], with a mean value equal to the fitted stiffness curve of Figure 33, and $CV = 0.25$, as visualised in Figure 34.

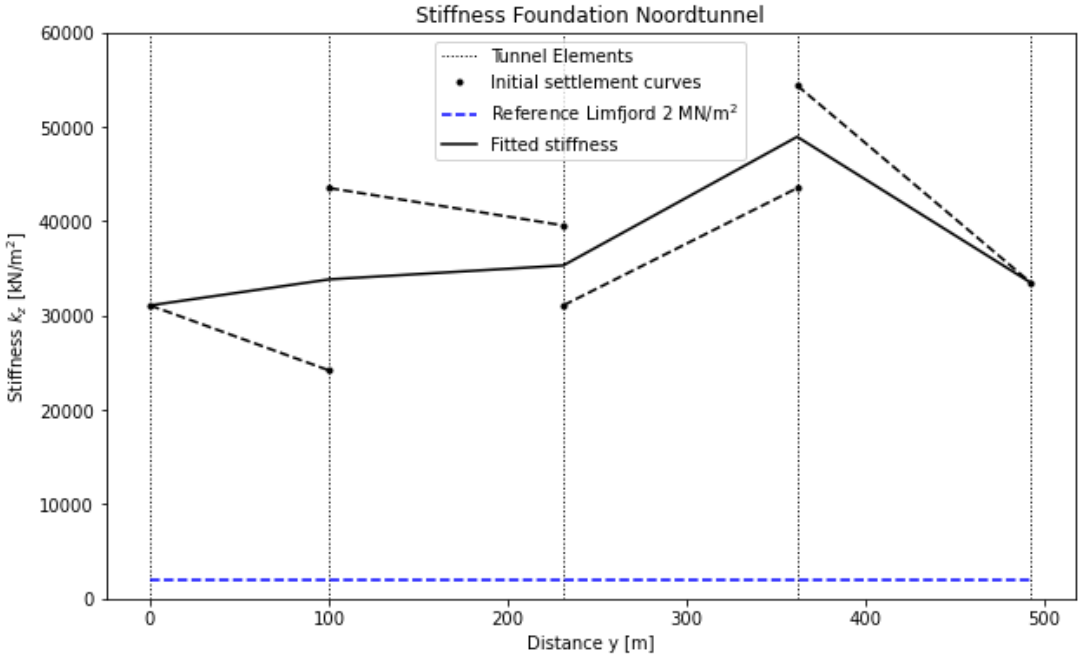

Figure 33: Derivation of the foundation stiffness of the Noordtunnel.

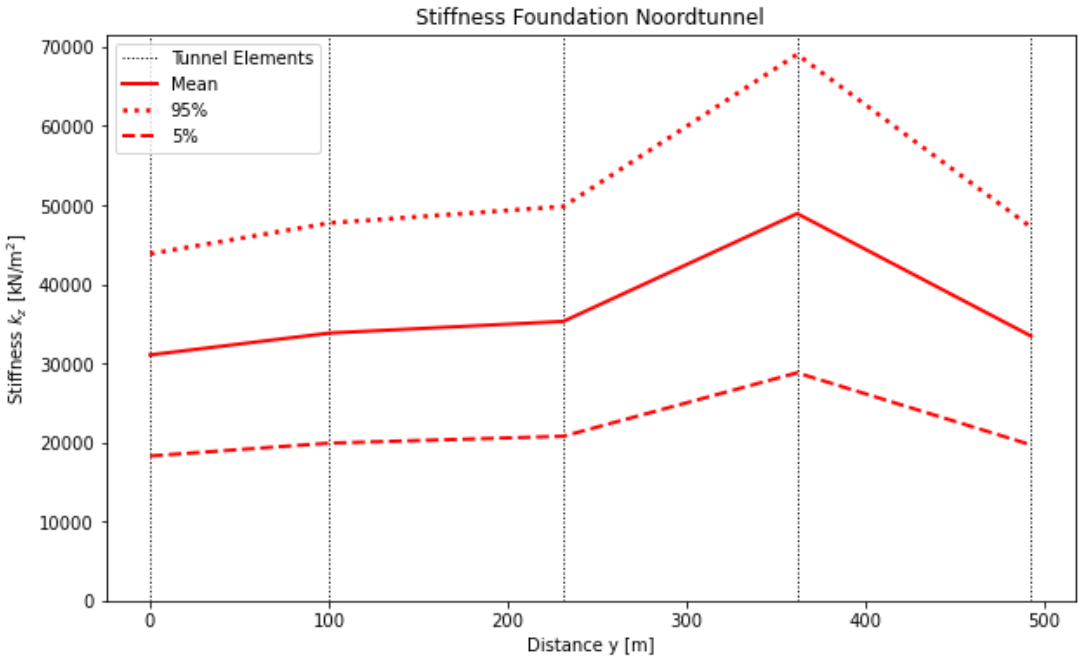

Figure 34: Normally distributed foundation stiffness of the Noordtunnel.

[72] The coefficient of variation ($CV = \mu/\sigma$) is based on the spread in obtained values for the initial settlements. It turned out that $CV = 0.24$, for the (initial) settlement array of $[13,8,10,14,14,18,11,10]$ mm (derived from Figure 65 to Figure 68 of Appendix C.2). Based on this, $CV = 0.25$ was used.

4.2.4. Capacity Segment Joint

The capacity of the segment joint is quantified for the failure mechanisms of shear force and rotation. In subsection 3.4, the mechanisms of shear force and rotation have already been qualitatively described. The quantification of the capacities will be further substantiated below.

For the shear force mechanism, the capacity is based on the design calculations of TEC (1989). Figure 35 illustrates the schematisation underlying the calculation (TEC, 1989). The mean value of the shear force capacity of the segment joints is estimated[73] to be $578.1\ kN/m$ over the collar width for TE1e, TE2 and TE4. For TE1abcd and TE3, the mean shear force capacity of the segment joints is estimated[74] to be $369.8\ kN/m$ over the collar width, as a lighter reinforcement configuration has been applied. After multiplying by the effective width of the cross section (according to Eurocode 2[75]), the total mean shear force capacities are estimated to be $9708\ kN$ for TE1e, TE2 and TE4, and $6211\ kN$ for TE1abcd and TE3. Using the Kiltunnel as a reference, the shear force capacity was calculated to be $1.3\ MN/m$ for the top outer collar, $0.8\ MN/m$ for the top inner collar, $1.1\ MN/m$ for the base inner collar, and $1.2\ MN/m$ for the base outer collar, based on 2D FEM calculations (Schols et al., 2013b)[76]. Additionally, the effective width of the tunnel cross section was determined to be $13\ m$ for the Kiltunnel, which is about 42% of the total tunnel width (Schols et al., 2013b)[77]. The shear force capacity is considered to be a normally distributed stochastic parameter[78] with $CV = 0.25$. Figure 36 presents the normally distributed shear force capacity for the segment joints of the Noordtunnel.

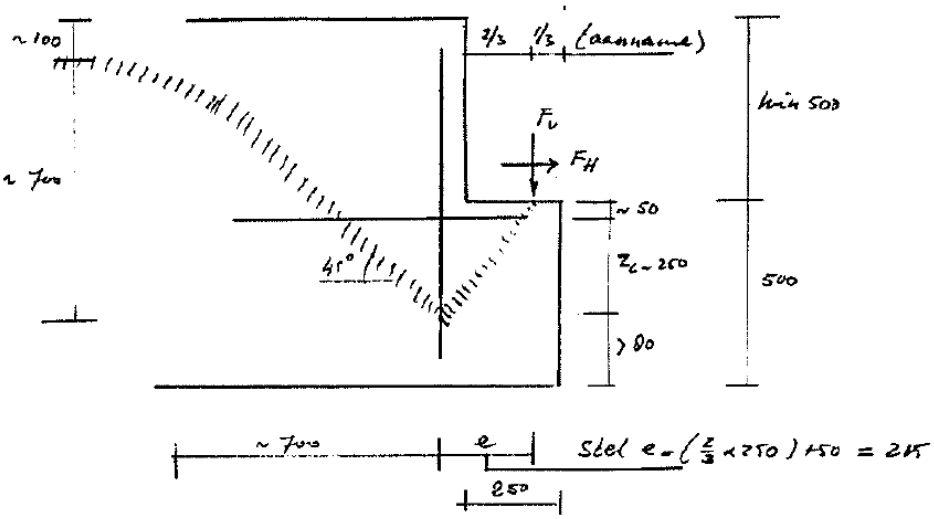

Figure 35: Schematisation of forces on the collar structure for the shear force capacity calculation (TEC, 1989).

[73] For TE1e, TE2 and TE4 there is $1300\ mm^2$/m reinforcement required over the width of the collars to bear a shear force of $281.4\ kN/m$, at which TEC (1989) applied a safety factor of 1.7. Note that this concerns the horizontal amount of reinforcement, since this seems to be normative for the shear force capacity (TEC, 1989). As $1571\ mm^2/m$ reinforcement is applied over the collar width, the mean value of the shear force capacity for TE1e, TE2 and TE4 is estimated to be $V_R = \frac{1.7}{1.0} \cdot \frac{1571}{1300} \cdot 281.4 = 578.1\ kN/m$ (TEC, 1989).

[74] For TE1abcd and TE3, there is $1005\ mm^2/m$ reinforcement applied over the collar width, as a result of which the mean shear force capacity is estimated to be $V_R = \frac{1005}{1571} \cdot 578.1 = 369.8\ kN/m$ (TEC, 1989).

[75] *NEN-EN 1992-1-1+C2:2011, Eurocode 2: Design of concrete structures - Part 1-1: General rules and rules for buildings* (p.61-62). The effective width is determined to be $16.8\ m$ for the Noordtunnel according to EC 2 (twice $4.11\ m$ for the outer wall sections, and $8.57\ m$ for the inner walls), which is 56% of the total width.

[76] The Finite Element Method software ATENA was used by Schols et al. (2013b).

[77] It should be noted that, in contrast to the cross section of the Noordtunnel (see Figure 20), the Kiltunnel has only one middle wall (no central tunnel channel).

[78] Considering uncertainty of execution performance during construction, degradation, and force redistribution.

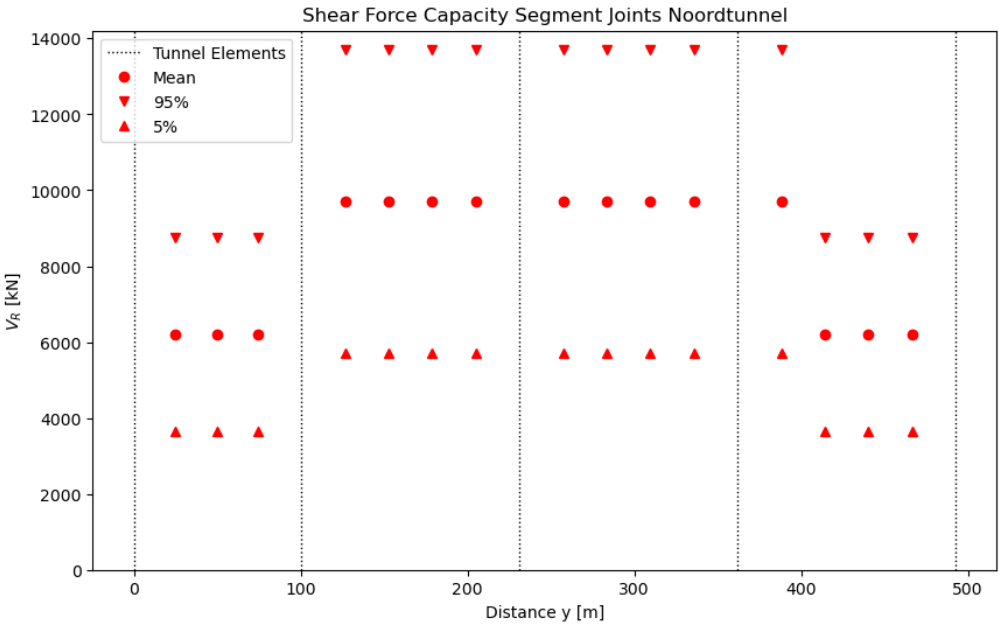

Figure 36: Normally distributed shear force capacity for the segment joints of the Noordtunnel.

For the rotational mechanism, the capacity is based on Eurocode 7 for geotechnical design of structures. According to the Eurocode[79], the maximum allowed differential rotation in a segment joint is equal to 1/500 and 1/150, for the Serviceability Limit State (SLS) and Ultimate Limit State (ULS), respectively. The mean rotational capacity for the segment joints of the Noordtunnel is assumed to be $2 \cdot 10^{-3}\ rad$, as the tunnel unavailability could be affected by (non-destructive) leakages, which is SLS related. This is in accordance with a rotation of $2.1 \cdot 10^{-3}$ for which the collar structure of the Kiltunnel is still intact (Schols et al., 2013b), and the used permissible rotation value for the Vlaketunnel of $2.5 \cdot 10^{-3}$ (Benhaddou, 2013). Similar to the shear force capacity, the rotational capacity is considered to be a normally distributed stochastic parameter with $CV = 0.25$. Figure 37 presents the normally distributed rotational capacity for the segment joints of the Noordtunnel.

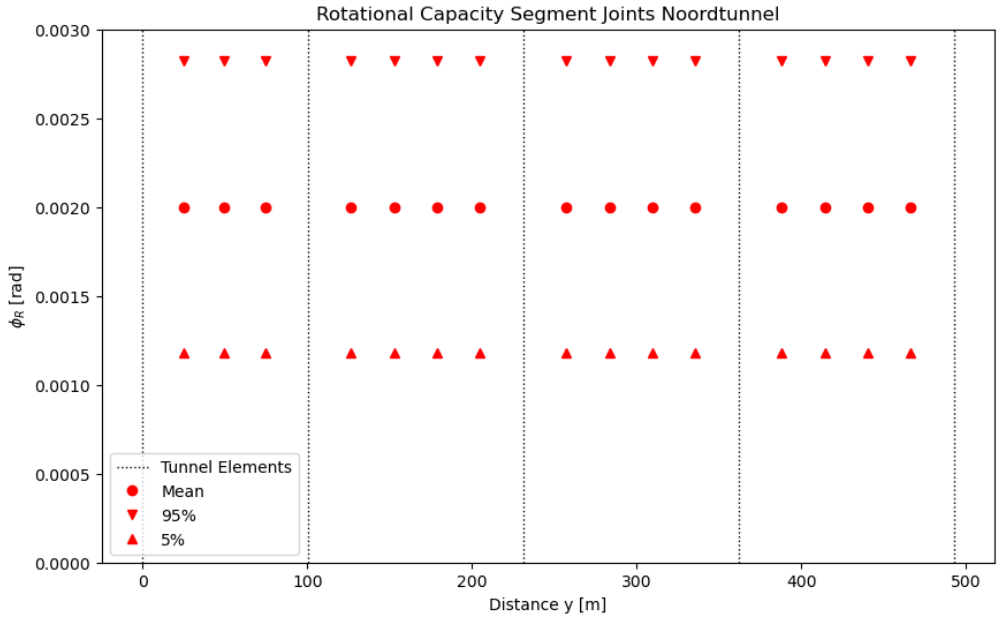

Figure 37: Normally distributed rotational capacity for the segment joints of the Noordtunnel.

[79] *NEN-EN 1997-1+C1+A1:2016, Eurocode 7: Geotechnical design - Part 1: General rules* (p.177-178).

4.2.5. Overview Parameters

The overview of all the parameters for the Noordtunnel case are presented here. Besides the parameters treated in the previous paragraphs 4.2.1 to 4.2.4, there are several additional parameters to consider, of which most are described in Appendix D. First of all, the years 2020, 2030, 2040 and 2050 are included for the time period (as seen in Figure 25 and Figure 26), as the renovation scope is defined to be 30 years. Secondly, an annual maximum temperature range of $\Delta T = 15\ K$ is taken into account, based on Saveur & Grantz (1997)[80]. It should be noted that temperature gradients over the tunnel are not considered. Moreover, the opening of the segment joints is based on the temperature shrinkage, which is extensively explained in subsection 3.3 (including the formula of footnote 42). Additionally, the axial and bending stiffness are quantified in Appendix D.3. Next, for the immersion joints just after immersion, the normal forces, bending moments, and the compression of the Gina gaskets are described in Appendix D.4. Furthermore, in Appendix D.5 the stiffness of the soil friction around the tunnel periphery has been computed. Finally, the probabilities of the axial deformation modes are specified in Appendix D.6. An overview of all the input parameters for the Noordtunnel case is presented in Table 2.

Table 2: Overview input parameters for the Noordtunnel case.

Parameter	Notation	Value	Distribution
Tunnel geometry	–	Figure 21	Deterministic
Axial stiffness	EA	$1.663 \cdot 10^9\ kN$	Deterministic
Bending stiffness	EI	$1.601 \cdot 10^{10}\ kNm^2$	Deterministic
Stiffness immersion joint (axial)	K_i	Figure 29	Deterministic
Stiffness immersion joint (rotational)	R_i	Figure 30	Deterministic
Stiffness segment joint (rotational)	r_i	Figure 31	Deterministic
Initial compression Gina gasket	c_{init}	Table 10	Deterministic
Normal force at immersion	F_{TEi}	Table 10	Deterministic
Moment at immersion	M_{TEi}	Table 10	Deterministic
Time	t	2020, 2030, 2040, 2050	Deterministic
Temperature difference	ΔT	$15\ K$	Deterministic
Probability axial deformation modes	P_{def}	Table 11	Deterministic
Opening segment joints[81]	Δu_i	$U(0.47\ mm, 4.71\ mm)$; $4.71\ mm$	Uniform; Deterministic
Settlements at joints	v_i	Figure 28 & Figure 69 to Figure 74	Lognormal
Vertical load	q_z	Figure 32	Normal
Stiffness tunnel foundation	k_z	Figure 34	Normal
Stiffness soil friction	k_y	Figure 82	Normal
Shear force capacity	V_R	Figure 36	Normal
Rotational capacity	φ_R	Figure 37	Normal

[80] As a reference, for the Limfjord tunnel the maximum temperature range between summer and winter was considered to be $\Delta T = 14\ K$ (ATKINS et al., 2019).

[81] Note that the outer opened segment joints are independent stochastic parameters (uniformly distributed), while the inner opened joints are deterministic (as explained in subsection 3.3). Noticeably, the presented values in Table 2 correspond to a segment length of $26.156m$ (tunnel elements 2 to 4, see Figure 21).

4.3. Case Results

This subsection presents the structural reliability and availability results for the Noordtunnel case, which are determined according to the research methodology described in section 3. The tunnel reliability (4.3.1), the tunnel unavailability (4.3.2), and the critical segment joints (4.3.3) are discussed successively. Noteworthy, the results were obtained for a number of simulations equal to $N = 10^4$, which number is extensively substantiated in Appendix E.1.

4.3.1. Tunnel Reliability

The failure probability and structural reliability are determined for the Noordtunnel case, with the research methodology for the years 2020, 2030, 2040 and 2050. Figure 38 and Figure 39 present the failure probability and reliability of the Noordtunnel for the two settlement projections (see Figure 25 and Figure 26), and the three structural models (described in subsection 3.2). In these figures, failure of the complete tunnel is considered, which is defined as failure of at least one segment joint due to either shear force or rotation. In the figures, third-order polynomials are fitted through the calculated values, for which the relation for the reliability is given with Equation 5. In Table 3 the values for the parameters a, b, c and d are displayed, belonging to the reliability curves of Figure 39. Appendix E.2 presents the results for the failure mechanisms of shear force and rotation separately, as well to properly analyse the differences between the outcomes for the failure mechanisms.

$$R(t) = a \cdot t^3 + b \cdot t^2 + c \cdot t + d$$

Equation 5: Third-order reliability polynomial format.

Table 3: Calculated parameters a, b, c and d for the reliability fit of the Noordtunnel over the years for N=10^4.

	Model 1		Model 2		Model 3	
Parameter	*Case A*	*Case B*	*Case A*	*Case B*	*Case A*	*Case B*
a	$-5.0 \cdot 10^{-8}$	$-6.7 \cdot 10^{-8}$	$-4.7 \cdot 10^{-7}$	$-8.1 \cdot 10^{-6}$	$-4.98 \cdot 10^{-6}$	$-1.0 \cdot 10^{-7}$
b	$1.5 \cdot 10^{-6}$	$4.0 \cdot 10^{-6}$	$9.8 \cdot 10^{-5}$	$7.1 \cdot 10^{-4}$	$2.4 \cdot 10^{-4}$	$2.8 \cdot 10^{-5}$
c	$1.0 \cdot 10^{-5}$	$-7.3 \cdot 10^{-5}$	$-6.1 \cdot 10^{-3}$	$-2.2 \cdot 10^{-2}$	$-3.1 \cdot 10^{-3}$	$-1.0 \cdot 10^{-3}$
d	$4.0 \cdot 10^{-4}$	$4.0 \cdot 10^{-4}$	$2.4 \cdot 10^{-1}$	$2.4 \cdot 10^{-1}$	$5.7 \cdot 10^{-1}$	$5.7 \cdot 10^{-1}$

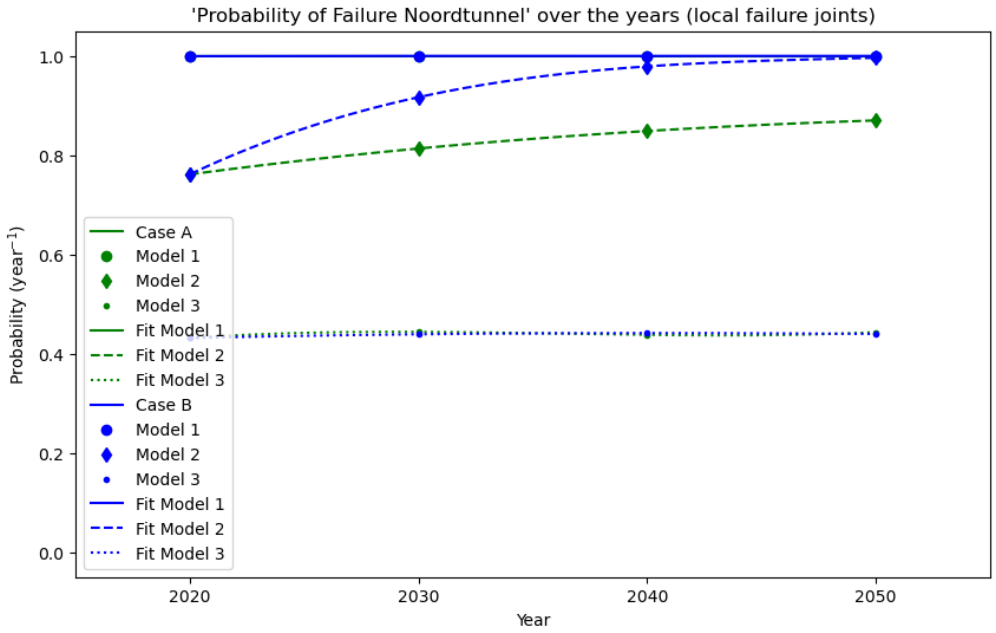

Figure 38: Calculated probability of failure for the Noordtunnel over the years (for N=10^4), where Case A and Case B concern the logarithmic and linear increase of settlements, respectively (identical to Figure 84 of Appendix E.2).

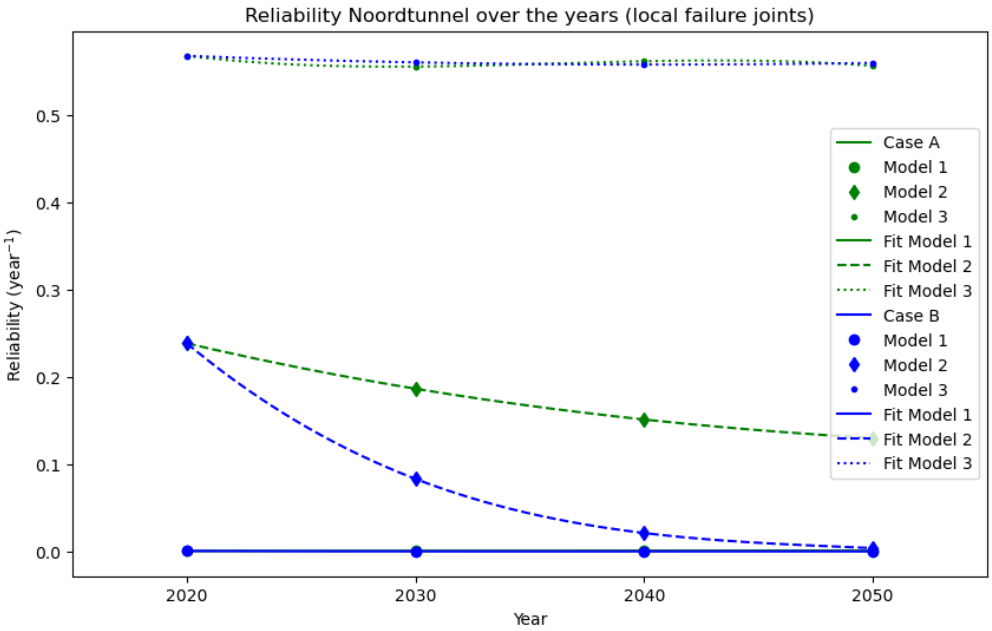

Figure 39: Calculated structural reliability for the Noordtunnel over the years (for N=10⁴), where cases A and B concern the logarithmic and linear increase of settlements, respectively (identical to Figure 85 of Appendix E.2).

As can be seen from the results of Appendix E.2, the failure probability increases over time, while the reliability decreases for all the models, both settlement projection cases and failure mechanisms. However, there are significant variances in both the extent to which the failure probability increases, and the order of magnitude values. First of all, the spread in results between the failure mechanisms is quantitatively the largest when compared to the spread for the different models and cases. The difference in results between the three models is roughly a factor of two, which also applies to the difference in results between the two cases. However, the difference in results between the two failure mechanisms is nearly a factor of 100. In addition, considering the failure mechanisms, it is clearly visible that shear force is the dominant failure mechanism above rotation, as there are hardly any differences between the failure probability due to shear force and rotation combined (Figure 84), and the failure probability due to shear force only (Figure 86). The rotational failure mechanism is not reflected in the total failure probability at all. Furthermore, it is remarkable that the spread in results for the shear force mechanism is comparable for all the models and cases, whereas the spread in results for the rotational mechanism is much larger for the two cases than for the three models. Moreover, it is noteworthy that *Model 1* shows the highest failure probabilities everywhere, except for the rotational failure mechanism regarding *Case B*, where *Model 2* is normative. Finally, comparing the settlement projections, the Noordtunnel always shows a higher failure probability for *Case B* (linear increase over time) than *Case A* (logarithmic increase over time).

It should be noted that the Noordtunnel failure probability does not concern the actual global failure of the tunnel, but is only determined to calculate the tunnel availability and unavailability, which is examined in paragraph 4.3.2. For this, the Noordtunnel reliability for the combination of both failure mechanisms will be used, which has been presented in Figure 39. In addition, the failure probability is considered more in depth at the joint level in paragraph 4.3.3, where the critical segment joints are evaluated for the different models.

4.3.2. Tunnel Unavailability

The tunnel availability and unavailability are determined for the Noordtunnel case, according to the research methodology. The results are presented in Table 4 to Table 6, for the three structural models and varying time periods where renewal is considered (2020-2030, 2020-2040, 2020-2050 and 2020-end of tunnel life). In the calculation, the mean down time (MDT) is equivalent to one day when failure occurs, during which time period it is assumed that a substantial settlement-related water leakage could be solved. The mean time between failure ($MTBF$) is based on the reliability curves for *Model 1*, *Model 2* and *Model 3*, which are presented in Figure 90, Figure 91 and Figure 92 of Appendix E.3[82], respectively. Noticeably, for *Model 1* with *Case B*, the time of renewal is indirectly limited to 10 years, because a failure probability of 1.0 occurs in 2030, which leads to similar results.

Table 4: Calculated MTBF, Availability, and Unavailability for different time periods of renewal and MDT = 1 day (Model 1).

Model 1	**Time of renewal (years)**		**MTBF (years)**		**Availability (%)**		**Unavailability (hours)**	
Period	*Case A*	*Case B*	*Case A*	*Case B*	*Case A*	*Case B*	*Case A*	*Case B*
2020-2030	10	10	0.005	0.0015	64.03	35.38	3151	5661
2020-2040	20	10	0.012	0.0015	81.42	35.38	1627	5661
2020-2050	30	10	0.020	0.0015	87.89	35.38	1061	5661
2020-∞	40.1	10	0.024	0.0015	89.75	35.38	898	5661

Table 5: Calculated MTBF, Availability, and Unavailability for different time periods of renewal and MDT = 1 day (Model 2).

Model 2	**Time of renewal (years)**		**MTBF (years)**		**Availability (%)**		**Unavailability (hours)**	
Period	*Case A*	*Case B*	*Case A*	*Case B*	*Case A*	*Case B*	*Case A*	*Case B*
2020-2030	10	10	2.6	1.6	99.89	99.83	9	15
2020-2040	20	20	4.5	2.0	99.94	99.86	5	12
2020-2050	30	30	6.0	2.1	99.95	99.87	4	11
2020-∞	70	33	7.8	2.1	99.96	99.87	3	11

Table 6: Calculated MTBF, Availability, and Unavailability for different time periods of renewal and MDT = 1 day (Model 3).

Model 3	**Time of renewal (years)**		**MTBF (years)**		**Availability (%)**		**Unavailability (hours)**	
Period	*Case A*	*Case B*	*Case A*	*Case B*	*Case A*	*Case B*	*Case A*	*Case B*
2020-2030	10	10	12.6	12.8	99.98	99.98	2	2
2020-2040	20	20	25.5	25.4	99.99	99.99	1	1
2020-2050	30	30	37.9	38.2	99.99	99.99	1	1
2020-∞	65.5	70	30.1	28.0	99.99	99.99	1	1

Surprisingly, most results reveal that the mean time between failure increases over time, while it is expected to decrease in reality. This is caused by the relatively flat reliability curves (Appendix E.3), inducing Equation 2 to increase for a later renewal year, which will be further discussed in subsection 5.3. Therefore, the unavailability results are interpreted as an order of magnitude for the different time periods of renewal. The spread in annual unavailability between the models is significant, with an order of magnitude of one day for *Model 2*, and a few hours for *Model 3*, while several months for *Model 1*. Based on current practice, *Model 2* and *Model 3* seem to be much more realistic than *Model 1*, but especially *Model 2* seems to match reality most. A rough estimate for the unavailability would therefore be one day annually, while further research is required for a more accurate assessment.

[82] Noteworthy, the upper limit of the integral in Equation 2 is bounded to a maximum of 70 years, under the assumption that the tunnel will reach its end of life after 100 years.

4.3.3. Critical Segment Joints

Following the research methodology, the failure probability is determined for each segment joint of the Noordtunnel in the years 2020, 2030, 2040, and 2050. Figure 40 presents the failure probability per joint for *Model 1*, considering the two failure mechanisms combined. Figure 41 displays the failure probability per joint for *Model 1*, taking only rotational failure into account. Failure due to shear force only is not shown separately, as it is similar to the plot of both failure mechanisms combined (see Figure 40). On top of that, Appendix E.4 presents the results for *Model 2* and *Model 3*, for both the combined failure mechanisms and rotational failure only.

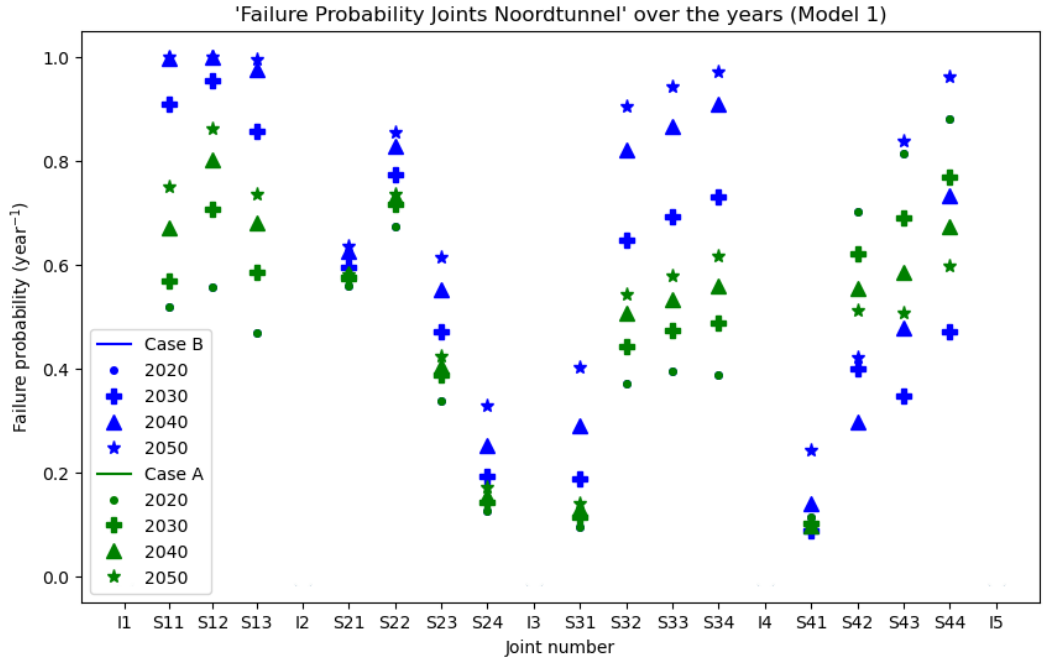

Figure 40: Failure probability segment joints of the Noordtunnel over the years for Model 1, where Case A and Case B concern the logarithmic and linear increase of settlements, respectively (identical to Figure 93 of Appendix E.4).

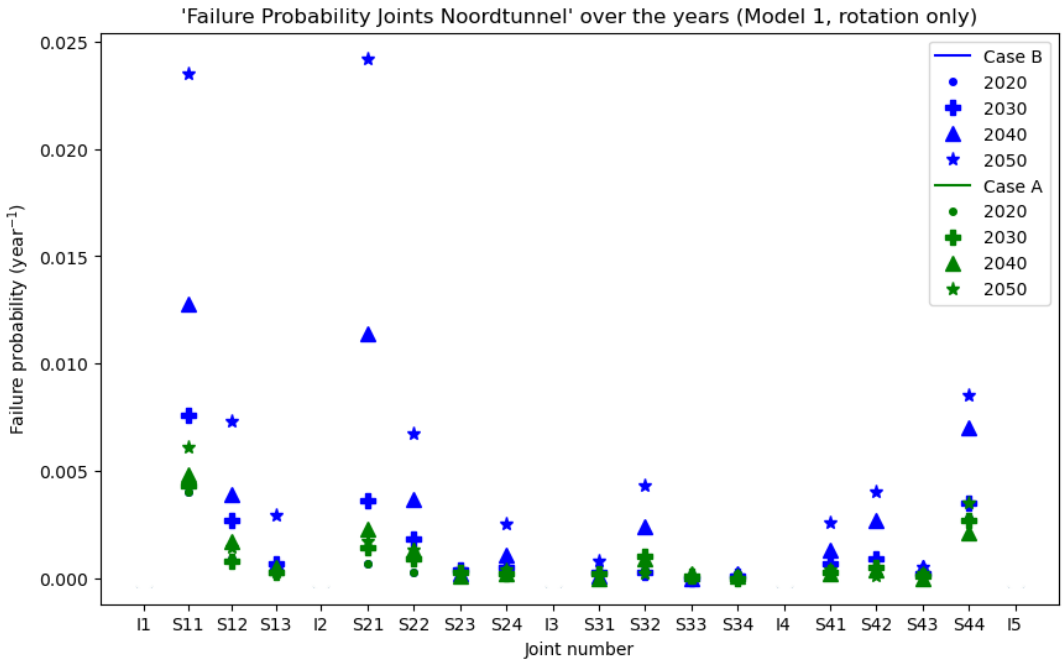

Figure 41: Failure probability segment joints of the Noordtunnel over the years for Model 1, considering only the rotational failure mechanism, where Case A and Case B concern the logarithmic and linear increase of settlements, respectively (identical to Figure 94 of Appendix E.4).

The results of Appendix E.4 demonstrate the increase of the failure probability for most segment joints over time, regardless of the model, case or failure mechanism used. Similar to the failure probability of the tunnel as a whole (described in paragraph 4.3.1), the failure probabilities of the segment joints show significant differences between the two failure mechanisms. Considering both failure mechanisms does not only lead to higher failure probabilities, but also to a completely different ratio between the joints, compared to rotational failure alone. For all the models, there appears to be more critical joints for both failure mechanisms than for rotation alone. In addition, it is noted that segment joints with high failure probabilities on rotational failure also show high failure probabilities, for the failure mechanisms combined. Furthermore, when comparing the settlement projections, the joints almost[83] always undergo a higher failure probability for *Case B* (linear increase over time) than *Case A* (logarithmic increase over time), which is consistent with the failure probability of the overall tunnel failure probability (see paragraph 4.3.1).

When comparing the structural models, the number of critical segment joints decreases from *Model 1* to *Model 3*, resulting in a more unambiguous outcome. *Model 1* shows many critical joints with a high failure probability, of which segment joints S11, S12, S13, S22, S32, S33, S34, S43, and S44 are the most noticeable. However, segment joints S21, S23, S24, S31, S41, and S42 appear to be highly critical for *Model 1* as well, albeit to a lesser extent. For *Model 2*, the critical joints are predominantly located on the leftmost tunnel element. The most critical joints seem to be segment joints S12, S13, and S21, followed by segment joints S22, S24, S31, and S32. For *Model 3*, all the critical joints are located in the outer two tunnel elements, and the failure probability increase is relatively small over the years. Herewith, segment joints S12, S13, S42, and S43 seem to be the most critical.

Segment joints S12, S13, and S43 appear to be the most critical joints of the Noordtunnel, when the three models are weighed equally. Additionally, segment joints S21, S22, S32, and S42 seem to be critical to a lesser extent. Next, the (future) critical segment joints are compared to the known occurred leakages. In the past, segment joints S13, S22, S32, and S34 have shown leakages, as displayed in Figure 23 (Kloosterman, 2014). Based on this, 75% of the segment joints with known leakages are identified as critical, according to the methodology. Thus, the assumed direct relationship between the occurrence of leakages and structural connection loss of a segment joint, seems to be reasonably well justified in this research.

Noteworthy, in reality some minor leakages will remain undetected, due to pumps functioning properly. On top of that, the water tightness of the joints is partly dependent on the performance during the execution phase, which could potentially have resulted in quality differences between various segment joints. This makes it difficult to draw firm conclusions about the exact connection between leakages and settlements.

[83] An exception of this is segment joint S42 for *Model 1*, where both failure mechanisms considered.

5. Sensitivity Analysis & Discussion

This section demonstrates the sensitivity analysis and the discussion of the research methodology, which is applied to the Noordtunnel case. In subsection 5.1, the approach of the sensitivity analysis is explained. Next, subsection 5.2 presents the results of the sensitivity analysis for Model 1, Model 2, and Model 3. Finally, the research methodology is discussed in subsection 5.3.

5.1. Approach

The sensitivity analysis aims to identify the parameters that mostly influence the failure probability of the segment joints. In addition, the uncertainty in failure probability is computed for all parameters. For each of the three models, the sensitivity analysis has been performed, distinguishing between the two failure mechanisms, which requires six different analyses to be executed. Thirteen parameters have been examined in the analysis (see Table 7), of which the quantification in the methodology is dependent on assumptions. The sensitivity of the parameters is assessed by the mean failure probability of the segment joints, for the failure mechanisms of either shear force or rotation.

For each parameter in the analysis, the influence has been quantified by considering an upper and lower limit. This involved two calculations per parameter (for both limits), according to the research methodology of section 3 (shown in Figure 19). The upper and lower limit are determined by considering the possible extreme values, which are partially based on the Noordtunnel parameter derivation of subsection 4.2. Herewith, the uncertainty differs for each parameter, causing the limits to consist of varying ratios over the parameters. Based on the settlement data of 2020, the sensitivity analysis has been conducted for the Noordtunnel.

An overview of the included parameters with the quantified upper and lower limits, is presented in Table 7, and the underlying assumptions are described further here. Firstly, the axial and bending stiffness are assumed to be a maximum factor of two higher or lower than the parameter value used ('the reference value'). For the settlements and segment joint capacities (shear force and rotation), the factor two has been used for both limits as well[84]. Besides this, the temperature difference is assumed to have a minimum of $1\ K$ and a maximum of $25\ K$. In addition, the limits of 0% and 50% are taken into consideration for the stress relaxation (in the year 2020). The limits of the initial compression of the GINA gaskets are assumed to be 90% and 110% of the reference value. Furthermore, the limits of the vertical load and soil friction stiffness are derived from the possible soil cover conditions above the tunnel[85]. Hereby, $1\ m$ and $3\ m$ cover are taken into account for the outer tunnel segments (TE1abcd and TE3), and $0.5\ m$ to $1.0\ m$ for the inner tunnel segments (TE1e, TE2 and TE4). Moreover, the foundation stiffness is considered to be at least a factor of 10 less stiff, and at most a of factor three stiffer than the reference value[86]. Additionally, the limits of the segment joint stiffness follow from the extreme values[87] of the maximum rotational stiffness (at zero joint opening)

[84] The mean and standard deviation for the limits of these stochastic parameters are determined by multiplying or dividing the reference value by two, respectively.
[85] In addition, for the soil friction stiffness the friction coefficient between concrete and sand is considered to be $f_{sc} = 0.5$ at minimum, and $f_{sc} = 1.0$ at maximum.
[86] The lower limit of the foundation stiffness is assumed to be a factor 10 less stiff compared to the reference value, based on the value that was used for the Limfjord tunnel (ATKINS et al., 2019), as explained in paragraph 4.2.3. For the upper limit of the foundation stiffness, the factor 3 stiffer is considered as realistic maximum.
[87] The limits of the maximum stiffness and joint opening are a factor 0.5 to 1.0 and $u_{max} = 10\ mm$ to $200\ mm$, for the lower and upper limit, respectively.

and the maximum joint opening (at which the rotational stiffness is zero), where the terms have been explained in paragraph 4.2.2. Finally, for the deformation modes, all the possible 45 options[88] have been considered separately, of which the lower and upper limit have been determined by the modes that resulted in the lowest and highest failure probabilities, respectively. Table 8 presents the deformation modes belonging to the lower and upper limits of the different sensitivity analyses.

Table 7: Overview parameters sensitivity analysis, including the upper and lower limits (for the settlement data of 2020).

Parameter	Reference Value	Lower Limit	Upper Limit
Axial stiffness (EA)	$1.663 \cdot 10^9\ kN$	$50\% \cdot EA$	$200\% \cdot EA$
Bending stiffness (EI)	$1.601 \cdot 10^{10}\ kNm^2$	$50\% \cdot EI$	$200\% \cdot EI$
Temperature difference (ΔT)	$15\ K$	$1\ K$	$25\ K$
Stress relaxation Gina gasket (rel)[89]	37.2%	0%	50%
Initial compression Gina gasket (c_{init})	Table 10	$90\% \cdot c_{init}$	$110\% \cdot c_{init}$
Vertical load (q_z)	Figure 32	$1.0\ m$ (TE1abcd/TE3), $0.5\ m$ (TE1e/TE2/TE4)	$3.0\ m$ (TE1abcd/TE3), $1.0\ m$ (TE1e/TE2/TE4)
Stiffness tunnel foundation (k_z)	Figure 34	$10\% \cdot EI$	$300\% \cdot EI$
Stiffness soil friction (k_y)	Figure 82	$1.0\ m$ (TE1abcd/TE3), $0.5\ m$ (TE1e/TE2/TE4) & $f_{sc} = 0.5$	$3.0\ m$ (TE1abcd/TE3), $1.0\ m$ (TE1e/TE2/TE4) & $f_{sc} = 1.0$
Shear force capacity (V_R)	Figure 36	$50\% \cdot V_R$	$200\% \cdot V_R$
Rotational capacity (φ_R)	Figure 37	$50\% \cdot \varphi_R$	$200\% \cdot \varphi_R$
Settlements at joints (v_i)	Figure 28	$50\% \cdot v_i$	$200\% \cdot v_i$
Probability axial deformation modes (P_{def})	Table 11	Mode for lowest mean failure probability of the joints (Table 11)	Mode for highest mean failure probability of the joints (Table 11)
Stiffness segment joint (r_i)	Figure 31	$u_{max} = 10\ mm$ & $0.5 \cdot r_{\phi,u0}$	$u_{max} = 200\ mm$ & $1.0 \cdot r_{\phi,u0}$

Table 8: Lower and upper limits of the deformation modes, for the different models and failure mechanisms.

Model	Failure mechanism	Limit	Tunnel Element 1	Tunnel Element 2	Tunnel Elements 3&4
Model 1	***Shear force***	*Lower*	Mode 3	Mode 1	Mode 4
		Upper	Mode 2	Mode 3	Mode 1
	Rotation	*Lower*	Mode 3	Mode 1	Mode 1
		Upper	Mode 1	Mode 3	Mode 3
Model 2	***Shear force***	*Lower*	Mode 3	Mode 1	Mode 5
		Upper	Mode 1	Mode 1	Mode 1
	Rotation	*Lower*	Mode 2	Mode 3	Mode 5
		Upper	Mode 1	Mode 1	Mode 2
Model 3	***Shear force***	*Lower*	Mode 3	Mode 2	Mode 5
		Upper	Mode 1	Mode 1	Mode 2
	Rotation	*Lower*	Mode 3	Mode 2	Mode 3
		Upper	Mode 2	Mode 1	Mode 2

[88] The possible 45 axial deformation options for the Noordtunnel follow from three considered modes for both tunnel element 1 and 2, and five considered modes of tunnel elements 3 and 4 combined (see Appendix D.6).
[89] The reference value follows from Figure 76 for $t = 30\ years$, as this corresponds to the 2020 situation (by taking the difference between 1.0 and the relaxation factor, and subsequently multiply by 100%).

5.2. Sensitivity Results

This subsection presents the results of the sensitivity analysis for *Model 1*, *Model 2* and *Model 3* subsequently in paragraphs 5.2.1, 5.2.2 and 5.2.3. *Model 1* prescribes the displacement at all the joints, *Model 2* the displacements at the immersion joints and the rotations at the segment joints, and *Model 3* the rotation at all the joints (as described in subsection 3.2).

5.2.1. Results Model 1

Figure 42 and Figure 43 demonstrate the results of the sensitivity analysis for *Model 1*, distinguishing between the failure mechanisms of shear force and rotation. For the shear force failure of Figure 42, four parameters have the most influence on the failure probability: bending stiffness, foundation stiffness, segment joint capacity, and settlements. The bending stiffness leads to an increase of a factor 1.2 (for $2 \cdot EI$), and a decrease of a factor 1.4 (for $0.5 \cdot EI$). The foundation stiffness causes the failure probability to increase with a factor of 2.0 (for $0.1 \cdot k_z$), and decrease with a factor of 0.6 (for $3 \cdot k_z$). For the segment joint capacity, the failure probability increases and decreases by the factors of 1.5 (for $0.5 \cdot V_R$) and 2.9 (for $2 \cdot V_R$), respectively. The settlements induce the failure probability to increase with a factor of 1.6 (for $2 \cdot v_z$), and decrease with a factor of 0.9 (for $0.5 \cdot v_z$). Noteworthy, the factor 0.6 for the foundation stiffness upper limit is contradicting relative to the lower limit, which is caused by the failure probability increase for almost all the segment joints. The discussion is further elaborated in subsection 5.3. In addition, note that the factor 0.9 for the settlements lower limit is induced by the increasing failure probability in the segment joints of tunnel elements 1 and 3 (outer elements), which is greater than the (absolute) net decrease of the other segment joints[90].

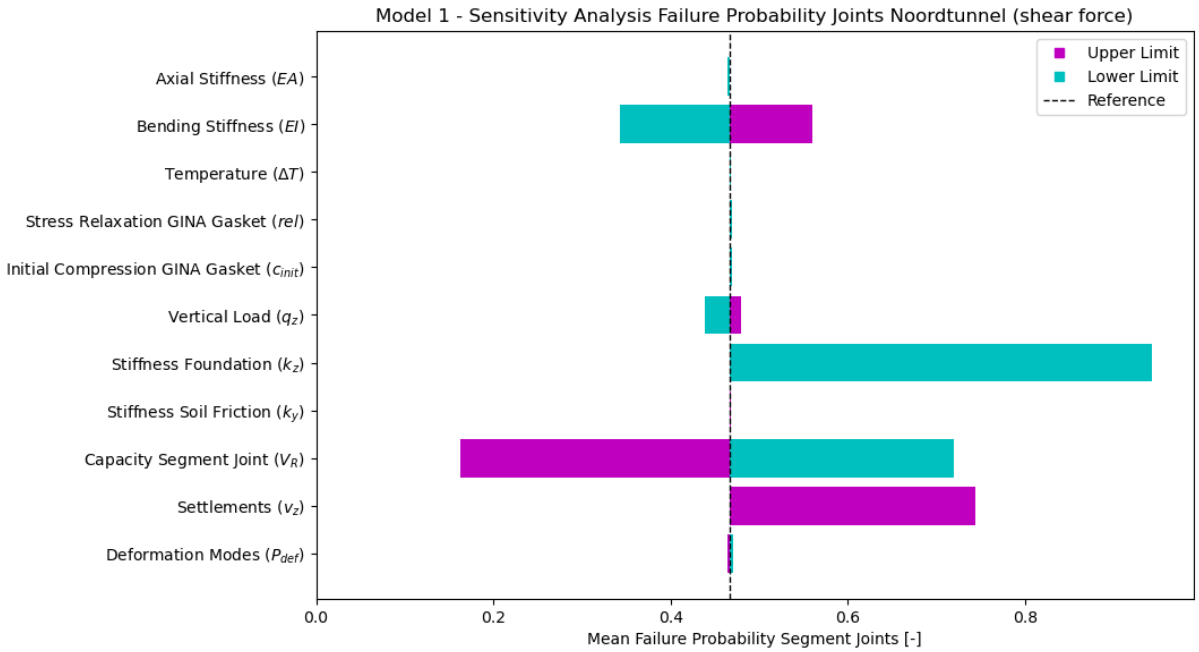

Figure 42: Results sensitivity analysis Model 1 for the shear force failure mechanism (considering the mean failure probability of the segment joints).

For the rotational failure of Figure 43, there are three very influential parameters: foundation stiffness, capacity segment joint, and settlements. The foundation stiffness causes the failure probability to increase with a factor of 33.3 (for $0.1 \cdot k_z$), and decrease with a factor of 2.9 (for $3 \cdot k_z$).

[90] The increase in failure probability for the segment joints of tunnel elements 1 and 3 (outer elements) is 50%, while the mean decrease for the joints of tunnel elements 2 and 4 (inner elements) is 56%. There is an absolute increase, as the failure probability of the segment joints in the outer elements is higher than for the inner ones.

For the segment joint capacity, the failure probability increases and decreases by the factors of 20.0 (for $0.5 \cdot \varphi_R$) and 5.2 (for $2 \cdot \varphi_R$), respectively. The settlements induce the failure probability to increase with a factor of 8.5 (for $2 \cdot v_z$), and decrease with a factor of 3.8 (for $0.5 \cdot v_z$).

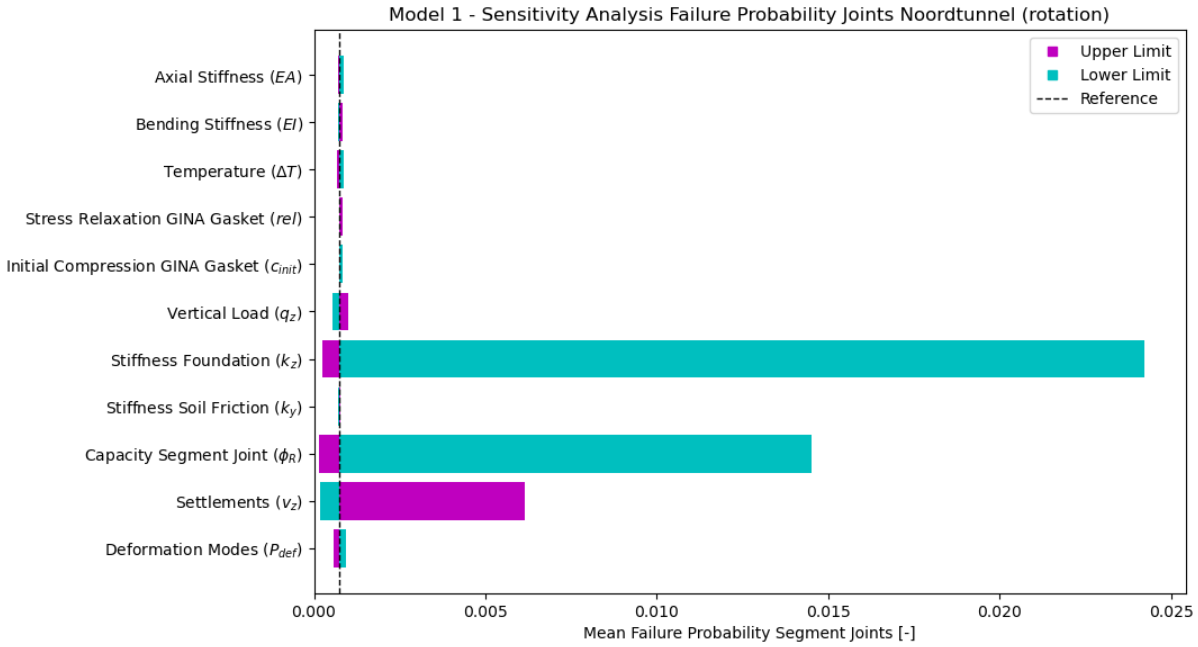

Figure 43: Results sensitivity analysis Model 1 for the rotational failure mechanism (considering the mean failure probability of the segment joints). Note the difference in scale between Figure 42 and Figure 43.

5.2.2. Results Model 2

Figure 44 and Figure 45 present the results for the sensitivity analysis of *Model 2*, regarding the failure mechanisms of shear force and rotation, respectively. Four influential parameters can be distinguished for the shear force failure (Figure 44): bending stiffness, foundation stiffness, segment joint capacity, and settlements. The bending stiffness leads to an increase of a factor 1.5 (for $2 \cdot EI$), and a decrease of a factor 1.5 (for $0.5 \cdot EI$). For the foundation stiffness, the failure probability increases and decreases by the factors of 5.5 (for $0.1 \cdot k_z$) and 0.3 (for $3 \cdot k_z$), respectively. The segment joint capacity causes the failure probability to increase with a factor of 3.3 (for $0.5 \cdot V_R$), and decrease with a of factor 5.8 (for $2 \cdot V_R$). The settlements induce the failure probability to increase with a factor of 3.1 (for $2 \cdot v_z$), and decrease with a factor of 2.2 (for $0.5 \cdot v_z$). Note that the factor 0.3 for the upper limit of the foundation stiffness[91] is again contradictory (similar to *Model 1* for shear force), which is further discussed in subsection 5.3.

The rotational failure mechanism of Figure 45 shows the foundation stiffness to be the most influential parameter, causing the failure probability to increase by a factor of 1069.1 (for $0.1 \cdot k_z$), and decrease by a factor of 1.5 (for $3 \cdot k_z$). Figure 46 provides a zoomed in version of Figure 45, by limiting the horizontal axis. The segment joint capacity and settlements have a much lower but still significant impact. The segment joint capacity leads to an increase of a factor 20.6 (for $0.5 \cdot \varphi_R$), and a decrease of a factor 4.1 (for $2 \cdot \varphi_R$). For the settlements, the failure probability increases and decreases by the factors of 18.9 (for $2 \cdot v_z$) and 0.8 (for $0.5 \cdot v_z$), respectively. Note that the factor 0.8 for the settlements lower limit is the consequence of an increasing failure probability in the outer two segment joints (S11 and S44), which is greater than the net decrease of the other joints together[92].

[91] The failure probability decreases with 62% in tunnel element 1, while increasing 263% for the other joints.
[92] The increase in failure probability for S11 with S44 is 72%, while the mean decrease for the other joints is 4%.

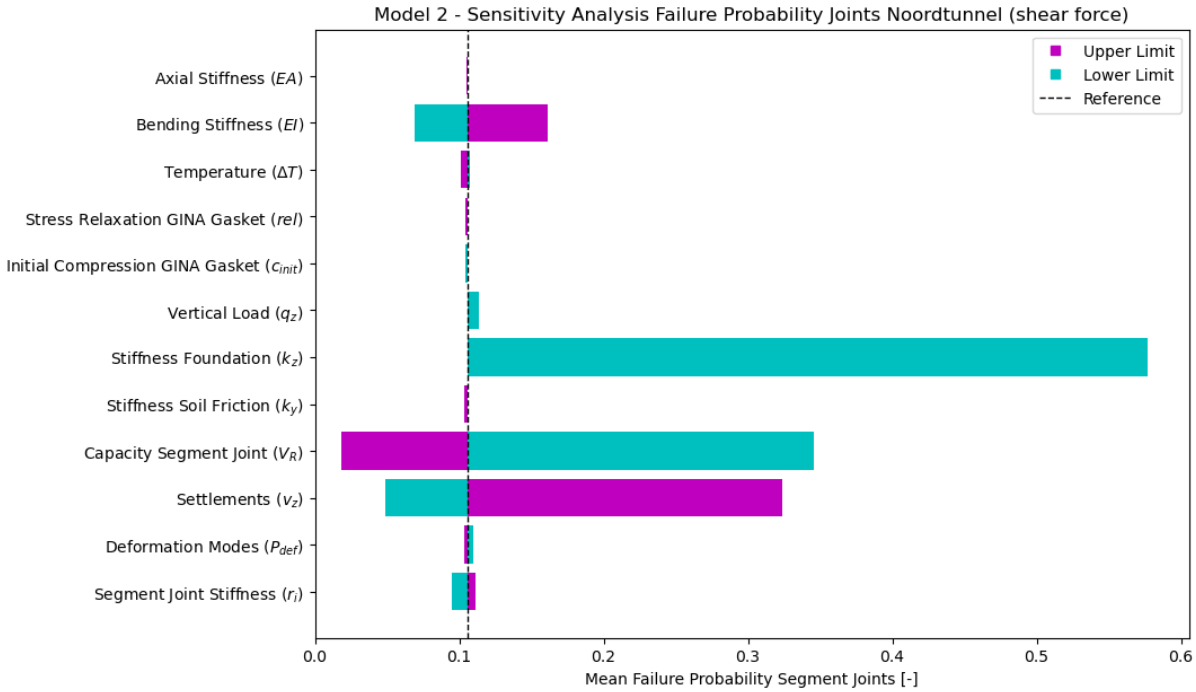

Figure 44: Results sensitivity analysis Model 2 for the shear force failure mechanism (considering the mean failure probability of the segment joints).

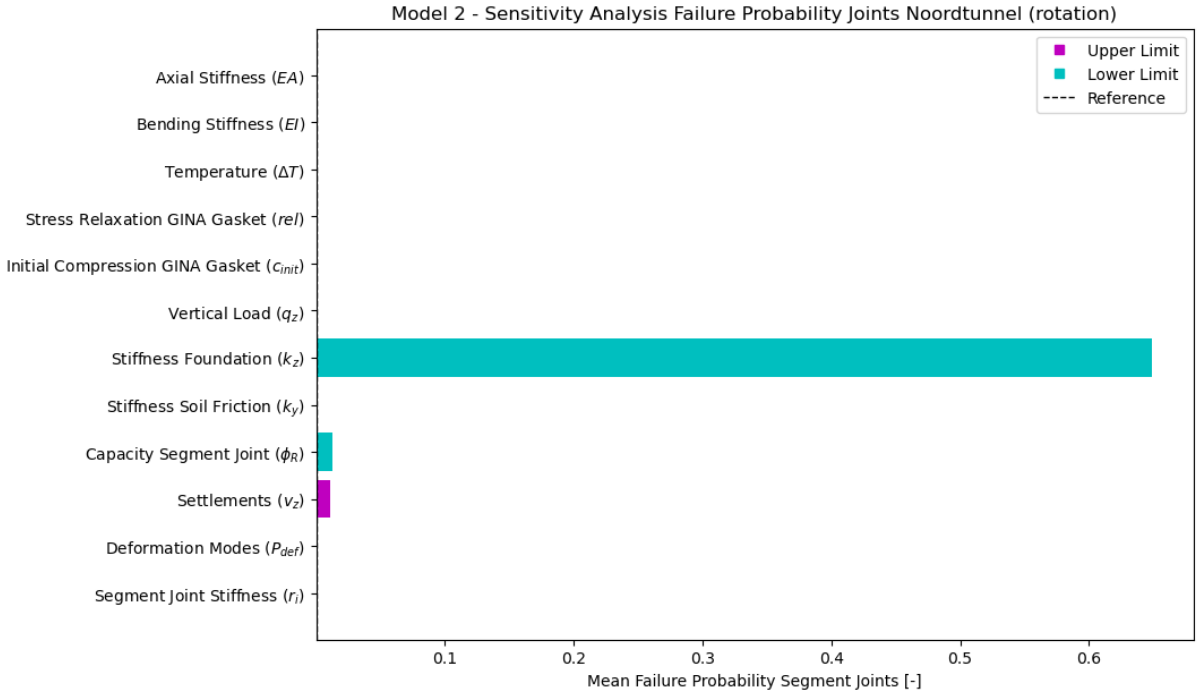

Figure 45: Results sensitivity analysis Model 2 for the rotational failure mechanism (considering the mean failure probability of the segment joints). Note the difference in scale between Figure 44 and Figure 45.

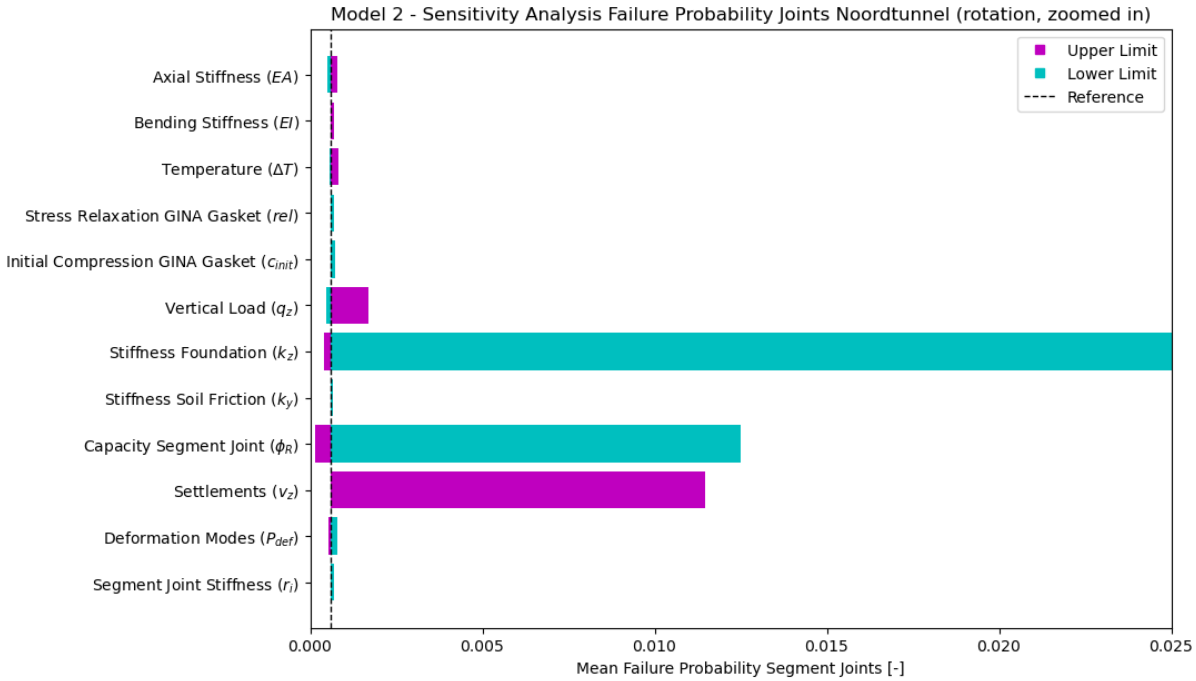

Figure 46: Results sensitivity analysis Model 2 for the rotational failure mechanism, zoomed in compared to Figure 45 by cutting off the upper limit of the foundation stiffness (considering the mean failure probability of the segment joints).

5.2.3. Results Model 3

Figure 47 and Figure 48 visualise the results of the sensitivity analysis for *Model 3*, where a distinction is made between the failure mechanisms of shear force and rotation. The shear force failure mechanism of Figure 47 contains four parameters with a major impact: bending stiffness, vertical load, foundation stiffness, and segment joint capacity. The bending stiffness leads to an increase of a factor 2.2 (for $2 \cdot EI$), and a decrease of a factor 2.3 (for $0.5 \cdot EI$). The vertical load induces the failure probability to increase with a factor of 2.1 (for max soil cover), and decrease with a factor of 4.0 (for min soil cover). The foundation stiffness causes the failure probability to increase with a factor of 8.2 (for $0.1 \cdot k_z$), and decrease with a factor of 3.8 (for $3 \cdot k_z$). For the segment joint capacity, the failure probability increases and decreases by the factors of 4.7 (for $0.5 \cdot V_R$) and 15.7 (for $2 \cdot V_R$), respectively.

For the rotational failure of Figure 48, the foundation stiffness is the most influential parameter, causing the failure probability to increase by a factor of 545.1 (for $0.1 \cdot k_z$), and decrease by a factor of 6.1 (for $3 \cdot k_z$). Figure 49 displays a zoomed in version of Figure 48, by restricting the horizontal axis. It follows that the segment joint capacity has a significant influence as well, albeit much smaller than the foundation stiffness, as the failure probability increases and decreases by the factors of 19.6 (for $0.5 \cdot \varphi_R$) and 4.5 (for $2 \cdot \varphi_R$), respectively.

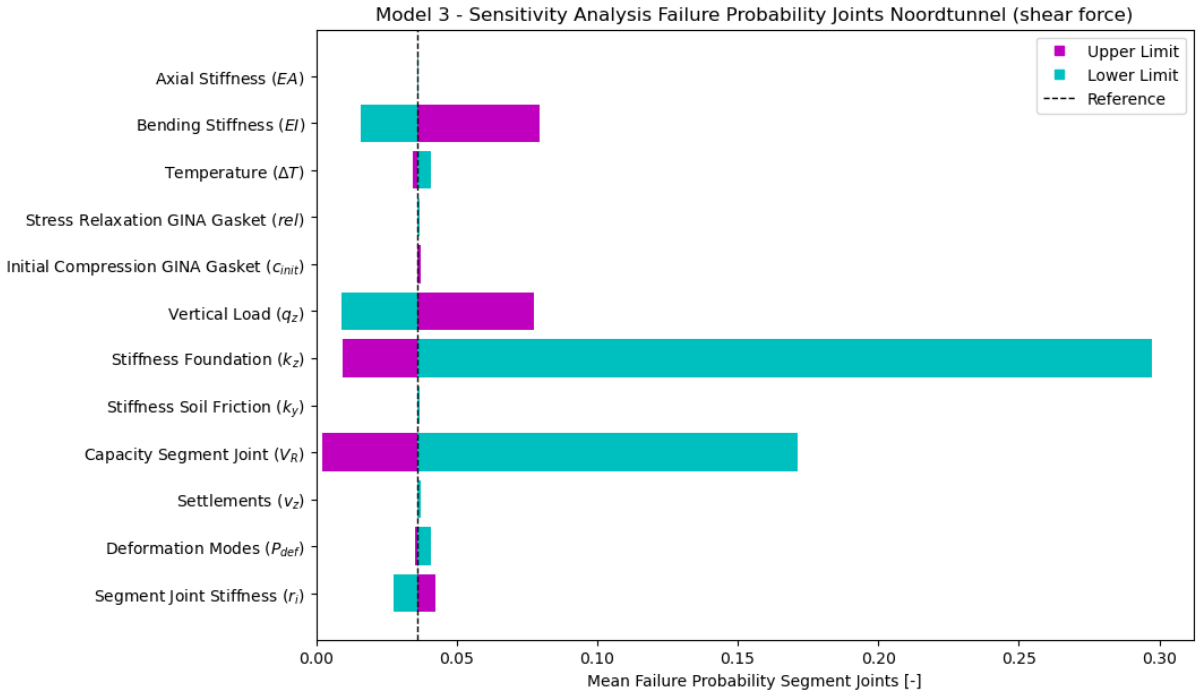

Figure 47: Results sensitivity analysis Model 3 for the shear force failure mechanism (considering the mean failure probability of the segment joints).

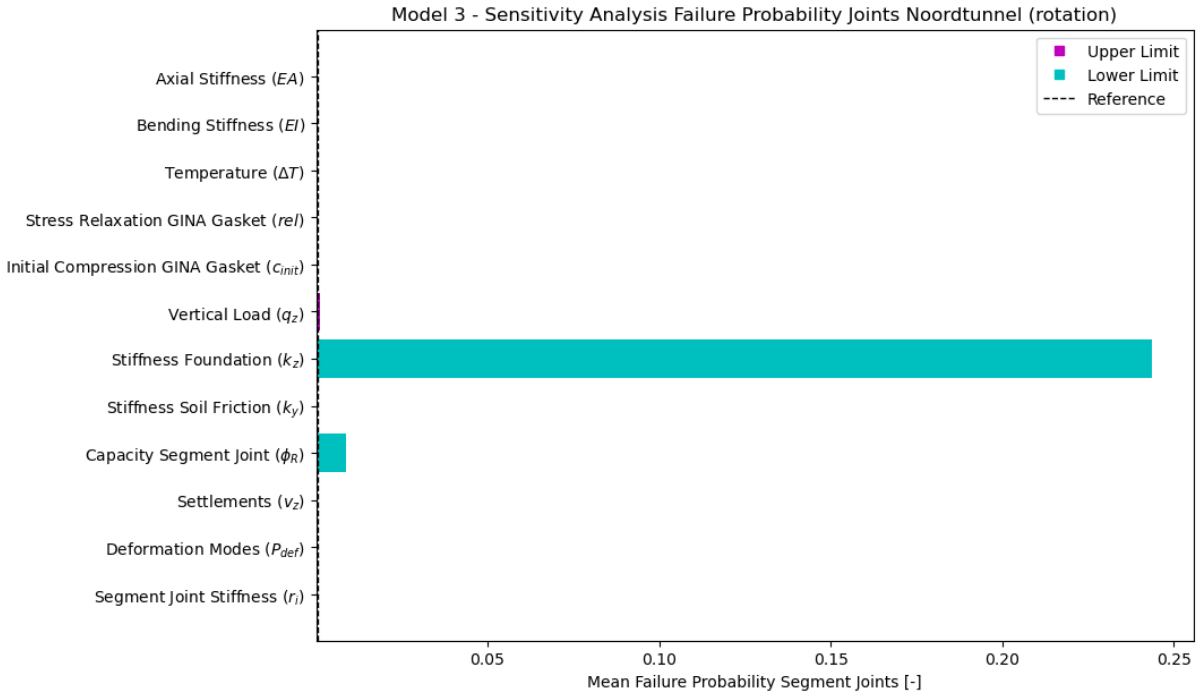

Figure 48: Results sensitivity analysis Model 3 for the rotational failure mechanism (considering the mean failure probability of the segment joints). Note the difference in scale between Figure 47 and Figure 48.

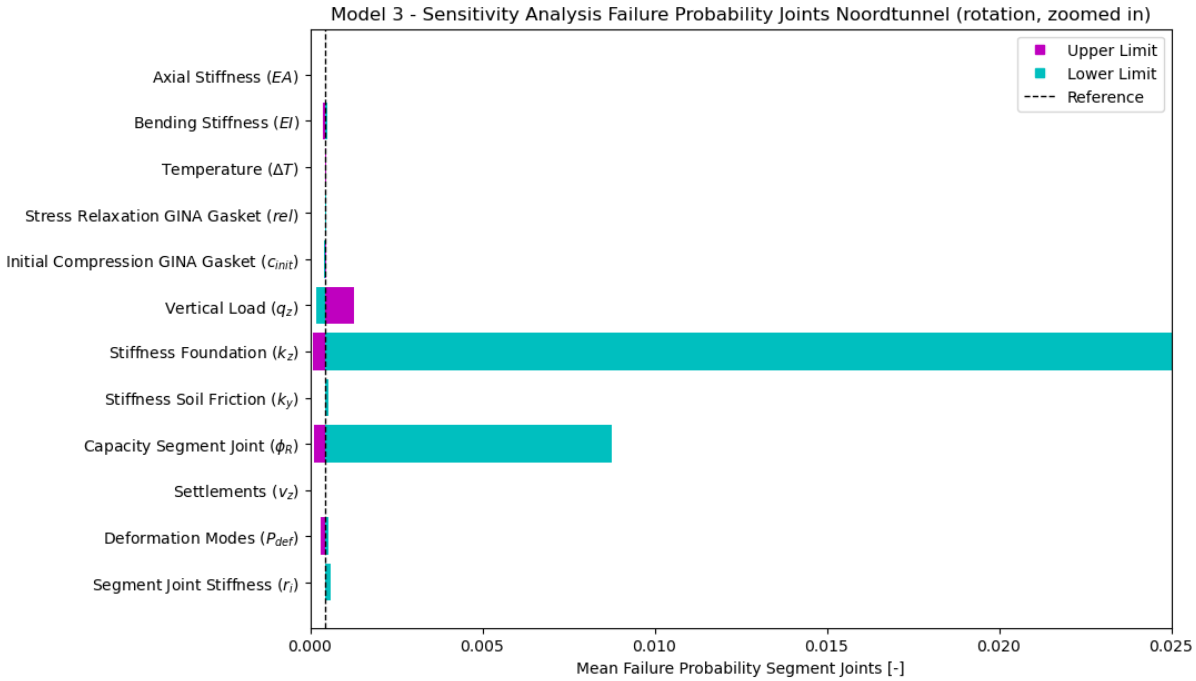

Figure 49: Results sensitivity analysis Model 3 for the rotational failure mechanism, zoomed in compared to Figure 48 by cutting off the upper limit of the foundation stiffness (considering the mean failure probability of the segment joints).

5.3. Discussion

This subsection presents the discussion of the research methodology. The influence and quantification of the parameters are discussed in paragraph 5.3.2. Next, the methodology itself will be discussed in paragraph 5.3.1, including the case results from subsection 4.3. Finally, paragraph 5.3.3 concludes the subsection with an overall interpretation.

5.3.1. Discussion Parameters

The results of the sensitivity analyses indicate a significant amount of uncertainty for the different structural models, especially for a few dominant parameters. First of all, the foundation stiffness is the parameter which involves the greatest uncertainty in the failure probability of the segment joints, both in absolute and relative terms, for all the models regardless of the failure mechanism. Particularly, the lower limit of the foundation stiffness causes the greatest uncertainty, leading to the highest failure probabilities. It is conflicting that for *Model 1* and *Model 2* regarding shear force, the upper limit of the foundation stiffness also result in higher failure probabilities of the segment joints. This has been examined in depth in Appendix E.5, which resulted in an explanation by the nonlinear relationship between the mean failure probability and the foundation stiffness. Secondly, the segment joint capacity is the next most impactful parameter in terms of uncertainty in the failure probability, irrespective of the model or failure mechanism. For the rotational failure mechanism, the lower limit of the segment joint capacity contains most of the uncertainty, both absolutely and relatively speaking. However, for shear force failure, the upper limit has relatively more uncertainty compared to the lower limit. In third place, after the foundation stiffness and segment joint capacity, the settlements are the most important parameter, due to its uncertainty in the failure probability. Noticeably, the settlements are not considered as an input for *Model 3*, as explained in subsection 3.2, which causes the settlements to show no impact for this model. Remarkably, the lower limit of the settlements for *Model 1* (shear force) and *Model 2* (rotation) involves a contradicting increase in the failure probability. However, the increase is relatively small and can be explained by an unequal change in the failure probability across the segment joints. Finally, the bending stiffness turns out to be the fourth important parameter, for the failure mechanism of shear force only.

Besides the four dominant parameters, the other parameters demonstrate interesting results as well. The vertical load entails quite some uncertainty in the failure probability, predominantly in *Model 3*, but is considerably less dominant for *Model 1* and *Model 2*. In addition, the segment joint stiffness[93] shows a relatively small spread in the failure probability, despite its rough quantification. Moreover, the parameters of temperature, stress relaxation, and initial Gina gasket compression hardly demonstrate any uncertainty in the failure probability. This results in little variation in the axial and rotational stiffness of the immersion joints. Furthermore, the parameters relating to the axial tunnel deformation (axial stiffness, temperature, soil friction stiffness, and the deformation modes) appear to have a relatively small influence on the spread in the probability of failure.

In the sensitivity analysis, the uncertainty per parameter consists of both its (relative) influence on the structural model, and the uncertainty in the parameter quantification. Parameters as foundation stiffness, segment joint capacity, and settlements contain a lot of uncertainty in the quantification, but also have a major impact on the outcome of the calculation. The three parameters have various reasons for their uncertainty in the quantification: too little information is known about the foundation stiffness, the segment joint capacity depends on a complex failure mechanism with an unknown actual condition, and the settlement data is of limited accuracy and frequency.

[93] The segment joint stiffness is only considered for *Model 2* and *Model 3*, as explained in subsection 3.2.

5.3.2. Discussion Methodology

The results of the research methodology for the Noordtunnel case demonstrated a large spread, mostly between the two failure mechanisms, with approximately a factor of 100 difference in the failure probability results (subsection 4.3). Also, the structural models and settlement cases contain a significant spread, with roughly a factor of two difference in the failure probability. The highest failure probability was observed for *Model 1* with *Case B*. In contrast to shear force failure, the rotational failure mechanism contains a smaller number of joints with a high failure probability, compared to the other joints. However, it was obtained that the segment joints with high failure probabilities considering rotational failure, often show high failure probabilities for the shear force failure as well. Besides the failure probability, the research methodology also presents a large spread in the unavailability results between the different models. In addition, it was shown that the mean time between failure ($MTBF$) increases over time, while it is expected to decrease in practice. This is because the structural reliability curves show a reducing decrease (Appendix E.3), for which the numerator of Equation 2 increases more than the denominator for a later year of renewal. Overall, the results of the research methodology could be interpreted as order of magnitude. Furthermore, the methodology appears to be able to qualitatively identify the critical segment joints of an immersed tunnel.

Reflecting on the structural model used in the methodology, the input parameters induce too much uncertainty in the results, which is why it is not worthwhile to further develop the model for the time being. First of all, the modelling of the segment joint stiffness does not have a significant effect on the outcomes, as shown in the sensitivity analysis. Additionally, the immersion joint stiffness modelling hardly displays any variation, and has even less impact compared to the segment joint stiffness. The influence of the vertical load in the model is significant, but minimal compared to the effect of the foundation stiffness. As the most influential input parameter, the foundation stiffness should be modelled more in depth. Here, it could be thought of applying two serial distributed springs layers, to model the tunnel foundation and the deeper soil layers separately. However, the data with respect to the foundation stiffness is insufficient to provide acceptable enough input for the modelling. Thus, the soil-structure interaction between the tunnel and its foundation requires further investigation and data gathering, before the model could be improved.

Zooming in on the segment joint level, several assumptions have been made underlying the structural model. First of all, the normal force in the segment joints has been assumed to act at the neutral axis of the tunnel cross section. However, in reality the normal force will concentrate in either the top or base slab of the tunnel, when a segment joint is subjected to a rotation (subsection 2.2). On top of that, in the structural model the relation between joint rotation and joint opening has not been taken into account, while in practice rotation is only possible after some opening of the joint. Even with these two assumptions, regarding normal force and rotation, the sensitivity analysis showed that the axial deformation entails a relatively small influence. In addition, for *Model 2* and *Model 3* the rotations of the segment joints have a maximum value of approximately $10^{-4}\ rad$ (see Appendix B), which would require an axial joint opening of about $1\ mm$. It is likely that some axial space is present in the joints, given the execution tolerance. But with *Model 1*, the rotations of the segment joints exceed $10^{-3}\ rad$ (see Appendix B), requiring an axial joint opening of more than $1\ cm$, which space can only be provided by axial deformation. Thus, regarding the relation between rotation and joint opening, especially *Model 1* contains unrealistically big assumptions, in contrast to the other models. Furthermore, in the research it has been assumed that the segment joints remain flat over the cross section, and the distribution of forces across the cross section has not been considered in detail. Despite the fact that the failure mechanism of shear force is more realistic than rotation, the results

obtained for shear force do not appear to correspond with reality, in contrast to the obtained results for the rotational failure mechanism. Noteworthy, the normal force in the segment joint has not been considered for the shear force resistance, while this could be favourable for the resistance. Nonetheless, all these possible improvements in modelling the segment joints more in depth, will always reduce less uncertainty than the soil-structure interaction, as followed from the foundation stiffness parameter in the sensitivity analysis. Hence, modelling the segment joints more thoroughly will only pay off, when the soil-structure interaction is established to a greater degree.

Reflecting on the two settlement projection cases, including the logarithmic increase of *Case A* and the linear increase of *Case B*, too much uncertainty is involved to establish the most realistic scenario. Admittedly, the logarithmic settlement projection would make more sense, as it could be explained from the geotechnical mechanisms. Moreover, for the Noordtunnel case it was demonstrated that a logarithmic settlement development occurred, based on the settlement data. However, as the settlement data of the Noordtunnel is of poor accuracy and frequency, reconstructing the exact deformation of the tunnel structure is impossible. On top of that, it cannot be excluded that settlement developments by non-geotechnical mechanisms occur in practice, although this does not seem obvious. Generally, *Case B* leads to higher failure probabilities of the segment joints, hence a larger tunnel unavailability. Therefore, both settlement projection cases should equally be considered when interpreting the results of the research methodology for the Noordtunnel case.

Comparing the three structural models (*Model 1*, *Model 2* and *Model 3*), the results obtained from *Model 2* seem to be the most realistic, for both structural reliability and availability. In addition, *Model 2* shows the least flaws in the structural modelling, both at a global and joint level. However, only regarding the direct settlement data input at all the joints, *Model 1* is more suitable by prescribing the displacements at all the segment joints[94]. Meanwhile, exactly the settlement data at the segment joints contains a lot of uncertainty, as there is a huge gap in the data for the Noordtunnel case. Therefore, *Model 2* currently seems to be the preferred model, although more investigation is required before this could be established.

5.3.3. Overall Interpretation

In short, from the results and sensitivity analysis for the Noordtunnel case, it follows that considerable uncertainty is involved in the research methodology. This uncertainty is made up of the uncertainties of the parameters, structural models, and failure mechanisms. Because of this, the research methodology contains a significant spread in the results, despite its thoroughness and thoughtfulness. Therefore, the results of the research methodology can only be used as order of magnitude, and should not be interpreted too precisely. However, the research methodology seems to be able to qualitatively identify the critical segment joints of an immersed tunnel. The most influential parameters contain the foundation stiffness, segment joint capacity, settlements, and bending stiffness, based on the sensitivity analysis results. Herewith, the settlements only relate to *Model 1* and *Model 2*, and the bending stiffness is only impactful for the shear force failure mechanism. Note that, currently there is a lack of information for determining the foundation stiffness. Additionally, the segment joint capacity faces many challenges for proper computation, and the settlement data is of limited accuracy and frequency. Furthermore, it cannot be validated which of the two settlement projection cases lead to the most realistic results of the research methodology, for the Noordtunnel case. Moreover, *Model 2* seems to correspond closest to reality out of the three

[94] For *Model 2*, the deformation at the immersion joints is prescribed based on the settlement data, while the rotations at the segment joints are prescribed based on the occurring bending moments with the rotational joint stiffness (as described in subsection 3.2).

structural models, but further research is required for establishing this. To conclude, presently gathering more data has a higher priority than improving the structural modelling of immersed tunnels. Especially the soil-structure interaction, between the tunnel structure and its foundation, needs further attention regarding the data collection. After more data has been gathered, modelling the soil-structure interaction could be conducted more comprehensively.

6. Maintenance & Renovation Strategy

In this section the maintenance and renovation strategy for the segment joints is demonstrated. Subsection 6.1 introduces several potential solutions that could form the maintenance and renovation strategy. Next, these solution alternatives are further described in subsection 6.2. Finally, the maintenance and renovation strategy are derived by evaluating the alternatives in subsection 6.3.

6.1. Introduction

Rijkswaterstaat, as executive agency of the Dutch Ministry of Infrastructure and Water Management, is responsible for the main infrastructure networks in the Netherlands. The focus of Rijkswaterstaat has been shifting over the years, from mainly constructing new infrastructure to high maintenance of existing infrastructure as well. This increasing maintenance trend will continue in the coming years, as most of the infrastructure network dates from the previous century, and requires modernising to keep the Netherlands safe, liveable and accessible. Meanwhile, Rijkswaterstaat will become more and more asset management driven from an organisational point of view. This trend will be enhanced with the developments in the field of data, digitalisation and automation. Most likely, Rijkswaterstaat will undergo many organisational changes in the upcoming years to reinvent itself for the future.

To address all of the urgent challenges, the infrastructure sector must evolve as a whole in the next years. There are currently fewer people working in the sector than necessary to solve all these challenges, especially since many professionals are leaving the sector nowadays. Hence, a higher efficiency of personnel is required, besides a better cooperation among all the stakeholders. Additionally, the current type of contracts between clients and contractors should be improved. The major efficiency gain in the sector should be accomplished by implementing standardisation, within a project and at portfolio level, in which several similar projects are combined.

The tens of tunnels, part of the main road network of Rijkswaterstaat, require maintenance and renovation to retain acceptable performance levels of safety and availability. Here, the difference between maintenance and renovation consists of the impact of the execution, and the duration of unavailability. For the Noordtunnel, a major renovation is planned before 2030 to accomplish significant maintenance. During this renovation, it should be ensured that the segment joints of the tunnel structure perform sufficiently for at least 30 years without drastic measures. Noteworthy, the ultimate goal is to apply a predictive maintenance strategy to the tunnels of Rijkswaterstaat in the future, to perform the maintenance as efficient and effective as possible.

This research differentiates five potential solutions that could contribute to the maintenance and renovation strategy of Rijkswaterstaat. Firstly, advanced monitoring and inspection indirectly support maintenance and renovation. In addition, the current maintenance of correctively injecting leakages could be improved. Ultimately, three drastic renovation solutions are included, such as repairing the structural connection, installing additional waterproofing, and compensation grouting. The solutions entail several benefits, which are deduced from the above together with the stakeholder analysis of Appendix F. The benefits of safety and availability to road users are extremely valuable, as pointed out above. Subsequently, maintaining tunnels more efficiently is a crucial advantage in dealing with the challenges. Moreover, using human resources more efficiently is a necessary advantage, given the limited number of professionals. Finally, applying standardisation induces a generalisability benefit.

6.2. Potential Solution Alternatives

This subsection describes five potential solution alternatives, which could be part of the maintenance and renovation strategy for the segment joints. Advanced monitoring and inspection (6.2.1), corrective injection of leakages (6.2.2), repairing the structural connection (6.2.3), installing additional waterproofing (6.2.4), and compensation grouting (6.2.5) are consecutively described.

6.2.1. Advanced Monitoring and Inspection

Advanced monitoring induces a tunnel to be maintained in a good condition more efficiently during its entire lifespan. Currently, Rijkswaterstaat measures the (vertical) deformation of the tunnel structures predominantly by manually levelling measuring bolts. The accuracy of the data is around $1\ mm$, and the frequency is limited to once a year. However, the frequency is much lower for most tunnels, as they should be closed for traffic to perform the measurements. If advanced monitoring instruments would be used, a lot of useful data would be obtained. In the first place, this data can be used to estimate the structural condition of the tunnel, as more insight is gained regarding the deformation behaviour. Moreover, maintenance will become more predictable, and the renovation scope could be better defined upfront. On top of that, advanced monitoring is less labour intensive, and thus more efficient. Finally, the data could be used for scientific research, which in the long run leads to more knowledge and accompanying advantages.

In the 1st Heinenoordtunnel, a pilot project has been implemented, where the tunnel deformation was measured by a distributed optical fiber sensor, as displayed in Figure 50. This monitoring system is remotely controlled, and does not affect the tunnel operation. The obtained data was of a higher frequency (twice an hour) and accuracy ($0.1\ mm$) than the conventional data from levelling the measuring bolts (Zhang & Broere, 2023a), by which the daily and seasonal deformation behaviour is obtained. The Noordtunnel is planned to be equipped with an advanced monitoring system in 2024, which would measure the deformations of the tunnel structure. The main objective here is to develop fundamental knowledge about the deformation behaviour of the tunnel, which is required to move towards a predictive maintenance strategy in the future. The monitoring system in the Noordtunnel will contribute to all of the abovementioned advantages.

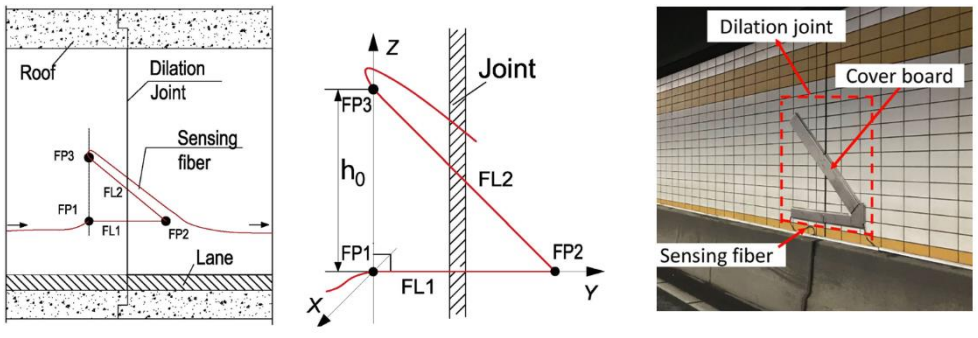

(a) (b) (c)

Figure 50: Developed distributed optical fiber sensor for the 1st Heinenoordtunnel, both schematically (a,b) and in practice (c) (Zhang & Broere, 2023a).

Besides advanced monitoring, flow measurements and visual inspection are also part of this solution alternative. By analysing flow measurements at various positions in the tunnel along with the rainfall data, it is possible to determine which joint is leaking and how much water is flowing inside. Visual inspection could also provide very useful information, especially when performed on the pump cellars and sewage system in the tunnel. Maintenance nights provide an opportunity of inspecting the sewage system and looking for potential leakages. Additionally, the composition of the water inside the central pump cellar could regularly be investigated (e.g. on sand of the foundation).

6.2.2. Corrective Injection of Leakages

The current way Rijkswaterstaat performs segment joint maintenance could be optimised, which involves corrective injection of leakages. Presently, appearing leakages in the joints are terminated by injection, in which the leakage path is sealed, preferably at night to limit hindrance. Most leakages appear during low temperatures in the winter period, as the segment joints are opened maximally at that time, due to the temperature shrinkage of the concrete segments. When a leakage occurs, this could result in water puddles on the road surface or icicles on the roof, which may lead to dangerous situations for road users. For these dangerous situations, tunnel tubes need to be closed off. Furthermore, a sand-carrying leakage could arise in a segment joint, as observed at the Kiltunnel in 2001, which is displayed in Figure 4 (Leeuw, 2008). For this particular example, foundation sand was transported into the tunnel, presumably after fracture of the spigot and socket structure took place (Leeuw, 2008). This affects the tunnel foundation and could further increase ongoing settlements. Note that not all (small) leakages are noticed, as the water is automatically drained by the system.

The drill and Injection method of Leeuw (2008)[95] enables to solve an active leakage during one night closure of the tunnel tube. The injection method requires extensive preparation, estimation of the leakage path, and determining the drilling strategy (Leeuw, 2008). In short, the method consists of drilling two holes, performing various checks for injection, and finally injecting with a special liquid. Noteworthy, the execution of this method is true craftsmanship and should only be performed by highly qualified professionals. Moreover, the costs of implementing the traffic measures are often more expensive than injecting the leakages themselves (Leeuw, 2008).

Technically, the current method for corrective injection of leakages in tunnels is very solid. However, there is still room for improvement regarding the cooperation between Rijkswaterstaat and the specialised contractors. Three changes are proposed here, which could result in a more efficient way of corrective maintenance. First and foremost, all relevant information about the segment joint detailing should be collected and stored at a single location, so that this information can be found efficiently. Additionally, one central contact point within Rijkswaterstaat could be appointed, where all information is known, as well as some expertise on tunnel leakages. Finally, a multi-year contract could be drafted with a specialised contractor, for injecting leakages in all the tunnels (including the reporting), apart from the regular maintenance and renovation contracts.

This improved cooperation would result in a faster operation, better knowledge assurance, and a higher execution performance. The risk of leakages in segment joints would therefore be much better controlled, which induces a higher tunnel availability, more efficient maintenance, and more efficient use of human resources. Furthermore, this solution causes the costs to be more predictable for Rijkswaterstaat, as a long-term collaboration is established with a suitable specialised contractor.

Figure 51: Injecting a leakage in the roof of a segment joint in the Noordtunnel (Leeuw, 2008).

[95] The complete injection approach has been described on page 66 of Leeuw (2008).

6.2.3. Repairing the Structural Connection

Repairing the structural connection of a segment joint restores structural integrity and prevents further differential settlements, after it would have failed due to exceeding loading. When the segment joint would no longer function structurally, differential settlements could occur, including the consequences of appearing leakages and damage to the asphalt. This causes increasing structural damage, and potential unsafe situations for road users, which requires repairing the structural connection. Hence, two different types of conceptual solutions are envisaged here, which are prestressing of the segment joint and structurally connecting the outer walls of the segment joint.

The prestressing of the segment joint(s) could be performed by post tensioning, which would reduce the tensile stresses and concrete cracking, due to seasonal temperature variations and ongoing settlements (ATKINS et al., 2019). Therefore, prestressing increases the durability of the tunnel and decreases the long-term maintenance costs (ATKINS et al., 2019). Figure 52 illustrates the alternative of additional post tensioning for the Limfjord Tunnel, where the cables are positioned next to the walls, as it is the only space available. For the Noordtunnel, in the most ideal situation use would be made of the old prestressing channels[96] to post tension the tunnel at the critical joints. However, further investigation is required to be able to estimate the technical feasibility and costs.

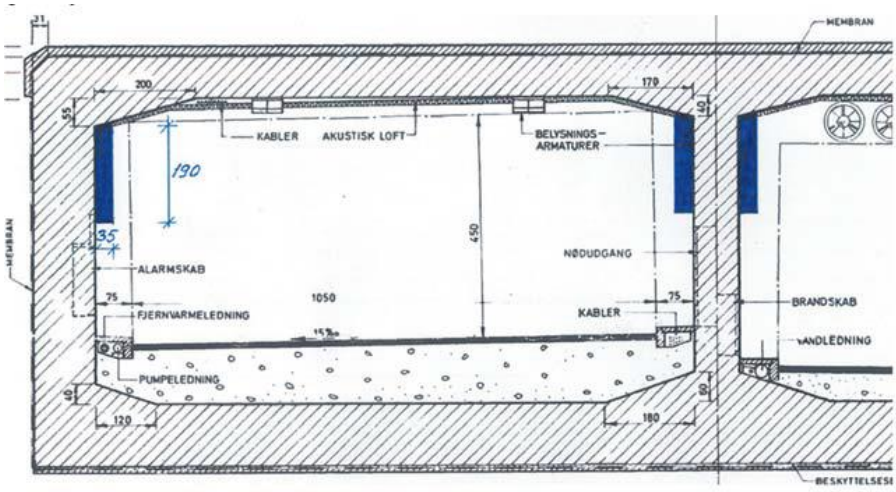

Figure 52: Additional prestressing for the Limfjord Tunnel, indicated with the blue boxes against the walls and just below the tunnel roof (ATKINS et al., 2019).

In addition to prestressing, one could also think of structurally connecting the outer walls of the tunnel in the segment joint. Conceptually, it may be possible to connect the adjacent segments structurally, by attaching a thick steel plate to the outer walls with many bolts. A potential advantage of this option involves the opportunity of optimising the stiffness of the segment joint somewhat, during the engineering of the solution.

Both options of prestressing the segment joint(s) and structurally connecting its outer walls recover the structural performance, by preventing the development of (further) differential settlements in the segment joint. During the renovation of the Noordtunnel, this solution would involve considerable costs and unavailability, but would lead to lower maintenance costs and less unavailability of the tunnel in the long run.

[96] During the construction of the Noordtunnel, the tunnel elements were prestressed for transportation (as described in subsection 2.1). Once the elements were immersed and the foundation was finished, the prestressing was cut, to allow the segment joints to perform their function (enabling some deformation).

6.2.4. Installing Additional Waterproofing

Installing additional waterproofing in a segment joint ensures watertightness, in case of (future) leakages appearing. The renovation of the Noordtunnel would offer the opportunity to install an additional waterproof gasket in the critical segment joint(s). This solution is quite drastic, but very effective when dealing with excessive leakages, whether it concerns the appearance of settlement-related leakages, or leakages due to poor construction performance. However, the installation of the additional gasket will be quite labour-intensive. Also, this solution will not recover the structural connection of the joint, in case of failure. Figure 53 presents the installation of a new waterproof gasket for the Roosendaal underpass A58. Installation of the additional gasket in an immersed tunnel is much more challenging than the underpass. Hence, the solution will not be cheap and closing of the tunnel is required for the execution, but this temporary unavailability could be minimised by optimising the renovation planning. In addition, the solution creates lower long-term maintenance costs and less unavailability of the tunnel, as leakages in critical joints are effectively solved.

Figure 53: A new waterproof gasket is installed for the Roosendaal underpass A58 (Leeuw, 2008).

Besides installing an additional waterproof gasket, also the drainage of leakage water could be improved, to avoid that the road surface gets affected. This could be achieved by installing a drainage channel in the segment joint, which drains the leakage water towards the tunnel drainage system. The main advantages are lower construction costs and less unavailability during execution, compared to installation of the additional gasket. However, the disadvantages are the poor durability and maintainability, which both lead to the associated maintenance costs. In one of the segment joints of the 1st Heinenoordtunnel, an enormous active leakage of 4-5 m^3/h has been controlled by an installed drainage channel, as displayed in Figure 54. Such a drainage channel needs to be designed for dynamic loads and vibrations from road traffic, as the channel and asphalt on top of it could be seriously damaged (Leeuw, 2008). Noticeably, the drainage solution may no longer be sufficient when leakages increase over time, due to increasing settlements for instance.

Figure 54: Drainage channel in the segment joint of the 1st Heinenoordtunnel to solve the leakage of 4-5 m^3/h (Leeuw, 2008).

6.2.5. Compensation Grouting

Compensation grouting could be a radical solution, when increasing tunnel deformations continue to deteriorate the structural condition of the tunnel, resulting in the appearance of concrete cracks and leakages. Compensation grouting is a geotechnical method that is used to control settlement of structures, and which could be used to lift a structure from its present position (ATKINS et al., 2019). With this method, grout is injected into the soil just below the structure, after which the soil will be expanded. Because of this, occurred settlements can be counteracted, and a controlled uplift of the tunnel structure can be provided to compensate for (future) settlements (ATKINS et al., 2019). Thus, compensation grouting would eliminate potential (future) risks for the tunnel structure, and ensures cheaper maintenance permanently. However, this technology will require an enormous investment, and the execution will not be without risks.

For the Limfjord Tunnel, an expert group took several geotechnical options into account that were based on typical industry proven ground engineering techniques, which could potentially be applied on the tunnel. Active horizontal compensation grouting seemed to be the preferred option, according to the experts (ATKINS et al., 2019). For the case of the Limfjord Tunnel, the grout injection could be performed from cofferdams, located in the waterway outside of the tunnel structure, to prevent significant disruptions to road users (ATKINS et al., 2019). The same execution method could also be applicable to the Noordtunnel, but directional drilling or grouting from land may be potential solutions as well. Figure 55 and Figure 56 visualise the horizontal compensation grouting for a cross-section of the Limfjord Tunnel, including a cross-sectional and top view.

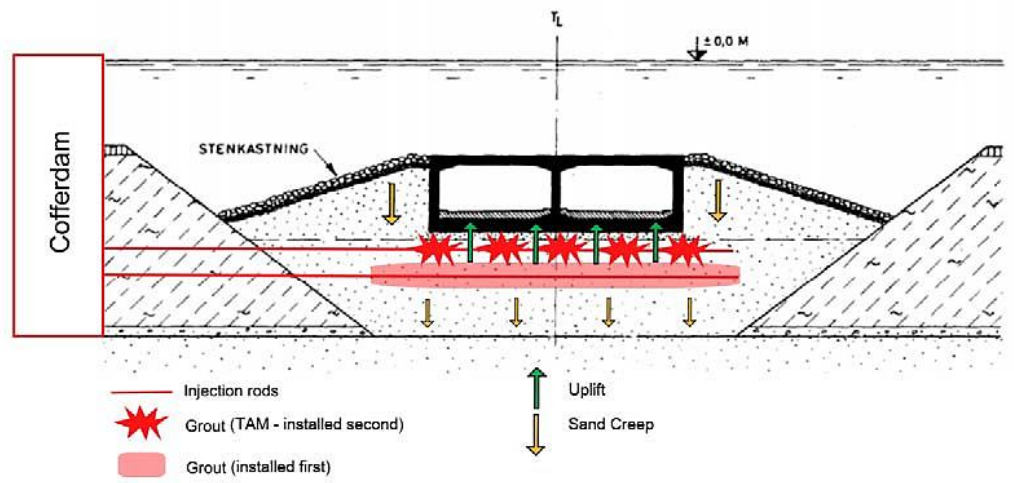

Figure 55: Cross-sectional view of the horizontal compensation grouting for the Limfjord Tunnel (ATKINS et al., 2019).

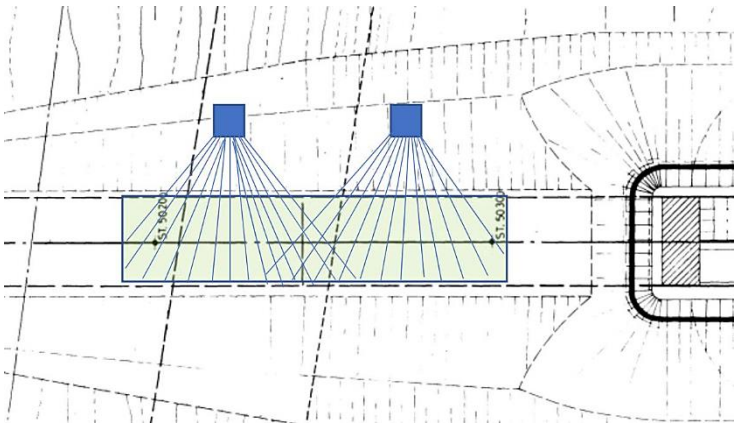

Figure 56: Top view of the horizontal compensation grouting for the Limfjord Tunnel (ATKINS et al., 2019). The blue squares indicate the cofferdams, from which the grouting could be performed.

6.3. Evaluation

This subsection evaluates the potential solutions, after which the maintenance and renovation strategy of Rijkswaterstaat is derived. Five solution alternatives were included, which involve advanced monitoring and inspection, corrective injection of leakages, repairing the structural connection, installing additional waterproofing, and compensation grouting. These solutions can roughly be divided into three groups, from a technical point of view. First of all, with advanced monitoring and inspection, a lot useful data and scientific knowledge could be obtained, which ensures maintenance and renovation to be performed more focused and efficient in the long-term. Secondly, the current way of correctively injecting leakages could be improved, resulting in improved maintenance. Eventually, three drastic renovation solutions are described that could induce more efficient maintenance over the lifespan of the tunnel structures. Here, repairing the structural connection recovers the structural performance, additional waterproofing ensures watertightness, and compensation grouting provides control over (future) ongoing settlements.

Table 9 presents the Technology Readiness Level (TRL) for each of the solution alternatives. The corrective injection of leakages and installing additional drainage (between brackets) both score the maximum, as the technologies have proven themselves. Advanced monitoring gains an 8, due to its successful pilot in an operational tunnel. Additional waterproofing and compensation grouting require further development, specifically in terms of application to immersed tunnels, and therefore both score a 7. Repairing the structural connection requires the most additional development, both in terms of effectiveness and technical feasibility, and consequently gets a score of 6.

Table 9: TRL levels of the solution alternatives.

Solution Alternatives	TRL
Advanced Monitoring	8
Corrective Injection of Leakages	9
Repairing the Structural Connection	6
Additional Waterproofing	7 (9)
Compensation Grouting	7

The benefits of the alternatives can be classified into different categories, which has already been touched upon in subsection 6.1. Firstly, safety to road users regards a main objective of Rijkswaterstaat, and thus a valuable benefit. On top of that, tunnel availability provides the benefit of social impact by guaranteeing accessibility. Additionally, more efficient and effective maintenance causes the benefit of lower long-term costs. Furthermore, efficiency of human resources contains the advantage to cope with the limited number of professionals working in the infrastructure sector. Finally, the generalisability benefit involves the opportunity of applying standardisation, which entails an efficiency gain in the sector as a whole.

A techno-economic evaluation is performed for the five potential maintenance and renovation alternatives for the segment joints, as described thoroughly in Appendix G. A cost-benefit analysis has been conducted from a societal perspective, by using the Net Present Value (NPV) and Internal Rate of Return (IRR). The alternatives were evaluated by making a comparison with the current tunnel maintenance approach, in which only the deviating costs and benefits were considered. For the benefits, five categories were differentiated, as derived above. In addition, the analysis assesses all alternatives separately, without considering any relationship between the alternatives. Moreover, the uncertainty in the costs was estimated based on the Technology Readiness Levels of Table 9.

In the techno-economic evaluation, a lot of assumptions have been performed, which makes the results to be order of magnitude valid (as discussed in Appendix G.7). Hence, only the interpretation of the financial results will be presented here, and the exact numbers of Appendix G are not shown again. The interpreted results are distinguished in three groups:

- The alternatives of advanced monitoring and inspection and corrective injection of leakages both seem to be worth considering for investment.
- The alternatives of repairing the structural connection and additional waterproofing require further research to establish in which extent a potential investment would pay off.
- The compensation grouting alternative currently does not seem to be worth its investment, but this may change in the future through technological innovation.

Therefore, advanced monitoring and inspection, as well as corrective injection of leakages, should be part of the maintenance strategy regarding the segment joints. These alternatives could be put into practice in the short term, given the developed TRL scores. With respect to the renovation strategy, the alternatives of repairing the structural connection and additional waterproofing need to be further investigated, for potential application in (future) critical segment joints during the renovation. The ultimate potential effectiveness of these two alternatives is currently not entirely clear, as can also be indicated from the TRL ratings of 6 and 7. On top of that, compensation grouting should not be part of the renovation strategy, for the time being.

Eventually, the relationships between the different alternatives and their technical feasibility are discussed. In the cost-benefit analyses, the alternatives are considered financially independent of each other, which is a valid approach, but technically there are opportunities by combining alternatives. The alternatives of advanced monitoring and correctively injecting leakages can be combined, as the monitoring data and the specialised contractor's experience together will lead to better insights. Based on these insights, it will be easier to make a decision when the other three alternatives (repairing the structural connection, additional waterproofing and compensation grouting) should be applied in practice. Additionally, a combination of repairing the structural connection and installing additional waterproofing could be quite obvious, when a segment joint would have lost both its structural and waterproof function.

7. Conclusions & Recommendations

This section demonstrates the conclusions and recommendations of the research. The conclusions are presented in subsection 7.1, where the main research question is answered, and the answers to the sub questions are presented. Next, the recommendations are described in subsection 7.2, where a distinction is made between scientific and practical recommendations.

7.1. Conclusions

In this subsection, the conclusions are demonstrated. First and foremost, the answer to the main research question is given, which was introduced in the introduction of section 1. Additionally, the answers to the sub question are presented, which are underlying the answer of the main question.

➢ **Main Question:** ***How to assess and optimise the performance of existing immersed tunnels subjected to ongoing settlements, regarding the segment joint functioning?***

The performance of an existing immersed tunnel could be assessed by determining its structural reliability over time, and subsequently establishing the tunnel unavailability, as a result of appearing leakages. On top of that, the critical segment joints can be identified, enabling to perform focused maintenance and renovation on the segment joints. In this way, the tunnel performance is optimised, and the remaining lifespan of the tunnel is maximised. The developed research methodology consists of a Monte Carlo approach, which is applied on a structural tunnel model, to determine the failure probabilities of the segment joints. Based on this, the structural reliability and tunnel availability could be derived, and the (future) critical segment joints could be identified. Hence, the performance of the segment joints can be assessed and optimised, for the threat of ongoing settlements.

The research methodology is implemented on the Noordtunnel case, as this tunnel showed excessive settlements, and a renovation will be performed in the coming years. The input parameters were quantified as stochastic parameters, including two settlement projection cases of a logarithmic and linear increase. The determined structural reliability of the Noordtunnel decreases over time, as the ongoing settlements increase. In addition, the unavailability of the tunnel is estimated to be roughly one day annually. Segment joints S12, S13, and S43 are the (future) most critical segment joints, and to a lesser extent joints S21, S22, S32, and S42. Noteworthy, the research methodology involves considerable uncertainty in the results and sensitivity analysis, allowing for a qualitative assessment only. The maintenance and renovation strategy for the segment joints contain various solutions. Advanced monitoring and inspection is required, and improved corrective leakage injection should be in the maintenance strategy. While repairing the structural connection and additional waterproofing should be further developed, as part of the renovation strategy (including the combination of both solutions). Figure 57 summarises the entire approach to assess and optimise the tunnel performance.

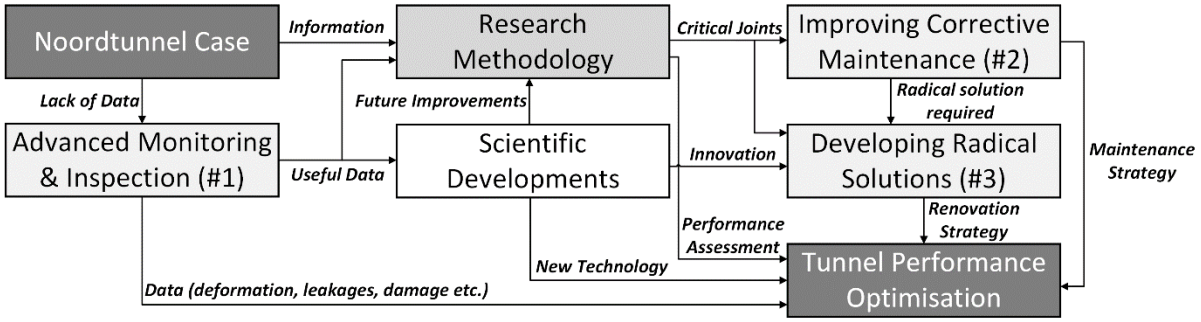

Figure 57: Overview assessing and optimising the performance of existing immersed tunnels subjected to settlements.

- **Sub question 1:** ***In which way could a parametric model simulate an immersed tunnel structure subjected to ongoing settlements?***

The research methodology consists of a model that embodies the structure of an immersed tunnel. The structure is modelled with beam elements that are supported by distributed springs, connected by translation and rotational springs, and subjected to a (vertical) distributed load. The soil-structure interaction is represented by the distributed springs, the stiffness of the immersion and segment joints is included in the discrete springs, and the resulting foundation loading is considered in the distributed load. The beam elements take three degrees of freedom into account: vertical deformation (v), axial deformation (u), and rotation (φ). In addition, the approach structures are assumed to be fixed points in the model.

By solving the differential equations of the beam elements at a given input, the structural model produces an output of the displacement, rotation, bending moment, and shear force diagrams over the tunnel length. Three different sets of boundary conditions have been considered for the differential equations of the structural model:

- *Model 1* prescribes the displacement at all the immersion and segment joints.
- *Model 2* prescribes displacements at immersion joints and rotations at segment joints.
- *Model 3* prescribes the rotation at all the immersion and segment joints.

The prescribed displacements follow from the settlement data, where the prescribed rotations are based on the bending moments with the rotational joint stiffness. The axial deformation of the concrete segments is included, by considering different deformation modes with a probability of occurrence, as no axial deformation measurements were available. Herewith, these modes are based on the seasonal behaviour of the tunnel structure, due to the temperature induced deformation.

For the segment joints, two failure mechanisms were taken into account. First of all, shear force failure of the collar in a segment joint was considered, which is the most likely mechanism in case of ongoing settlements. Moreover, rotational failure was defined as exceeding the maximum deformation of a segment joint, when the tunnel structure is examined from a geotechnical perspective. For the Noordtunnel case, the outcomes of the structural models were demonstrated for a parametric input, where ongoing settlements were one of the input parameters for the models.

- **Sub question 2:** ***How to assess the structural reliability and availability over time of an immersed tunnel subjected to ongoing settlements?***

The reliability and availability of the immersed tunnel structure are determined by using a Monte Carlo approach for the ongoing settlements. In this approach, an N number of simulations was executed, where each simulation solves the structural model for a random set of parameters, based on their stochastic distribution. The failure probability has consequently been determined by dividing the number of simulations that lead to failure over the total amount of simulations ($P_f = n_f/N$). Subsequently, the structural reliability was established by taking the difference between 1.0 and the failure probability ($R = 1 - P_f$). Next, the availability was estimated based on the reliability, by considering the tunnel as a fully repairable system. Note that a key assumption contains the failure definition, which involves failure of at least one segment joint, due to either shear force or rotation.

The input parameters were quantitatively determined, by means of including the uncertainty in the stochastic parameters. For the Noordtunnel case, the settlements were projected until 2050, where the extreme cases of logarithmically and linearly increasing settlements were distinguished. The determined structural reliability of the Noordtunnel decreases over time, as the ongoing settlements increase, regardless of the model, settlement projection or failure mechanism. However, the extent

to which the reliability develops over time is quite aberrant for the aforementioned. Shear force turned out to be the dominant failure mechanism over rotation. Subsequently, the unavailability of the tunnel has been estimated, assuming a direct relationship between the appearance of leakages and the loss of structural connection at a segment joint. The availability results of the Noordtunnel contain a lot of uncertainty, and could therefore only be interpreted as an order of magnitude. As a result, the availability development over time could not be assessed properly. A rough estimation for the unavailability would be one day annually, however further research is required for a more accurate assessment. Noteworthy for the Noordtunnel case, *Model 2* seems to correspond closest to reality out of the three structural models.

- **Sub question 3:** ***To which extent could the (future) critical segment joints of an immersed tunnel be identified?***

The critical segment joints can be identified qualitatively, for an immersed tunnel subjected to ongoing settlements, according to the research methodology. The uncertainty which is involved in the methodology, causes the results to be interpretable as order of magnitude only. For the Noordtunnel case, the critical segment joints were determined by identifying the joints with high failure probabilities, for the three structural models. Examining the three structural models equally, indicates that S12, S13, and S43 are the (future) most critical segment joints. On top of that, segment joints S21, S22, S32, and S42 seem to be critical to a lesser extent. In the past, leakages appeared at the segment joints S13, S22, S32, and S34, of which 75% was indicated as (semi) critical, according to the research methodology. It should be noted that in reality (small) leakages will remain undetected, and poor execution performance could also be the cause of leakages. Therefore, it is not possible to firmly conclude the validation of the methodology, although the fact that three out of four joints with known leakages were indeed indicated to be critical by the model does not contradict this either.

- **Sub question 4:** ***Which maintenance and renovation strategy could potentially improve the performance of the segment joints?***

In the research, several solutions have been investigated to determine the maintenance and renovation strategy for the segment joints of immersed tunnels. Five solution alternatives were taken into consideration, including advanced monitoring and inspection, corrective injection of leakages, repairing the structural connection, installing additional waterproofing, and compensation grouting. With the advanced monitoring and inspection alternative, a lot of useful data and scientific knowledge could be obtained, which supports future maintenance and renovation to be performed more focused and efficient. Additionally, the present corrective way of maintenance, by injecting leakages, could be improved in terms of process and organisation. Moreover, three drastic renovation solutions could induce more efficient maintenance over the tunnel lifespan. Repairing the structural connection recovers the structural performance, additional waterproofing ensures watertightness, and compensation grouting provides control over (future) ongoing settlements.

The solution alternatives have been assessed techno-economically, by a societal cost-benefit analysis. The analysis could be interpreted as an order of magnitude only, since there are several assumptions underlying the approach. It followed that, advanced monitoring and inspection (TRL 8), and improved corrective injection of leakages (TRL 9) are worth considering investing in. These solutions should therefore be part of the maintenance strategy. Furthermore, repairing the structural connection (TRL 6), and additional waterproofing (TRL 7) require further research to establish the technical and financial feasibility. Further developing these solutions should be part of the renovation strategy, including the combination of both solutions. Finally, compensation grouting (TRL 7) currently does not seem to be worth its investment, and should not be part of the renovation strategy.

7.2. Recommendations

This subsection presents the recommendations, where the scientific recommendations for further research are extensively explained (7.2.1), and the practical recommendations to Rijkswaterstaat are described (7.2.2).

7.2.1. Scientific Recommendations

The scientific recommendations are threefold. First and foremost, more data of the tunnel structure and its environment should be collected, as a lack of data is the main obstacle for further improving the research methodology. Additionally, the global structural model could be enhanced, by further contemplation of the soil-structure interaction, and optimisation of the boundary conditions. Finally, the structural model could be further developed at joint level, including the relation between joint opening and rotation, and a more detailed consideration of the failure mechanisms, which could be done by using Finite Element Method techniques in three dimensions. These are explained in more detail below:

1. It is highly recommended to gather more data of tunnel structures and their environment. The foundation stiffness, segment joint capacity, and the settlements demonstrated to be very influential parameters, while containing a significant amount of uncertainty. Too limited subsurface data is available for the foundation stiffness, the actual condition of the segment joints is unknown, and the settlement data is of limited frequency and accuracy. More data is required to better quantify these parameters. This includes gathering data more frequently, and acquiring a higher data quality. It should be considered to install advanced monitoring systems in the tunnels, which could measure deformations, stresses or water flow. On top of that, it should be attempted to collect more data with innovative technologies, for example in the fields of ultrasonics or digitalisation. In addition, investigating the option of applying Cone Penetration Testing through the tunnel slab, as well as measuring the water pressure below the slab, could be very advantageous to determine the foundation stiffness.

2. Moreover, further development of the structural model would be recommended, especially regarding the soil-structure interaction. The foundation stiffness proved to have a crucial impact on the outcomes of the structural model, compared to the stiffness of the joints or the vertical loading. It could be thought to apply two serial distributed spring layers, to model the tunnel (sand flow) foundation and the deeper soil layers separately. However, this requires more data in the first place, as described in the recommendation above. Furthermore, optimisation of the boundary conditions in the structural model requires further research. For instance, it could be investigated whether it is possible to use five boundary conditions at a joint, by using an ‘overdetermined system’.

3. Ultimately, it is recommended to enhance the structural model at the level of the segment joints as well. The failure mechanism of the segment joint could be considered in more depth, by means of performing 3D Finite Element Method calculations. This causes the segment joint capacity to be determined more accurately, including both the (favourable) influence of the normal force and soil-structure interaction at the resistance side. Also, the relation between the opening of a segment joint and a developing rotation within the joint, should be further investigated. Additionally, the cross-sectional deformation of the joint could be taken into consideration more in depth. This relates to the redistribution of forces across the cross section of a segment joint.

7.2.2. Practical Recommendations

The main practical recommendation is to explicitly include the segment joints of immersed tunnels into the maintenance and renovation scope of Rijkswaterstaat. Notably, it will be a challenge to put the maintenance and renovation strategy for the segment joints into practice. In addition, first more research is required to determine how critical the segment joints will exactly be in the future. However, Rijkswaterstaat has the responsibility to perform at the best level possible, and to prepare for future risks that could affect the structural performance of immersed tunnels. Therefore, the following three recommendations are prescribed (and their relations are presented in Figure 57):

1. It is recommended to install advanced (deformation) monitoring systems in the Noordtunnel and other immersed tunnels of Rijkswaterstaat. These systems generate lots of useful data, which provides insight into the structural tunnel condition, encourages the development of scientific knowledge, enables optimising maintenance and renovation in the long-term, and requires fewer human resources. In addition to deformation monitoring, other types of monitoring such as flow measurements and visual inspection, are also recommended to be applied. It should be noted that, advanced monitoring and improved regular inspection are conditionally required for further developing the future predictive maintenance strategy, for the tunnels of Rijkswaterstaat.

2. Furthermore, it is recommended to optimise the corrective way of maintenance by injecting leakages (in segment joints). The current approach of injection in tunnels is technically very solid, but process wise and organisationally there is room for improvement. Hence, three proposals are made, which are described as follows. Firstly, all relevant information regarding the tunnel structure (including the segment joint detailing) should be collected and stored at a single location (for instance, as-built drawings and appeared leakages). Secondly, one central point of contact within Rijkswaterstaat should be organised (for all regional departments combined), where all information and leakage expertise is available. Finally, a multi-year contract with a specialised contractor should be drafted, for the injection of leakages in tunnels (including the reporting), apart from the regular maintenance and renovation contracts. This would allow better injection preparation and knowledge assurance, through cooperation between Rijkswaterstaat and the contractor. In spite that the maintenance approach will be still corrective, it will become more efficient and risks will be reduced.

3. Finally, it is recommended to further research and develop the radical renovation solutions for very critical segment joints. This includes repairing the structural connection, and installing additional waterproofing of a segment joint. The combination of both solutions should also be further developed, as the solutions complement each other well. It is simply not an option to be unprepared for risky events like the failure of a segment joint, as the current practice of some newsworthy tunnels have demonstrated. For the Noordtunnel, the radical solutions could be further developed for the considered critical segment joint(s), e.g. ‘S13’. The upcoming renovation of the Noordtunnel is the perfect opportunity to first and foremost further investigate an intended critical segment joint in practice, with a similar approach as the immersion joints were researched in recent years.

References

ATKINS, COWI, TEC, ChristiansenEssenbak, DeltaMarineConsultants, nmGeo & RAMBOLL (2019). *Limfjord Tunnel assessment and retrofitting-technical summary report, v1.0.* Technical report.

Atmakusuma, P. A. (2023). *Settlement Predictions of The Noordtunnel – A Numerical Simulation.* Master Thesis, Delft University of Technology. TU Delft Repository.

Arcadis (2015). *Verbetervoorstellen monitoring tunnels* (Nr. 078346567:A). Rijkswaterstaat Grote Projecten en Onderhoud.

Bakker, K. J., Vervuurt, A. H. J. M., & Hendrix, B. (2012). *Monitoradvies voor afzinktunnels: Eindrapportage 2012* (TNO-060-DTM-2012-03344). InfraQuest, Competence centre for roads and structures.

Benhaddou, N. (2013). *Invloed Getijdewerking op de stabiliteit van de Vlaketunnel – Geotechnisch en constructief beoordeling status tunnel.* Master Thesis, Delft University of Technology. TU Delft Repository.

Birolini, A. (2014). *Reliability Engineering, Theory and Practice*. Berlin: Springer-Verlag.

Broere, W., & Zhang, X. (2023). Monitoring daily and seasonal movement of an immersed tunnel. In *CRC Press eBooks* (pp. 2999–3006). https://doi.org/10.1201/9781003348030-362

COB (2020). *Overzicht zinkvoegonderzoeken: Een samenvatting van vijf jaar onderzoek aan (klemverbindingen van) zinkvoegen.* Het Nederlands kenniscentrum voor ondergronds bouwen en ondergronds ruimtegebruik (COB). https://www.cob.nl/kennisbank

COB (2022). *Werkwijzer monitoring zinktunnels: Gids voor het gestructureerd meten van tunneldeformaties.* Het Nederlands kenniscentrum voor ondergronds bouwen en ondergronds ruimtegebruik (COB). https://www.cob.nl/kennisbank

COB (2023). *Handboek Tunnelbouw versie 2023.1: Civieltechnisch Ontwerp en Realisatie van Tunnels.* Het Nederlands kenniscentrum voor ondergronds bouwen en ondergronds ruimtegebruik (COB). https://www.handboektunnelbouw.nl/

Deltares (2023). *WNZ Tunnels functieoverschrijding 2021-2022 (02-02-2023).*

Gavin, K., Broere, W., Kovačević, M., & De Haas, K. (2019). Investigation of the remaining life of an immersed tube tunnel in The Netherlands. *Tunnels and Underground Cities: Engineering and Innovation meet Archaeology, Architecture and Art*, 4831–4838. https://doi.org/10.1201/9780429424441-512

Grantz, W. C. (2001a). Immersed tunnel settlements. Part 1: nature of settlements. *Tunnelling and Underground Space Technology, 16*(3), 195–201. https://doi.org/10.1016/s0886-7798(01)00039-6

Grantz, W. C. (2001b). Immersed tunnel settlements. Part 2: case histories. *Tunnelling and Underground Space Technology, 16*(3), 203–210. https://doi.org/10.1016/s0886-7798(01)00040-2

Holschemacher, K., & Löber, P. (2019). Experimental investigation on friction between foundation slabs and substructure. *Modern building materials, structures and techniques.* https://doi.org/10.3846/mbmst.2019.143

Lunniss, R., & Baber, J. (2013). *Immersed tunnels*. CRC Press.

Kloosterman, J. (2014). *Lekkage Noordtunnel noordbuis voeg 2c-2d.* Memo t.a.v. Rijkswaterstaat West-Nederland Zuid.

Leeuw, L. (2008). *Lekkage in Tunnels.* Rijkswaterstaat Bouwdienst. https://www.cob.nl/kennisbank

Leeuw, L. (2018). *Lekkage in Tunnels II.* Uitgave RWS-GPO. https://www.cob.nl/kennisbank

NEN (2011). *NEN-EN 1992-1-1+C2:2011, Eurocode 2: Design of concrete structures–- Part 1-1: General rules and rules for buildings.* https://connect.nen.nl/

NEN (2016). *NEN-EN 1997-1+C1+A1:2016, Eurocode 7: Geotechnical design–- Part 1: General rules.* https://connect.nen.nl/

Olsen, T., Kasper, T., & De Wit, J. (2022). Immersed tunnels in soft soil conditions experience from the last 20 years. *Tunnelling and Underground Space Technology*, *121*, 104315. https://doi.org/10.1016/j.tust.2021.104315

Parwani, K. (2014). *Quantifying the impact of loads on connections between segments of an immersed tunnel.* Master Thesis, Delft University of Technology. TU Delft Repository.

Rijkswaterstaat (2019). *Adviesrapport behorend bij Deformatiemeting Tunnel onder de Noord – 38C-113-01-18*. Opnamedatum 2019-04-11 & 2019-04-12, Versie: 06-09-2019.

Saveur, J., & Grantz, W. C. (1997). Chapter 3 Structural Design of Immersed tunnels. *Tunnelling and Underground Space Technology, 12*(2), 93–109. https://doi.org/10.1016/s0886-7798(97)90015-8

Schols, I. (2012a). *Segmentvoegcapaciteit van de Kiltunnel, Deel 1 – Afgezonken tunnels en zettingen.* Master Thesis, Delft University of Technology. TU Delft Repository.

Schols, I. (2012b). *Segmentvoegcapaciteit van de Kiltunnel, Deel 2 – Capaciteitsbepaling.* Master Thesis, Delft University of Technology. TU Delft Repository.

Schols, I., Braam, R., & Vervuurt, A. (2013a). Zettingen en rotaties zinktunnels: Zettingsgedrag en de capaciteit van mootvoegen in zinktunnels (1). *Cement.* Retrieved from https://www.cementonline.nl/artikel/zettingen-en-rotaties-zinktunnels

Schols, I., Braam, R., & Vervuurt, A. (2013b). Dwarskrachten kraagconstructie: Zettingsgedrag en de capaciteit van mootvoegen in zinktunnels (2). *Cement.* Retrieved from https://www.cementonline.nl/artikel/dwarskrachten-kraagconstructie

Steunpunt Economische Expertise (2022). *Waarderingskengetallen verkeersveiligheid.* Rijkswaterstaat Water, Verkeer en Leefomgeving. Retrieved from https://www.rwseconomie.nl/documenten/publicaties/2016/februari/18/waarderingskengetallen-verkeersveiligheid

Sweco (2020). *Risicoanalyse Noordtunnel–- Onderdeel van het tunnelprogramma COB* (Nr. SWNL0270141). COB Commissie Deformaties. https://www.cob.nl/kennisbank

Tang, C., He, S., Guan, Z., Zhou, W., & Yin, Z. (2023). Enhanced elastic beam model with BADS integrated for settlement assessment of immersed tunnels. *Underground Space*, *12*, 79–88. https://doi.org/10.1016/j.undsp.2023.02.005

TEC (1989). *Tunnel onder de Noord – Berekening Tunnelelementen.* Identificatienummer: NT.02.02.KP22.1

TEC (1992). *De Noordtunnel referentie meting hoogteligging tunnel–- Bijlage 2 zettingsresultaten TE 1 t/m 4.* Referentie: 1000N/CB/LG/B92512.

TNO (2021). *Data-enhanced reliability assessment method for tunnels* (Nr. TNO-2021-R12021A). https://www.cob.nl/kennisbank

Van Montfort, R. (2018). *Insufficiency of immersion joints in existing immersed tunnels – Case study on functioning of Gina-seal and Omegaseal in the Kil Tunnel.* Master Thesis, Delft University of Technology. TU Delft Repository.

Van Oorsouw, R. S. (2010). *Behaviour of segment joints in immersed tunnels under seismic loading.* Master Thesis, Delft University of Technology. TU Delft Repository.

Wang, Y., Wang, L., Min, X., & Wu, M. C. (2023). Deformation analysis for an immersed tunnel considering cyclic degradation of substratum soil. *Applied Ocean Research*, *138*, 103681. https://doi.org/10.1016/j.apor.2023.103681

Zhang, X., & Broere, W. (2019). Settlements of immersed tunnel on soft ground: A case study. *Tunnels and Underground Cities: Engineering and Innovation meet Archaeology, Architecture and Art*, 1234–1241. https://doi.org/10.1201/9780429424441-132

Zhang, X., & Broere, W. (2023a). Design of a distributed optical fiber sensor system for measuring immersed tunnel joint deformations. *Tunnelling and Underground Space Technology*, *131*, 104770. https://doi.org/10.1016/j.tust.2022.104770

Zhang, X., & Broere, W. (2023b). Monitoring of Tidal Variation and Temperature Change-Induced movements of an immersed Tunnel using Distributed Optical Fiber Sensors (DOFSs). *Structural control & health monitoring*, *2023*, 1–17. https://doi.org/10.1155/2023/2419495

Zhang, X., & Broere, W. (2023c). Monitoring seasonal deformation behavior of an immersed tunnel with distributed optical fiber sensors. *Measurement*, *219*, 113268. https://doi.org/10.1016/j.measurement.2023.113268

Zhang, X. (2023). *Monitoring the deformation behavior of an immersed tunnel with Distributed Optical Fiber Sensor (DOFS)*. Doctoral Thesis, Delft University of Technology. https://doi.org/10.4233/uuid:2d76b1f1-a60e-48e0-acbf-051628a76da7

A. Mechanical Beam Models

This appendix presents the models and accompanying ordinary differential equations for an axially loaded beam (A.1) and a Timoshenko beam (A.2), consecutively. Both beams are continuously elastically supported.

A.1. Axially Loaded Beam

The ordinary differential equation for an axially loaded beam, which is continuously elastically supported, is given by Equation 6. The mechanical model is shown in Figure 58, assuming a constant axial stiffness EA over the length of the beam.

$$\left.\begin{aligned} \varepsilon &= \frac{du}{dx} \\ N &= EA\varepsilon \\ \frac{dN}{dx} &= -q_x + k_x u \end{aligned}\right\} EA\frac{d^2u}{dx^2} - k_x u = -q_x$$

Equation 6: Derivation of an axially loaded beam equation, which is continuously elastically supported.

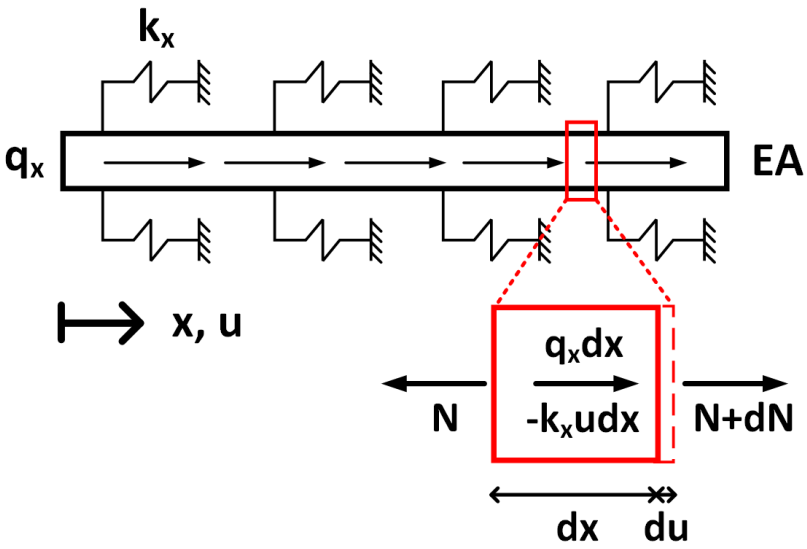

Figure 58: Mechanical model of a continuously elastically supported, axially loaded beam.

A.2. Timoshenko Beam

The Timoshenko beam theory is used for a continuously elastically supported beam with both bending and shear deformation included. The ordinary differential equation is given by Equation 7, and the mechanical model is displayed in Figure 59. The beam is assumed to be homogeneous with a constant cross section.

$$\left.\begin{aligned} \gamma &= \frac{dv}{dx} + \varphi \\ \kappa &= \frac{d\varphi}{dx} \\ V &= GA_{eff}\gamma \\ M &= EI\kappa \\ \frac{dM}{dx} &= V \\ \frac{dV}{dx} &= k_z v - q \end{aligned}\right\} \quad \begin{aligned} EI\frac{d^2\varphi}{dx^2} - GA_{eff}\left(\frac{dv}{dx} + \varphi\right) &= 0 \\ GA_{eff}\left(\frac{d^2v}{dx^2} + \frac{d\varphi}{dx}\right) - k_z v &= -q_z \end{aligned} \quad \left.\begin{aligned} EI\frac{d^3\varphi}{dx^3} - k_z v + q_z &= 0 \\ \frac{dv}{dx} &= -\varphi + \frac{EI}{GA_{eff}}\frac{d^2\varphi}{dx^2} \end{aligned}\right\}$$

Equation 7: Derivation of the Timoshenko beam equation, which is continuously elastically supported.

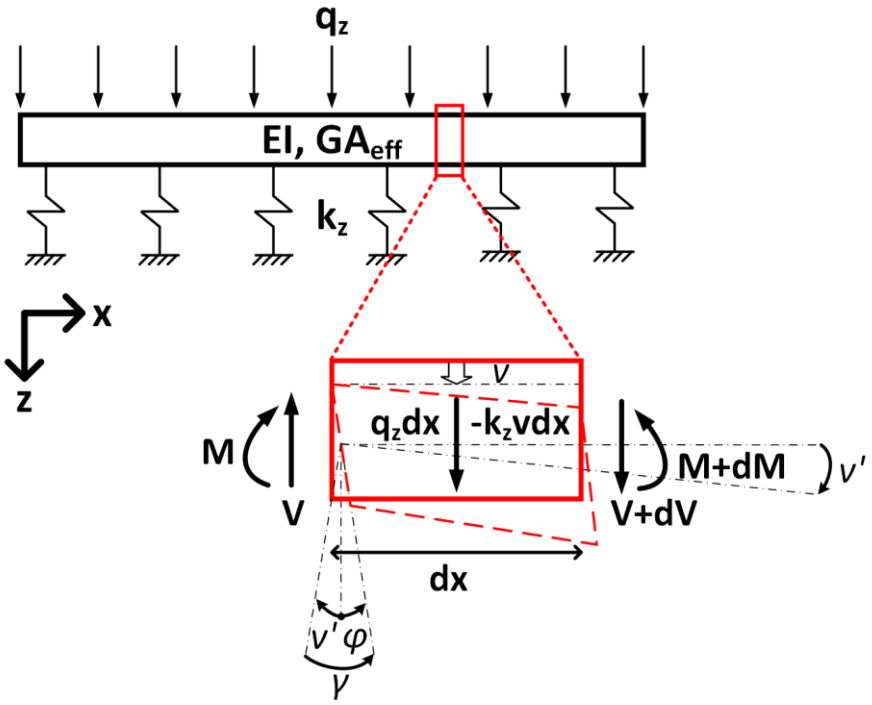

Figure 59: Mechanical model of a continuously elastically supported Timoshenko beam.

The Timoshenko beam is equivalent to the Euler-Bernoulli beam, if the last term of the second equation is negligible. An approximation when this is valid holds:

$$\frac{3EI}{GA_{eff}L^2} \ll 1$$

This would lead to Equation 8, which is shown below.

$$EI\frac{d^4v}{dx^4} + k_z v = q_z$$

Equation 8: Euler-Bernoulli beam equation for a homogeneous beam of constant cross section.

B. Comparison Outcomes Models

This appendix shows the displacement, rotation, moment and shear force curves for the three models. These are illustrated for the Noordtunnel case, with the mean parameter values in the 2020 situation.

B.1. Model 1

The displacement, rotation, moment and shear force curves for *Model 1* are displayed in Figure 60. Herewith, the displacements are prescribed at all the joints, which causes the rotations to be free.

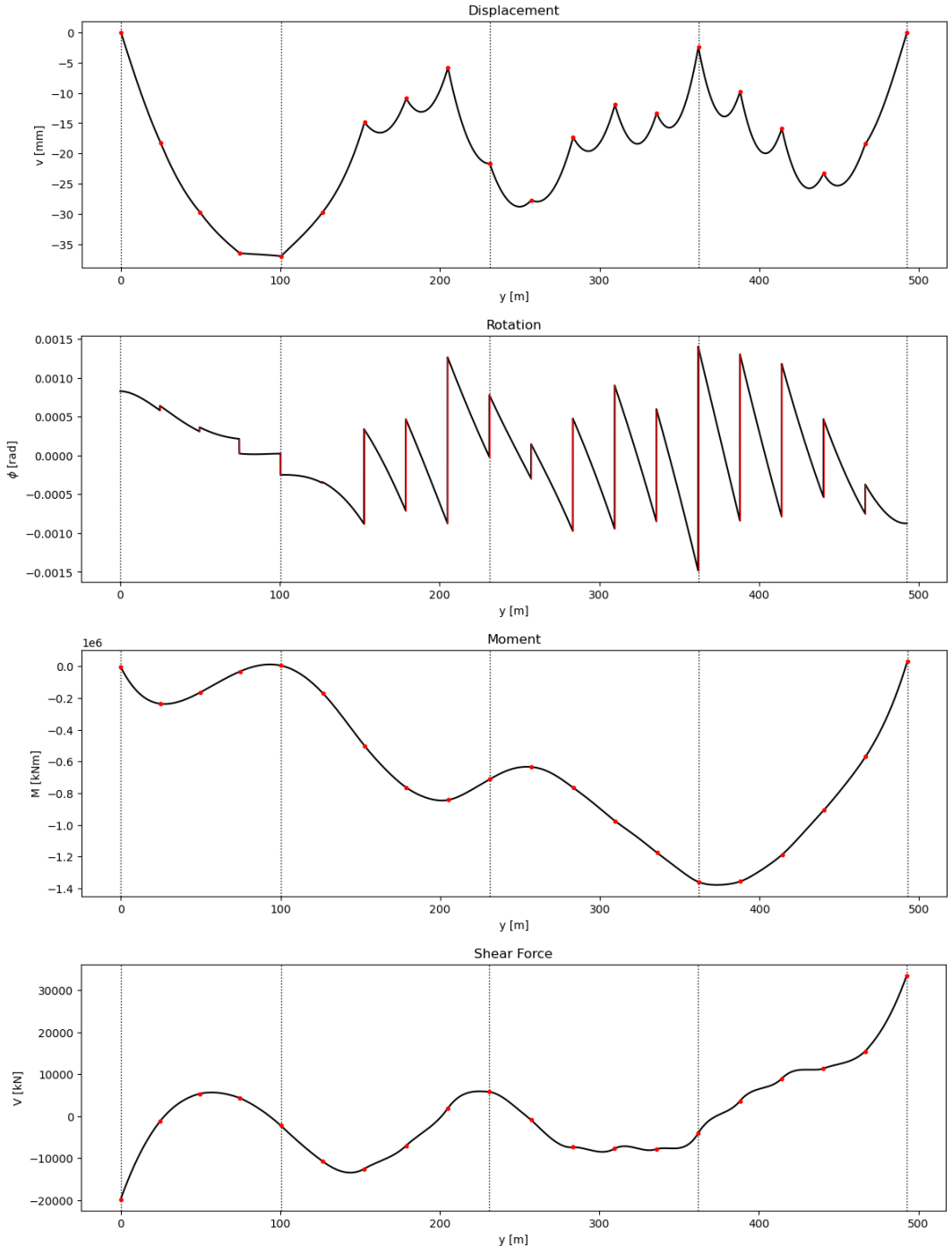

Figure 60: The displacement, rotation, moment and shear force curves of the Noordtunnel obtained for the mean parameters in the 2020 situation, according to Model 1 (prescribed displacements & free rotations).

B.2. Model 2

For *Model 2*, the displacement, rotation, moment and shear force curves are presented in Figure 61. In this model, the displacements are prescribed at the immersion joints, and the rotations are prescribed at the segment joints. Thus, the rotations at the immersion joints are free, as well as the displacements at the segment joints.

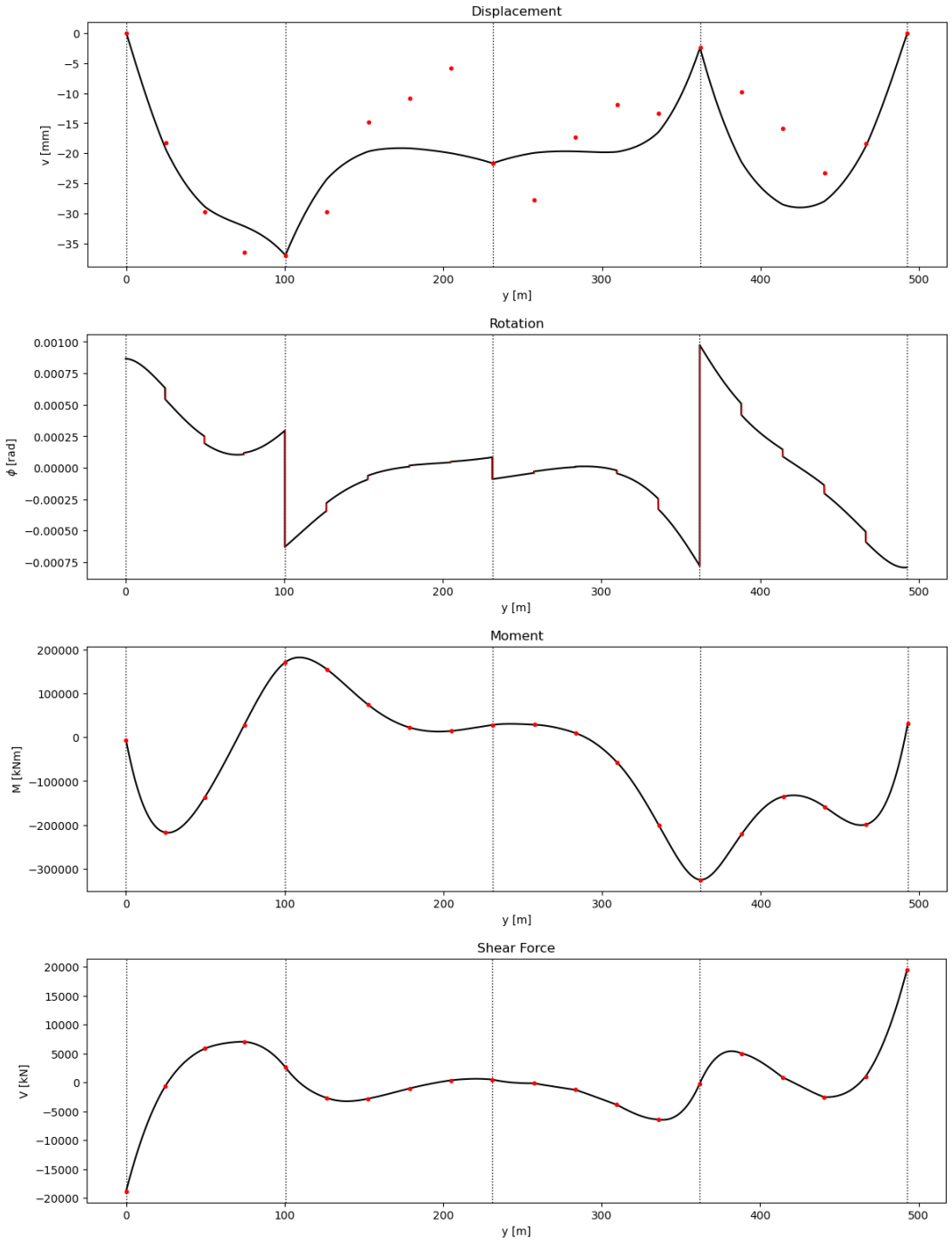

Figure 61: The displacement, rotation, moment and shear force curves of the Noordtunnel obtained for the mean parameters in the 2020 situation, according to Model 2 (prescribed displacements & free rotations at the immersion joints, and prescribed rotations & free displacements at the segment joints).

B.3. Model 3

The displacement, rotation, moment and shear force curves for *Model 3* are visualised in Figure 62. For this model the rotations are prescribed at all the joints, resulting in free displacements.

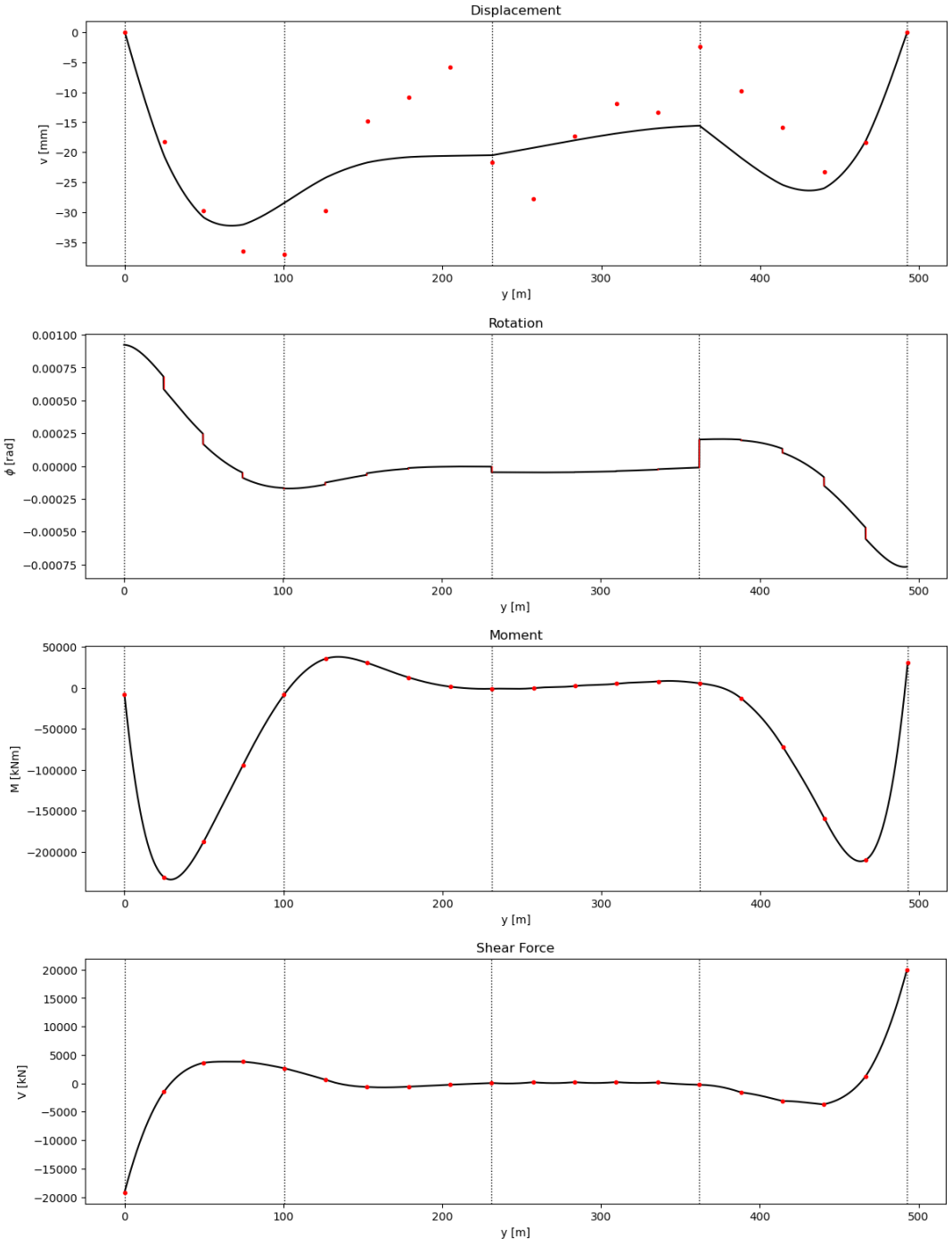

Figure 62: The displacement, rotation, moment and shear force curves of the Noordtunnel obtained for the mean parameters in the 2020 situation, according to Model 3 (prescribed rotations & free displacements).

C. Information Noordtunnel Case

In this appendix, some background documentation of the Noordtunnel is presented, in which primarily the as-built drawings are presented (C.1). Subsequently, the initial settlement measurements from immersion are demonstrated (C.2).

C.1. As-Built Drawings

Figure 63 and Figure 64 display the longitudinal section and detailed cross section for the case of the Noordtunnel.

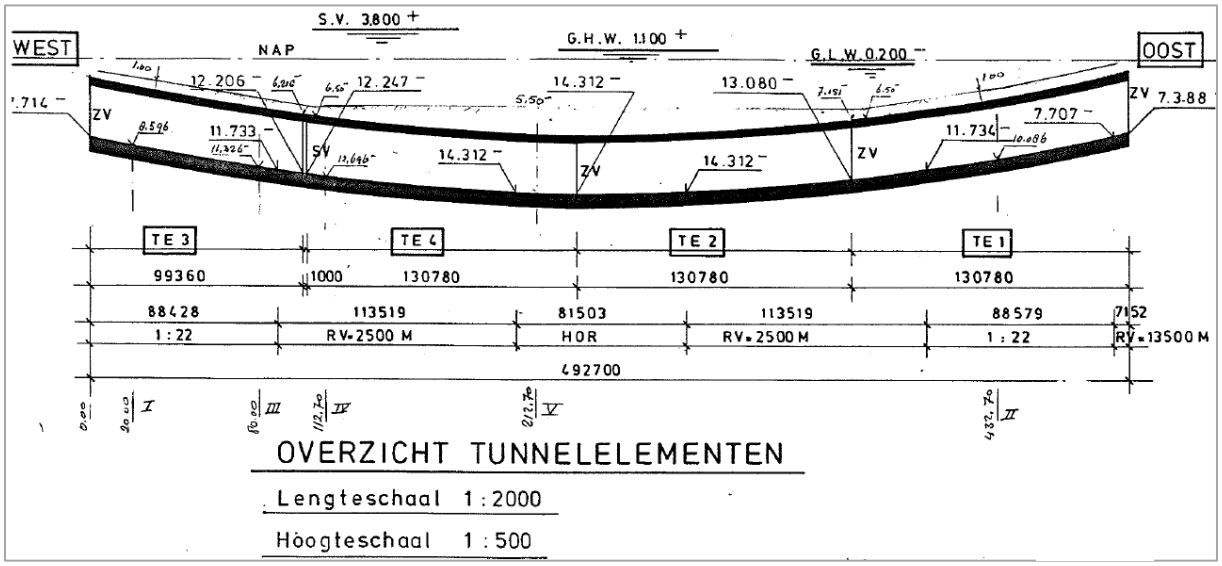

Figure 63: Longitudinal section of the Noordtunnel (TEC, 1989).

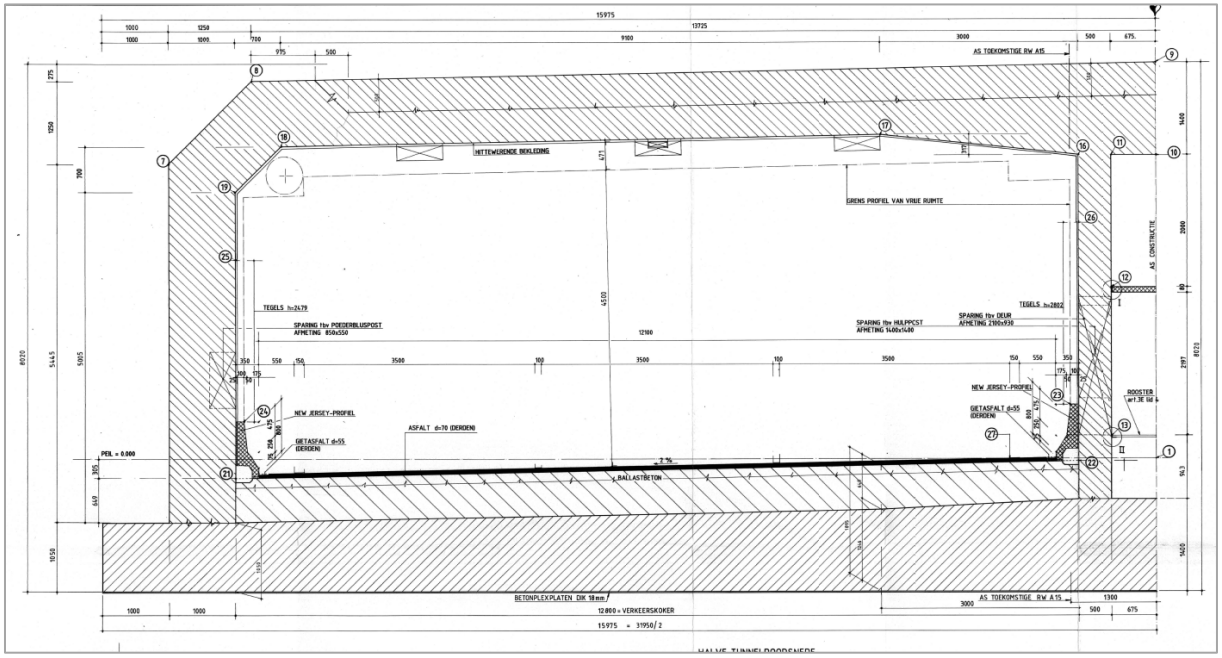

Figure 64: Details of the Noordtunnel cross section (archive Rijkswaterstaat).

C.2. Initial Settlement Measurements

The initial settlement measurements are shown in Figure 65 to Figure 68, for tunnel elements 1 to 4.

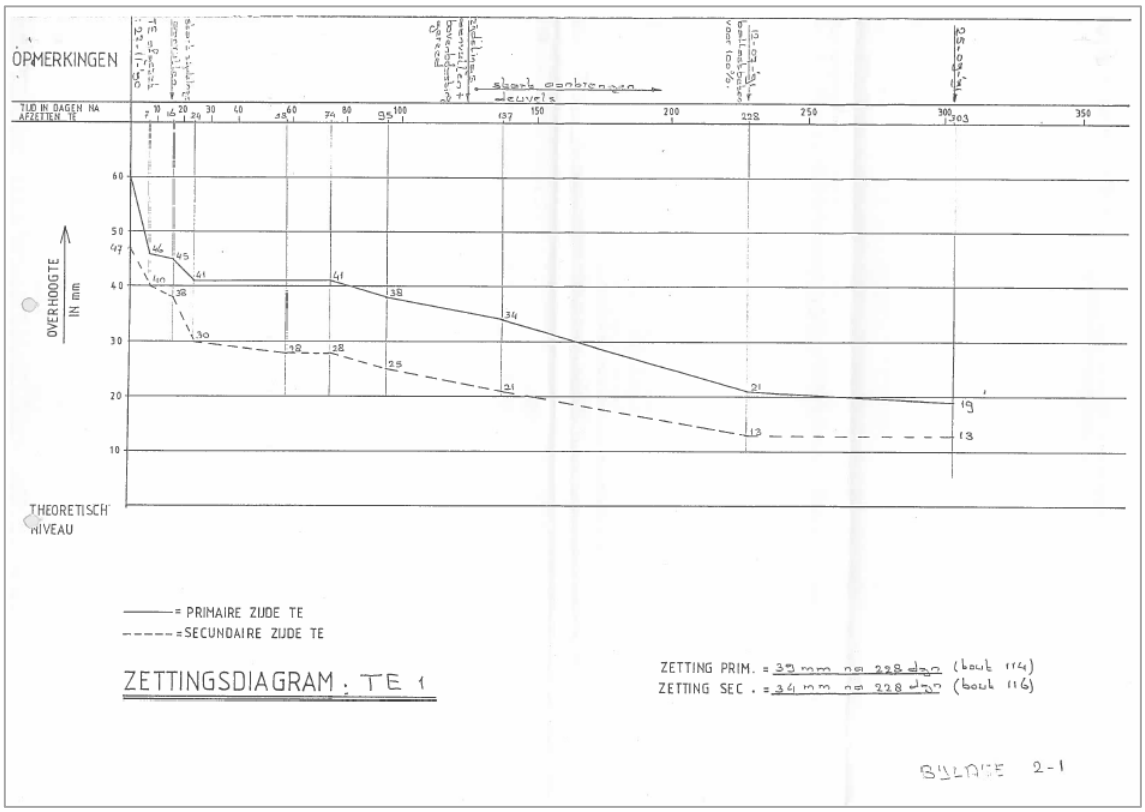

Figure 65: Settlement measurements at both ends of Tunnel Element 1, for the initial 303 days after immersion (TEC, 1992).

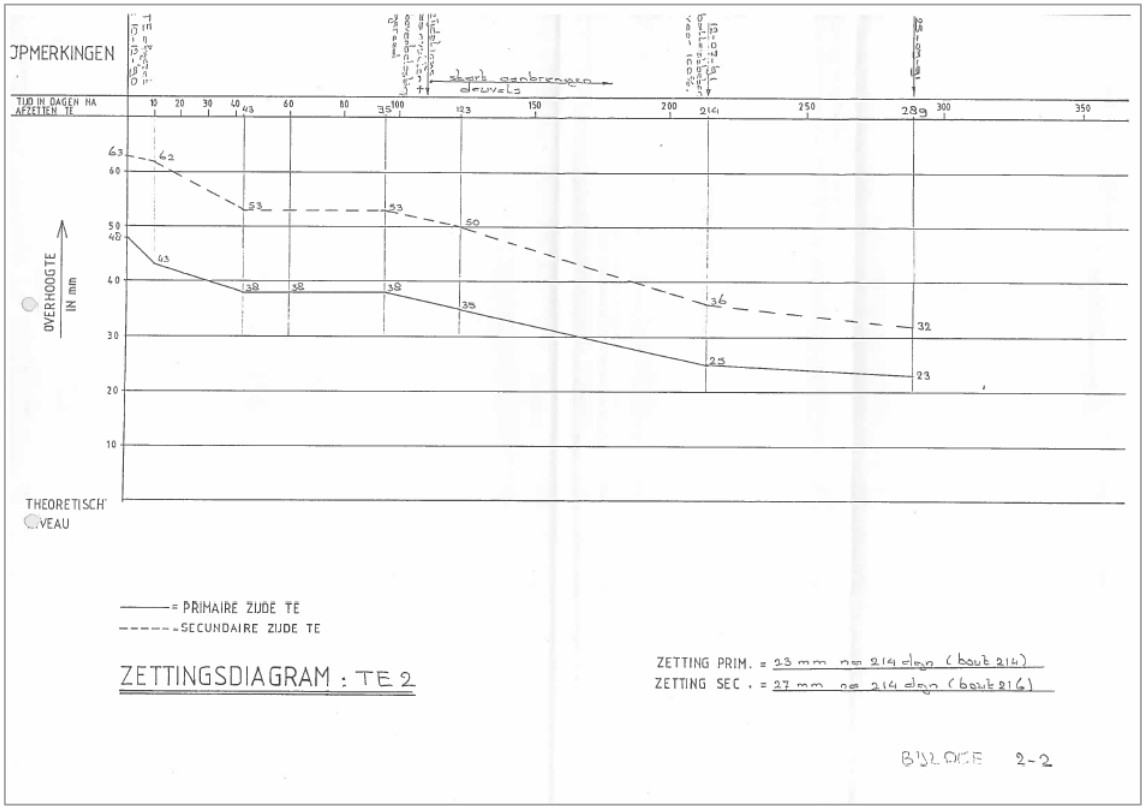

Figure 66: Settlement measurements at both ends of Tunnel Element 2, for the initial 289 days after immersion (TEC, 1992).

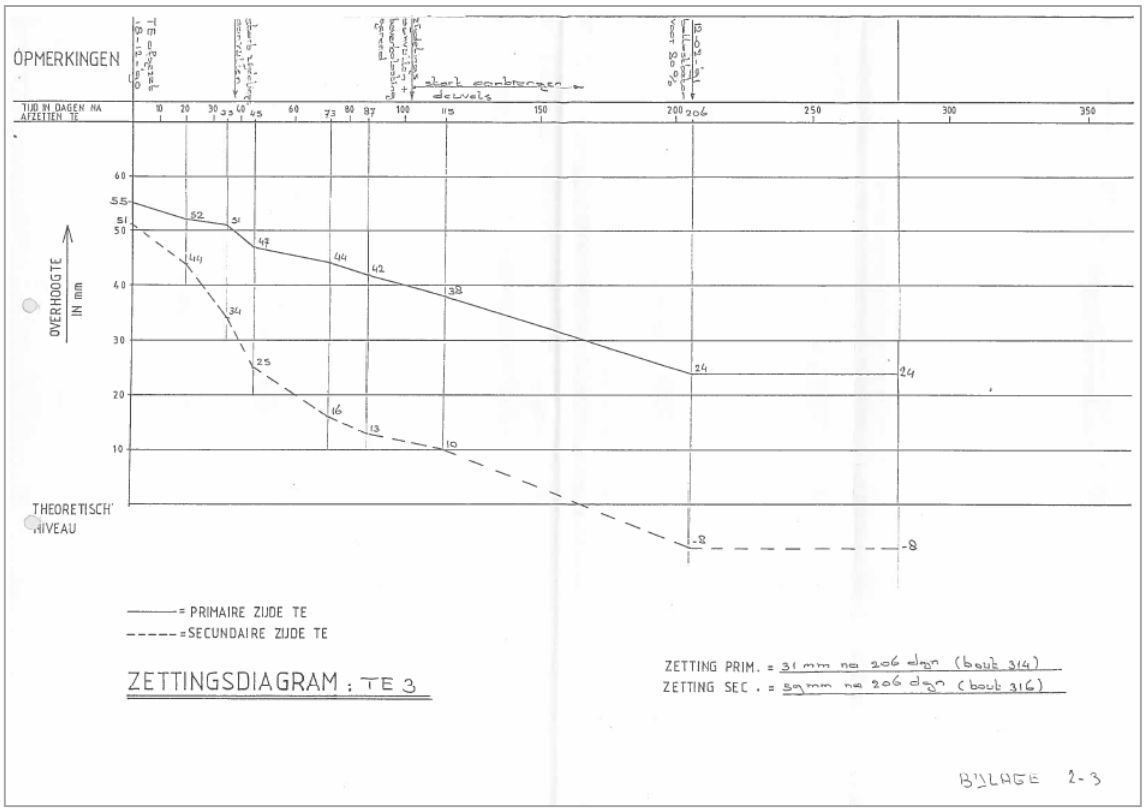

Figure 67: Settlement measurements at both ends of Tunnel Element 3, for the initial 281 days after immersion (TEC, 1992).

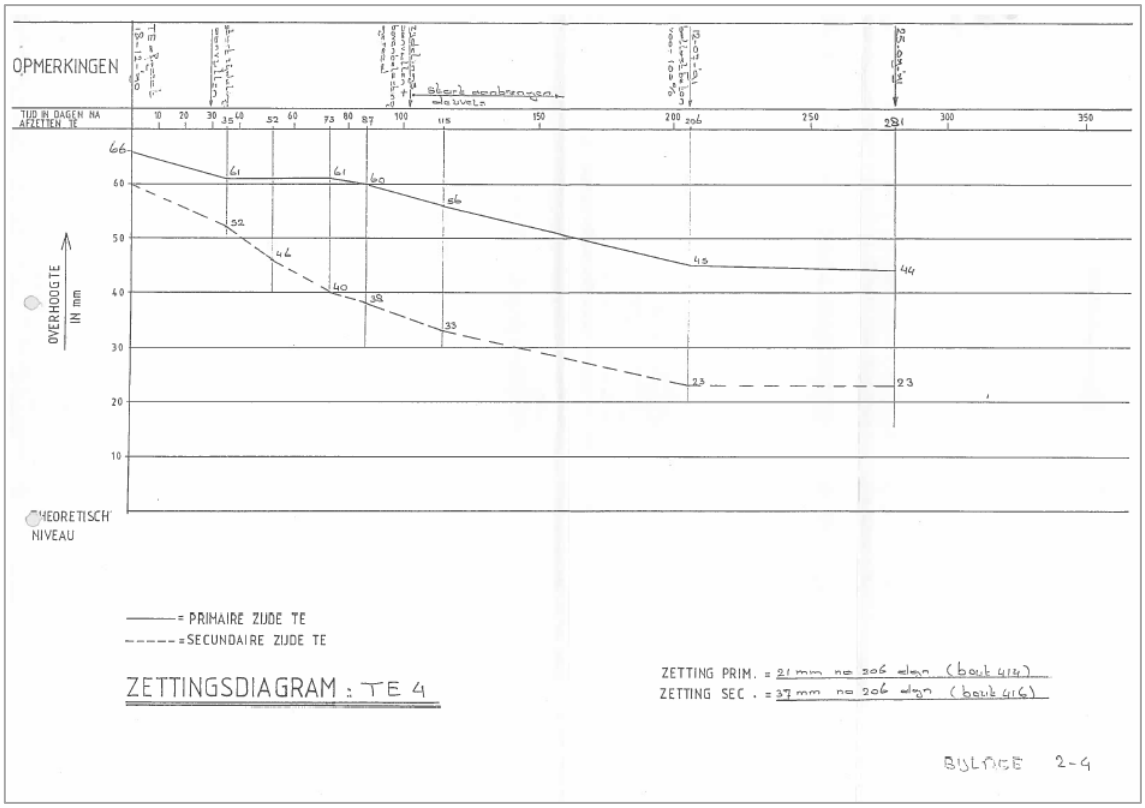

Figure 68: Settlement measurements at both ends of Tunnel Element 4, for the initial 281 days after immersion (TEC, 1992).

D. Additional Input Parameters

In this appendix, the additional input parameters are substantiated for the Noordtunnel case. This includes the settlements for the years 2030, 2040 and 2050 (D.1), the immersion joint stiffness derivation (D.2), the axial and bending stiffness (D.3), the characteristic immersion parameters (D.4), the stiffness of the soil friction (D.5), and the probability of the axial deformation modes (D.6).

D.1. Settlements 2030, 2040 and 2050

The settlement distributions for the years 2030, 2040 and 2050 are presented for *Case A* and *Case B*, in Figure 69 to Figure 71 and Figure 72 to Figure 74, respectively. For *Case A*, the distributions are based on the logarithmically increasing settlement projection of Figure 25. At the same time, the distributions of *Case B* are derived from the linearly increasing settlement projection, which is displayed in Figure 26. Both figures are discussed extensively in subsection 4.2 (paragraph 4.2.1).

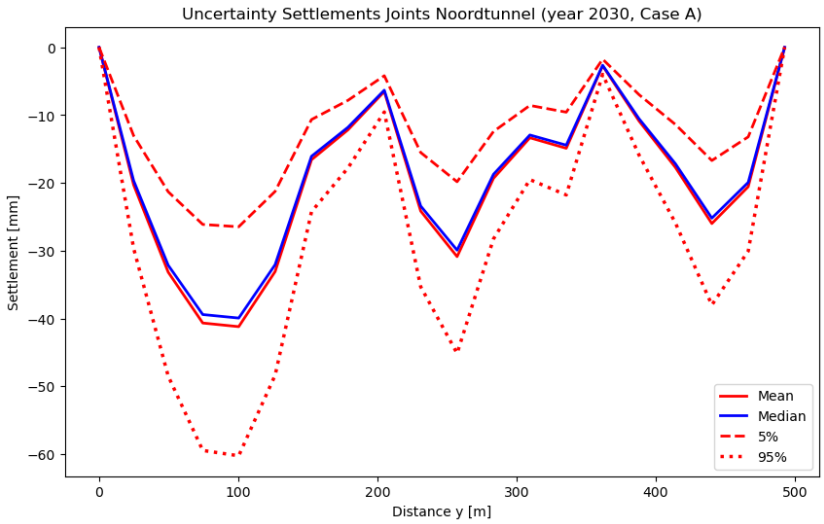

Figure 69: Lognormal distributed settlements at the joints of the Noordtunnel for the year 2030, considering the logarithmic settlement increase of Case A.

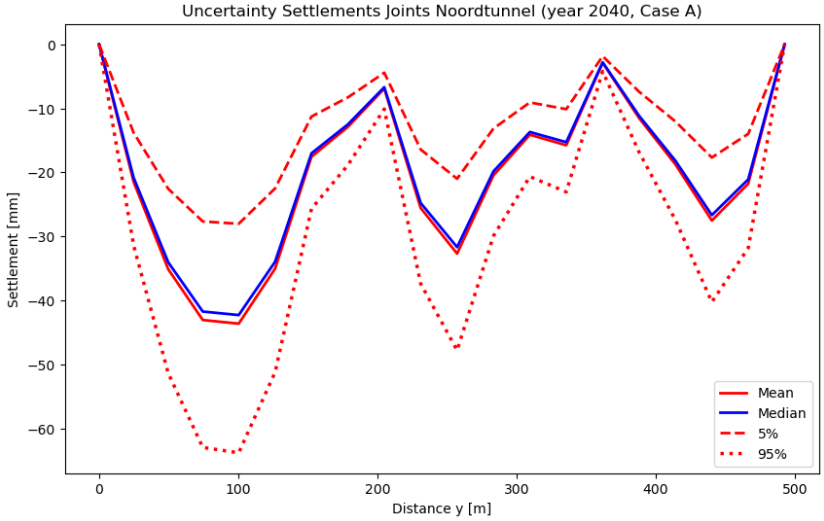

Figure 70: Lognormal distributed settlements at the joints of the Noordtunnel for the year 2040, considering the logarithmic settlement increase of Case A.

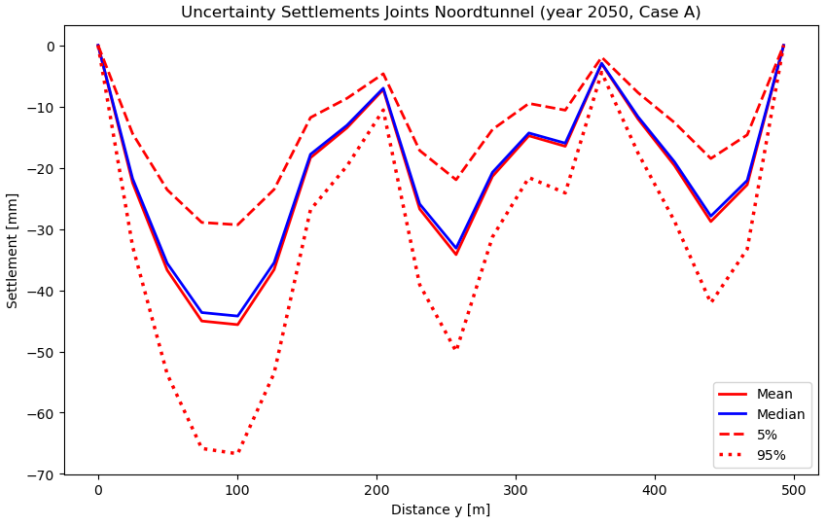

Figure 71: Lognormal distributed settlements at the joints of the Noordtunnel for the year 2050, considering the logarithmic settlement increase of Case A.

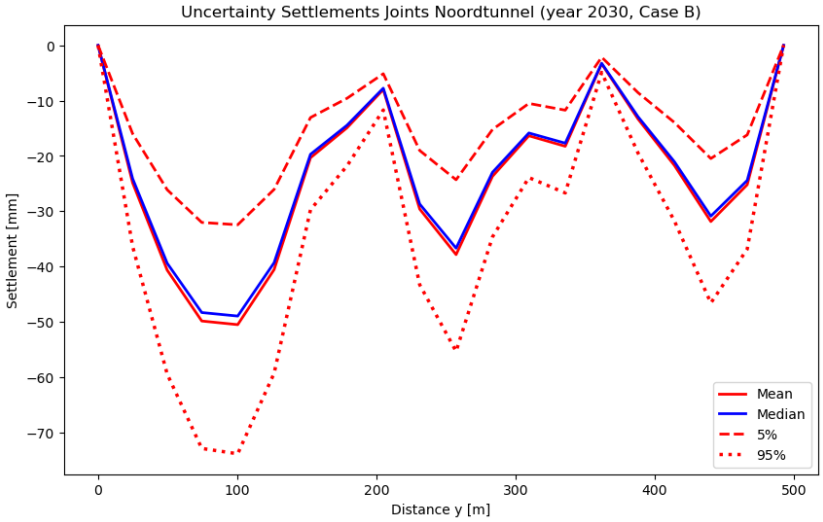

Figure 72: Lognormal distributed settlements at the joints of the Noordtunnel for the year 2030, considering the linear settlement increase of Case B.

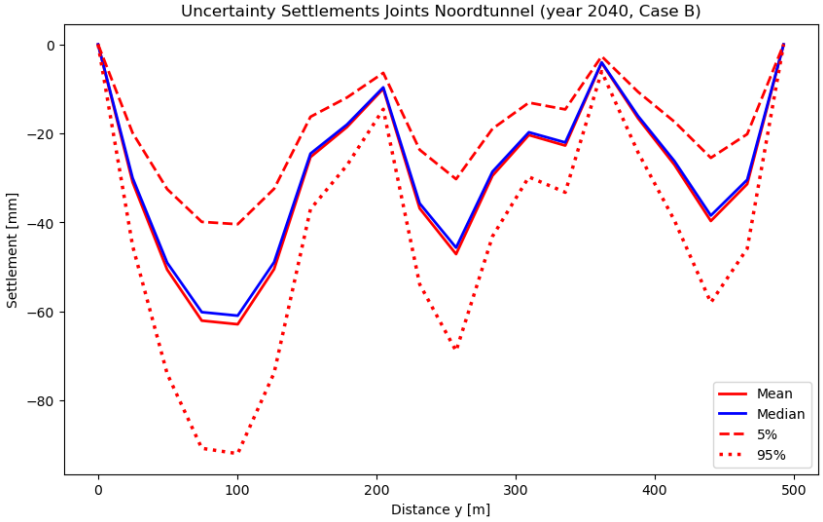

Figure 73: Lognormal distributed settlements at the joints of the Noordtunnel for the year 2040, considering the linear settlement increase of Case B.

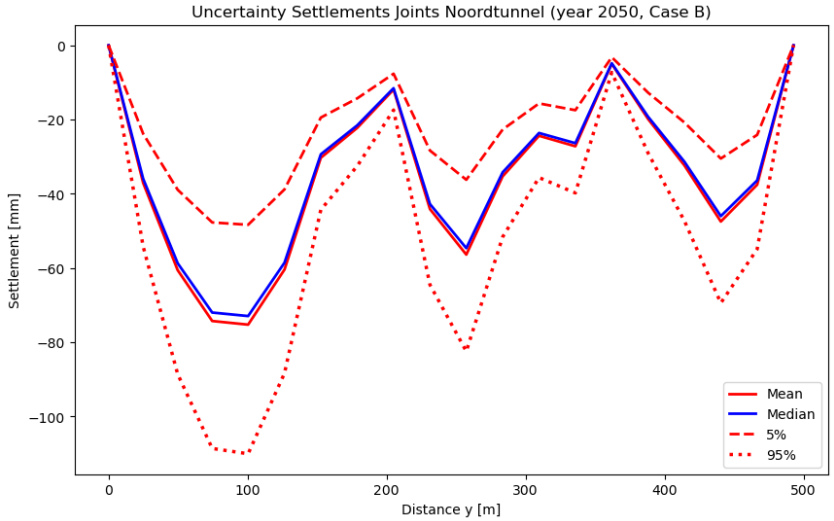

Figure 74: Lognormal distributed settlements at the joints of the Noordtunnel for the year 2050, considering the linear settlement increase of Case B.

D.2. Derivation Stiffness Immersion Joints

For the Noordtunnel case, the Gina gasket type ETS-130-160 has been used in the immersion joints, for which the fitted force-displacement graph is given in Figure 75. It is assumed that the rubber will be subjected to 50% stress relaxation after 100 years, according to the logarithmic trend displayed in Figure 76 (COB, 2022; Saveur & Grantz, 1997). Figure 77 presents the force-displacement graph for the Gina gasket type ETS-130-160, including stress relaxation after 0, 30, 50 and 100 years (based on Figure 75 and Figure 76). In Figure 78 the initial stiffness of the rubber gasket (k_0) is presented, which is determined by the derivative of the force-displacement relation (slope of graph in Figure 77). Noticeably, based on Figure 75 to Figure 78, the axial and rotational stiffness of the immersion joints can be obtained, as demonstrated in Figure 29 and Figure 30 of subsection 4.2 (paragraph 4.2.2).

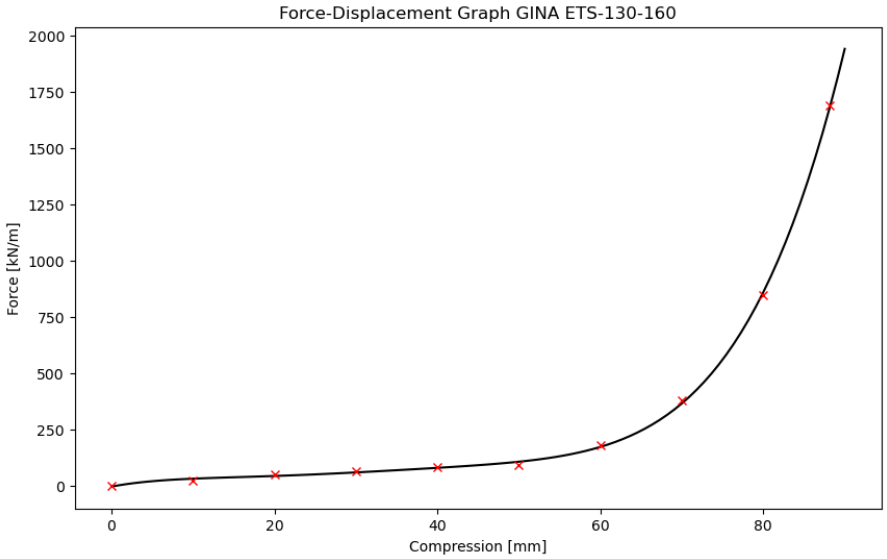

Figure 75: Force-displacement graph GINA ETS-130-160 rubber gasket (fitted polynomial).

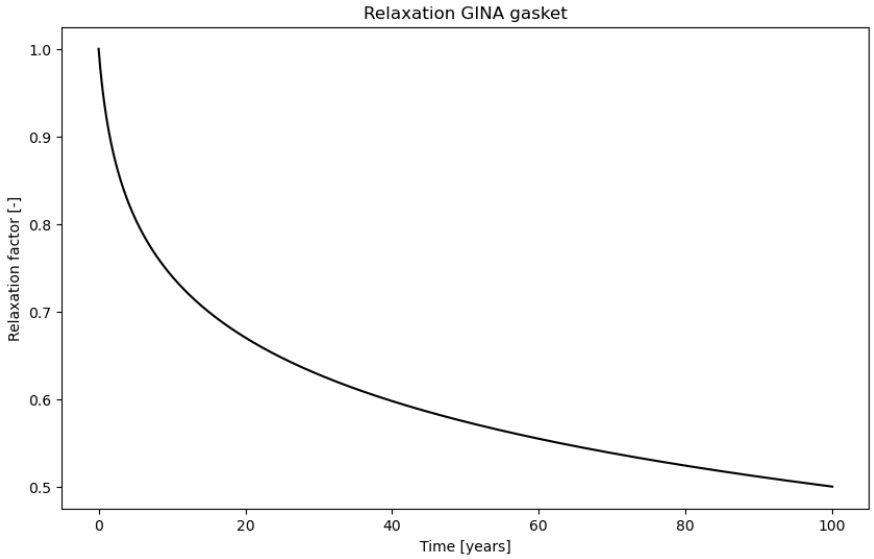

Figure 76: Assumed stress relaxation of the rubber GINA gasket over the years.

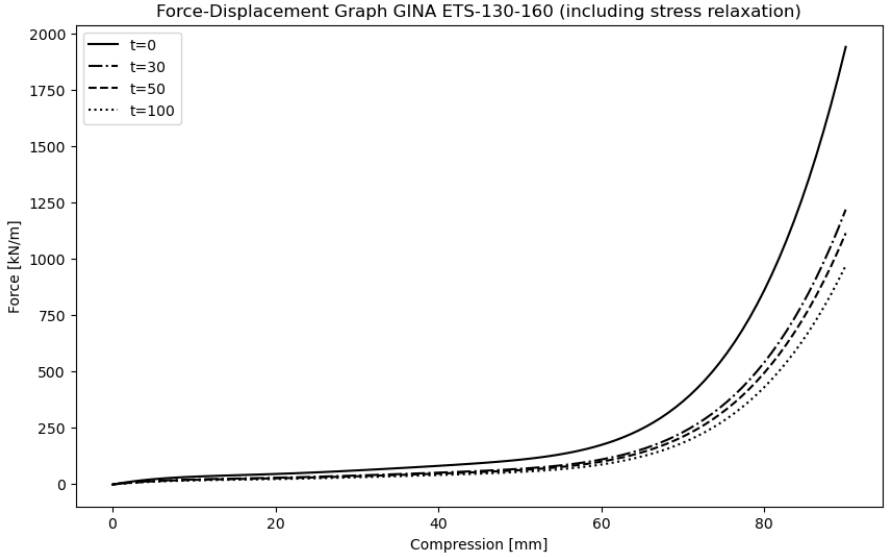

Figure 77: Force-displacement graph GINA ETS-130-160 rubber gasket (including stress relaxation).

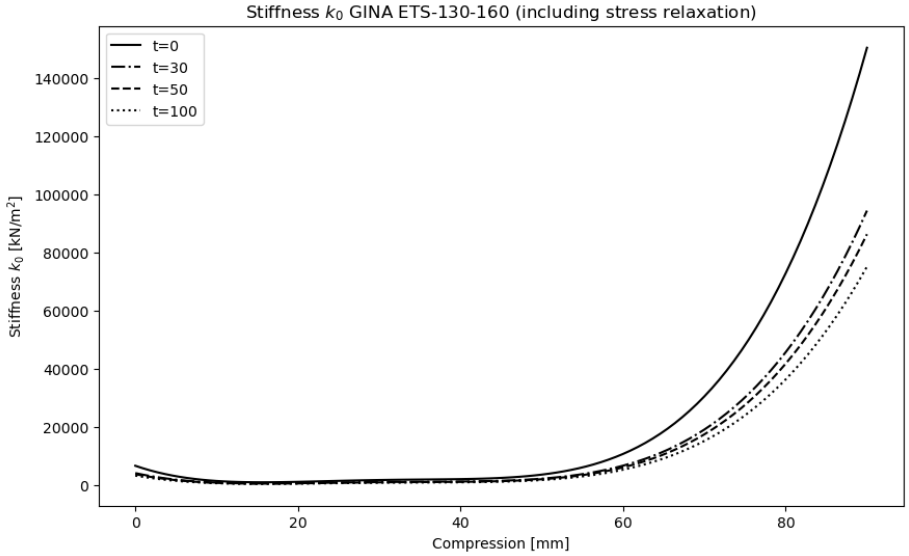

Figure 78: Stiffness k_0 GINA ETS-130-160 rubber gasket Noordtunnel (including stress relaxation).

D.3. Axial and Bending Stiffness

The axial stiffness EA, bending stiffness EI and shear stiffness GA_{eff} are calculated based on the cross-sectional as-built drawings of the Noordtunnel. From the drawings, it follows that the steel class is FeB500 and the concrete class concerns C25/30, indicated with B30 in the notation at that time. The moduli of elasticity are considered to be $200000\ MPa$ and $18857\ MPa$ for the steel and concrete[97], respectively. The shear modulus is calculated by $G = E/2(1+\nu)$, based on the modulus of elasticity and assuming isotropic material conditions. It follows that $EA = 1.663 \cdot 10^9\ kN$, $EI = 1.601 \cdot 10^{10}\ kNm^2$ and $GA_{eff} = 6.917 \cdot 10^8\ kN$. Noteworthy, the Noordtunnel contains two types of cross sections in terms of reinforcement, of which the difference in stiffness is negligible[98].

D.4. Characteristic Immersion Parameters

The normal forces, bending moments and the compression of the Gina gaskets are determined for the immersion joints after immersion. Herewith, the force-displacement graph of Figure 77 is used, without considering stress relaxation of the rubber gasket. The resulting normal forces in the immersion joints are determined by multiplying the average water pressure times the bulkhead area of the elements. For the Noordtunnel, the average water level is $NAP + 1.1m$ and the bulkhead area is equal to $237\ m^2$ (TEC, 1989). The water weight is assumed to be $10\ kN/m^3$ and the water depth at the secondary end of the element follows from TEC (1989). The bending moments in the immersion joints are a consequence of the eccentricity[99] of the resulting normal force. Table 10 presents the overview of the determined parameters for each of the immersion joints. In Figure 79 the definition of primary and secondary end during immersion is given. Figure 80 shows the force-displacement graph including each of the immersion joints at the primary ends of the tunnel elements.

Table 10: Parameters of the immersion joints, just after immersion.

Tunnel Element	Joint	Normal force [kN]	Bending moment [MNm]	Initial compression [mm]
TE1	I5	28837	-12.7	71.16
TE2	I4	31757	-12.7	72.30
TE3	I1	26863	-12.7	70.32
TE4	I3	26863	-12.7	70.32

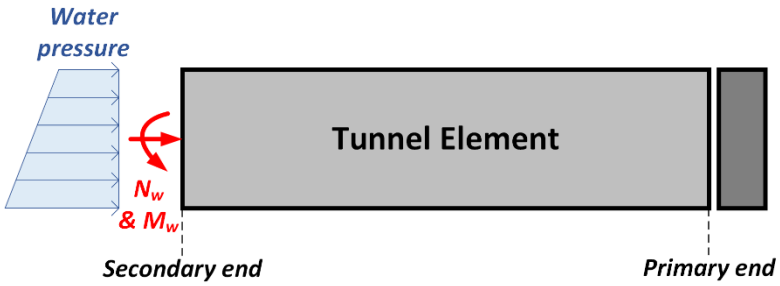

Figure 79: Definition of primary and secondary end during the immersion process.

[97] For the concrete stiffness E_c, the mean (longterm) value was used: $E_c = f_{cm}/\varepsilon_{c3} = 33/(1.75 \cdot 10^{-3})$.
[98] For TE1 (except segment TE1e) & TE3 the cross section of the tunnel contains less reinforcement, causing the stiffnesses to change negligibly: $EA = 1.661 \cdot 10^9\ kN$, $EI = 1.599 \cdot 10^{10}\ kNm^2$ and $GA_{eff} = 6.910 \cdot 10^8\ kN$.
[99] The water pressure at the bottom of the tunnel is higher than the water pressure at the top. A hydrostatic water pressure results in a (negative) bending moment at the immersion joint which is determined with: $M_{wp} = -\left(\frac{1}{2} \cdot 10 \cdot h_{tunnel} \cdot A_{bulkhead}\right) \cdot \left(\frac{1}{6} \cdot h_{tunnel}\right) = -\frac{10}{12} \cdot h_{tunnel}^2 \cdot A_{bulkhead}$

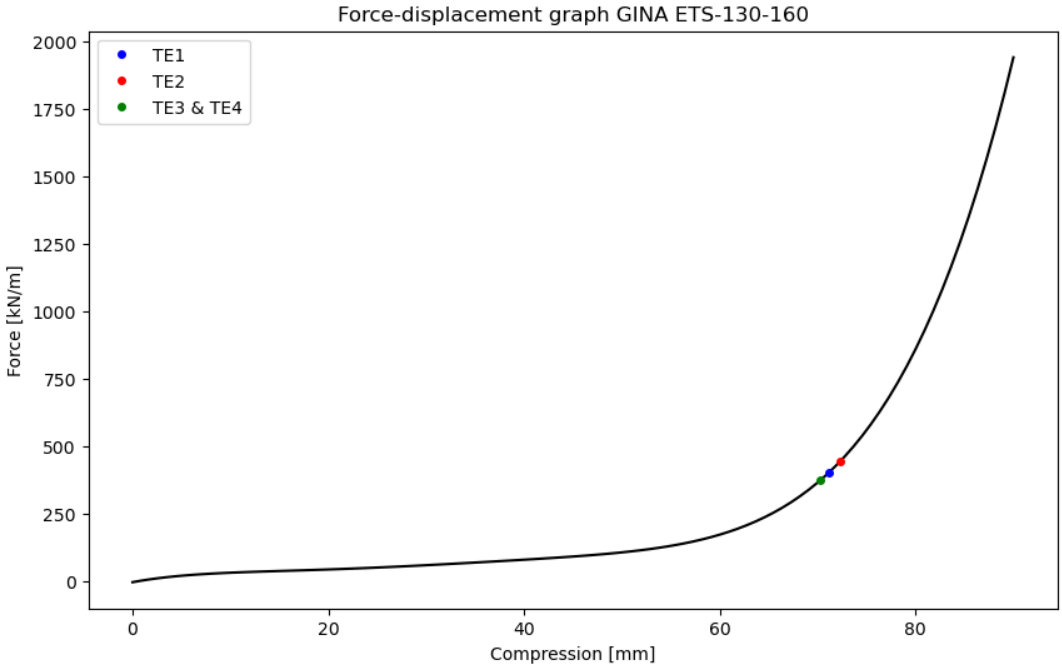

Figure 80: Force-displacement graph GINA ETS-130-160 rubber gasket for the tunnel elements just after immersion.

D.5. Stiffness Soil Friction

The stiffness of the soil friction around the tunnel is estimated here. As the tunnel segments deform axially, the soil that surrounds the tunnel cross section, will exert some resistance to this deformation due to friction. This friction resistance is modelled by continuously axially distributed springs, which are connected to the tunnel segments over the tunnel length. Figure 81 presents the effective soil pressures working on the tunnel cross section schematically. Similar to the vertical load (described in paragraph 4.2.3), it is assumed that TE1e, TE2 and TE4 have $1m$ of soil cover, while TE1abcd and TE3 have $2m$ of soil cover, where the joints between these two levels contain the average of $1.5m$. Equation 9 shows the quantification[100] of the total friction force, by the soil around the circumference of the tunnel cross section. It should be noted that the outcome of the equation depends on the thickness of the cover layer on top of the tunnel (t_c). A friction coefficient of $f_{sc} = 0.9$ is assumed between concrete and sand (Holschemacher & Löber, 2019). The other parameters[101] in the equation are visually Indicated in Figure 81.

$$Q_f = \begin{pmatrix} t_c \cdot w_{top} \cdot \gamma_s' + 2 \cdot (t_c + h_{ear}) \cdot w_{ear} \cdot \gamma_s' + K \cdot \left((t_c + 0.5 \cdot h) \cdot h \cdot \gamma_s'\right) \\ + q_{res} + (t_c - 1) \cdot w_{bot} \cdot \gamma_s' \end{pmatrix} \cdot f_{sc}$$

Equation 9: Total friction force of the soil around the circumference of the tunnel cross section (in y-direction).

[100] Note that $\gamma_s' = 10\ kN/m^3$, as it is assumed that the cross section is fully surrounded by sand with a hydrostatic water pressure. In addition, a neutral earth pressure for loose sand ($\phi = 30°$) on the outer walls of the tunnel is considered, as a result of which $K = 0.5$. Moreover, the load at the tunnel bottom is the resultant of the tunnel weight, 1m of soil cover weight and the upward water pressure: $q_{res} = 734.1\ kN/m$ (TEC, 1989).
[101] The following values were used: $h = 8.02\ m$, $h_{ear} = 6.97\ m$, $w_{top} = 29.95\ m$ and $w_{bot} = 31.95\ m$.

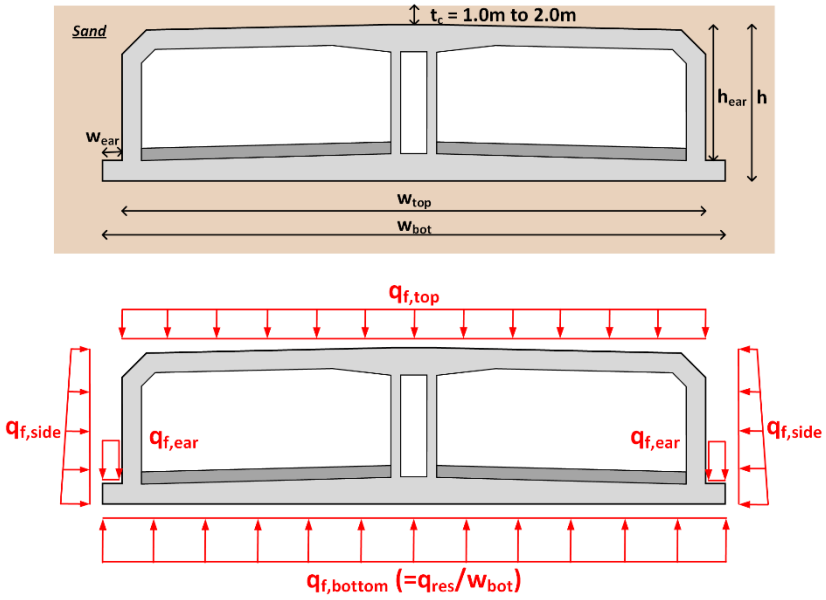

Figure 81: Schematic representation of the Noordtunnel cross section with present effective soil pressures.

Figure 82 presents the maximum friction force normally distributed over the Noordtunnel, at which it is considered that $CV = 0.1$ for the soil overburden[102], and $CV = 1/27$ for the friction coefficient[103]. Hereafter, the soil friction stiffness is determined by dividing the friction force over the relative displacement. The common relative displacement value of $10mm$ is used in accordance to Van Oorsouw (2010). Figure 83 shows the normally distributed soil friction stiffness over the Noordtunnel.

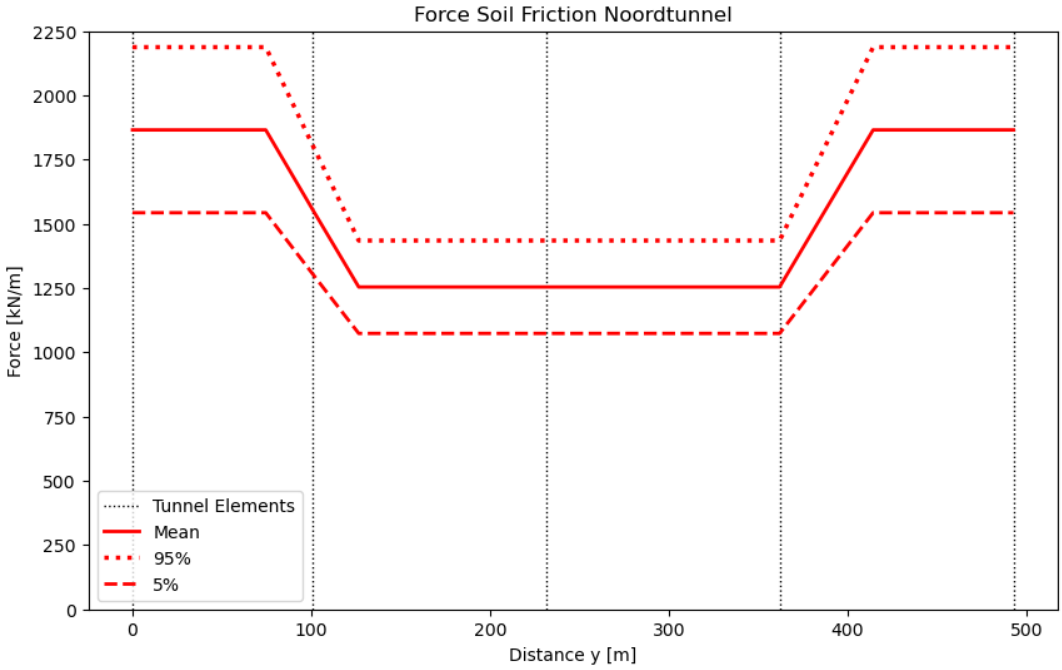

Figure 82: Normally distributed friction force of the soil around the circumference of the Noordtunnel cross section, of which the maximum value is considered.

[102] The substantiation of $CV = 0.1$ for the soil overburden, which was explained in paragraph 4.2.3.

[103] It is assumed that the maximum friction coefficient is $f_{sc} = 1.0$, and regards the $\mu + 3\sigma$ upper boundary of the distribution. From this it follows that: $CV = \frac{\sigma}{\mu} = \frac{1.0-0.9}{0.9 \cdot 3} = \frac{1}{27}$

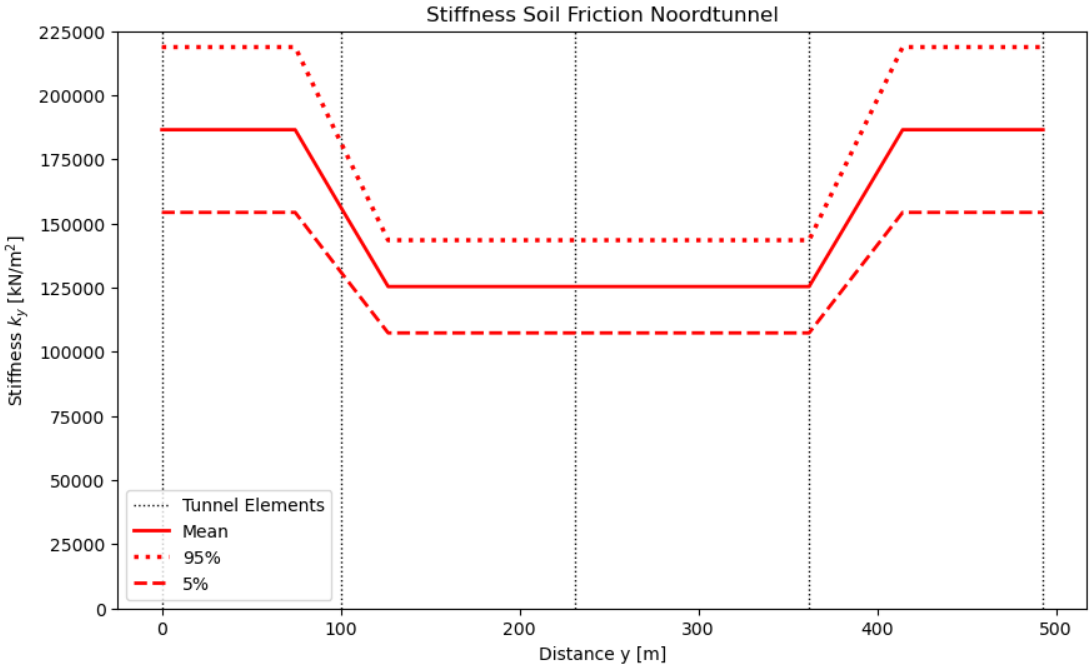

Figure 83: Normally distributed soil friction stiffness of the Noordtunnel.

D.6. Probability Axial Deformation Modes

The probabilities of the axial deformation modes are derived for the Noordtunnel case, by using Figure 14, Figure 15 and Figure 16 of subsection 3.3. The combined tunnel elements 3 and 4 are supposed to exert six different possible deformation modes (as shown in Figure 15). For tunnel element 1 and 2, a similar type of behaviour is considered, with four different possible deformation modes (see Figure 16). Mode 4 of tunnel element 1 or 2, and mode 6 of tunnel elements 3 and 4 combined are not included, as mathematically comparable solutions are found, for consecutively mode 3 (tunnel element 1 or 2), and mode 5 (tunnel element 3 and 4 combined)[104].

For each of the modes, the probability of occurrence is determined, by examining the soil friction and the normal force. Figure 13 demonstrates this mechanism of forces on a segment joint. The probability that one or more segments move axially is calculated with $P(Z = R - S < 0)$, where R is the resistance of the segment(s) by soil friction, and S is the normal force occurring on the specific segment(s)[105]. The normal force is assumed to be a normally distributed stochastic parameter[106], without considering the stress relaxation of the rubber Gina gasket. The resistance is also considered to be normally distributed[107]. As explained above, the probability of mode 4 (tunnel element 1 or 2) and mode 6 (tunnel element 3 and 4 combined) are assumed to be zero. Table 11 presents the calculated probabilities of the axial deformation modes for each of the elements of the Noordtunnel.

[104] A similar solution of the differential equation is found for mode 4 (TE1/TE2) and mode 6 (TE3+TE4), as with mode 3 (TE1/TE2) and mode 5 (TE3+TE4), because of zero normal force in the outer two segment joints.

[105] Thus, modes 1, 2, and 3 (TE1/TE2) occur for $R_{2\ segments} < S$, $R_{1\ segment} < S$, and $R_{1\ segment} > S$, respectively.

[106] $N(\mu_{F_{TE}}, \frac{F_{TE,max} - \mu_{F_{TE}}}{3})$, with $\mu_{F_{TE}}$ as mean normal force at immersion (Table 10 of Appendix D.4). Besides, $F_{TE,max}$ is the maximum normal force, under the assumption that the initial compression of the rubber Gina gaskets increases with the complete temperature shrinkage of a tunnel element, by $\Delta L = \alpha \cdot L_0 \cdot \Delta T$ (Van Montfort, 2018), for $\Delta T = 10\ K$ and $\alpha = 12 \cdot 10^{-6}\ K^{-1}$.

[107] $N(\mu_{Q_f} \cdot L_{seg}, \sigma_{Q_f} \cdot L_{seg})$, with μ_{Q_f} and σ_{Q_f} as the mean and standard deviation of the soil friction resistance, which can be derived from Figure 82 of Appendix D.5, and L_{seg} equal to the length of one or more segments.

Table 11: Estimated probabilities of the axial deformation modes for the different elements of the Noordtunnel.

Modes	Tunnel Element 1	Tunnel Element 2	Tunnel Elements 3&4
Mode 1	0.0076	0.1249	$1.60 \cdot 10^{-6}$
Mode 2	0.2214	0.3606	$2.62 \cdot 10^{-4}$
Mode 3	0.7709	0.5145	0.0164
Mode 4	0.0	0.0	0.2620
Mode 5	-	-	0.7213
Mode 6	-	-	0.0

E. Results Noordtunnel Case

This appendix demonstrates the results for the Noordtunnel case, by successively describing the Monte Carlo approach validation (E.1), the results for the tunnel reliability (E.2), the derivation of the tunnel availability (E.3), and the failure probability of the segment joints (E.4). Finally, an analysis for the influence of the foundation stiffness parameter is conducted (E.5).

E.1. Validation Monte Carlo Approach

This appendix presents the validation of the Monte Carlo approach for the Noordtunnel case, with the mean parameter values of the 2020 situation, in which the results of the three different models are compared. Table 12 to Table 14 presents the failure probability results of the Noordtunnel case, for a varying number of simulations (N). Table 12 offers the results without taking stress relaxation into account, with zero temperature change and only considering deformation mode 1. In Table 13, the results are shown with temperature change included and all deformation modes considered. Table 14 includes stress relaxation as well, besides the temperature change and all the deformation modes. In the tables a distinction is made between the failure probability due to shear force, rotation and the combined failure probability (due to either shear force or rotation).

The tables demonstrate a large spread in the calculated failure probabilities, depending on the failure mechanism examined, the respective model and other considerations. *Model 1* shows the greatest failure probabilities, followed by the intermediate values of *Model 2*, and the smallest results of *Model 3*. Besides, as can be seen in the results, there is a large difference between the two failure mechanisms of shear force and rotation. For *Model 1* the total failure probability is completely determined by failure due to shear force, where the total failure probabilities of *Model 2* and *Model 3* are almost entirely determined through this mechanism as well. Furthermore, minor differences are present in the results between the tables, in which varying considerations are included regarding stress relaxation, temperature change and deformation modes. Relatively, these differences are larger for the rotation mechanism compared to the shear force mechanism.

Table 12: Failure probability results Noordtunnel (year 2020) by the Monte Carlo approach for a varying number of simulations (N=10-10⁴), without stress relaxation, zero temperature change, and considering only deformation mode 1.

Calculation	Number of simulations (N)	Failure probability shear force ($P_{f,V}$)			Failure probability rotation ($P_{f,\varphi}$)			Failure probability (P_f)		
		Mod1	*Mod2*	*Mod3*	*Mod1*	*Mod2*	*Mod3*	*Mod1*	*Mod2*	*Mod3*
#1	N=10	1.0	0.8	0.7	0.0	0.0	0.0	1.0	0.8	0.7
#2	N=100	1.00	0.78	0.45	0.00	0.00	0.00	1.00	0.78	0.45
#3	N=1000	1.000	0.772	0.481	0.011	0.006	0.003	1.000	0.775	0.481
#4	N=10000	0.9994	0.7794	0.4713	0.0130	0.0092	0.0063	0.9994	0.7812	0.4744

Table 13: Failure probability results Noordtunnel (year 2020) by the Monte Carlo approach for a varying number of simulations (N=10-10⁴), without stress relaxation, temperature change, and considering all the deformation modes.

Calculation	Number of simulations (N)	Failure probability shear force ($P_{f,V}$)			Failure probability rotation ($P_{f,\varphi}$)			Failure probability (P_f)		
		Mod1	*Mod2*	*Mod3*	*Mod1*	*Mod2*	*Mod3*	*Mod1*	*Mod2*	*Mod3*
#5	N=10	1.0	0.5	0.2	0.0	0.0	0.0	1.0	0.5	0.2
#6	N=100	1.00	0.82	0.42	0.01	0.02	0.01	1.00	0.82	0.43
#7	N=1000	1.000	0.761	0.426	0.009	0.014	0.009	1.000	0.765	0.431
#8	N=10000	0.9995	0.7536	0.4316	0.0112	0.0093	0.0056	0.9995	0.7547	0.4352

Table 14: Failure probability results Noordtunnel (year 2020) by the Monte Carlo approach for a varying number of simulations (N=10-10⁴), with stress relaxation, temperature change, and considering all the deformation.

Calculation	Number of simulations (N)	Failure probability shear force ($P_{f,V}$)			Failure probability rotation ($P_{f,\varphi}$)			Failure probability (P_f)		
		Mod1	*Mod2*	*Mod3*	*Mod1*	*Mod2*	*Mod3*	*Mod1*	*Mod2*	*Mod3*
#9	N=10	1.0	0.7	0.6	0.0	0.0	0.0	1.0	0.7	0.6
#10	N=100	1.00	0.74	0.49	0.00	0.01	0.00	1.00	0.74	0.49
#11	N=1000	1.000	0.740	0.444	0.016	0.012	0.006	1.000	0.743	0.446
#12	N=10000	0.9997	0.7540	0.4310	0.0121	0.0098	0.0060	0.9997	0.7561	0.4345

It is deducted from the tables, that an increase in number of simulations obviously lead to a higher accuracy in the calculated failure probability. For *Model 1* this is perfectly illustrated, as the failure probability is 1.0 for N=10 to N=1000 simulations, but slightly lower than 1.0 for N=10000 simulations. Therefore, it is concluded that accuracy could be lost when the number of simulations would be lower than N=10000. Apart from *Model 1*, the differences in failure probability for N=1000 and N=10000 simulations seem generally to be relatively small. Based on this, it is assumed that using an even higher number of simulations, such as $N=10^5$, would not drastically change the calculated failure probability.

It should be noted that, in order to run the model a single time for N=10000 simulations, the computation time is already more than half an hour. As the computation time of the calculation increases with the number of simulations, the number of simulations cannot simply be increased endlessly. Thus, a balance should be found between accuracy of the results and the computation time. As the computation time will increase enormously for simulations above N=10000, and the accuracy of the calculated failure probability could only be slightly increased, it is considered that N=10000 is the balanced number of simulations. TNO (2021) used 10000 samples as well in the Monte Carlo simulation, for the performance of a Drechttunnel case study, in which the reliability of immersion joints regarding leakage was determined. In this research, N=10000 is used, as the calculated failure probability is considered accurate enough, seen in order of magnitude.

E.2. Tunnel Reliability

Figure 84 and Figure 85 display the developments of the failure probability and structural reliability, for the Noordtunnel case over the years, distinguishing between *Model 1*, *Model 2* and *Model 3*.

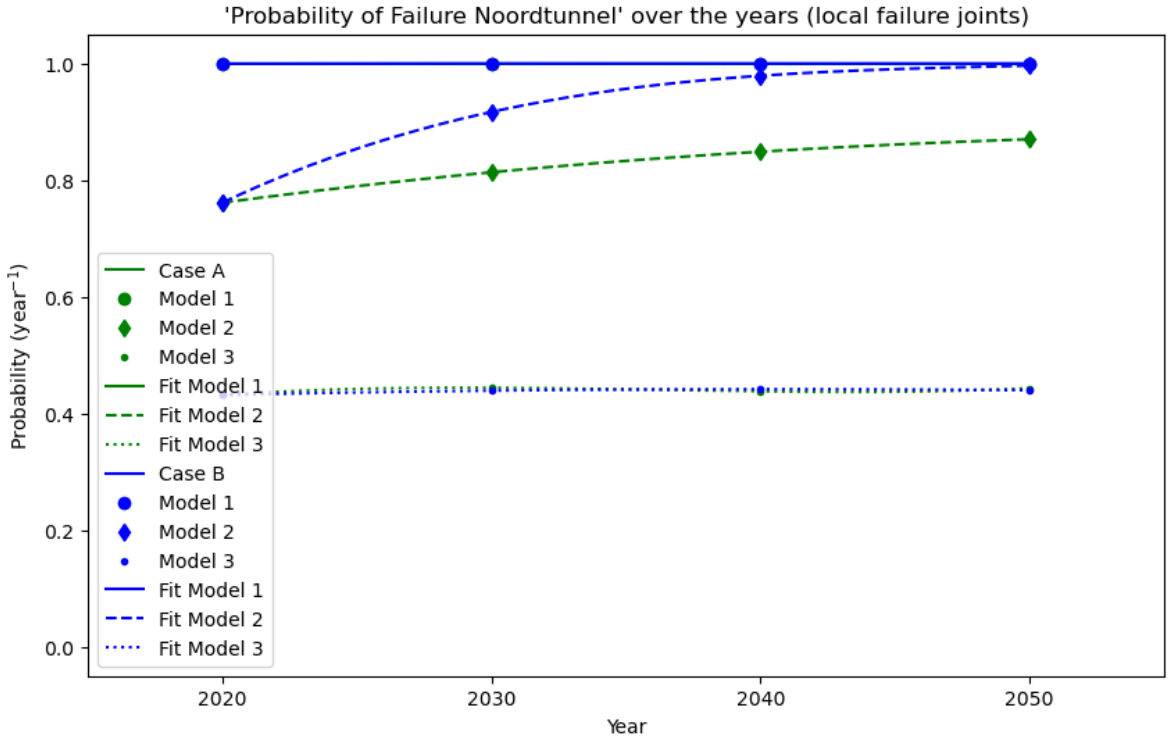

Figure 84: Calculated probability of failure for the Noordtunnel over the years (for N=10⁴), where Case A and Case B concern the logarithmic and linear increase of settlements, respectively.

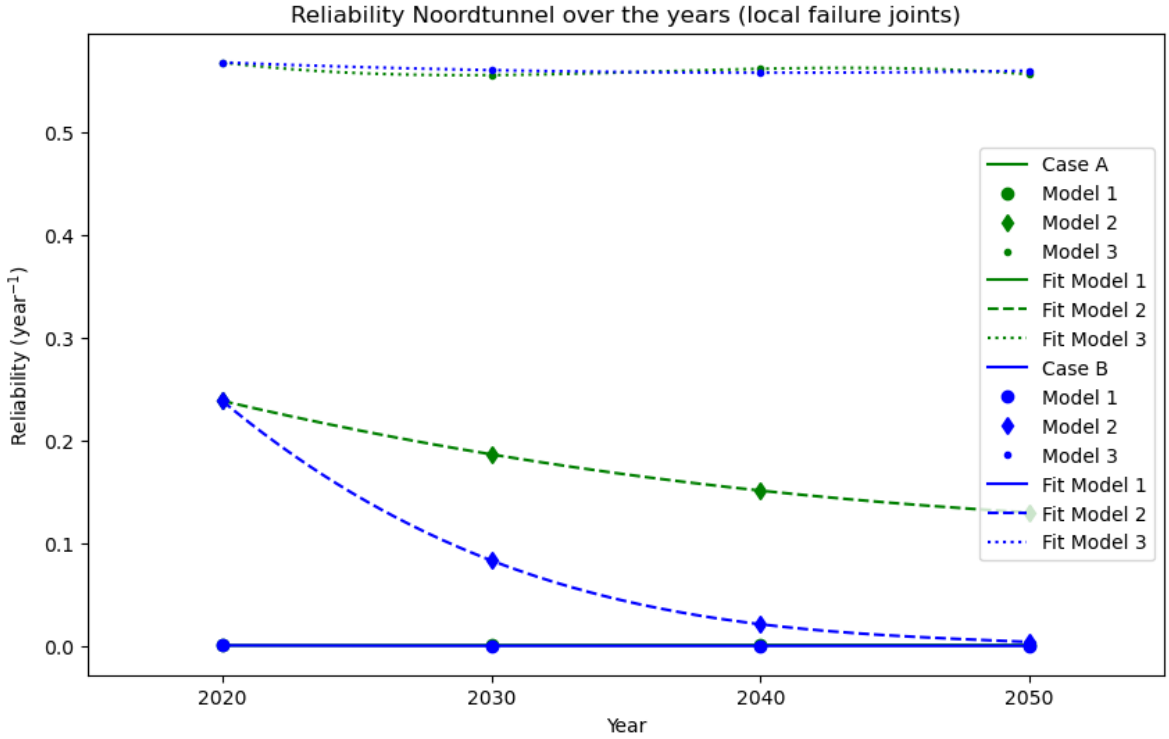

Figure 85: Calculated structural reliability for the Noordtunnel over the years (for N=10⁴), where Case A and Case B concern the logarithmic and linear increase of settlements, respectively.

Figure 86 and Figure 87 illustrate the developments of the failure probability and structural reliability, for the Noordtunnel case over time, considering only the shear force failure mechanism, in which a distinction is made between *Model 1*, *Model 2* and *Model 3*.

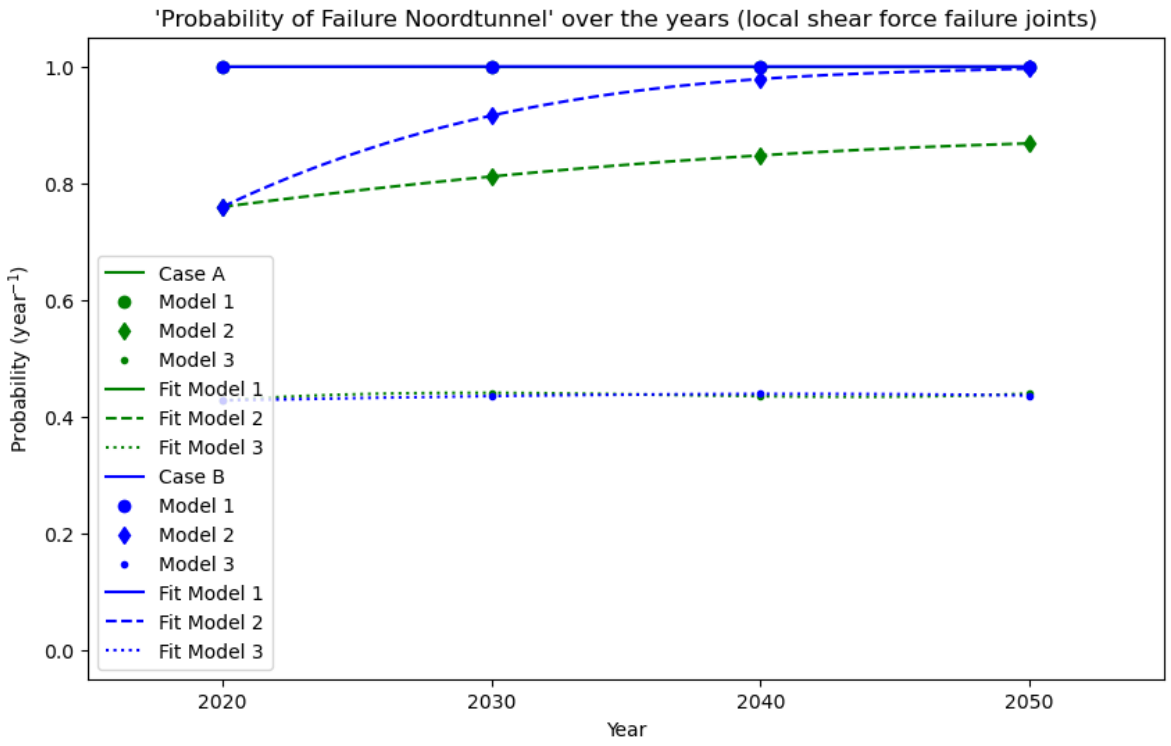

Figure 86: Calculated probability of failure for the Noordtunnel over the years (for N=10⁴), considering only the shear force failure mechanism, where Case A and Case B concern the logarithmic and linear increase of settlements, respectively.

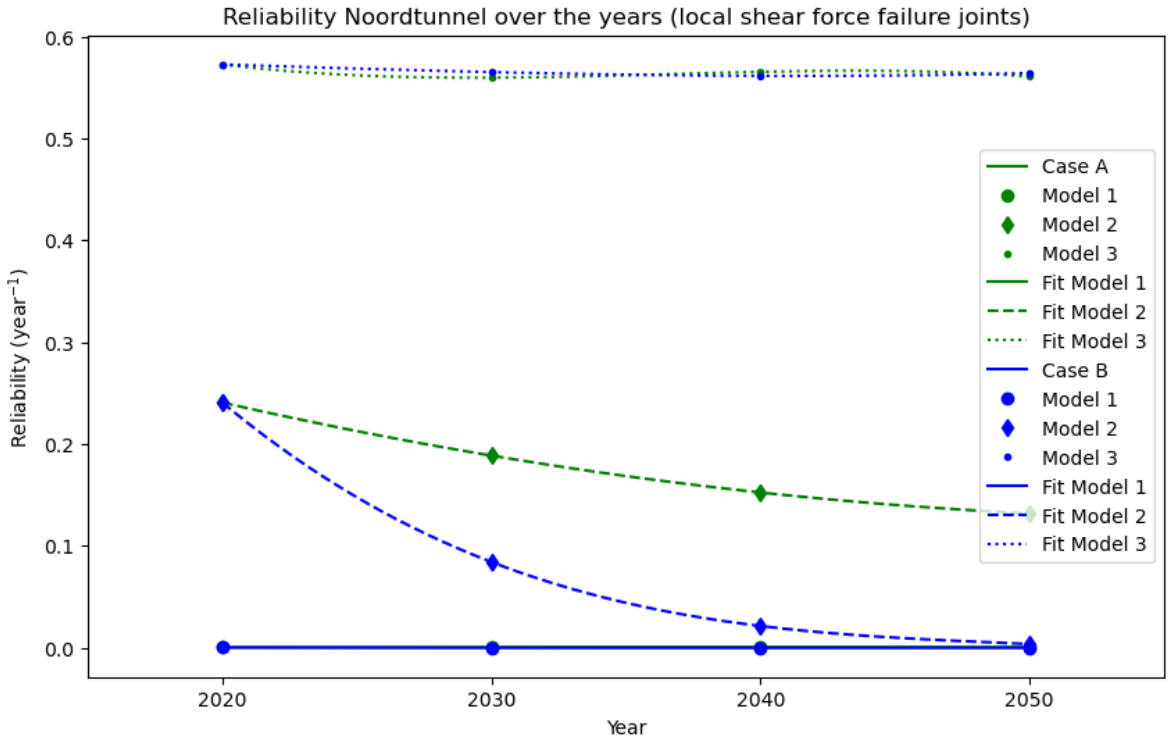

Figure 87: Calculated structural reliability for the Noordtunnel over the years (for N=10⁴), considering only the shear force failure mechanism, where Case A and Case B concern the logarithmic and linear increase of settlements, respectively.

In Figure 88 and Figure 89 the developments of the failure probability and structural reliability are presented, for the Noordtunnel case over time, considering only the rotational failure mechanism, where *Model 1*, *Model 2* and *Model 3* are distinguished.

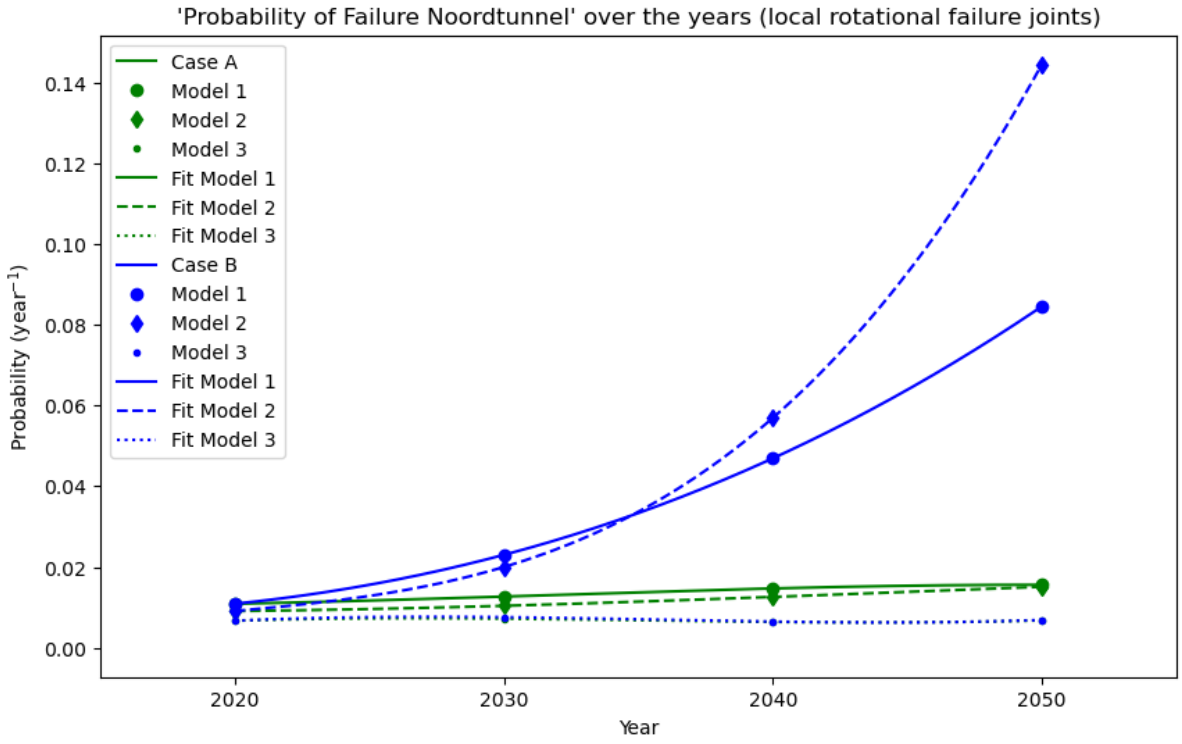

Figure 88: Calculated probability of failure for the Noordtunnel over the years for (for N=10⁴), considering only the rotational failure mechanism, where Case A and Case B concern the logarithmic and linear increase of settlements, respectively.

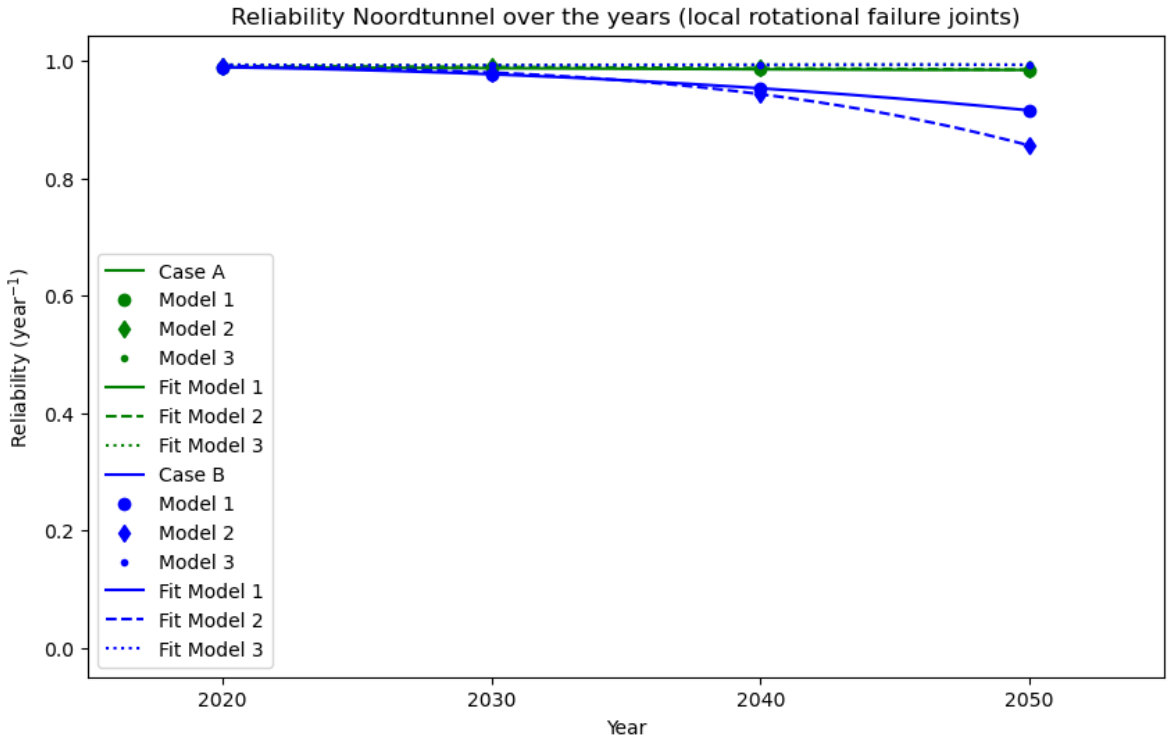

Figure 89: Calculated structural reliability for the Noordtunnel over the years (for N=10⁴), considering only the rotational failure mechanism, where Case A and Case B concern the logarithmic and linear increase of settlements, respectively.

E.3. Derivation Tunnel Availability

This appendix presents the structural reliability of the Noordtunnel over the time period 2020-2090, including some necessary assumptions, in order to determine the (un)availability of the tunnel in paragraph 4.3.2. In Figure 90, Figure 91 and Figure 92 the reliability of the Noordtunnel is presented for *Model 1*, *Model 2* and *Model 3*, respectively. Based on these figures, the mean time between failure ($MTBF$) can be determined with Equation 2 (see subsection 3.5). The upper limit of the integral in Equation 2 is held to a maximum of 70 years, under the assumption that the tunnel will reach its end of life after 100 years. For *Model 2* with *Case A* (Figure 91) and *Model 3* with *Case B* (Figure 92), the reliability curves are corrected to linearly decrease to zero between the years 2050 and 2090, as the fitted third-order polynomial curves are not realistic after 2050[108]. In addition, the reliability polynomial for *Case B* of *Model 1* (Figure 90) is corrected to be zero after 2030, as the calculated reliabilities at 2030, 2040 and 2050 are zero as well. Noteworthy, the remarkable increase of reliability for *Case A* of *Model 1* over the period 2020-2050 is not adjusted for the availability determination, because this does not concern a fit error as the values are computed with the research methodology.

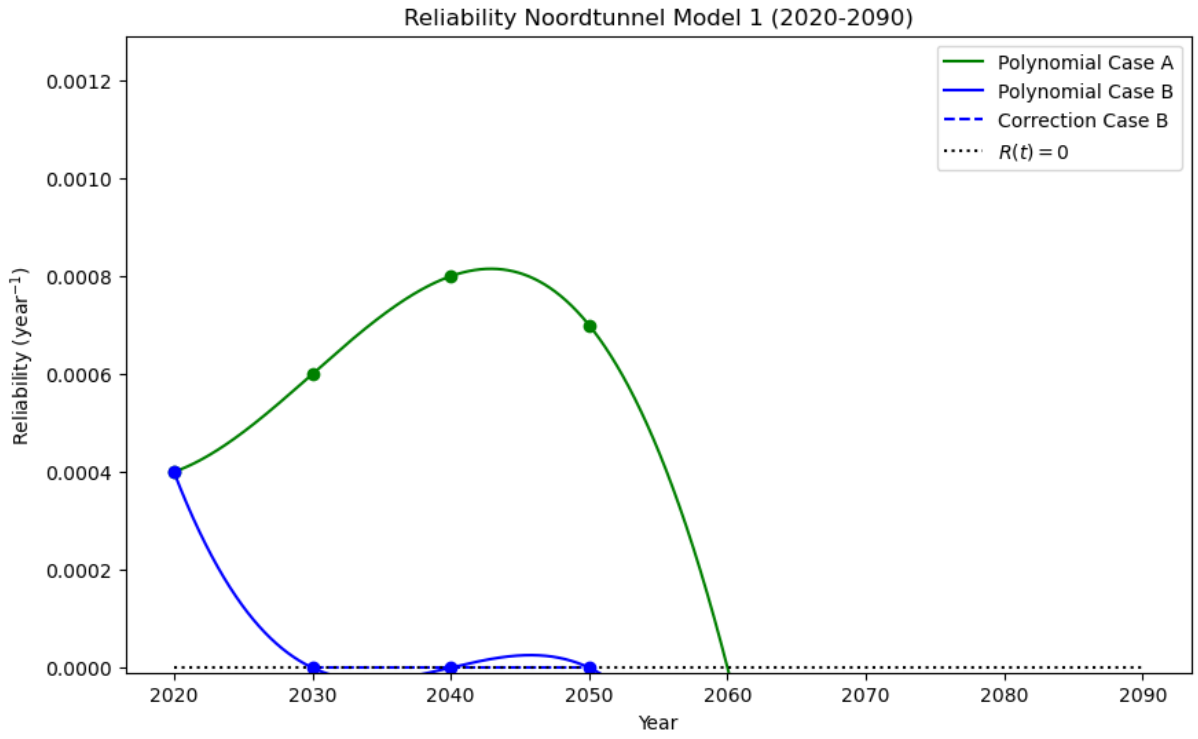

Figure 90: Determined structural reliability for the Noordtunnel over the time period 2020-2090, obtained with Model 1. The figure is based on the polynomial fit of Equation 5, with the values of Table 3. The dots in the figure represent the calculated reliability for years 2020, 2030, 2040, and 2050, of Figure 85 from Appendix E.2 (for N=10⁴), and Case A and Case B concern the logarithmic and linear increase of settlements, respectively.

[108] Without considering maintenance, it is definitely not expected that the reliability of the structure will increase after 2050. The reason for this increase is a lack of fitted data points for $R(t)$ after 2050.

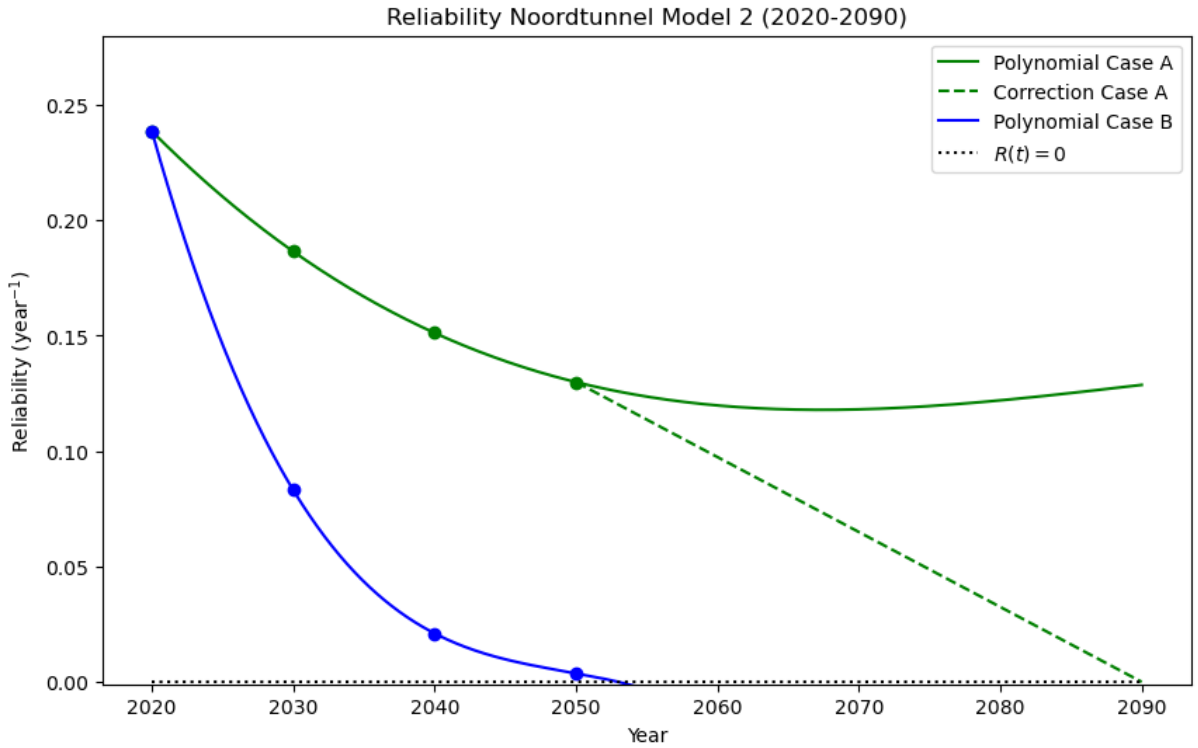

Figure 91: Determined structural reliability for the Noordtunnel over the time period 2020-2090, obtained with Model 2. The figure is based on the polynomial fit of Equation 5, with the values of Table 3. The dots in the figure represent the calculated reliability for years 2020, 2030, 2040, and 2050, of Figure 85 from Appendix E.2 (for N=10⁴), and Case A and Case B concern the logarithmic and linear increase of settlements, respectively.

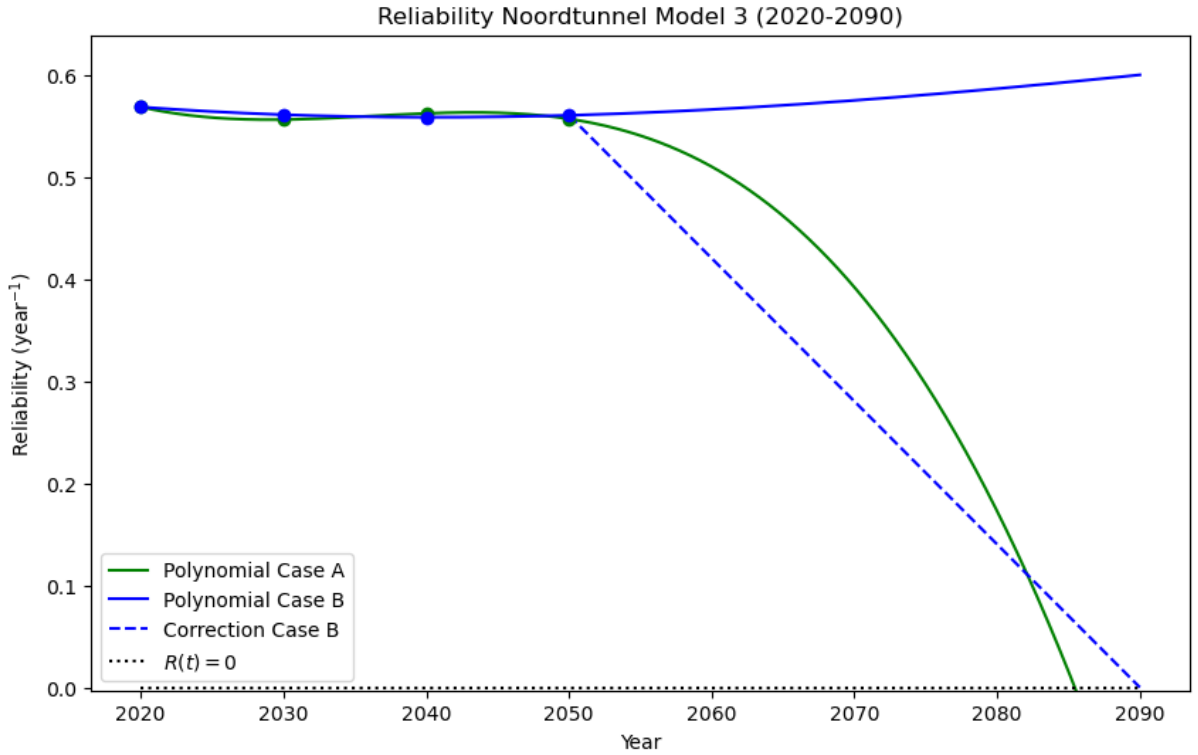

Figure 92: Determined structural reliability for the Noordtunnel over the time period 2020-2090, obtained with Model 3. The figure is based on the polynomial fit of Equation 5, with the values of Table 3. The dots in the figure represent the calculated reliability for years 2020, 2030, 2040, and 2050, of Figure 85 from Appendix E.2 (for N=10⁴), and Case A and Case B concern the logarithmic and linear increase of settlements, respectively.

E.4. Critical Segment Joints

Figure 93 and Figure 94 display the failure probabilities of the segment joints of the Noordtunnel, obtained with *Model 1*, including the developments over the years for *Case A* and *Case B*.

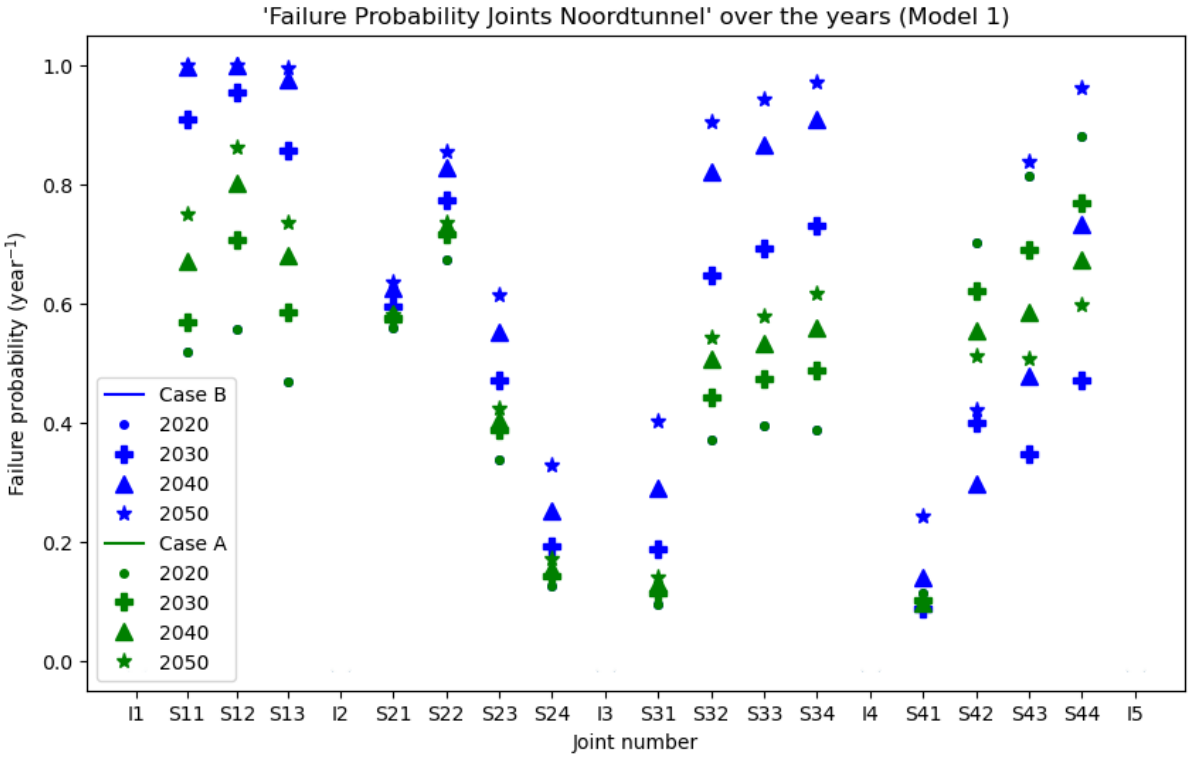

Figure 93: Failure probability segment joints of the Noordtunnel over the years for Model 1, where Case A and Case B concern the logarithmic and linear increase of settlements, respectively.

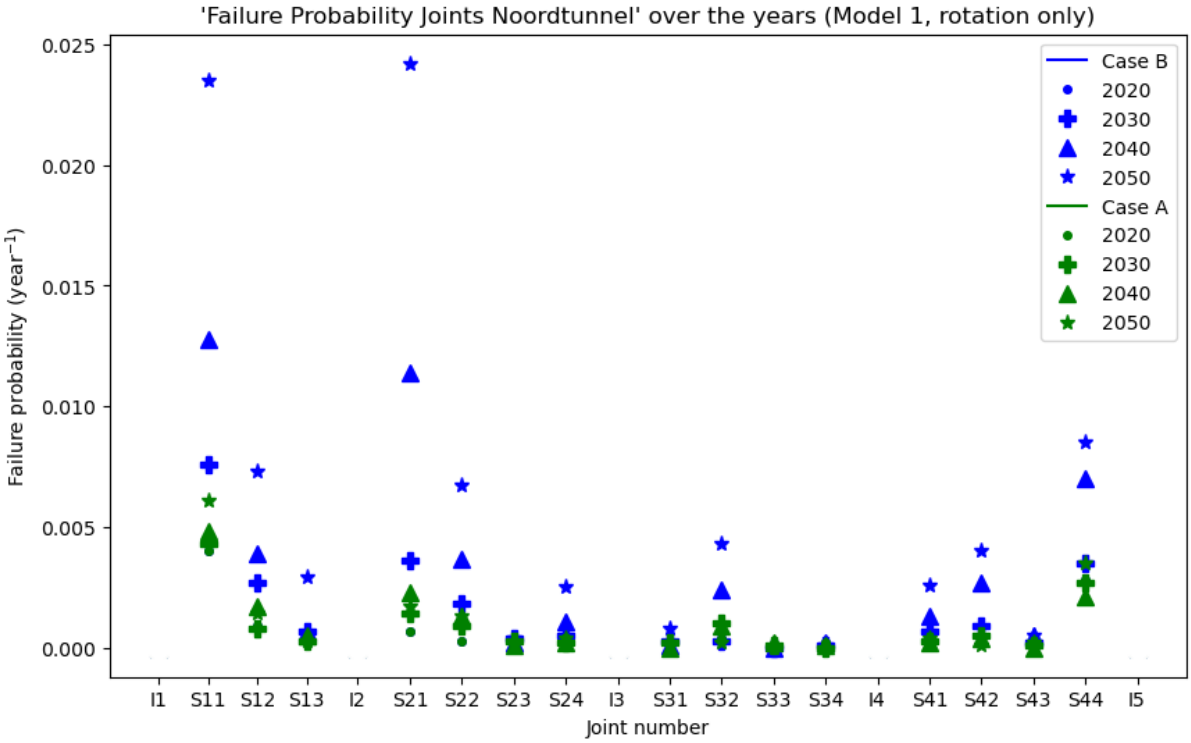

Figure 94: Failure probability segment joints of the Noordtunnel over the years for Model 1, considering only the rotational failure mechanism, where Case A and Case B concern the logarithmic and linear increase of settlements, respectively.

In Figure 95 and Figure 96 the failure probabilities of the segment joints of the Noordtunnel are shown, received with *Model 2*, including the developments over time for *Case A* and *Case B*.

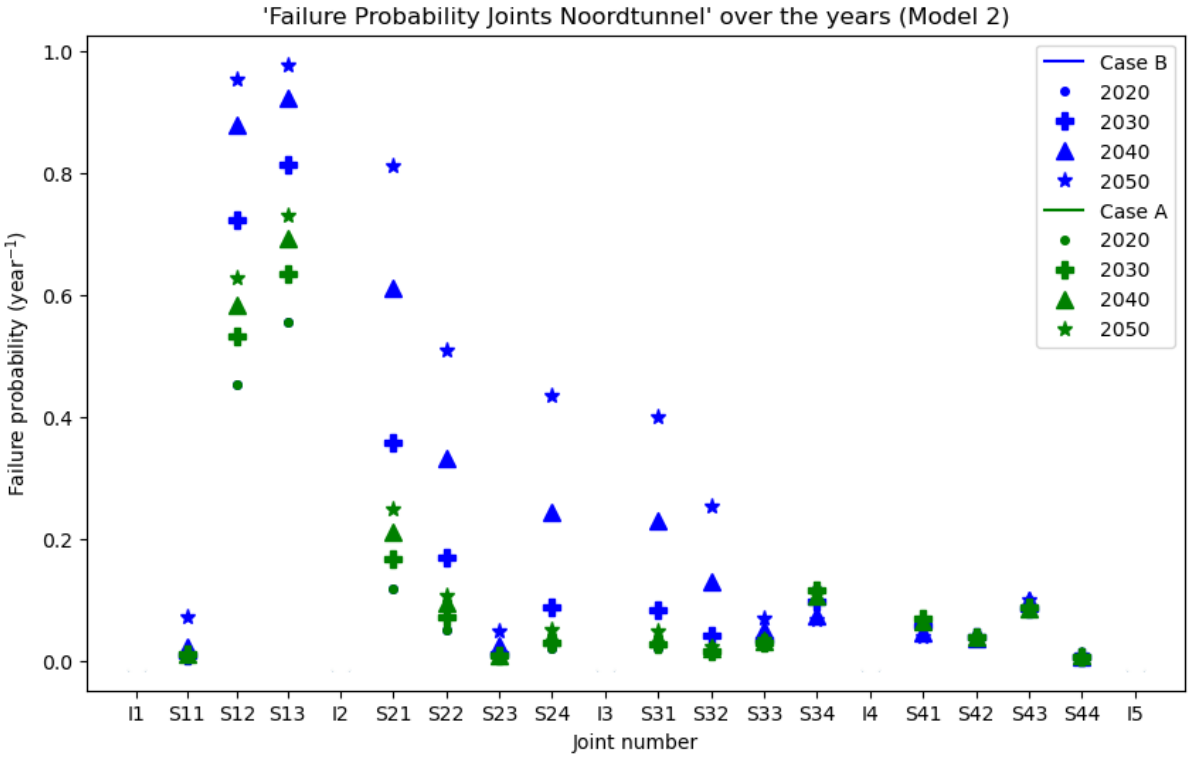

Figure 95: Failure probability segment joints of the Noordtunnel over the years for Model 2, where Case A and Case B concern the logarithmic and linear increase of settlements, respectively.

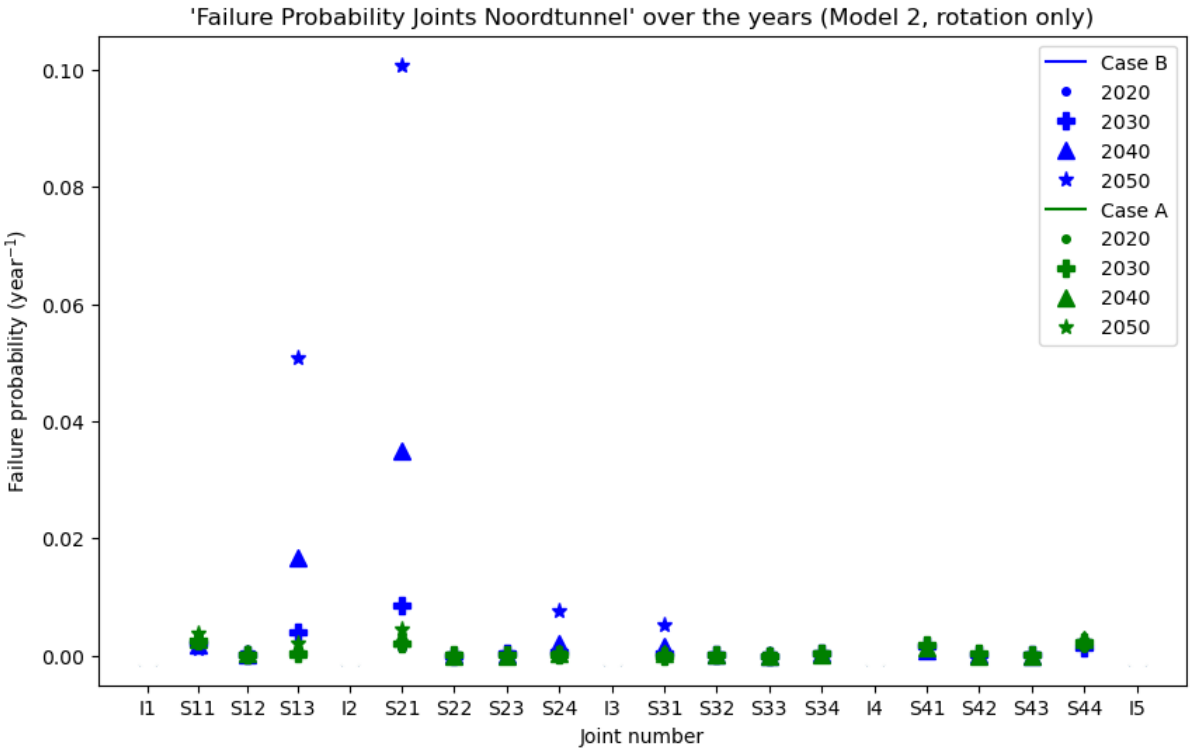

Figure 96: Failure probability segment joints of the Noordtunnel over the years for Model 2, considering only the rotational failure mechanism, where Case A and Case B concern the logarithmic and linear increase of settlements, respectively.

Figure 97 and Figure 98 presents the failure probabilities of the segment joints of the Noordtunnel, realised with *Model 3*, including the developments over time for *Case A* and *Case B*.

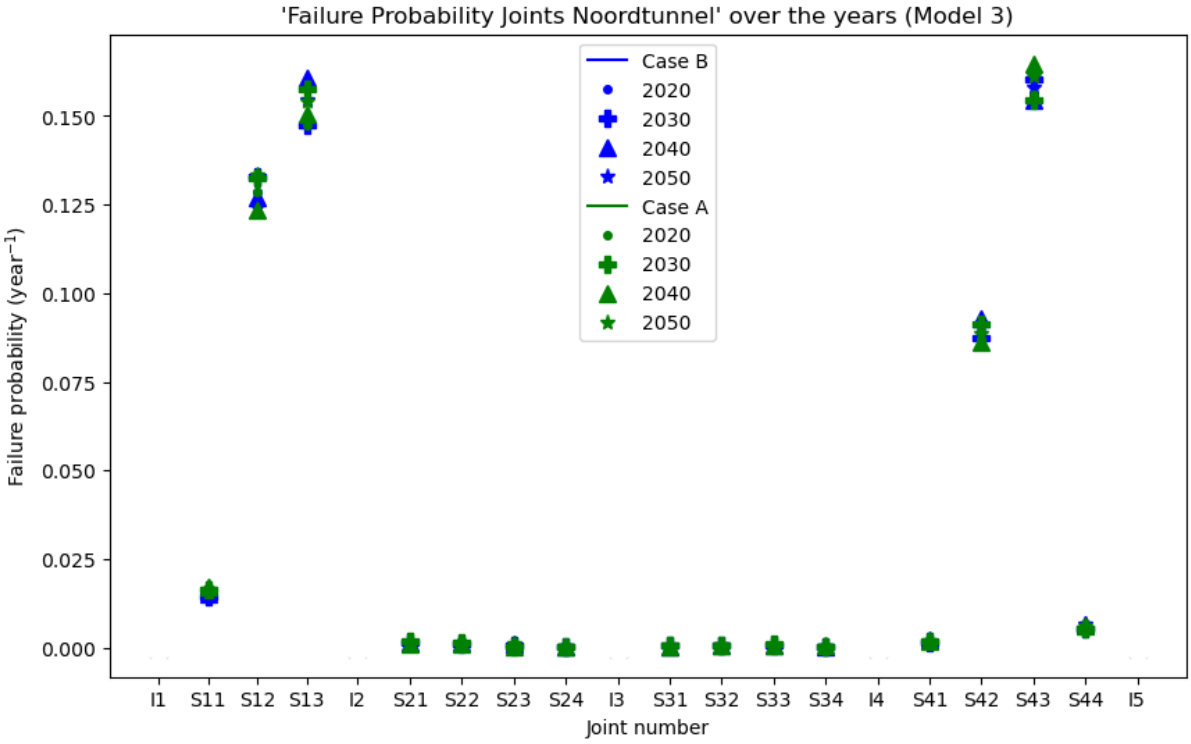

Figure 97: Failure probability segment joints of the Noordtunnel over the years for Model 3, where Case A and Case B concern the logarithmic and linear increase of settlements, respectively.

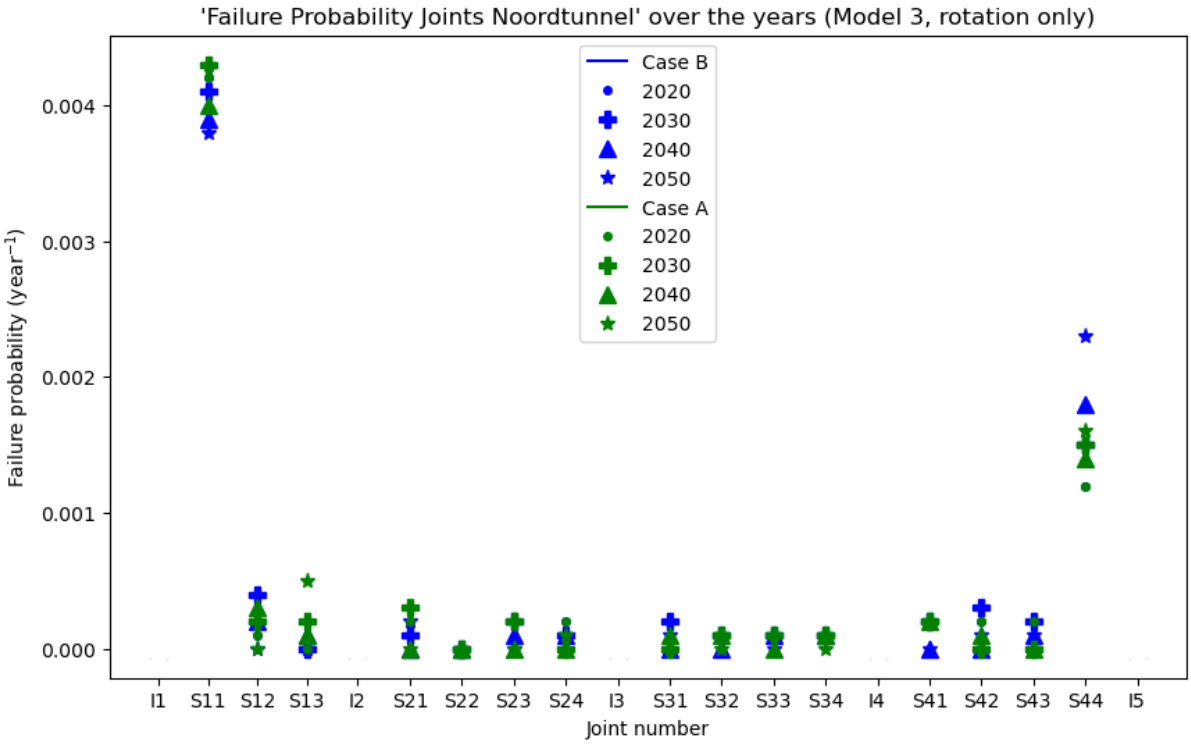

Figure 98: Failure probability segment joints of the Noordtunnel over the years for Model 3, considering only the rotational failure mechanism, where Case A and Case B concern the logarithmic and linear increase of settlements, respectively.

E.5. Analysis Foundation Stiffness Parameter

The contradictory results for the foundation stiffness in the sensitivity analysis of subsection 5.2 ensured that this parameter required further investigation. Therefore, an additional analysis was conducted to determine the influence of the foundation stiffness parameter on the mean failure probability of the segment joints. Figure 99 and Figure 100 present the results of this analysis for the shear force and rotational failure mechanisms. Here, the foundation stiffness is evenly distributed over the tunnel for values ranging between $k_z = 10000$ to $150000\ kN/m^2$.

In the figures, the results are visualised for the three structural models based on two approaches. The first approach uses the research methodology of section 3, with all the parameters as deterministic values, for which the stochastic parameters are simplified to the mean value. In addition, the second approach (illustrated by the dots) has a similar input for the research methodology as described subsection 4.2, except for the foundation stiffness that is assumed to be as an evenly distributed stochastic parameter. Note that $N = 10^3$ is used here, to limit the computation time. Moreover, the coloured symbols in the figures indicate the results of the foundation stiffness for the used parameter value (averaged over the tunnel length), and the limits in the sensitivity analysis, with the crosses and triangles, respectively.

The results show that for shear force failure with *Model 1* and *Model 2*, a remarkable relation is clearly obtained between the foundation stiffness and the mean failure probability. This causes the upper and lower limit of the foundation stiffness (indicated by the red and green triangles) to lead to an increase in the failure probability. This is why there is no upper limit visualised for the foundation stiffness in Figure 42 and Figure 44 of subsection 5.2. Notice that the coloured symbols differentiate from the dots of the second approach, as the underlying foundation stiffness quantification of Figure 34 is not evenly distributed. In addition, the fluctuating results of the first approach follows from the combination of the different developments in failure probability, for the segment joints.

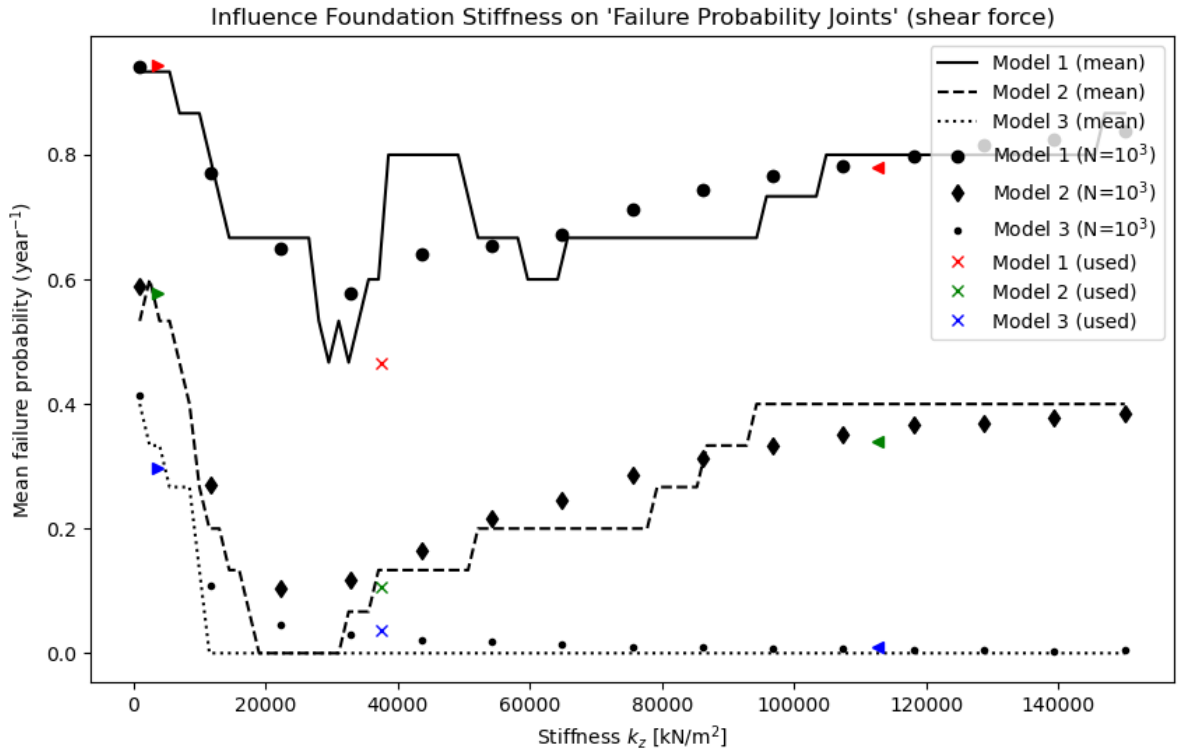

Figure 99: Influence of the foundation stiffness parameter on the mean failure probability of the segment joints, considering the three structural models and the shear force failure mechanism, under the assumption of an even parameter distribution.

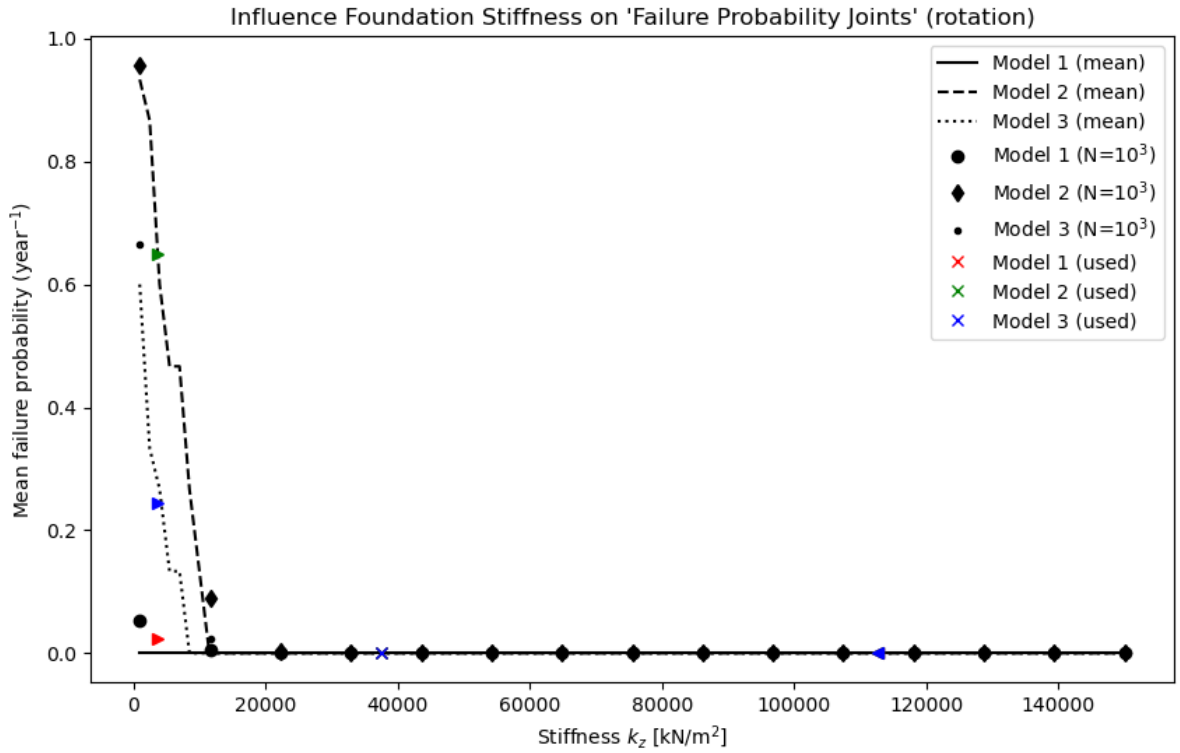

Figure 100: Influence of the foundation stiffness parameter on the mean failure probability of the segment joints, considering the three structural models and the rotational failure mechanism, under the assumption of an even parameter distribution.

F. Stakeholder Analysis EngD Project

In this Appendix, the stakeholder analysis of the EngD research project is described. The scope of the analysis is quite broad to provide a complete overview of all the involved parties for the operation, maintenance and renovation of the immersed tunnels of Rijkswaterstaat.

Figure 101 shows the stakeholder map for the EngD research project. In this figure, various stakeholders have been taken into account, which are involved in the operation, maintenance and renovation of immersed tunnels. The main stakeholders are Rijkswaterstaat, Delft University of Technology and COB, which are all part of this project. Besides these, many more stakeholder have an indirect relation with the project, such as research institutes, engineering firms and contractors.

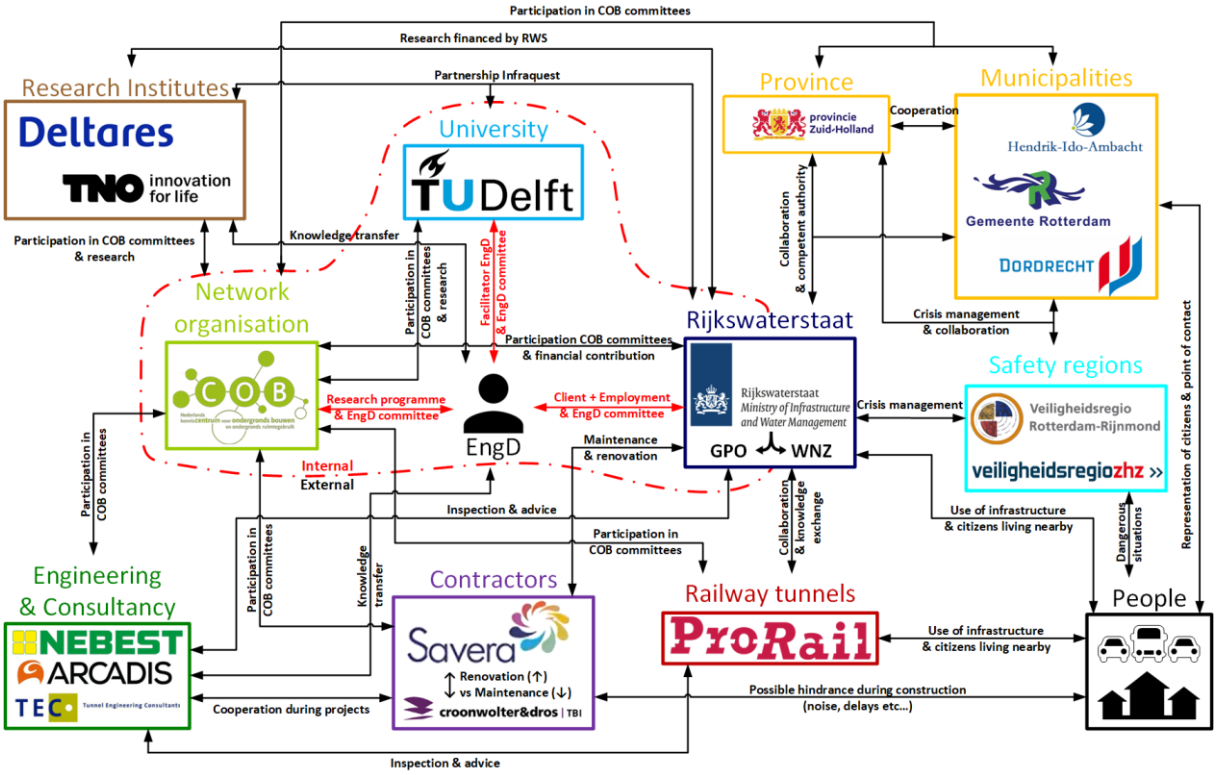

Figure 101: Stakeholder map of the EngD research project.

Rijkswaterstaat

Rijkswaterstaat is responsible for the main infrastructure that should keep the Netherlands safe, liveable and accessible. The tunnels are important links in this road network and there is a major maintenance and renovation challenge, especially for the tunnel structures that have been constructed in the previous century. The renovations should be executed cost effectively and with a high performance, in view of future tunnel maintenance.

Rijkswaterstaat GPO (*'Grote Projecten en Onderhoud'*) is a national department within Rijkswaterstaat and the initiator of the EngD research project. Rijkswaterstaat WNZ (*'West-Nederland Zuid'*) is the regional department that is responsible for managing all the tunnels in South Holland, including the maintenance and renovation. Rijkswaterstaat GPO advices the tunnel managers of South Holland (RWS WNZ) on the structural aspects of the tunnels, amongst others. As a result, this EngD research project should in the end contribute to the predictive maintenance strategy of the tunnel managers. Thus, Rijkswaterstaat WNZ could be seen as the 'client' of the project.

Delft University of Technology

Delft University of Technology considers its social duty to provide ground-breaking technical-scientific solutions that contribute to impact for a better society. With facilitating this EngD project, innovation in the field of tunnels is strengthened. This stimulates tunnel maintenance and renovations to be conducted in a more effective and efficient manner in the future.

COB

As a network and knowledge organisation in underground constructions and underground use of space, the COB is committed to solve tunnel related challenges. Numerous experts participate within the network, so that broadly supported solutions can be found together. This EngD project is part of the research programme 'Future Proof Tunnels' of the COB, to solve the knowledge gaps that tunnels are dealing with. After all, by working well together all parties will benefit somehow.

Research Institutes

Research institutes Deltares and TNO perform applied scientific research with respect to tunnels, when the technical questions become very complex. Herewith, regular calculation methods and standards are not sufficient for use. Obviously, these institutes require the necessary budget and time in order to succeed their research.

Engineering & Consultancy Firms

Engineering and consultancy firms have the experience to help Rijkswaterstaat with the major tunnel renovation challenge. Their calculations, advices and inspections will help Rijkswaterstaat to estimate the risks for the tunnel structures, and technical solutions are offered to overcome the tunnel threats. Of course, when providing these services to Rijkswaterstaat, engineering and consultancy firms are commercially driven.

Contractors

Contractors are always ready to face the maintenance and renovation challenges for the tunnels of Rijkswaterstaat, and they have a lot of experience in executing projects like these. Croonwolter&dros is currently responsible for the regular maintenance of the tunnels in South Holland. Savera III is the contractor combination for the renovation of the 1st Heinenoordtunnel. Contractors use their pragmatic attitude to realise creative solutions that could actually be applied in practice. When the projects are completed, contractors always need to make a profit, which is often challenging given the small profit margins, and the tremendous risks in infrastructure projects.

ProRail

ProRail is a governmental task organisation, which is responsible for the railway tunnels in the Netherlands. The organisation is part of the same ministry as Rijkswaterstaat, and is dealing with similar problems in their infrastructure. Both organisations share knowledge and experiences with each other, also regarding the maintenance and renovation of tunnel structures.

Province and municipalities

The province of South Holland and the municipalities within, want their domain to be easily accessible (by car) and they want clarity about the required tunnel maintenance (including nuisance). Tunnel closures due to maintenance or calamities should be minimised, and preferably planned well in advance.

Safety regions

Safety regions want to prevent calamities in tunnels, but they are prepared for any risk that could affect the safety of the respective region.

People

People using or living nearby road infrastructure of Rijkswaterstaat, want the region to be easily accessible (by car), with an optimal travel time and without nuisance (e.g. noise and traffic jams). Both road users and citizens demand clear communication, regarding maintenance or renovation of tunnels.

G. Techno-Economic Evaluation

This appendix presents the techno-economic evaluation of the potential solutions, as part of the maintenance and renovation strategy of the segment joints. Firstly, the approach and limitations underlying the evaluation are demonstrated (G.1). Subsequently, the financial feasibility is assessed of the potential solutions: Advanced Monitoring (G.2), Corrective Injecting of Leakages (G.3), Repairing the Structural Connection (G.4), Installing Additional Waterproofing (G.5), and Compensation Grouting (G.6). Finally, the results are compared and discussed (G.7).

G.1. Approach

The techno-economic evaluation is performed for the potential maintenance and renovation solutions of the segment joints, by means of a cost-benefit analysis. The cost-benefit analysis is formulated from a societal perspective, and it has been assumed that this fully corresponds the perspective of Rijkswaterstaat. The analysis involves the determination of the Net Present Value (NPV) and Internal Rate of Return (IRR), for each of the solutions. Note that the solution alternatives are evaluated financially independently, thus neglecting any technical relationship. In addition, each specific solution is compared to the current approach of tunnel maintenance, so only the deviating costs and benefits are considered. For the solutions of advanced monitoring and corrective injection of leakages (paragraphs 6.2.1 and 6.2.2), the scope of the analysis entails the current situation of the Noordtunnel. Besides, for the other three solutions (paragraphs 6.2.3, 6.2.4 and 6.2.5), the cost-benefit analysis is conditional to the presence of a critical segment joint, which is assumed for the Noordtunnel case.

Regarding the costs in the analysis, an extra investment and/or operational expenses of a solution are included. With respect to the benefits, five categories are considered: increased safety to road users, a higher tunnel availability, less maintenance costs, more efficient use of human resources & generalisability of the solution. These categories are derived in subsection 6.3, and are based upon the stakeholder analysis (Appendix F) and the strategy of Rijkswaterstaat (described in subsection 6.1). Table 15 gives the overview of the solution alternatives with the corresponding relevant potential benefit categories.

Table 15: Relevant potential benefit categories for each solution alternative.

Solution Alternatives	Safety	Availability	Maintenance efficiency	HR efficiency	Generalisability
Advanced Monitoring	X	X	X	X	X
Corrective Injection of Leakages	–	X	X	X	X
Repairing the Structural Connection	X	X	X	–	X
Additional Waterproofing	X	X	X	–	X
Compensation Grouting	X	X	X	–	X

In Table 9, the estimated Technology Readiness Level (TRL) was displayed for the potential solution alternatives. It should be noted that the levels are just a rough indication, as the exact levels are very debatable. Based on the TRL, it is stated that the first two alternatives do not require additional development costs. However, additional development costs must be taken into account for the other three alternatives. This is done by multiplying the estimated costs with an additional factor.

G.2. Advanced Monitoring

The investment for an advanced monitoring system in an immersed tunnel is considered for a period of 10 years. It is estimated that the monitoring system will be at the end of its economic life after 10 years. This is because the innovation of new technology is rapidly developing, and the performance of the installed system decreases after a certain time. It should be noted that only the deformation monitoring system is taken into account in the cost-benefit analysis.

The investment of the total deformation monitoring system of an immersed tunnel, is estimated to be order of magnitude €600k for a period of 10 years, based on two commercial offers. Herewith, the initial investment of purchasing and installing the monitoring system is considered to be half of the total investment (€300k). Maintenance of the system and data storage are considered as the other part of the investment, divided into equal amounts over a period of ten years (ten times €30k).

The benefits of the obtained data by the advanced monitoring instruments would quantitatively be subdivided into safety, availability, maintenance efficiency, HR efficiency, and generalisability:

- The safety benefit consists of better predictability of unsafe situations for road users, as a consequence of tunnel structure deformation, which is estimated to be €6.96k annually[109].
- The data of the advanced monitoring will lead to a higher availability of the Noordtunnel, as insight is given into the structural condition of the tunnel. Through this insight, the corrective maintenance strategy will be more predictable, utilizing tunnel closures more efficiently. As a result of this, it is estimated that the tunnel is in total half a day less unavailable over a period of ten years. The availability benefit is therefore estimated to be €50k annually[110].
- Maintenance of the tunnel structure will be more predictable and hence more cost efficient, as the advanced monitoring system enables estimating the structural condition of the tunnel, and identifying the critical segment joints. The maintenance efficiency benefit will increase over time and is considered to be €100k in total over 10 years of monitoring[111]. It is assumed that the maintenance efficiency benefit is €5k in the first year and increases to €15k in the tenth year.
- Manually levelling of the measuring bolts is not required to be performed anymore, as the advanced monitoring system will generate data automatically. This saves approximately €20k over a period of 10 years[112]. Thus, the benefit of human resources efficiency by automation is estimated to be €2k annually.
- The advanced monitoring system creates generalisability benefits, as acquired knowledge will lead to new systems with improved performance or lower costs, which could be applied in other tunnels. Also, the existing data platform for the monitoring system in the Noordtunnel could be used for other tunnels that will be equipped with monitoring in the future. Therefore, the generalisability benefits are estimated to be €3k per year (1% of the initial investment costs). Furthermore, it is assumed that the advanced monitoring system has a residual value of €30k after the 10 years lifespan (10% of the initial investment costs).

[109] It is assumed that an unsafe situation can arise once every 10 years, as a consequence of tunnel structure deformation. The probability that a person gets a serious traffic injury during this event is assumed to be 0.1, and according to Steunpunt Economische Expertise (2022) the societal costs of a serious traffic injury are €696k.
[110] The availability of the tunnel is increased by roughly half a day every 10 years. The societal benefits are set on €1M per day in case the Noordtunnel is fully available. Annually, this leads to the estimated benefit of €50k.
[111] Tunnel maintenance costs roughly concern €500k per year (standard number). Assuming a 2% efficiency gain on average for a period of 10 years, gives a total benefit of €100k (starting at 1%, linearly increasing to 3%).
[112] Over a period of 10 years, approximately 4 manual measurement events are performed for the Noordtunnel, given that three were done since the end of 2013 according to Rijkswaterstaat (2019), and one is planned in 2023. The costs per measurement event are approximately €5k.

Considering all the costs and benefits for the advanced monitoring alternative as described above, the overview is given in Table 16 and Figure 102. The subsequent NPV is calculated to be **€39k** (for 5% interest rate), and the IRR is determined to be **7.4%**.

Table 16: Cost-benefit analysis for the alternative of advanced monitoring.

Advanced Monitoring		Year										
		0	1	2	3	4	5	6	7	8	9	10
Costs	*Investment*	-€300k										
	Maintenance & data storage		-€30k	-€30k	-€30k	-€30k	-€30k	-€30k	-€30k	-€30k	-€30k	-€30k
Benefits	*Safety*		€7k	€7k	€7k	€7k	€7k	€7k	€7k	€7k	€7k	€7k
	Availability		€50k	€50k	€50k	€50k	€50k	€50k	€50k	€50k	€50k	€50k
	Maintenance efficiency		€5k	€6k	€7k	€8k	€9k	€11k	€12k	€13k	€14k	€15k
	HR efficiency		€2k	€2k	€2k	€2k	€2k	€2k	€2k	€2k	€2k	€2k
	Generalisability		€3k	€3k	€3k	€3k	€3k	€3k	€3k	€3k	€3k	€33k
Net Benefit		**-€300k**	**€37k**	**€38k**	**€39k**	**€40k**	**€41k**	**€43k**	**€44k**	**€45k**	**€46k**	**€77k**

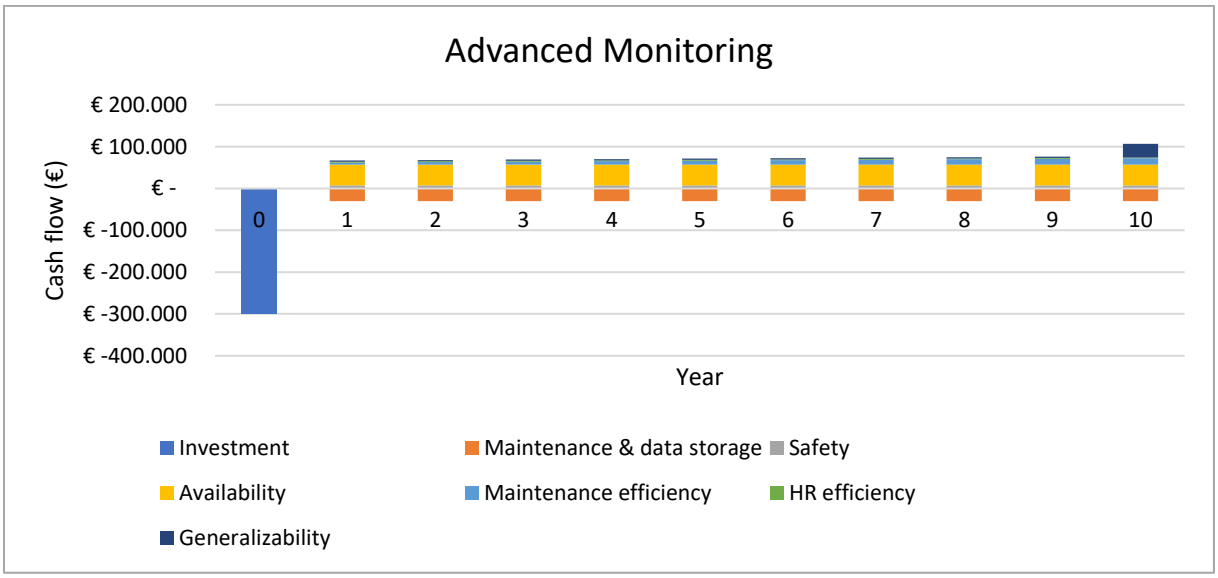

Figure 102: Cost-benefit analysis for the alternative of advanced monitoring.

G.3. Corrective Injection of Leakages

The investment for the alternative of correctively injecting leakages is considered for a period of 10 years. As described in paragraph 6.2.2, the alternative consists of three changes compared to the current corrective maintenance of injecting leakages: (1) collecting and ordering all relevant information, (2) organising a central point of contact within Rijkswaterstaat, and (3) concluding a multi-year contract with a specialised contractor for injecting all leakages in the tunnels. The cost-benefit analysis is performed for ten years, as the multi-year contract is intended to last this period.

The costs for this alternative are split into two parts. Firstly, it is estimated that collecting information, reorganising within Rijkswaterstaat, and preparing the tender for the multi-year contract, will costs in total approximately €1M for all Rijkswaterstaat tunnels[113]. In addition, the multi-year contract is

[113] So this includes predominantly personnel costs and software (and hardware) costs.

estimated to amount €100k annually for the period of 10 years (€1M in total[114]). Assuming an even distribution of costs among roughly 20 tunnels of Rijkswaterstaat, this leads to €50k initial costs and €5k annual costs for the Noordtunnel[115], for the total organisational and annual contractual costs, respectively.

The benefits of the injecting approach for appearing leakages would quantitatively be subdivided into availability, maintenance efficiency, HR efficiency, and generalisability:

- The improved injection approach will lead to a higher availability of the Noordtunnel, as a result of better preparation and organisation. Because of this, it is estimated that the tunnel is in total 0.1 day less unavailable over a period of ten years. The availability benefit is therefore estimated to be €10k annually[116].
- Maintenance of the tunnel structure will be executed more efficiently in the future because of the multi-year contract with the specialised contractor. Through preparation and good cooperation, the contractor will deliver higher quality within a shorter time duration. It is assumed that this leads to a benefit of €1k annually[117].
- Human resources efficiency is achieved by using both a permanent team for injection of the appearing leakages at all tunnels, and with the shorter lines of communication at Rijkswaterstaat. The HR efficiency benefit is estimated to be €1k annually[118].
- Generalisability benefits, through uniform documentation of experiences for all tunnels by the contractor, which allows for standardisation of the lessons learned, amounts €2k annually[119].

Considering all the costs and benefits for the corrective injection of leakages alternative as described above, the overview is given in Table 17 and Figure 103. The subsequent NPV is calculated to be **€19k** (for 5% interest rate), and the IRR is determined to be **12.4%**.

Table 17: Cost-benefit analysis for the alternative of corrective injection of leakages.

Corrective Injection of Leakages		Year										
		0	1	2	3	4	5	6	7	8	9	10
Costs	*Organisational costs*	-€50k										
	Contractual costs		-€5k	-€5k	-€5k	-€5k	-€5k	-€5k	-€5k	-€5k	-€5k	-€5k
Benefits	*Availability*		€10k	€10k	€10k	€10k	€10k	€10k	€10k	€10k	€10k	€10k
	Maintenance efficiency		€1k	€1k	€1k	€1k	€1k	€1k	€1k	€1k	€1k	€1k
	HR efficiency		€1k	€1k	€1k	€1k	€1k	€1k	€1k	€1k	€1k	€1k
	Generalisability		€2k	€2k	€2k	€2k	€2k	€2k	€2k	€2k	€2k	€2k
Net Benefit		**-€50k**	**€9k**	**€9k**	**€9k**	**€9k**	**€9k**	**€9k**	**€9k**	**€9k**	**€9k**	**€9k**

[114] Based on 5% of the €20M (including tax and rounded) contract awarded regarding the engineering services for the Project Tunnel Renovations South Holland.
[115] The Noordtunnel costs are determined by €1M/20 = €50k (initial organisational costs), and €100k/20 = €5k (annual contractual costs).
[116] The availability of the tunnel is increased by roughly 0.1 day every 10 years. The societal benefits are set on €1M per day in case the Noordtunnel is fully available. Annually, this leads to the estimated benefit of €10k.
[117] Tunnel maintenance costs roughly concern €500k per year (standard number) and with an assumed 0.2% efficiency gain, this leads to an annual benefit of €1k.
[118] It is estimated that 20 manhours (€50 each) are saved every year, which leads to an annual benefit of €1k.
[119] Assumed to be 0.4% of the standard number of €500k (annual tunnel maintenance costs), which leads to €2k annually.

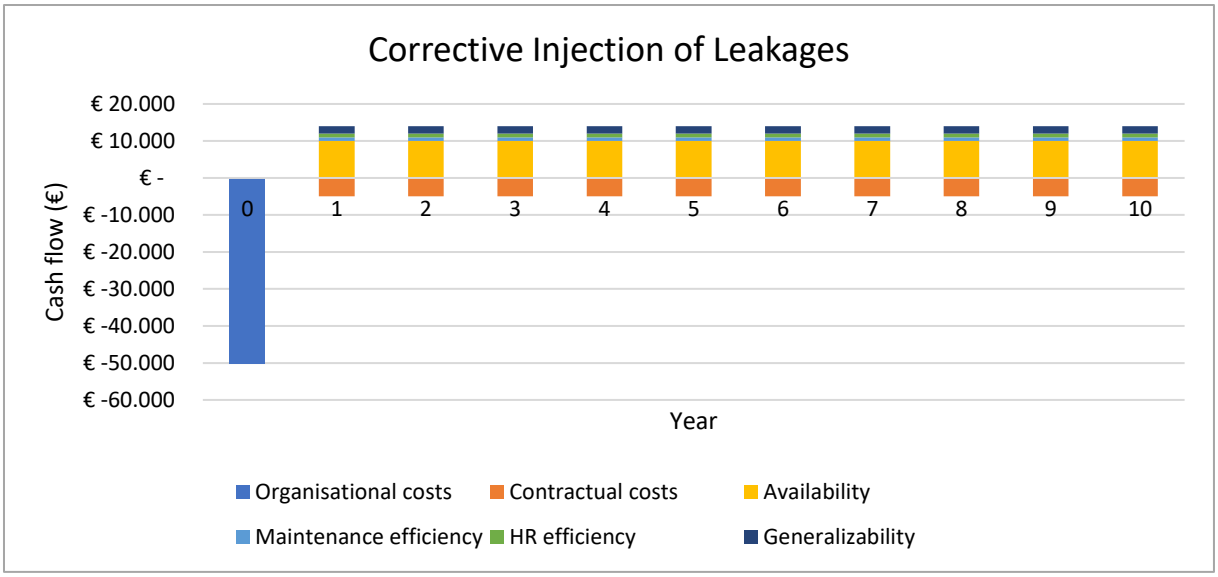

Figure 103: Cost-benefit analysis for the alternative of corrective injection of leakages.

G.4. Repairing the Structural Connection

The investment for the alternative of repairing the structural connection is considered for a period of 50 years, which is equal to half the intended lifespan of the Noordtunnel. Repairing the structural connection of a segment joint is a very major operation, and should therefore only be considered if it is sure that the original structural connection of a joint has failed. Note that for the cost-benefit analysis of this alternative, it is assumed that the Noordtunnel contains such a critical segment joint.

The costs for this alternative consist of an investment part and an operational part. It is estimated that the investment for (the critical part of) the Noordtunnel would be €2M (including 200% additional development costs because of TRL 6), based on the cost estimation for prestressing of the Limfjord Tunnel, which is approximately €5M (ATKINS et al., 2019). The operational costs (inspection and maintenance) are estimated to be 1% of the investment, thus consisting of €20k annually.

The benefits of the alternative of repairing the structural connection would quantitatively be subdivided into safety, availability, maintenance efficiency, and generalisability:

- The safety benefit consists of less unsafe situations for road users, as a consequence of repairing the structural connection of the critical segment joint. It is estimated to be twice the quantified value of the advanced monitoring alternative (described in G.2), which results in €13.9k annually.
- The alternative will lead to a higher availability, as less maintenance disruption is required. It is estimated that the tunnel will in total be 1 day less unavailable over a period of ten years. Thus, the availability benefit is therefore estimated to be €100k annually[120].
- Maintenance of the tunnel structure could be conducted more efficiently in the future, after the alternative is applied in the critical segment joint. It is assumed that this leads to a benefit of €5k annually [121].
- Generalisability benefits through gained experience could pay off for all other tunnels when standardisation is being applied, which involves €2k annually[122].

[120] The availability of the tunnel is increased by roughly 1 day every 10 years. The societal benefits are set on €1M per day in case the Noordtunnel is fully available. Annually, this leads to the estimated benefit of €100k.
[121] It is assumed to save 1% of the €500k tunnel maintenance costs per year (standard number), which is €5k.
[122] Assumed to be 0.1% per year of the initial investment, which leads to a benefit of €2k annually.

Considering all the costs and benefits for the repairing the structural connection alternative as described above, the overview is given in Table 18 and Figure 104. The subsequent NPV is calculated to be **-€158k** (for 5% interest rate), and the IRR is determined to be **4.5%**.

Table 18: Cost-benefit analysis for the alternative of repairing the structural connection.

Repairing the Structural Connection		Year(s)										
		0	1-5	6-10	11-15	16-20	21-25	26-30	31-35	36-40	41-45	46-50
Costs	*Investment*	-€2M										
	Operational costs		-€100k	-€100k	-€100k	-€100k	-€100k	-€100k	-€100k	-€100k	-€100k	-€100k
Benefits	*Safety*		€70k	€70k	€70k	€70k	€70k	€70k	€70k	€70k	€70k	€70k
	Availability		€500k	€500k	€500k	€500k	€500k	€500k	€500k	€500k	€500k	€500k
	Maintenance efficiency		€25k	€25k	€25k	€25k	€25k	€25k	€25k	€25k	€25k	€25k
	Generalisability		€10k	€10k	€10k	€10k	€10k	€10k	€10k	€10k	€10k	€10k
Net Benefit	**For five consecutive years**	**n/a**	**€505k**	**€505k**	**€505k**	**€505k**	**€505k**	**€505k**	**€505k**	**€505k**	**€505k**	**€505k**
	For a single year	**-€2M**	**€101k**	**€101k**	**€101k**	**€101k**	**€101k**	**€101k**	**€101k**	**€101k**	**€101k**	**€101k**

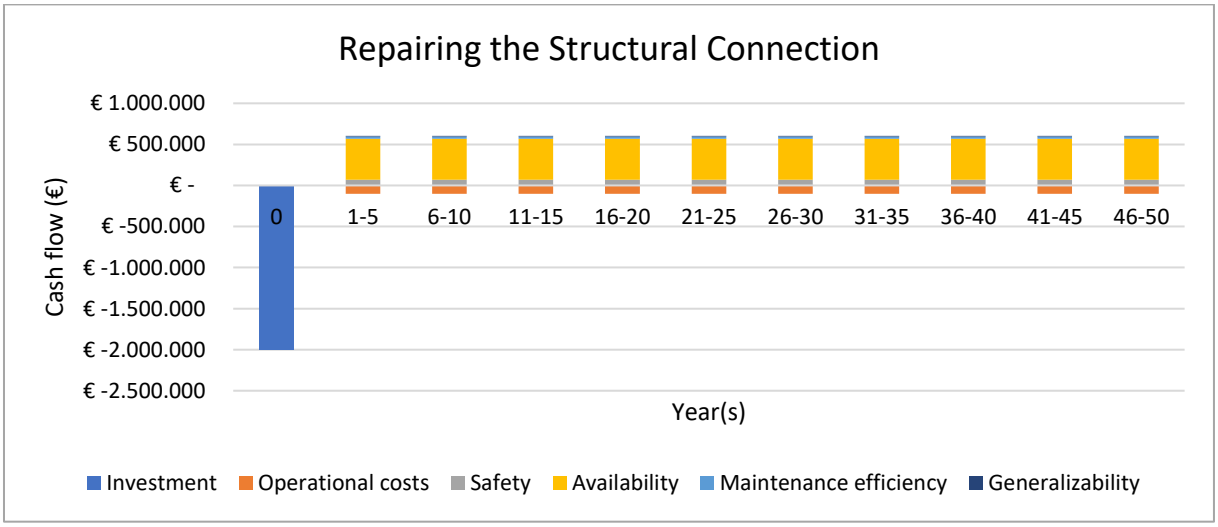

Figure 104: Cost-benefit analysis for the alternative of repairing the structural connection.

G.5. Installing Additional Waterproofing

The investment for the alternative of installing additional waterproofing is considered for a period of 50 years, which is equal to half the intended lifespan of the Noordtunnel (similar to previous alternative). Installing an additional waterproof gasket in a segment joint is a very major operation, and should therefore only be considered if a joint has lost (or is likely to lose) its waterproof function, resulting in significant leakages. Note that for the cost-benefit analysis of this alternative, it is assumed that the Noordtunnel contains such a critical segment joint.

The costs for this alternative consist of an investment part and an operational part. It is estimated that the investment for one critical joint of the Noordtunnel would be €3M (including 150% additional development costs because of TRL 7). Note that this is a very rough estimate, based on cost estimates for other renovation activities planned for the Noordtunnel. The operational costs (mainly inspection) are estimated to be 0.1% of the investment, thus consisting of €3k annually.

The benefits of the additional waterproofing alternative would quantitatively be subdivided into safety, availability, maintenance efficiency, and generalisability:

- The safety benefit consists of less unsafe situations for road users, as the additional waterproof gasket prevents future leakages in the critical joint. It is estimated to be similar to the quantified value of the advanced monitoring alternative (described in G.2), which is €6.96k annually.
- The alternative will lead to a higher availability, as less maintenance disruption is required. It is estimated that the tunnel will in total be 1 day less unavailable over a period of ten years. Thus, the availability benefit is therefore estimated to be €100k annually[123].
- Maintenance of the tunnel structure could be conducted more efficiently in the future, after this alternative is applied in a critical segment joint. It is assumed that this leads to a benefit of €5k annually [124].
- Generalisability benefits through gained experience could pay off for all other tunnels when standardisation is being applied, which involves €3k annually[125].

Considering all the costs and benefits for the additional waterproofing alternative as described above, the overview is given in Table 19 and Figure 105. The subsequent NPV is calculated to be **-€956k** (for 5% interest rate), and the IRR is determined to be **2.8%**.

Table 19: Cost-benefit analysis for the alternative of installing additional waterproofing.

Installing Additional Waterproofing		Year(s)										
		0	1-5	6-10	11-15	16-20	21-25	26-30	31-35	36-40	41-45	46-50
Costs	*Investment*	-€3M										
	Operational costs		-€15k	-€15k	-€15k	-€15k	-€15k	-€15k	-€15k	-€15k	-€15k	-€15k
Benefits	*Safety*		€35k	€35k	€35k	€35k	€35k	€35k	€35k	€35k	€35k	€35k
	Availability		€500k	€500k	€500k	€500k	€500k	€500k	€500k	€500k	€500k	€500k
	Maintenance efficiency		€25k	€25k	€25k	€25k	€25k	€25k	€25k	€25k	€25k	€25k
	Generalisability		€15k	€15k	€15k	€15k	€15k	€15k	€15k	€15k	€15k	€15k
Net Benefit	**For five consecutive years**	**n/a**	**€560k**	**€560k**	**€560k**	**€560k**	**€560k**	**€560k**	**€560k**	**€560k**	**€560k**	**€560k**
	For a single year	**-€3M**	**€112k**	**€112k**	**€112k**	**€112k**	**€112k**	**€112k**	**€112k**	**€112k**	**€112k**	**€112k**

[123] The availability of the tunnel is increased by roughly 1 day every 10 years. The societal benefits are set on €1M per day in case the Noordtunnel is fully available. Annually, this leads to the estimated benefit of €100k.
[124] It is assumed to save 1% of the €500k tunnel maintenance costs per year (standard number), which is €5k.
[125] Assumed to be 0.1% per year of the initial investment, which leads to a benefit of €3k annually.

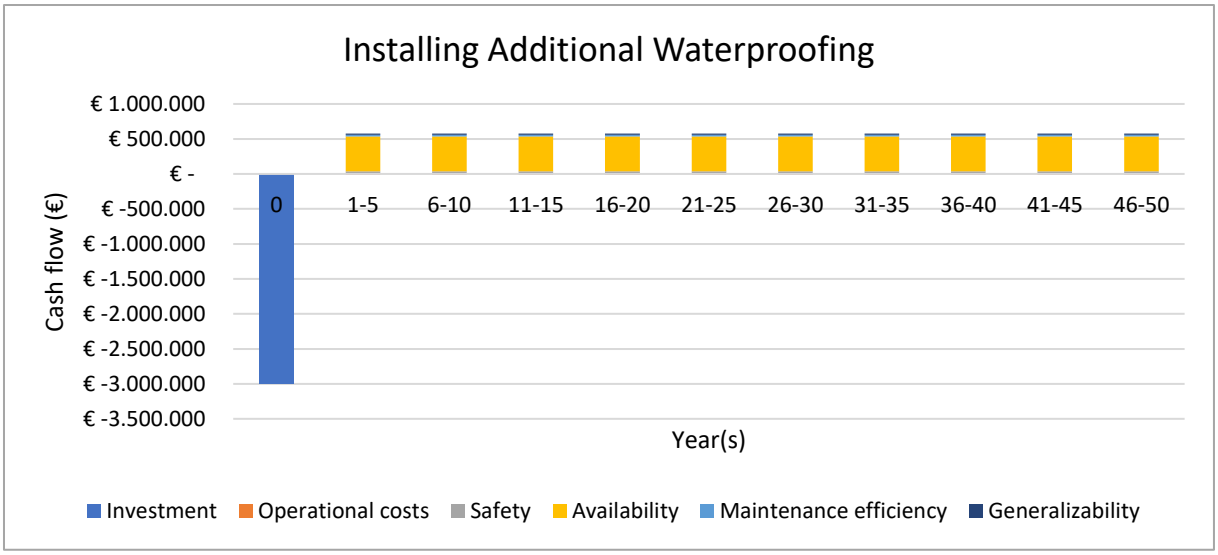

Figure 105: Cost-benefit analysis for the alternative of installing additional waterproofing.

G.6. Compensation Grouting

The investment for the compensation grouting alternative is considered for a period of 50 years, similar to the previous two alternatives, which is equal to half the intended lifespan of the Noordtunnel. Compensation grouting is by far the most expensive alternative, and should therefore only be considered if increasing deformations continue to deteriorate the structural tunnel condition. Note that for the cost-benefit analysis of this alternative, this has been assumed to be the case for the Noordtunnel.

The costs for this alternative consist of an investment part and an operational part. It is estimated that the investment of compensation grouting (of only the critical element) at the Noordtunnel would be €15M (including 150% additional development costs because of TRL 7), based on the cost estimation for compensation grouting of the Limfjord Tunnel, which is approximately €30M (ATKINS et al., 2019). The operational costs (mainly monitoring) are estimated to be 0.1% of the investment, thus consisting of €15k annually.

The benefits of the compensation grouting alternative would quantitatively be subdivided Into safety, availability, maintenance efficiency, and generalisability:

- The safety benefit consists of less unsafe situations for road users, as the tunnel settlements are reversed and additional risks are avoided. It is estimated to be thrice the quantified value of the advanced monitoring alternative (described in G.2), which results in €20.9k annually.
- The alternative will lead to a higher availability as less maintenance disruption is required. It is estimated that the tunnel will in total be 2 days less unavailable over a period of ten years. Thus, the availability benefit is therefore estimated to be €200k annually[126].
- Maintenance of the tunnel structure could be conducted more efficiently in the future, after this alternative is applied. It is assumed that this leads to a benefit of €10k annually [127].
- Generalisability benefits through gained experience could pay off for all other tunnels when standardisation is being applied, which involves €15k annually[128].

[126] The availability of the tunnel is increased by roughly 2 days every 10 years. The societal benefits are set on €1M per day in case the Noordtunnel is fully available. Annually, this leads to the estimated benefit of €200k.
[127] It is assumed to save 2% of the €500k tunnel maintenance costs per year (standard number), which is €10k.
[128] Assumed to be 0.1% per year of the initial investment, which leads to a benefit of €15k annually.

Considering all the costs and benefits for the compensation grouting alternative as described above, the overview is given in Table 20 and Figure 106. The subsequent NPV is calculated to be **€-10.8M** (for 5% interest rate), and the IRR is determined to be **-1.0%**.

Table 20: Cost-benefit analysis for the alternative of compensation grouting.

Compensation Grouting		Year(s)										
		0	1-5	6-10	11-15	16-20	21-25	26-30	31-35	36-40	41-45	46-50
Costs	*Investment*	-€15M										
	Operational costs		-€75k	-€75k	-€75k	-€75k	-€75k	-€75k	-€75k	-€75k	-€75k	-€75k
Benefits	*Safety*		€105k	€105k	€105k	€105k	€105k	€105k	€105k	€105k	€105k	€105k
	Availability		€1M	€1M	€1M	€1M	€1M	€1M	€1M	€1M	€1M	€1M
	Maintenance efficiency		€50k	€50k	€50k	€50k	€50k	€50k	€50k	€50k	€50k	€50k
	Generalisability		€75k	€75k	€75k	€75k	€75k	€75k	€75k	€75k	€75k	€75k
Net Benefit	**For five consecutive years**	**n/a**	**€1.15M**	**€1.15M**	**€1.15M**	**€1.15M**	**€1.15M**	**€1.15M**	**€1.15M**	**€1.15M**	**€1.15M**	**€1.15M**
	For a single year	**-€15M**	**€231k**	**€231k**	**€231k**	**€231k**	**€231k**	**€231k**	**€231k**	**€231k**	**€231k**	**€231k**

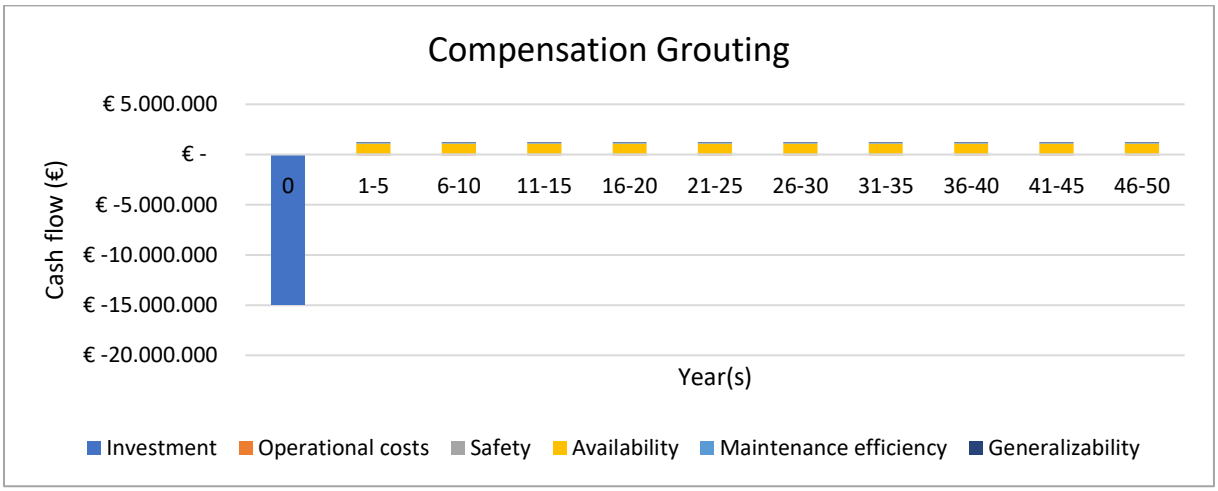

Figure 106: Cost-benefit analysis for the alternative of compensation grouting.

G.7. Discussion

The techno-economic evaluation is discussed here, regarding the potential maintenance and renovation solutions of segment joints, and the financial results are compared. A cost-benefit analysis has been conducted from a societal perspective, where the Net Present Value (NPV) and Internal Rate of Return (IRR) were determined. The alternatives were evaluated by making a comparison with the current tunnel maintenance approach[129], thus only considering deviating costs and benefits[130]. Furthermore, no relationships have been taken into account between the alternatives. Moreover, the Technology Readiness Level (TRL) of Table 9 was used to estimate the uncertainty in the costs.

[129] For advanced monitoring (G.2) and corrective injection of leakages (G.3), the scope of the analysis entails the current situation of the Noordtunnel. However, the presence of a critical segment joint is assumed for the cost-benefit analyses of repairing the structural connection (G.4), installing additional waterproofing (G.5), and compensation grouting (G.6). Whether there is actually a critical joint in the Noordtunnel is debatable.
[130] The benefit categories (see Table 15) have been derived in subsection 6.3.

In the approach of the cost-benefit analysis, several assumptions have been made. The costs and benefits of the alternatives were compared to the current tunnel maintenance, however this is difficult as some of the current costs and benefits are unknown. Nevertheless, the approach of the quantification in the business case is considered to be suitable, apart from the cost-benefit estimates themselves. Additionally, with the NPV and IRR, two different investment evaluation tools were used in the analysis, resulting in more interpretable outcomes. The periods for which the cost-benefit analyses were chosen, were reasonably substantiated and considered as appropriate, for all the alternatives.

In terms of cost-benefit estimates, there is still some uncertainty included within the estimates. Regarding the cost quantification, some of the alternatives are technically still at a conceptual level, and therefore it is impossible to estimate the costs accurately. In addition, the development costs for the alternatives with TRL 6 or 7, are based on a rough estimation as well. In the quantification of the benefit categories, some comments could be made for the different alternatives. The availability benefit has the greatest impact of all the alternatives, which makes it the most important category to discuss. The societal benefits of the Noordtunnel being available (€1M per day) might be a little high. Besides this, the complete closure of the tunnel is assumed indirectly (for both tunnel tubes), and the difference between closure during the day or night is not considered. Also, potential unavailability costs of the execution have not been taken into account, under the premise of planning optimisation within the renovation. However, the estimated time advantage[131] in the availability benefit is likely to be underestimated, for the alternatives. Additionally, the image risk for Rijkswaterstaat has not been taken into consideration, due to its intangibility. This image risk, which is linked to the tunnel unavailability, is expected to be quite significant. Therefore, the potential under and overestimates of the availability benefit roughly seem to cancel each other out, so that the benefit is estimated reasonably. Overall, the business case of the alternatives is therefore considered to be order of magnitude valid.

Table 21 presents the overview of the calculated Net Present Value (NPV) and Internal Rate of Return (IRR) for the solution alternatives. Based on these results, three groups are distinguished within the alternatives. First of all, the alternatives of advanced monitoring and corrective injection of leakages, show positive results for both the NPV (5% interest rate) and the IRR. Therefore, these alternatives seem to be worth considering for investment. Secondly, the alternatives of repairing the structural connection and additional waterproofing, display a negative NPV and a positive IRR result. Hence, for these alternatives it is still uncertain to what extent a potential investment would pay off. Finally, the compensation grouting alternative demonstrates negative results for both the NPV and IRR, causing this alternative not to seem worth its investment at this moment.

Solution Alternatives	NPV (k€)	IRR (%)
Advanced Monitoring	39	7.4
Corrective Injection of Leakages	19	12.4
Repairing the Structural Connection	-158	4.5
Additional Waterproofing	-956	2.8
Compensation Grouting	-10785	-1.0

Table 21: Overview results of the cost-benefit analyses for the five solution alternatives.

[131] For the different alternatives this is assumed between the 0.1 to 2 days per 10 years.